First Principles Conceptual Models Of Chemical Reactivity: Quantitative Curly Arrows And Frontier Orbitals

Cardiff University

A thesis presented for the degree of Doctor of Philosophy

Josh Kirsopp

June 5, 2020

Abstract

The computational expense associated with evaluating the electrostatic potential at a series of points stems from the presence of the position vector of each point in the denominator of a complicated 3D integral. A multipole expansion of the potential is significantly less computationally demanding, and yields a good approximation to the exact potential far from the charge distribution, but penetration effects lead to erroneous potentials at short range. In this work we present a new, computationally efficient method for approximating molecular electrostatics, the Reduced Orbital Potential Approximation, which combines multipole information with the full electrostatic potential arising from a simple model density, which can be evaluated at a fraction of the cost of the full density and incorporates some of the penetration correction without the need for damping functions.

A new tool for the chemical interpretation of *ab initio* wavefunctions is also introduced which aims to establish a rigorous link between accurate computations of the potential energy surface and widely employed chemical descriptions of change during a reaction, such as frontier orbitals and "curly arrows". To achieve this, the total energy is partitioned tensorially into a global potential energy containing no quantities associated with chemical bonding and a covalency energy, for which the necessary assumptions and approximations for the use of chemically intuitive notions of reactivity can be considered valid. The scheme is applied first to canonical orbitals and shown to provide quantitative bonding information in line with classical molecular orbital diagrams, and then to localised orbitals in an attempt to recover frontier orbitals and curly-arrows. An extension to the method is also explored which enforces the assumption that core orbitals are mere spectators to reactions. The method is shown to give good results for a simple test system, and then applied to an S_N2 reaction.

Acknowledgements

My supervisor, Peter Knowles, without whom I could never have managed it and whose conversations over lunch kept me excited about quantum chemistry through even the most difficult periods of this research. Similarly, my colleagues and friends from the Knowles group and wider School of Chemistry.

Danny and Eddie, for having never failed to brighten my day and for the most bulletproof friendships I could ever have hoped for.

Paige, for being a constant source of love and inspiration. You are a force of nature and I could not be more proud of you.

My family Joanne, Alan and Aidan, your love and encouragement are the things I value most in this world, and I hope this makes you proud.

My grandparents John and Maureen, you gave me a magical first five years of life and filling the pages of this thesis with gratitude would not be enough. This is for you.

Declaration

- This thesis is being submitted in partial fulfilment of the requirements for the degree of Doctor of Philosophy (PhD).
- This work has not been submitted in substance for any other degree or award at this or any other university or place of learning, nor is it being submitted concurrently in candidature for any other degree or award.
- I hereby give consent for my thesis, if accepted, to be available in the University's Open Access repository, and for the title and summary to be made available to outside organisations.
- This thesis is the result of my own independent work, except where otherwise stated, and the views expressed are my own. Other sources are acknowledged by explicit references. The thesis has not been edited by a third party beyond what is permitted by Cardiff University's policy on the Use of Third Party Editors by Research Degree Students.

Candidate signature:

Josh J. M. Kirsopp

"Sometimes it seems to me that a bond between two atoms has become so real, so tangible, so friendly, that I can almost see it. And then I awake with a little shock: for a chemical bond is not a real thing: it does not exist: no-one has ever seen it, no-one ever can. It is a figment of our own imagination."

- Charles A. Coulson

Contents

Acronyms

ALMO Absolutely Localised Molecular Orbital.

AO Atomic Orbital.

BFGS Broyden-Fletcher-Goldfarb-Shanno.

BO Born-Oppenheimer.

BS-ISA Basis Space Iterative Stockholder Algorithm.

CASSCF Complete Active Space Self Consistent Field.

CC Coupled Cluster.

CI Configuration Interaction.

CSF Configuration State Function.

DFP Davidson-Fletcher-Powell.

DFT Density Functional Theory.

DMA Distributed Multipole Analysis.

EDA Energy Decomposition Analysis.

ESP Electrostatic Potential.

ETS Extended Transition State.

FB Foster-Boys.

FCI Full Configuration Interaction.

GEM Gaussian Electrostatic Model.

GMM Gaussian Multipole Model.

GTO Gaussian-Type Orbital.

HF Hartree-Fock.

HL Heitler-London.

IBO Intrinsic Bond Orbital.

ISA Iterative Stockholder Algorithm.

KM Kitaura-Morokuma.

LCAO Linear Combination of Atomic Orbitals.

LMO Localised Molecular Orbital.

MBIS Minimal Basis Iterative Stockholder.

MCSCF Multiconfigurational Self Consistent Field.

MM Molecular Mechanics.

MO Molecular Orbital.

MP Møller-Plesset.

NAO Natural Atomic Orbitals.

NBO Natural Bond Orbitals.

NO Natural Orbital.

OFA Orbital Field Approximation.

OFGA Orbital Field Gradient Approximation.

OMA Orbital Multipole Approximation.

PES Potential Energy Surface.

PM Pipek-Mezey.

QM/MM Quantum Mechanics/Molecular Mechanics.

RHF Restricted Hartree-Fock.

RO Reaction Orbital.

ROFA Reduced Orbital Field Approximation.

ROFGA Reduced Orbital Field Gradient Approximation.

ROPA Reduced Orbital Potential Approximation.

SALC Symmetry Adapted Linear Combination.

SAPT Symmetry-Adapted Perturbation Theory.

SCF Self-Consistent Field.

SCGVB Spin-Coupled Generalized Valence Bond.

SD Slater Determinant.

STO Slater-Type Orbital.

SVD Singular Value Matrix Decomposition.

UHF Unrestricted Hartree-Fock.

VB Valence Bond.

Chapter 1

Introduction

1.1 Quantum Mechanics

The laws of classical mechanics defined our understanding of the universe exclusively, and successfully, for almost three centuries. The first clues as to the inadequacy of classical mechanics as the sole descriptor of the world around us came at the hands of technological advances at the beginning of the 20th century, which posed the question of how one should describe particles at large velocities or on small scales. The theory of relativistic mechanics solved the high velocity problem, while the small scale problem was solved by the construction of a new branch of physics: quantum mechanics.

The impact of the early quantum mechanical theories cannot be overstated. Not only did they provide scientists with predictive powers over atomic and sub atomic systems, they changed the way physicists think about macroscopic systems. Erwin Schrödinger's wave mechanics approach to the quantum problem is perhaps the most famous, and is foundational to this work. [1]

1.1.1 The Postulates of Quantum Mechanics

In any discussion of quantum mechanics, the start is almost invariably the comparison of the postulates of quantum and classical mechanics. [2] This section will cover this ground and include a short disussion of each postulate in turn. The list items X.C and X.Q correspond to the X^{th} classical and quantum postulates, respectively.

1.C The state of a particle can be described at any time t by two variables, position $x(t)$, and momentum $p(t)$, by Newton's Laws.

1.Q The state of a particle is described by a vector $\psi(\vec{r}, t)$ belonging to a Hilbert Space.

A Hilbert space is a complex vector space which contains vectors (representing functions) normalisable to unity, and vectors normalisable only to the dirac delta function. The importance of this feature is made clear in the discussion of the next postulate.

2.C Any measurable quantity exhibited by the particle can be described by some combination of $x(t)$ and $p(t)$ using the appropriate equation. The measurement of a variable has no impact on the state of the system.

2.Q The analogues of the classical variables for 2.C are not simple functions of time, but the expectation values of the operators $\hat{x}$ and $\hat{p}$. The measurement of an observable changes the state vector of the particle to a basis vector contained within the eigenbasis of the operator used to take the measurement.

The classical postulate requires little discussion, the state of a ball at x is not changed by the observation that the ball is at x. Upon the measurement of a quantum particle in state $|\psi(\vec{r}, t)\rangle$ with the position operator, $\hat{x}$, the state is changed to an eigenvector of $\hat{x}$ contained within the Hilbert space of the previous postulate, with eigenvalue (i.e the measured position) $x\delta(x - x_0)$. In this basis, the matrix representation of $\hat{x}$, $\mathbf{x}$, is diagonal. The form of the operators used in quantum mechanics are given quite simply, by mapping the classical expression for a variable to the operator form in the same combination (if we ignore some constants).

The modification of the state vector as a result of measurement is known as the "collapse" of the state vector. One obtains upon the measurement of variable Λ eigenvalue λ_i, with probability $P(\lambda_i) \propto |\langle \lambda_i | \psi \rangle|^2$.

3.C The change in the state variables stays within the superstructure that is Hamilton's equations.

3.Q The state vector $|\psi(\vec{r},t)\rangle$ obeys at all times the Schrödinger equation,

$$i\hbar\frac{\partial}{\partial t}|\psi(\vec{r},t)\rangle = \hat{H}|\psi(\vec{r},t)\rangle \tag{1.1}$$

The collapse of the state vector into an eigenvector of the chosen Hamiltonian introduces an uncertainty which sits at the core of quantum mechanics. That is, to measure two observables associated with a particle, apply their Hamiltonian operators one after another, and if they are diagonal in the same basis, one can know both precisely. In the case that they are not diagonal in the same basis, both can never be known simultaneously. The most famous example of this is Heisenberg's uncertainty principle, which states that increasing the accuracy of a measurement of a component of the position operator is to the detriment of the accuracy of any momentum measurement along that component.

There are two representations used frequently in quantum mechanics: the position space and the momentum space, which are simply the Hilbert spaces in which the position and momentum operators, respectively, are diagonal. In this thesis we are concerned only with position space, and also not at all with the evolution of the wavefunction with time.

1.1.2 Quantum Chemistry

There are several terms which are commonly used synonymously with quantum chemistry, such as computational, or theoretical chemistry. In this work the term quantum chemistry will be used and defined, loosely, as the treatment of molecular systems within the framework above, with the view to use the wavefunction for the calculation of quantities of chemical interest.

While the Schrödinger equation is too difficult to solve analytically for systems of chemical interest, there are a number of available methods and approximations which allow us to gather numerical solutions. A selection of the most popular ones are discussed in the next chapter.

1.2 Current Work

A review of the most commonly used methods for finding approximate solutions to the Schrödinger equation is contained in chapter 2. Chapter 3 provides useful mathematical context to the optimisation problems encountered throughout this thesis, and outlines a popular algorithm for solving problems of this sort, which has been much used in the preparation of this thesis. Chapter 4 contains a review of methods, theory and historical setting related to the new work on approximating molecular electrostatic potentials and forcefields which is then presented in chapter 5. Chapter 6, much like chapter 4, is entirely review and sets the stage for the introduction of a new method for extracting chemically intuitive bonding information from molecular wavefunctions in chapter 7.

Chapter 2

Electronic Structure Theory

Electronic structure theory comprises a vast array of approaches for solving the Schrödinger equation. As such, this discussion is limited to those not including relativistic effects, nor those including any nuclear motion. It is assumed that nuclear and electronic eigenstates are completely decoupled and as such our problem is reduced to constructing a wavefunction which satisfies the requirements of the electrons. How this is done, and the most popular models built on this assumption are outlined in this chapter, along with the general form of the electronic wavefunction and the most commonly used basis sets.

2.1 The Born-Oppenheimer Approximation

The time-independent Schrödinger equation for a molecule takes the following form,

$$\hat{H}\psi(\mathbf{r},\mathbf{R}) = E\psi(\mathbf{r},\mathbf{R}) \tag{2.1}$$

$$\hat{H} = \hat{T}_e + \hat{T}_N + \hat{V}_{ee} + \hat{V}_{eN} + \hat{V}_{NN} \tag{2.2}$$

where $\mathbf{r}$ and $\mathbf{R}$ are the electronic and nuclear co-ordinates, respectively, and

$$\hat{T}_e = -\sum_i^N \frac{1}{2}\nabla_i^2, \qquad (2.3)$$

$$\hat{T}_N = -\sum_A^M \frac{\nabla_A^2}{2M_A}, \qquad (2.4)$$

$$\hat{V}_{ee} = \sum_{i>j}^N \frac{1}{r_{ij}}, \qquad (2.5)$$

$$\hat{V}_{eN} = -\sum_{i,A} \frac{Z_A}{r_{iA}}, \qquad (2.6)$$

$$\hat{V}_{NN} = \sum_{A>B} \frac{Z_A Z_B}{R_{AB}}, \qquad (2.7)$$

in atomic units. Kinetic energy operators are denoted $\hat{T}$ and potential energy operators are denoted $\hat{V}$. Subscripts correspond to electrons, e, of which there are N and nuclei, A, of which there are M. Assuming that the electronic and nuclear co-ordinates are separable, one can write a trial eigenfunction of the molecular Hamiltonian written above as

$$|\Psi(\mathbf{r};\mathbf{R})\rangle = \psi(\mathbf{r};\mathbf{R})\gamma(\mathbf{R}), \qquad (2.8)$$

where $\psi(\mathbf{r};\mathbf{R})$ is the electronic wavefunction which depends explicitly on the electronic co-ordinates and parametrically on the nuclear co-ordinates, and $\gamma(\mathbf{R})$ is the nuclear wavefunction. Inserting the above into the Schrödinger equation yields

$$\hat{H}\psi\gamma = \left[\psi\hat{T}_N\gamma + U(\mathbf{r};\mathbf{R})\right] + \left\{\gamma\hat{T}_e\psi + (\hat{V}_{ee} + \hat{V}_{NN} + \hat{V}_{eN})\psi\gamma\right\}. \qquad (2.9)$$

$U(\mathbf{r};\mathbf{R})$ represents the coupling terms between the nuclear and electronic wavefunctions, and is assumed negligible. The second set of parentheses contains terms dependent only on electronic co-ordinates and fixed nuclear positions, and under the clamped nuclei approximation is the only surviving term in the above equation. Moreover, any contribution to the energy from $\hat{V}_{NN}$ is constant under this approximation and simply shifts the eigenvalues of the operator. Under the Born-Oppenheimer (BO) approximation, the operator for nuclear motion is applied after the solution to the electronic problem has been found. The justification rests upon the differences in mass of the electrons, protons and neutrons, which have a ratio of 0.00054:1:1; the protons and neutrons are expected to move much more slowly than the electrons, thus in the frame of reference of an electron the nuclei are stationary. [3] As a result, the potential energy surface the nuclei move along un-

der the BO approximation can be found by repeated evaluation of the electronic Schrödinger equation at fixed geometries.

This approximation is not valid for excited states, or where electronic states are near-degenerate at the same nuclear geometry. In this thesis we are concerned only with ground state wavefunctions, so the breakdown of the approximation under these circumstances will not present an issue.

2.2 Electronic Wavefunctions

The description of an electron's state requires, in total, four parts: three spatial co-ordinates, $\mathbf{r}$, and one spin function. The spin functions, $\alpha(\omega)$ and $\beta(\omega)$ identify the spin of the electron as spin up ($m_s = +\frac{1}{2}$) or spin down ($m_s = -\frac{1}{2}$), respectively. A complete description of a single electron can be written as,

$$\chi(\mathbf{r},\omega) = \begin{cases} \psi(\mathbf{r})\alpha(\omega) \\ \psi(\mathbf{r})\beta(\omega) \end{cases} . \tag{2.10}$$

With the available tools for describing a single electron, we can generalise to many electrons so long as we keep in mind a set of requirements which must be fulfilled: That the electrons are treated as indistinguishable particles - one can never say electron one is described by this function and electron two by a second function exclusively - and that any trial wavefunction be antisymmetric with respect to the interchange of the space and spin co-ordinates of any pair of electrons. The latter requirement arises from the fermionic nature of electrons. If this thesis concerned the description of protons, which are bosons, we would require the wavefunction to be symmetric, rather than antisymmetric.

For any system of N electrons one can quite simply write the wavefunction as a Slater determinant (SD), named so after John C. Slater. [4,5] A Slater determinant takes advantage of the features of the determinants one calculates in linear algebra from the elements of a square matrix. Those features are the change in sign upon interchange of any two columns or rows, and that the determinant vanishes if any two columns or rows happen to be identical. Perhaps best illustrated by example

for two electrons,

$$\Psi(\mathbf{x}_1, \mathbf{x}_2) = \begin{vmatrix} \chi_p(\mathbf{x}_1) & \chi_q(\mathbf{x}_1) \\ \chi_p(\mathbf{x}_2) & \chi_q(\mathbf{x}_2) \end{vmatrix} = \chi_p(\mathbf{x}_1)\chi_q(\mathbf{x}_2) - \chi_q(\mathbf{x}_1)\chi_p(\mathbf{x}_2) \tag{2.11}$$

wherein it is clear that if both columns were identical, the determinant would be naught, and interchanging the two sets of variables $\mathbf{x}_1$ and $\mathbf{x}_2$ leaves us with the same wavefunction but for a change in sign. More generally, one can write

$$\Psi(\mathbf{x}_1, \mathbf{x}_2, \ldots, \mathbf{x}_N) = \begin{vmatrix} \chi_p(\mathbf{x}_1) & \chi_q(\mathbf{x}_1) & \cdots & \chi_r(\mathbf{x}_1) \\ \chi_p(\mathbf{x}_2) & \chi_q(\mathbf{x}_2) & \cdots & \chi_r(\mathbf{x}_2) \\ \vdots & \vdots & \ddots & \vdots \\ \chi_p(\mathbf{x}_N) & \chi_q(\mathbf{x}_N) & \cdots & \chi_r(\mathbf{x}_N) \end{vmatrix}. \tag{2.12}$$

The orthogonality of the spin functions used in the description of these electrons builds into this wavefunction a deficiency in correlating the motions of electrons of opposite spins. This is remedied in higher-level methods by using more than one Slater determinant, as will be discussed in later sections of this chapter.

2.3 The Slater-Condon Rules

The Slater-Condon rules are central to deriving the working equations for all methods which construct approximate solutions to the Schrödinger equation as a SD, or a linear combination of SDs, of orthonormal orbitals. They were defined for the diagonal elements of a matrix representation of an operator, $\hat{H}$, in terms of individual orbitals by John C. Slater, and for the off diagonal elements by Edward Condon the following year. [4, 6] That is, they provide the means for evaluating the matrix elements,

$$H_{IJ} = \langle \Psi_I | \, \hat{H} \, | \Psi_J \rangle \,, \tag{2.13}$$

for SDs $|\Psi_I\rangle$ and $|\Psi_J\rangle$. Taking one determinant as a reference, it is then possible to define all other determinants belonging to the same space by how they differ from the reference,

$$\Psi = ||\psi_1(\mathbf{x}_1), \psi_2(\mathbf{x}_2), \ldots, \psi_i(\mathbf{x}_i), \ldots, \psi_j(\mathbf{x}_j), \ldots, \psi_k(\mathbf{x}_k), \ldots, \psi_N(\mathbf{x}_N)||, \tag{2.14}$$

where the notation $||\cdot||$ indicates a normalised SD. It is then simple to write excited determinants in the form

$$\Psi_i^a = ||\psi_1(\mathbf{x}_1), \psi_2(\mathbf{x}_2), \ldots, \psi_a(\mathbf{x}_i), \ldots, \psi_j(\mathbf{x}_j), \ldots, \psi_k(\mathbf{x}_k), \ldots, \psi_N(\mathbf{x}_N)||, \quad (2.15)$$

$$\Psi_{ij}^{ab} = ||\psi_1(\mathbf{x}_1), \psi_2(\mathbf{x}_2), \ldots, \psi_a(\mathbf{x}_i), \ldots, \psi_b(\mathbf{x}_j), \ldots, \psi_k(\mathbf{x}_k), \ldots, \psi_N(\mathbf{x}_N)||, \quad (2.16)$$

$$\Psi_{ijk}^{abc} = ||\psi_1(\mathbf{x}_1), \psi_2(\mathbf{x}_2), \ldots, \psi_a(\mathbf{x}_i), \ldots, \psi_b(\mathbf{x}_j), \ldots, \psi_c(\mathbf{x}_k), \ldots, \psi_N(\mathbf{x}_N)||, \quad (2.17)$$

and so on. The superscripts denote virtual orbitals which are now occupied and have replaced the orbital in coincidence in the subscript. Pauli exclusion prevents double occupation of spin orbitals.

In this work we are interested only in the orbitals which minimise the energy of the operator,

$$\hat{H} = \sum_i \hat{h}(i) + \frac{1}{2}\sum_{i,j}\frac{1}{r_{ij}}, \quad (2.18)$$

as discussed in section 2.1. The Slater-Condon rules for the integrals across $\hat{H}$ are

$$\langle\Psi|\,\hat{H}\,|\Psi\rangle = \sum_i^N \langle\psi_i|\,\hat{h}\,|\psi_i\rangle + \frac{1}{2}\sum_{i,j}^N \left[\langle\psi_i\psi_j|\,\frac{1}{r_{12}}\,|\psi_i\psi_j\rangle - \langle\psi_i\psi_j|\,\frac{1}{r_{12}}\,|\psi_j\psi_i\rangle\right] \quad (2.19)$$

$$\langle\Psi_i^a|\,\hat{H}\,|\Psi\rangle = \langle\psi_a|\,\hat{h}\,|\psi_i\rangle + \sum_j \left[\langle\psi_a\psi_j|\,\frac{1}{r_{12}}\,|\psi_a\psi_j\rangle - \langle\psi_a\psi_j|\,\frac{1}{r_{12}}\,|\psi_j\psi_a\rangle\right] \quad (2.20)$$

$$\langle\Psi_{ij}^{ab}|\,\hat{H}\,|\Psi\rangle = \langle\psi_a\psi_b|\,\frac{1}{r_{12}}\,|\psi_a\psi_b\rangle - \langle\psi_a\psi_b|\,\frac{1}{r_{12}}\,|\psi_b\psi_a\rangle \quad (2.21)$$

$$\langle\Psi_{ijk}^{abc}|\,\hat{H}\,|\Psi\rangle = 0. \quad (2.22)$$

These results are valuable. We now know that states which differ by more than one orbital do not couple through the one electron operator, and those which differ by more than two orbitals do not couple through the two electron operator. [3,7,8] In the case that we build a wavefunction for a system which is a linear combination of SDs, we then have valuable information about the form of the matrix representation of $\hat{H}$ - it is very sparse. These results will be useful in the coming sections.

The integrals shown in this section take the form,

$$\langle\psi_i|\,\hat{h}\,|\psi_j\rangle = \int d\vec{x}_1 \quad \psi_i^*(\vec{x}_1)\hat{h}\psi_j(\vec{x}_1), \tag{2.23}$$

$$\langle\psi_i\psi_j|\,\frac{1}{r_{12}}\,|\psi_k\psi_l\rangle = \int d\vec{x}_1 \int d\vec{x}_2 \quad \psi_i^*(\vec{x}_1)\psi_j^*(\vec{x}_2)\frac{1}{r_{12}}\psi_k(\vec{x}_1)\psi_l(\vec{x}_2). \tag{2.24}$$

The integral shown in equation 2.24 is often abbreviated to $\langle\psi_i\psi_j|\psi_k\psi_l\rangle$, and $(\langle\psi_i\psi_j|\psi_k\psi_l\rangle - \langle\psi_i\psi_j|\psi_l\psi_k\rangle)$ to $\langle\psi_i\psi_j|\,|\psi_k\psi_l\rangle$.

2.4 Basis Sets

In this thesis, approximate molecular wavefunctions are always represented by an expansion in some appropriately designed set of functions, which are referred to as "basis sets". The topic of this section is the design and features of modern basis sets used frequently in quantum chemistry as a means to express the orbitals mentioned in section 2.3. It is first worth noting that the algebraic approach to solving the electronic problem outlined in this section is not the only one available. One could more accurately solve the electronic problem numerically using a dense grid, however this is hardly done as it comes at intractable computational cost except where symmetry is high. [7, 9, 10]

In a complete basis, one could write exactly the wavefunction of a single electron as a linear combination of the member functions of the set, $\{\chi_\alpha\}$. That is,

$$\psi_i = \sum_\alpha C_{\alpha i}\chi_\alpha(\mathbf{r}), \tag{2.25}$$

where ψ_i is the ith molecular orbital and $C_{\alpha i}$ is the coefficient of basis function $\chi_\alpha(\mathbf{r})$ in the expansion of that molecular orbital. These basis functions are often referred to as the atomic orbitals (AOs). In reality, infinitely large bases are of course not possible, and choices must be made as to which functions to include in the basis set, both for computational effficiency and accuracy of the numerical solutions to the Schrödinger equation they provide.

In principle, one could use any set of appropriately defined functions as a basis set for a quantum chemical calculation. It is also not unreasonable to centre these basis functions randomly throughout space, not associating them with any nucleus

in particular. However, in modern applications of electronic structure methods, basis functions are almost always centred at the nuclear positions, and take the form of atomic orbitals, thus giving rise to the linear combination of atomic orbitals (LCAO) picture of molecular orbital (MO) theory. Features which are desirable for basis functions are observed quite clearly in the eigenfunctions of the Schrödinger equation for the hydrogen atom, seen in figures 2.1 and 2.2.

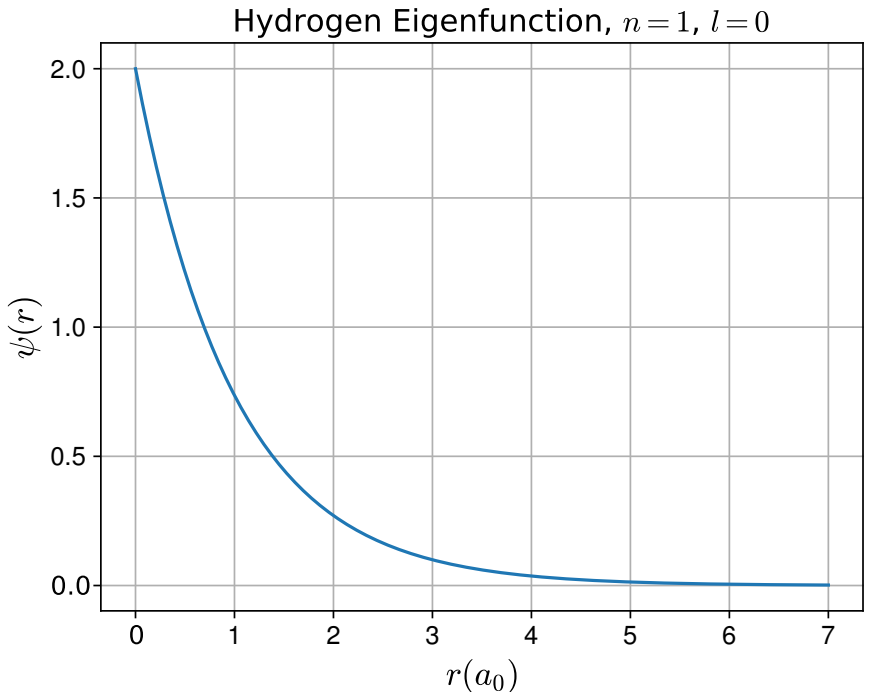

Figure 2.1: The radial part of the first solution to the Schrödinger equation for the H atom - the 1s orbital, which corresponds to quantum numbers $n = 1$ and $l = 0$.

Singularities arise in the wavefunction for any system containing both electrons and nuclei. The conditions under which they occur are,

$$\lim_{r_{ij}\to 0}\left(\frac{\partial\Psi}{\partial r_{ij}}\right)_{\text{av.}} = \frac{1}{2}\Psi(r_{ij}=0) \tag{2.26}$$

$$\lim_{r_{Ai}\to 0}\left(\frac{\partial\Psi}{\partial r_{Ai}}\right) = -Z_A\Psi(r_{Ai}=0). \tag{2.27}$$

Equation 2.26 is known as the electronic cusp condition and arises where the position of two electrons is identical, and equation 2.27 is known as the nuclear cusp condition, and is observed in the $l = 0$ orbitals (seen in figures 2.1 and 2.2). The LCAO formalism of MO theory results in the shape of the wavefunction close to

the nuclei being dominated by the analytic form of the AOs, which is in turn dominated by the nuclear cusp condition.

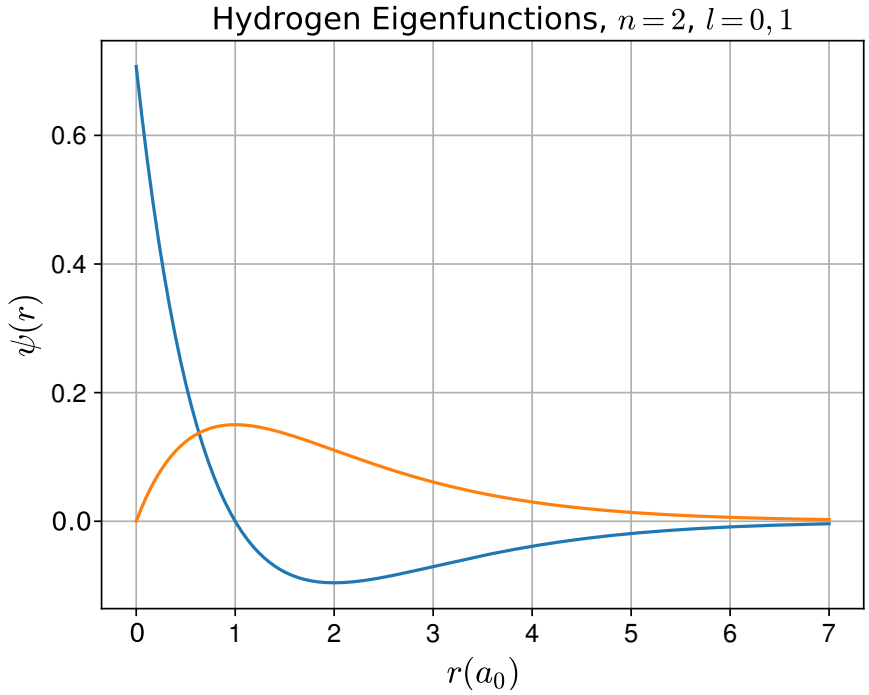

Figure 2.2: Second and third solutions to the Schrödinger equation for the H atom - the 2s and 2p orbitals, which correspond to quantum numbers $n = 2$, $l = 0$ (blue line) and $l = 1$ (orange line)

An early solution was offered by Slater, who proposed a nodeless analytic form for the AOs known as Slater-type atomic orbitals (STOs), which are written as

$$\chi^{\mathrm{STO}}_{\xi_{nl}lm}(r, \theta, \phi) = R_{\xi_{nl}lm}(r) Y_{lm}(\theta, \phi) \tag{2.28}$$

$$R^{\mathrm{STO}}(r) = \frac{(2\xi_{nl})^{\frac{3}{2}}}{\sqrt{(2l+2)!}} (2\xi_{nl} r)^l \exp(-\xi_{nl} r) \tag{2.29}$$

where the radial dependence is given by $R_{\xi_{nl}lm}(r)$, the angular part by the Legendre polynomial $Y_{lm}(\theta, \phi)$ and n, l are the usual quantum numbers. In this way each ξ_{nl} may be optimised, and the best basis set generated for each atomic number. As an example, the H 1s function ($\xi_{nl} = 1$), the slater orbital is identical to the exact solution seen in figure 2.1.

In modern day quantum chemical calculations, STOs are rarely used. Rather, it has become the *de facto* approach to use Gaussian-type AOs (GTOs) in their

place. The Gaussian product theorem, which guarantees that the product of any two Gaussians is another Gaussian, provides a means to reduce products of many Gaussians to a single Gaussian. By taking advantage of this, one can reduce 3- and 4-centre integrals to finite sums of two centre integrals, and then again to finite sums of one-centre integrals and thus reduce the computation associated with integration by several orders of magnitude. [7] Gaussian-type orbitals (GTOs) take the analytic form,

$$\chi^{\mathrm{GTO}}_{\alpha_{nl}lm}(r,\theta,\phi) = R_{\alpha_{nl}lm}(r)Y_{lm}(\theta,\phi) \tag{2.30}$$

$$R_{\alpha_{nl}lm}(r) = \frac{2(2\alpha_{nl})^{\frac{3}{4}}}{\pi^{\frac{1}{4}}}\sqrt{\frac{2^l}{(2l+1)!!}}(\sqrt{2\alpha_{nl}}r)^l \exp(-\alpha_{nl}r^2), \tag{2.31}$$

where the exponent is here denoted α. Either of the function definitions in equation 2.28 or 2.30 could be used to form a complete basis. The lack of a cusp at $r = 0$ in the Gaussian-type orbitals is concerning; however they are so computationally efficient one can include many Gaussians where it might only be possible to include a few Slater-type orbitals. To take advantage of this, Pople and co-workers created the STO-KG basis sets, which include K functions which are fitted by the least squares method to the Slater-type orbitals. One can achieve in this way arbitrary accuracy in the fit by simply including more GTOs, as seen in figures 2.3 and 2.4.

The linear combination of Gaussians which gave the green and red orbitals in figures 2.3 and 2.4 need only be optimised once, then the coefficients and exponents stored. In this way one can avoid the duplication of effort by using contracted basis sets made up of *contracted* Gaussians (such as the STO-KG basis sets), rather than *primitive* Gaussians. Contracted Gaussians take the form

$$\chi^{\mathrm{CGTO}}_{\mu} = \sum_{p} d_{p\mu}\chi^{\mathrm{PGTO}}_{p}, \tag{2.32}$$

where $d_{p\mu}$ is the coefficient of the p^{th} primitive Gaussian in the expansion of the μ^{th} contracted Gaussian. Optimizing exponents and coefficients for GTOs is a complex problem with many solutions, and thus must be re-performed for as many systems as there are elements in the periodic table. One way in which this optimisation is simplified is to place a constraint upon the ratio between exponents within the same

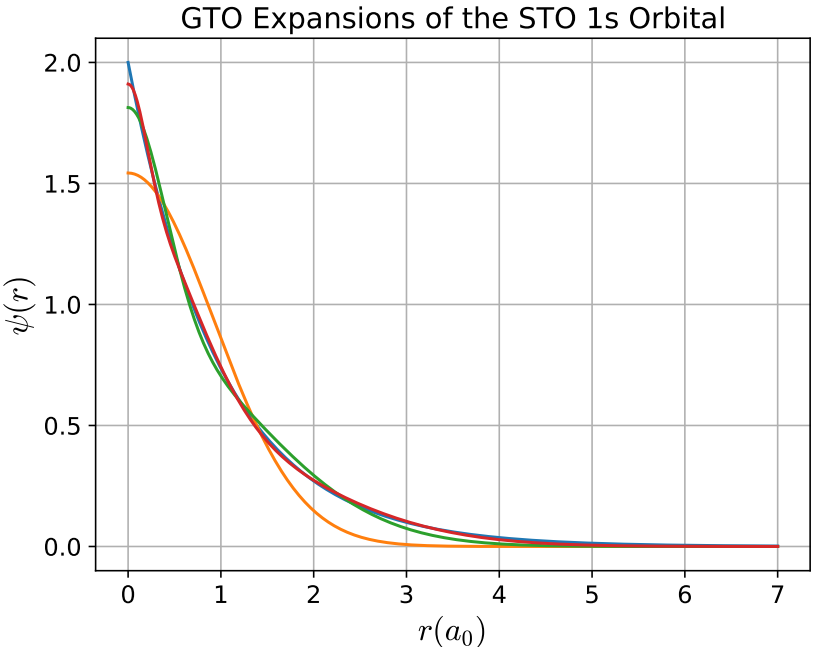

Figure 2.3: Expansion of the hydrogen STO 1s (blue line) function in GTOs, generated using a least squares approach. Shown are the GTO expansions using a single GTO (orange line), two GTOs (green line) and three GTOs (red line).

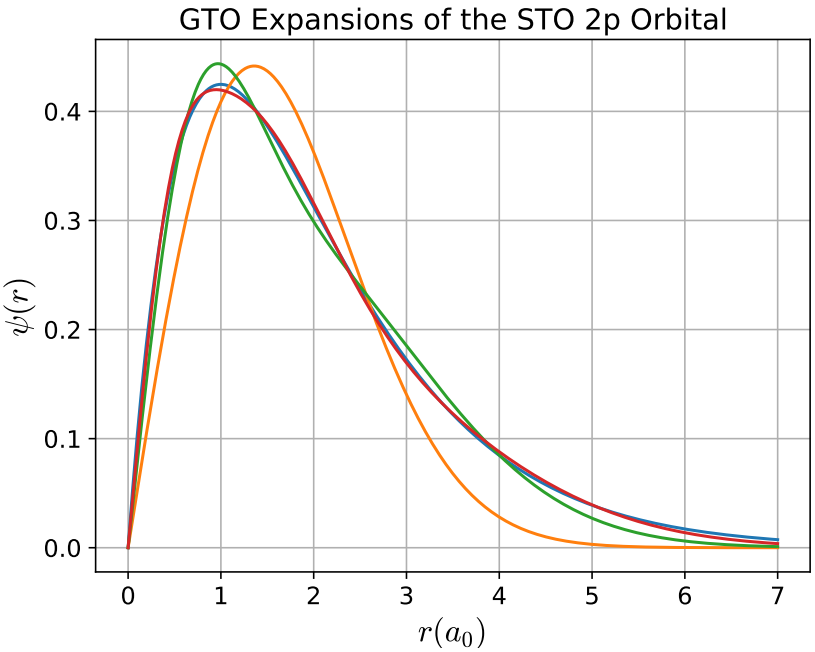

Figure 2.4: Expansion of the hydrogen STO 2p (blue line) function in GTOs, generated using a least squares approach. Shown are the GTO expansions using a single GTO (orange line), two GTOs (green line) and three GTOs (red line).

shell, requiring that the exponent in each term of the expansion have a predefined ratio with the exponent in the previous term. Basis sets generated in this way are referred to as *even-tempered* basis sets, named so after the evenly spaced peaks of their constituent Gaussians. [7,11–14] Expansions of the basis functions defined in this way form a good starting point for moving towards the HF limit in a controlled manner, as opposed to beginning arbitrarily. [7]

It was made clear at the outset that this thesis is concerned with solving the electronic problem for *molecules*. So far the discussion has been limited to atoms, and much has been made of the deficiency of GTOs in comparison with STOs. When one makes the move to modelling systems containing multiple nuclei (particularly those with different atomic numbers), atomic symmetry is destroyed and consequently there is a need for polarization functions to appear in the basis set. One has available two approaches to including polarization functions: functions positioned away from nuclear centres, or the inclusion of more atom-centred functions. The variational optimisation of positions of GTOs away from nuclear centres is numerically and computationally difficult, and so is rarely done. Moreover, the inclusion of basis functions only at nuclear positions allows one to compare the sizes of basis sets in a consistent way. The terminology usually used for basis sets containing the minimum possible number of functions is a minimal basis. For carbon, a minimal basis would simply contain a total of five basis functions; two s-type functions and three p-type functions. If one then includes two basis functions for each atomic orbital and has a total of ten basis functions: four s-type functions and six p-type functions, one has a strictly "double-zeta" basis. A triple-zeta basis contains three basis functions for each atomic orbital, and so on. In the description of molecules it is common to employ split-valence basis sets, in which a smaller number of basis functions are included for core orbitals than are included for valence orbitals. In the description of molecules, it is also necessary to provide enough flexibility to the wavefunction that it is able to distort in the presence of any nearby charge distribution. This is usually achieved by the inclusion of polarisation functions in the form of basis functions of higher l. For instance, an s-orbital is able to shift its position and shape by mixing with p-orbitals, and p-orbitals by mixing with d-orbitals, and so on. Thus, one introduces to a basis set functions of

$l_{\max} + 1$ angular momentum, where $l_{\max}$ is the largest l of the valence orbitals of the atom. For instance, to introduce polarisation functions to a carbon nucleus, one expands the basis to include functions for which $l = 2$.

2.5 Hartree-Fock Theory

The Hartree-Fock (HF) method is concerned with the clamped-nucleus, mean-field treatment of the electrons in a system. The wavefunction is approximated by a single SD. As such, using the results presented in section 2.3, one can write the energy expression for a single SD as

$$E = \sum_{i}^{N} \langle \psi_i | \, \hat{h} \, | \psi_i \rangle + \frac{1}{2} \sum_{i,j}^{N} \left[\langle \psi_i \psi_j | \, \frac{1}{r_{ij}} \, | \psi_i \psi_j \rangle - \langle \psi_i \psi_j | \, \frac{1}{r_{ij}} \, | \psi_j \psi_i \rangle \right] + E_{\text{nuc}}. \quad (2.33)$$

Self-interaction of the electrons is not present, *i.e*, the second term in the energy equation is zero when $i = j$. The factor of a half is to prevent double counting. The first term is a sum over one-electron contributions,

$$\langle \psi_i | \, \hat{h} \, | \psi_i \rangle = -\frac{1}{2} \langle \psi_i | \, \nabla_1^2 \, | \psi_i \rangle - \sum_{I=1}^{M} \langle \psi_i | \, \frac{Z_I}{|\vec{r}_1 - \vec{R}_I|} \, | \psi_i \rangle \,, \quad (2.34)$$

each term of which is the energy arising from an electron in orbital i interacting with M nuclei independent of the other electrons in the system. The quantity in square brackets in equation 2.33 - the two electron terms - describe the inter-electron interactions. The first term in the square brackets is the coulomb term, and is the classical repulsive interaction between two charge distributions. The second term is a consequence of the antisymmetry of the wavefunction and is known as the exchange interaction energy and has no simple classical interpretation.

2.5.1 Closed-Shell Hartree-Fock Theory

In the case that one has a molecular wavefunction of singlet spin and all orbitals are doubly occupied (*i.e*, two spin orbitals have identical spatial parts and orthogonal

spin parts), one can integrate out the spin functions in 2.33 according to,

$$\langle\alpha(\omega)|\alpha(\omega)\rangle = \langle\beta(\omega)|\beta(\omega)\rangle = 1, \tag{2.35}$$

$$\langle\alpha(\omega)|\beta(\omega)\rangle = \langle\beta(\omega)|\alpha(\omega)\rangle = 0, \tag{2.36}$$

and thus obtain the energy expression containing only the spatial parts of the orbitals defined in equation 2.10,

$$E = 2\sum_{i}^{N} \langle\psi_i|\,\hat{h}\,|\psi_i\rangle + \sum_{i,j}^{N}\left[2\,\langle\psi_i\psi_j|\,\frac{1}{r_{12}}\,|\psi_i\psi_j\rangle - \langle\psi_i\psi_j|\,\frac{1}{r_{12}}\,|\psi_j\psi_i\rangle\right] + E_{\text{nuc}}. \tag{2.37}$$

It is then straightforward to obtain an expression for the closed-shell energy within the LCAO picture of MO theory by substituting equation 2.25 into equation 2.37 to obtain,

$$E = 2\sum_{\alpha,\beta}\sum_{i} C_{\alpha i}C_{\beta_i}\left\{h_{\alpha\beta} + \frac{1}{2}\sum_{\gamma,\delta} 2\sum_{j}^{N} C_{\gamma j}C_{\delta j}\left[\langle\alpha\gamma|\beta\delta\rangle - \frac{1}{2}\langle\alpha\gamma|\delta\beta\rangle\right]\right\} + E_{\text{nuc}} \tag{2.38}$$

$$= \sum_{\alpha,\beta} D_{\alpha\beta}\left\{h_{\alpha\beta} + \frac{1}{2}\sum_{\gamma,\delta} D_{\gamma\delta}\left[\langle\alpha\gamma|\beta\delta\rangle - \frac{1}{2}\langle\alpha\gamma|\delta\beta\rangle\right]\right\} + E_{\text{nuc}} \tag{2.39}$$

$$= \sum_{\alpha,\beta} D_{\alpha\beta}\left\{h_{\alpha\beta} + \frac{1}{2}\Gamma_{\alpha\beta}\right\} + E_{\text{nuc}}. \tag{2.40}$$

where the abbreviation $\langle\chi_\alpha\chi_\gamma|\chi_\beta\chi_\delta\rangle = \langle\alpha\gamma|\beta\delta\rangle$ has been introduced for integrals over basis functions, and

$$D_{\alpha\beta} = 2\sum_{i}^{N} C_{\alpha i}C_{\beta i}, \tag{2.41}$$

$$\Gamma_{\alpha\beta} = \sum_{\gamma,\delta} D_{\gamma\delta}\left[\langle\alpha\gamma|\beta\delta\rangle - \frac{1}{2}\langle\alpha\gamma|\delta\beta\rangle\right]. \tag{2.42}$$

$\mathbf{D}$ is the *density matrix* in the atomic orbital basis, and $\mathbf{\Gamma}$ is the two-electron matrix, which has a parametric dependence on $\mathbf{D}$. One can now write a compact

expression for the HF energy in matrix form,

$$E = \mathrm{tr}\left[\mathbf{D}\cdot\left(\mathbf{h}+\frac{1}{2}\mathbf{\Gamma}\right)\right] + E_{\mathrm{nuc}}. \tag{2.43}$$

Thus during any calculation of E one need only calculate the one-electron integrals in the AO basis once. Thereafter, they are stored and transformed according to the equations above to give the energy of any SD defined in the current basis.

2.5.2 Variational Conditions

The HF method provides an upper bound on the exact energy, so we can vary the MO coefficients as we wish in order to minimize the energy and thus obtain the best approximation to the energy within the space spanned by the chosen basis. It is customary to also demand the orbitals be orthonormal with respect to the atomic orbital overlap matrix,

$$S_{\alpha\beta} = \langle\alpha|\beta\rangle = \int d\vec{x}_1 \quad \chi^*_\alpha(\vec{x}_1)\chi_\beta(\vec{x}_1). \tag{2.44}$$

That is,

$$\mathbf{C}^\dagger\mathbf{S}\mathbf{C} = \mathbf{1}. \tag{2.45}$$

There are several ways one can solve this problem. One could start with orthonormal orbitals and rotate them together, thus retaining their orthonormality and allowing an unconstrained optimisation of elements of the rotation generator. Another method might be to define a Lagrangian, L, and perform an unconstrained optimisation. The latter is the way this is usually presented, and so will be briefly shown here and the former will be used extensively in later chapters for a different problem.

Consider the function

$$L = E - 2\sum_{i,j}\epsilon_{ij}([\mathbf{C}^\dagger\mathbf{S}\mathbf{C}]_{ij} - \delta_{ij}) = E - g. \tag{2.46}$$

We wish to find the MO coefficients for which

$$\frac{\partial L}{\partial C_{\alpha i}} = 0 \quad \forall \quad \alpha, i. \tag{2.47}$$

One obtains for the derivatives of the energy with respect to the MO coefficients and AO density matrix elements,

$$\frac{\partial E}{\partial C_{\alpha i}} = \sum_{\gamma\delta} \left(\frac{\partial E}{\partial D_{\gamma\delta}} \right) \left(\frac{\partial D_{\gamma\delta}}{\partial C_{\alpha i}} \right), \tag{2.48}$$

$$\frac{\partial E}{\partial D_{\gamma\delta}} = h_{\gamma\delta} + G_{\gamma\delta} = F_{\gamma\delta} \tag{2.49}$$

respectively. $\mathbf{F}$ is the *Fock matrix*. The derivative of the density with respect to the MO coefficients is

$$\frac{\partial D_{\gamma\delta}}{\partial C_{\alpha i}} = 2[\delta_{\gamma\alpha} C_{\delta i} + \delta_{\delta\alpha} C_{\gamma i}]. \tag{2.50}$$

Now differentiating the constraint, g,

$$\frac{\partial g}{\partial C_{\alpha i}} = 4 \sum_j [\mathbf{SC}]_{\alpha j} \epsilon_{ij} = 4[\mathbf{SC}\epsilon]_{\alpha i}. \tag{2.51}$$

Then, writing the derivative of the Lagrangian out in full, assuming we have found a stationary point, one has

$$\frac{\partial L}{\partial C_{\alpha i}} = 4[\mathbf{FC} - \mathbf{SC}\epsilon]_{\alpha i} = 0. \tag{2.52}$$

And thus the *Hartree-Fock-Roothaan equations* are obtained,

$$\mathbf{FC} = \mathbf{SC}\epsilon. \tag{2.53}$$

In order to find the undetermined multipliers, ϵ_{ij}, one multiplies on the left with $\mathbf{C}^\dagger$. The density matrix in HF, given by equation 2.41 is invariant to unitary transformations, and depends only on the occupied orbitals. This is easily shown, by inserting $\mathbf{C}' = \mathbf{CU}$ into the equation for the density matrix,

$$\mathbf{D}' = 2\mathbf{CUU}^\dagger\mathbf{C} = 2\mathbf{C1C}^\dagger = \mathbf{D}. \tag{2.54}$$

Thus the Fock operator is also invariant to unitary transformations of the occupied orbitals. This allows us to choose $\mathbf{U}$ such that ϵ is diagonal. The diagonal elements of ϵ are then defined as the "orbital energies" of the molecular system of interest.

Having spoken only about optimising the occupied molecular orbitals, we have neglected a famous feature of the Hartree-Fock-Roothaan equations, and that is that they can be extended to include the virtual orbitals, and consequently become self consistent after a sufficient number of iterations. That is, if one calculates the Fock matrix (using a density calculated with only the occupied orbitals), then diagonalises in the full orbital space, the mixing between the occupied and virtual orbitals changes the energy, the occupied orbitals, and the density. Repeatedly performing this procedure leads to a solution for which the Fock operator in the MO basis is diagonal, in both the occupied and virtual blocks. At this point, the orbitals stop changing (there is no longer any mixing between spaces), and self consistency is achieved.

An alternative way to do this is to transform the Fock matrix (AO basis) into the symmetrically orthogonalised AO basis, by multiplying by $\mathbf{S}^{-\frac{1}{2}}$. That is,

$$\bar{\mathbf{F}} = \mathbf{S}^{-\frac{1}{2}}\mathbf{F}\mathbf{S}^{-\frac{1}{2}}, \tag{2.55}$$

$$\mathbf{C} = \mathbf{S}^{-\frac{1}{2}}\bar{\mathbf{C}}. \tag{2.56}$$

Substituting into equation 2.53, we then have an eigenvalue problem,

$$\bar{\mathbf{F}}\bar{\mathbf{C}} = \bar{\mathbf{C}}\bar{\epsilon}. \tag{2.57}$$

Diagonalisation of $\bar{\mathbf{F}}$ yields $\bar{\mathbf{C}}$ from which one obtains the next $\mathbf{C}$ though the back-transformation of the MO coefficients in the orthogonalised AO basis, *i.e,* using equation 2.56.

2.5.3 Open-Shell Hartree-Fock

So far, we have assumed that for a system containing N electrons, of which N_α are of α spin and N_β are of β spin, that $N_\alpha = N_\beta$. This is not always true in reality and so it is important to also consider open-shell systems wherein one or

more spatial orbitals contain only one electron. One usually refers to these states by quantum number $S = 0, 1/2, 1, 3/2, \ldots$, or as singlet, doublet, triplet or quartet states, respectively. It is easy to see from the integration of the spin functions that if we wish to describe these states with a single Slater determinant, all of the open-shell orbitals must contain electrons of the same spin. This is an artefact of the two electron terms in the energy expression vanishing where the electrons are of opposite spins.

Now consider the case that $N_\alpha > N_\beta$. One can either treat the system in an analogous way to that described in section 2.5.1 - that is, to require α and β spin electrons to occupy identical spatial orbitals - or one can lift this restriction and optimise the spatial functions for individual electrons, rather than pairs. The former case is known as the *restricted Hartree-Fock* method (RHF), and the latter is known as the *unrestricted Hartree-Fock* method (UHF).

The UHF method will not be treated in detail here, as it is not of much interest in this work, and the results obtained are similar to those presented in section 2.5.1. The difference is simply that where one has a single quantity in RHF, one has two quantities in UHF. The coupled equations are obtained,

$$\mathbf{F}^\alpha \mathbf{C}^\alpha = \mathbf{S}\mathbf{C}^\alpha \epsilon^\alpha, \tag{2.58}$$

$$\mathbf{F}^\beta \mathbf{C}^\beta = \mathbf{S}\mathbf{C}^\beta \epsilon^\beta, \tag{2.59}$$

which must be solved simultaneously. [3] It is worth noting that the RHF equations are a special case of the UHF equations. Thus, solutions to the RHF problem represent a subset of the set of solutions to the UHF problem.

2.5.4 Deficiencies of the Hartree-Fock Method

While the HF method can provide reasonable and qualitatively useful results for systems which can be described by a single determinant (for instance some equilibrium geometries of closed shell systems), there are some glaring issues and it cannot be relied upon for all cases. The particular weaknesses of the HF method are the modelling of bond dissociation, and the capture of electron correlation effects; the former is hostage to the latter, both are discussed together here.

In the homolytic cleavage of a chemical bond, one begins with a singlet wavefunction, and must retain that singlet wavefunction as the nuclei are pulled away from one another. Consider the H_2 molecule. [15] One can write the wavefunction for this system in terms of the hydrogen 1s orbitals centered at H_A and H_B. That is,

$$\Psi = \frac{1}{\sqrt{2}}\left[||\mathrm{s}_A^\alpha(1)\mathrm{s}_B^\beta(2)|| - ||\mathrm{s}_A^\beta(1)\mathrm{s}_B^\alpha(2)||\right]. \tag{2.60}$$

The above features *two* SDs. In HF theory we have only one SD. From basic MO theory we know that the in-phase and out-of-phase combinations of the atomic orbitals gives the molecular bonding and anti-bonding orbitals,

$$\sigma_g = \frac{1}{\sqrt{2(1+s)}}[\mathrm{s}_A + \mathrm{s}_B], \tag{2.61}$$

$$\sigma_u = \frac{1}{\sqrt{2(1-s)}}[\mathrm{s}_A - \mathrm{s}_B], \tag{2.62}$$

where s is the overlap between the two s functions, which tends to zero as internuclear distance increases. One can then write the atomic orbitals in terms of these molecular orbitals,

$$\mathrm{s}_A = \frac{1}{\sqrt{2}}(\sigma_g + \sigma_u), \tag{2.63}$$

$$\mathrm{s}_B = \frac{1}{\sqrt{2}}(\sigma_g - \sigma_u), \tag{2.64}$$

thus obtaining the correct, singlet wavefunction for H_2 in the molecular orbital basis,

$$\Psi = \frac{1}{\sqrt{2}}\left[||\sigma_g^\alpha(1)\sigma_g^\beta(2)|| - ||\sigma_u^\alpha(1)\sigma_u^\beta(2)||\right]. \tag{2.65}$$

The RHF determinant is just the first term in this expansion,

$$\Psi_{\mathrm{RHF}} = ||\sigma_g^\alpha(1)\sigma_g^\beta(2)||, \tag{2.66}$$

$$= \frac{1}{2}\left[||\mathrm{s}_A^\alpha(1)\mathrm{s}_A^\beta(2)|| + ||\mathrm{s}_B^\alpha(1)\mathrm{s}_B^\beta(2)|| + ||\mathrm{s}_A^\alpha(1)\mathrm{s}_B^\beta(2)|| + ||\mathrm{s}_B^\alpha(1)\mathrm{s}_A^\beta(2)||\right], \tag{2.67}$$

and represents a mixture of the correct wavefunction, and two degenerate ionic states (last two terms and first two terms in square brackets, respectively). This

leads to the dissociation curve having ionic character - the electrons have a 50% chance of being at *both* atoms, and 50% chance of both being on the *same* atom. In the UHF treatment, the symmetry of the wavefunction is broken, and is actually a mixture of triplet and singlet states, but given the degeneracy of the states, the lineshape of the dissociation curve is correct, albeit for the wrong reasons. [3] These results are shown in figure 2.5.

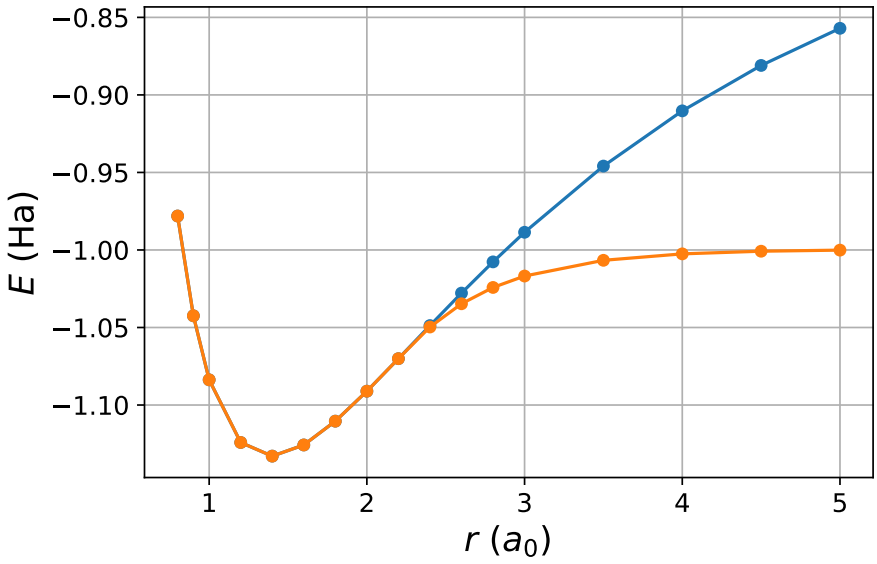

Figure 2.5: Energy of H_2 with internuclear distance r, calculated using RHF (blue line) and UHF (orange line) in the cc-pVTZ basis.

It is obvious from equation 2.65, that the correct wavefunction is a 50:50 mixing of *two* Slater determinants. The energy arising from degenerate states such as these is known as the *static correlation* energy. Static correlation is responsible for returning the appropriate spin symmetry of the asymptotic wavefunction and cannot be captured by a single SD by definition.

Dynamic correlation, which is associated with satisfying the electronic cusp condition (equation 2.26), would do nothing to address the dissociation of the bond, and thus a distinction is drawn between the two types. Dynamic correlation is partly captured by the HF method, as two electrons of parallel spins cannot occupy the same point in space, however, electrons of opposite spins can. This is unphysical and steps can be taken to account for this, as outlined in the following sections.

2.6 Configuration Interaction

In full CI (FCI) theory, the electronic wavefunction is written as an expansion of all configurations formed by exciting electrons from some reference wavefunction. Where one is concerned with a closed shell system, the RHF wavefunction makes a good reference from which one then constructs all singly, doubly, triply, *etc* excited configurations and forms a linear combination of these determinants,

$$|\Psi_{FCI}\rangle = c_0 |\Psi_0\rangle + \sum_{i,a} c_i^a |\Psi_i^a\rangle + \sum_{i<j} \sum_{a<b} c_{ij}^{ab} |\Psi_{ij}^{ab}\rangle + \sum_{i<j<k} \sum_{a<b<c} c_{ijk}^{abc} |\Psi_{ijk}^{abc}\rangle + \cdots , \tag{2.68}$$

where the quantities $\{\Psi\}$ are as defined in section 2.3. While there are computational advantages to using SDs (as above), one could opt to use configuration state functions (CSFs) which are spin adapted linear combinations of SDs, are eigenfunctions of $\hat{S}^2$ and explicitly retain the spin multiplicity of the total wavefunction. [7, 16] In terms of the problem at hand (obtaining the parameters $C_0, c_i^a, c_{ij}^{ab}, c_{ijk}^{abc}, \ldots$), the manner in which one writes the wavefunction makes little difference.

Writing the FCI wavefunction in a more general form,

$$|\Psi_0\rangle = \sum_m c_m |\Psi_m\rangle \tag{2.69}$$

where m runs over all SDs (or CSFs), one can minimise the expectation value of the energy, E, with respect to the expansion coefficients c_m, and this does not modify the orbital coefficients. In matrix notation, this is

$$\mathbf{Hc} = E\mathbf{Sc}, \tag{2.70}$$

where $\mathbf{c}$ is a vector containing the expansion coefficients, c_m. Given the results in section 2.1, we know that matrix $\mathbf{H}$ is sparse. As one can imagine from the discussion of the bonding in H_2 in section 2.5.4, a wavefunction generated in this way includes all correlation effects, and gives the correct form of the wavefunction at all points - the FCI wavefunction (if one had a complete basis set) is the exact solution to the clamped-nucleus non-relativistic Schrödinger equation.

This problem is computationally unwieldy, with **H** being difficult to diagonalise numerically, and the number of generated SDs being so large they become impossible to store. Various methods have been developed for tackling this issue, perhaps the most famous is the direct CI method developed by Roos. [17]

To further reduce the cost of CI methods, one can make a decision about the level of excitations to include in the expansion 2.68. For example in the CISD method, one stops at the third term in the expansion. Doing this requires making a sacrifice - the method is no longer *size extensive*. Size extensivity is a property of a wavefunction which states that the wavefunction of two coexisting, non-interacting systems is the same as the product of the wavefunctions for the two systems where they do not coexist. Consider, for example CID (double excitations only) for $2H_2$, where the distance between the molecules is infinite. By definition our wavefunction consists of the ground state wavefunction and double excitations. The wavefunction for H_2 consists of the ground state and double excitations. The product of two H_2 wavefunctions infinitely separated consists of double and quadruple excitations, and thus is not the same as the wavefunction where the molecules coexist.

Where one has a reference wavefunction of the form of equation 2.69, one can construct excitations from the set of configurations $\{|\Psi_m\rangle\}$. This is known as the *multi-reference* configuration interaction method. One simply has the job of generating those $|\Psi_m\rangle$ which are most important for the region of the potential energy surface (PES) of interest.

2.7 Multiconfigurational SCF Theory

Multiconfigurational Self-Consistent Field (MCSCF) theory is essentially a hybrid HF-CI method, or a HF method for a linear combination of SDs rather than a single SD. [7, 16] That is, in standard configuration interaction (CI) methods one optimises only the CI coefficients whereas in MCSCF one optimises both the CI coefficients, and the molecular orbital coefficients. By the appropriate selection of determinants to include in the expansion, one can describe very well chemical features, and degenerate states.

The exponential generator of orbital rotations mentioned in section 2.5.2 is now

applied to equation 2.69 to give

$$|\Psi_0(\theta, \mathbf{C})\rangle = \exp(-\theta) \sum_m c_m |\Psi_m\rangle , \tag{2.71}$$

where $\theta^\dagger = -\theta$. The energy of this wavefunction,

$$E = \min_{\theta, \mathbf{C}} \frac{\langle \Psi_0(\theta, \mathbf{C})| \hat{H} |\Psi_0(\theta, \mathbf{C})\rangle}{\langle \Psi_0(\theta, \mathbf{C})|\Psi_0(\theta, \mathbf{C})\rangle}, \tag{2.72}$$

is of course invariant to the rotations if the expansion forms a complete set. That is, if one chooses all excited configurations and performs FCI.

In terms of the applications to chemical problems, MCSCF is a powerful tool in the prediction of bond dissociation energies, as one can be sure that the wavefunction has the right symmetry and the problems encountered in section 2.5.4 are not met again. Moreover, by choosing states which are degenerate and including them in the expansion (equation 2.69) one can capture reliably the static correlation. Of course, the dynamic correlation captured in these methods depends on the size of the space one explores in the second expansion of the wavefunction.

2.7.1 Complete Active Space Self-Consistent-Field Theory

Complete active space SCF theory (CASSCF) is simply a regime by which one can choose the determinants included in the initial expansion by generating excited states from a single reference wavefunction. It is done by dividing the full orbital space into three subspaces: the inactive, active and virtual spaces. The inactive space is treated with the usual HF mean-field approach with a single SD and all orbitals are doubly occupied. The active space consists of both occupied and virtual orbitals and is defined by the user, then all excited configurations within this space are used for the expansion of the wavefunction. The virtual space remains unoccupied throughout.

Usually the active space is defined by the user's chemical intuition and how it aligns with the graphical depiction of the orbitals (usually localised by the minimisation of some functional). It is not much of a stretch to imagine how one might choose an active space for a bond dissociation, for example. One hopes to find an

orbital which points along the bond and resembles the LCAO in-phase mixing of MO theory and a virtual which resembles the out-of-phase mixing of MO theory. Performing CI within this space, then, one returns a good representation of the PES in the direction of the nuclear separation of the bonding atoms.

2.8 Coupled Cluster Theory

Coupled cluster (CC) theory involves exponential ansätze where one expands the wavefunction in terms of excitation operators acting upon a reference wavefunction, exciting electrons in singles, pairs, triples, and so on as the power increases in the series. CC has at its disposal a unique feature and one which sets it apart from other electronic structure methods, which is that, in constrast to truncated CI methods, it is size-extensive in all of its flavours. One can truncate the expansion at any point and not suffer the same loss of this feature that FCI does. This arises from the form of the wavefunction,

$$|\Psi_{CC}\rangle = \exp\left(\sum_{i,a} t_i^a \hat{\tau}_i^a + \sum_{i>j}\sum_{a>b} t_{ij}^{ab}\hat{\tau}_{ij}^{ab} + \cdots\right). \tag{2.73}$$

Where the quantities t_i^a and τ_i^a are the weighting of the excitations in the expansion, and the excitation operators, respectively. The excitation operators simply generate the state where orbitals corresponding to the lower indices are replaced by the orbitals corresponding to the upper indices.

Just as in section 2.6, consider two H_2 molecules infinitely separated, and the wavefunction generated by the application of the CCD operator on an RHF reference. The wavefunction for each fragment would include only the ground state and double excitations, and the system wherein the molecules coexist would also be described by a wavefunctions which includes only the ground state and double excitations. One can write a simple example of this and show that the wavefunction is multiplicatively separable. [7, 16]

2.9 Many-Body Perturbation Theory

Perturbation theory rests on the idea that one can take a solution to an ideal problem, and perturb it to make it better suit reality. There is only the requirement that the ideal case is close to the real case. In terms of electronic structure, electron correlation is very small by comparison to the total energy, thus the energy is not dominated by correlation and nor is the wavefunction. Using this method to acquire the correlation energy will be the subject of section 2.9.1. Here, a short introduction to Rayleigh-Schrödinger perturbation theory is given.

One begins by writing the quantities we are interested in as a Taylor series in some parameter, λ,

$$\hat{H}(\lambda) = \hat{H}^{(0)} + \lambda\hat{H}^{(1)} + \lambda^2\hat{H}^{(2)} + \cdots, \tag{2.74}$$

$$\Psi(\lambda) = \Psi^{(0)} + \lambda\Psi^{(1)} + \lambda^2\Psi^{(2)} + \cdots, \tag{2.75}$$

$$E(\lambda) = E^{(0)} + \lambda E^{(1)} + \lambda^2 E^{(2)} + \cdots, \tag{2.76}$$

where

$$\hat{H}^{(k)} = \frac{1}{k!}\frac{\partial^k \hat{H}}{\partial\lambda^k}, \tag{2.77}$$

$$\Psi^{(k)} = \frac{1}{k!}\frac{\partial^k \Psi}{\partial\lambda^k}, \tag{2.78}$$

$$E^{(k)} = \frac{1}{k!}\frac{\partial^k E}{\partial\lambda^k}. \tag{2.79}$$

The power of this method, alongside its application to the theory of intermolecular forces, is in the choice of the parameter λ. One can choose it to represent an external field imparted by a nearby molecule, for instance. Inserting into the Schrödinger equation the expansions in equations 2.74, 2.75 and 2.76 one obtains a sequence of equations of increasing order in λ,

$$[\hat{H}^{(0)} - E^{(0)}]\,|\Psi^{(0)}\rangle = 0, \tag{2.80}$$

$$\lambda[\hat{H}^{(0)} - E^{(0)}]\,|\Psi^{(1)}\rangle + \lambda[\hat{H}^{(1)} - E^{(1)}]\,|\Psi^{(0)}\rangle = 0, \tag{2.81}$$

$$\lambda^2[\hat{H}^{(0)} - E^{(0)}]\,|\Psi^{(2)}\rangle + \lambda^2[\hat{H}^{(1)} - E^{(1)}]\,|\Psi^{(1)}\rangle + \lambda^2[\hat{H}^{(2)} - E^{(2)}]\,|\Psi^{(0)}\rangle = 0. \tag{2.82}$$

In order to ensure unique solutions to the above and avoid the construction of linear combinations of eigenstates with the zeroth order wavefunction, which are just further eigenstates and equally valid solutions, we insist that the wavefunctions $\{\Psi^{(k)} : \forall k > 0\}$ be orthogonal to $\Psi^{(0)}$. Projecting on the left of equations 2.80, 2.81 and 2.82 with $\langle\Psi^{(0)}|$, one obtains the energies corresponding to each order of the perturbation parameter,

$$E^{(0)} = \langle\Psi^{(0)}|\,\hat{H}^{(0)}\,|\Psi^{(0)}\rangle\,, \tag{2.83}$$

$$E^{(1)} = \langle\Psi^{(0)}|\,\hat{H}^{(1)}\,|\Psi^{(0)}\rangle\,, \tag{2.84}$$

$$E^{(2)} = \left[\langle\Psi^{(0)}|\,\hat{H}^{(1)}\,|\Psi^{(1)}\rangle + \langle\Psi^{(0)}|\,\hat{H}^{(2)}\,|\Psi^{(0)}\rangle\right]. \tag{2.85}$$

As a result, one requires only the zeroth and first order wavefunctions to correct the energy up to second order in λ.

2.9.1 Møller-Plesset Perturbation Theory

Møller-Plesset (MP) perturbation theory is concerned with using the framework of section 2.9 in order to approximately capture as much of the correlation energy as possible. [18, 19] The zeroth order wavefunction is just a single SD and the zeroth order Hamiltonian is chosen to be a sum of Fock operators for all electrons and the first order operator is the difference between the exact operator and the fock operator. That is,

$$\hat{H}^{(0)} = \sum_{i}^{N} \hat{f}(i), \tag{2.86}$$

$$\hat{H}^{(1)} = \hat{H} - H^{(0)}. \tag{2.87}$$

These are convenient definitions: the zeroth order wavefunction is the optimised HF determinant, and the zeroth order energy is the sum of the orbital eigenvalues, as discussed in section 2.5, with the difference between the HF energy and the zeroth order energy being that in MP perturbation theory we do not correct for double counting. Rather, this is corrected by the first order Hamiltonian. Thus,

$$\langle\Psi^{(0)}|\,H^{(0)} + H^{(1)}\,|\Psi^{(0)}\rangle = E^{(0)} + E^{(1)} = E_{HF}. \tag{2.88}$$

So to improve upon the HF energy one has to go up to second order, which requires a first order wavefunction as in equation 2.85. The first order wavefunction is a combination of SDs,

$$\Psi^{(1)} = \sum_i \sum_a t_i^a \Psi_i^a + \sum_{j>k} \sum_{b>c} t_{jk}^{bc} \Psi_{jk}^{bc} + \cdots , \tag{2.89}$$

where t are the weighting coefficients in the expansion. To find them, project on the left with all excited determinants, and take advantage of the fact that we are in an eigenbasis of the zeroth order Hamiltonian. This yields

$$t_i^a = -\frac{\langle \Psi_i^a | \hat{H} | \Psi \rangle}{\epsilon_a - \epsilon_i}, \tag{2.90}$$

$$t_{ij}^{ab} = -\frac{\langle \Psi_{ij}^{ab} | \hat{H} | \Psi \rangle}{\epsilon_a + \epsilon_b - \epsilon_j - \epsilon_i}. \tag{2.91}$$

For single excitations this amounts to naught where Brillouin's conditions are satisfied, as the occupied virtual block of the Fock matrix is zero. That is, for all closed shell HF problems, and for all UHF wavefunctions there is no contribution from singly excited determinants. We are also aware from section 2.3 that integrals between determinants differing by more than 2 orbitals vanish, thus only double excitations can contribute to the zeroth order wavefunction and the second order energy (this is true for the third order energy too, but the algebraic manipulation needed to show this is omitted). Moreover, the only terms remaining where determinants differ by two orbitals are the two-electron integrals, thus the amplitude is given by

$$t_{ij}^{ab} = -\frac{\langle \psi_a \psi_b | \psi_i \psi_j \rangle - \langle \psi_a \psi_b | \psi_j \psi_i \rangle}{\epsilon_a + \epsilon_b - \epsilon_i - \epsilon_j}, \tag{2.92}$$

and the second order correction to the energy is

$$E^{(2)} = \sum_{i>j} \sum_{a>b} t_{ij}^{ab} \langle \Psi_{ij}^{ab} | \hat{H} | \Psi_0 \rangle = -\sum_{i>j} \sum_{a>b} \frac{[\langle \psi_a \psi_b | \psi_i \psi_j \rangle - \langle \psi_a \psi_b | \psi_j \psi_i \rangle]^2}{\epsilon_a + \epsilon_b - \epsilon_j - \epsilon_i}. \tag{2.93}$$

Thus the second order correction to the energy arises from the pairwise correlation of the electrons in the system. Higher order terms couple only to excited determinants whose importance diminishes. The physical interpretation of this result is that the pairwise correlations are more important than three-and-higher-body

correlations. An attractive consequence of only considering certain excitations is that the method is size extensive.

The order to which one corrects the energy through this method is written MPX, where X indicates at which order the expansion terminates. Here we have only discussed MP2 but the same framework applies to all higher orders. MP2 is computationally very cheap to perform given that only double excitations need be generated. It is rare in modern electronic structure applications to see higher orders than this. MP2 reliably gives an energy closer to the true energy, whereas increasing the order can sometimes lead to a divergence in the series and unreliable results. MPX can be performed for any reference wavefunction, restricted or otherwise, and will yield an energy which behaves similarly asymptotically. That is, any deficiency in the HF energy of the reference is carried over to the MPX energy. A similar procedure to this can also be carried out for multireference wavefunctions. [7, 16]

2.10 Density Functional Theory

Density functional theory (DFT) is built upon the foundations laid by Hohenberg and Kohn, who proved that the ground-state electronic energy is determined only by the electron density. [20] The features of the density which provide some insight into why this may be true are that the integration over the density is equal to the electron number and that there are cusps at the nuclei (of a height dependent on the atomic number) in the electron density of any system, atomic or molecular. [8]

In orbital-free DFT, there are only ever 3 variables which define the density and thus the energy, however, the accuracy of these methods is very low and they will not be discussed here. Rather, one makes the sacrifice of increasing the number of variables to $3N$ and introduces orbitals to DFT in the form of Kohn-Sham theory. [21] The Kohn-Sham model sits on top of what has already been discussed in section 2.5 - the kinetic, electron-nuclear and coulomb electron-electron terms in the energy being of identical form. The difference in approach comes in the use of natural orbitals (NO) in place of the canonical HF orbitals. The NOs are those orbitals which diagonalise the electron density. The kinetic energy, then, is given

by,

$$T[\rho_{\text{exact}}] = -\frac{1}{2}\sum_i n_i \langle\psi_i| \nabla^2 |\psi_i\rangle . \tag{2.94}$$

Where the ψ_i are natural orbitals, and n_i are the eigenvalues of the density matrix, referred to as the occupation numbers. Where the exact density is not known (it can never be known as we can never have an infinite number of natural orbitals), the n_i are exactly one or zero, as in the case for HF theory. So one can write the approximate density, ρ, as,

$$\rho = \sum_i |\psi_i|^2 \tag{2.95}$$

The use of a single Slater determinant in HF theory, and the use of binary occupation numbers in DFT leaves us with some error in the kinetic energy, which arises from the assumption that each electron is moving independently of the rest. In DFT, a term exists which soaks up "the rest" of any omitted interactions. Since this missing energy arises only from the independent treatment of the electrons, it is called the *exchange-correlation* term, $E_{\text{xc}}[\rho]$. By contrast, the electron-nuclear interaction is truly an independent particle term and so if one wishes to return the exact energy using DFT, the form of the exchange correlation term must be,

$$E_{\text{xc}}[\rho] = T[\rho] - T_{\text{HF}} + V_{ee}[\rho] - J[\rho]. \tag{2.96}$$

And thus the form of the density functional be,

$$E[\rho] = T[\rho] + V_{Ne} + J[\rho] + E_{\text{xc}}[\rho]. \tag{2.97}$$

The art in DFT is the design of the exchange-correlation functional. There are so many DFT functionals in existence one could not hope to keep up with them all. Each one is tuned according to some regime, some according to physics, others according to large data sets. [21–24] The design of density functionals is beyond the scope of this discussion. It suffices to say that the vast majority of the kinetic energy of the electrons comes in the same form as in HF theory, and that in the Kohn-Sham formulation of DFT, one has an orbital-based, independent electron model.

Chapter 3

Numerical Optimisation Methods

Much of this thesis is concerned with the minimisation of functionals. This chapter provides a short mathematical background, and motivation for certain approximations and methods. It is by no means a complete review of numerical optimisation methods, but is pertinent given the content of chapters 5 and 7.

3.1 Useful Results and Definitions

It is usual to assume the objective function $f(\mathbf{x})$ which is to be minimised is smooth, continuous and continuously differentiable ($\mathbb{C}_1$), so one can then define the gradient vector,

$$\nabla f = \begin{bmatrix} \frac{\partial f}{\partial x_1} \\ \frac{\partial f}{\partial x_2} \\ \vdots \\ \frac{\partial f}{\partial x_n} \end{bmatrix}. \tag{3.1}$$

For our purposes, we shall also assume $\mathbf{x}$ contains only real values. In the case the function is twice continuously differentiable ($\mathbb{C}_2$), one can also define the Hessian matrix,

$$\mathbf{G} = \nabla^2 f = \begin{bmatrix} \frac{\partial^2 f}{\partial x^2} & \frac{\partial^2 f}{\partial x_1 x_2} & \cdots & \frac{\partial^2 f}{\partial x_1 x_n} \\ \frac{\partial^2 f}{\partial x_2 x_1} & \frac{\partial^2 f}{\partial x_2^2} & \cdots & \frac{\partial^2 f}{\partial x_2 x_n} \\ \vdots & \vdots & \ddots & \vdots \\ \frac{\partial^2 f}{\partial x_n x_1} & \frac{\partial^2 f}{\partial x_n x_2} & \cdots & \frac{\partial^2 f}{\partial x_n x_n} \end{bmatrix}. \tag{3.2}$$

All functionals encountered in this thesis are $\mathbb{C}_2$ or higher. Given these expressions, it is possible to calculate the gradient and second derivative of the function $f(\mathbf{x})$ along any line,

$$\mathbf{x}(=\mathbf{x}(\alpha)) = \mathbf{x}' + \alpha\mathbf{s} \quad \forall\alpha. \tag{3.3}$$

$\mathbf{x}'$ is a point along the line, α is the distance between $\mathbf{x}$ and $\mathbf{x}'$ if the direction vector, $\mathbf{s}$, is normalised. The measure most commonly used for this normalisation is the L_2 norm. That is that $||\mathbf{s}||_2 = \sqrt{\mathbf{s}^\dagger\mathbf{s}} = 1$. [25]

The slope along the line is given by

$$\frac{\mathrm{d}f}{\mathrm{d}\alpha} = \mathbf{s}^\dagger\nabla f = (\nabla f)^\dagger\mathbf{s}. \tag{3.4}$$

And the curvature along the line, by

$$\frac{\mathrm{d}^2 f}{\mathrm{d}\alpha^2} = \mathbf{s}^\dagger\nabla((\nabla f)^\dagger\mathbf{s}) = \mathbf{s}^\dagger\nabla^2 f\mathbf{s}. \tag{3.5}$$

Let us consider the quadratic function,

$$q(\mathbf{x}) = \frac{1}{2}\mathbf{x}^\dagger\mathbf{G}\mathbf{x} + \mathbf{b}^\dagger\mathbf{x} + c, \tag{3.6}$$

which when differentiated using the product rule ($\nabla(\mathbf{u}^\dagger\mathbf{v}) = (\nabla\mathbf{u}^\dagger)\mathbf{v} + (\nabla\mathbf{v}^\dagger)\mathbf{u}$) yields the gradient vector

$$\nabla q(\mathbf{x}) = \frac{1}{2}(\mathbf{G} + \mathbf{G}^\dagger)\mathbf{x} + \mathbf{b} = \mathbf{G}\mathbf{x} + \mathbf{b} \tag{3.7}$$

from the symmetry of $\mathbf{G}$, and thence the Hessian

$$\nabla^2 q(\mathbf{x}) = \mathbf{G}. \tag{3.8}$$

An interesting consequence of equation 3.7 is that differences in position are mapped to differences in gradient by the Hessian. That is, if one has points $\mathbf{x}$ and $\mathbf{x}'$, one can find the associated gradients, $\mathbf{g}$ and $\mathbf{g}'$, according to

$$\mathbf{g} - \mathbf{g}' = \mathbf{G}(\mathbf{x} - \mathbf{x}'). \tag{3.9}$$

Equations 3.7 and 3.8 are enough to fully characterise any stationary point defined by equation 3.6. We are interested in solving the minimisation problem,

$$\min_{\mathbf{x}} f(\mathbf{x}), \quad \mathbf{x} \in \mathbb{R}. \tag{3.10}$$

But it is worth mentioning that everything discussed here can be used to find maxima through a simple transformation of the objective function,

$$\max_{\mathbf{x}} f(\mathbf{x}) = -\min_{\mathbf{x}} -f(\mathbf{x}). \tag{3.11}$$

Usually one operates under the assumption that the minimiser (the location of a minimum in $f(\mathbf{x})$), $\mathbf{x}^*$, exists and is unique, though neither of these assumptions always holds.

The criteria for what constitutes a minimum are divided into two sets; the *necessary* conditions and the *sufficient* conditions. [25] The necessary conditions arise from the observation that any line $\mathbf{x}(\alpha)$ passing through $\mathbf{x}^*$ must have zero slope and non-negative curvature at $\mathbf{x}^*$. That is,

$$\mathbf{g}^* = 0, \tag{3.12}$$

$$\mathbf{s}^\dagger \mathbf{G} \mathbf{s} \geq 0. \tag{3.13}$$

The possibility of zero in the second equation is perhaps surprising at first glance, but arises as the line passing through $\mathbf{x}^*$ from which the implication is drawn cannot completely characterise the point. Rather, one combines the necessary conditions with the sufficient conditions, which imply that the point $\mathbf{x}^*$ is a minimum. The first is identical to equation 3.12, the second is that $\mathbf{G}^*$ is a positive semi-definite matrix. [25]

The eigenvalues of a Hessian matrix give information about the function along the corresponding eigenvectors. Where all eigenvalues are positive, the function increases in all directions, and one is at a minimum. Where all of the eigenvalues are negative, the function decreases in all directions, and one is at a maximum. If one eigenvalue is negative and the rest positive, and the gradient is zero then one has arrived at a saddle point, and the function decreases in one direction and

increases in the rest.

In the design of a numerical optimisation method one must make a choice of both the model used to approximate the objective function (usually a quadratic model), and some algorithm which chooses the length of the step in the direction chosen, such as a trust-region, restricted-step or line search model. In this discussion we will limit ourselves to a quadratic model with a line search.

A line search method is a procedure by which one walks along the objective function in some pre-computed descent direction, then chooses the step size to be the distance from the current point to the minimum along that walk.

3.2 Newton's Method

Newton's method is a simple way of employing a quadratic model. One performs a Taylor expansion of the objective function about $\mathbf{x}^{(n)}$ and truncates at second order,

$$f(\mathbf{x}^{(n)} + \delta) \approx q^{(n)}(\delta) = f^{(n)} + \mathbf{g}^{(n)\dagger}\delta + \frac{1}{2}\delta^{\dagger}\mathbf{G}^{(n)}\delta. \tag{3.14}$$

Where $\delta = \mathbf{x} - \mathbf{x}^{(n)}$. Then we take $\mathbf{x}^{(n+1)} = \mathbf{x}^{(n)} + \delta^{(n)}$ where $\delta^{(n)}$ minimises the model function. That is, the update in position is given uniquely by $\nabla q^{(n)}(\delta^{(n)}) = 0$. Taking the derivative of equation 3.14, rearranging and multiplying on the left by $\mathbf{G}^{(n)^{-1}}$, we obtain

$$\delta^{(n)} = -\mathbf{G}^{(n)^{-1}}\mathbf{g}^{(n)}. \tag{3.15}$$

There is, of course, no guarantee that the point on the objective function will behave similarly enough to a quadratic that this method yields a decrease in the value of f. One can protect against this by taking $\delta^{(n)}$ as the direction for a line search in order to make a step of informed length and ensure descent. A more difficult problem to solve arises remote from the minimum, where the Hessian may not be positive definite. In such a situation the stationary point in the model function is not a minimising point, and the algorithm is ill-defined. Moreover, there is then no minimum. One further disadvantage of the Newton method is the demand placed on the user; $f, \mathbf{g}$ and $\mathbf{G}$ must be available at all points on the surface and provided to the algorithm.

3.3 Quasi-Newton Methods

Quasi-Newton methods are those which approximate the Hessian in a way which ensures positive definiteness, and thus robustness of the method at all points on the objective function. All quasi-Newton methods need only the gradient vector (and f, if a line search is performed) to be provided by the user.

The structure of a quasi-Newton method is to have some way of constructing a positive definite $\mathbf{H} \approx \mathbf{G}^{(n)^{-1}}$, solving for the direction of the linesearch using

$$\mathbf{s}^{(n)} = -\mathbf{H}^{(n)}\mathbf{g}^{(n)}, \tag{3.16}$$

performing the linesearch to get $\mathbf{x}^{(n+1)} = \mathbf{x}^{(n)} + \alpha^{(n)}\mathbf{s}^{(n)}$ and updating the approximate inverse Hessian to $\mathbf{H}^{(n+1)}$. Defining the useful quantities,

$$\delta^{(n)} = \alpha^{(n)}\mathbf{s}^{(n)} = \mathbf{x}^{(n+1)} - \mathbf{x}^{(n)}, \tag{3.17}$$

$$\gamma^{(n)} = \mathbf{g}^{(n+1)} - \mathbf{g}. \tag{3.18}$$

From the mapping of the differences in position to differences in gradient by the hessian,

$$\gamma^{(n)} \approx \mathbf{G}^{(n)}\delta^{(n)}. \tag{3.19}$$

Since the quantities defined in equations 3.17 and 3.18 contain updated terms (those with superscript $(n+1)$), the approximate inverse Hessian fails to relate them properly. $\mathbf{H}^{(n+1)}$ is chosen such that this is remedied,

$$\mathbf{H}^{(n+1)}\gamma^{(n)} = \delta^{(n)}. \tag{3.20}$$

This is known as the *quasi-Newton condition*. [25] This can be achieved through a number of formulae, a famous one is the Davidson-Fletcher-Powell update of the Hessian,

$$\mathbf{H}^{(n+1)}_{\mathrm{DFP}} = \mathbf{H} + \frac{\delta\delta^{\dagger}}{\delta^{\dagger}\gamma} - \frac{\mathbf{H}\gamma\gamma^{\dagger}\mathbf{H}}{\gamma^{\dagger}\mathbf{H}\gamma}, \tag{3.21}$$

where the superscripts on the right hand side are suppressed. This form of the approximate inverse Hessian is clearly defined at the solution as the second and third terms vanish. Moreover, this formula also preserves positive definiteness

and thus the descent property. The quasi-Newton method with the Davidson-Fletcher-Powell (DFP) Hessian update and exact line search performs very well for most optimisation problems. [25] A method which performs better than DFP with inexact line searches is the quasi-Newton method with the Broyden-Fletcher-Goldfarb-Shanno (BFGS) Hessian update with line search,

$$\mathbf{H}^{(n+1)}_{\mathrm{BFGS}} = \mathbf{H} + \left(1 + \frac{\gamma^\dagger \mathbf{H} \gamma}{\delta^\dagger \gamma}\right) \frac{\delta \delta^\dagger}{\delta^\dagger \gamma} - \left(\frac{\delta \gamma^\dagger \mathbf{H} + \mathbf{H} \gamma \delta^\dagger}{\delta^\dagger \gamma}\right). \tag{3.22}$$

This also preserves positive definiteness. [25] This method is the one used frequently throughout this work.

A full exposition with example problems and of greater depth can be found in ref. [25], which this discussion has followed closely, omitting proofs and finer details.

Chapter 4

Approximating Molecular Electrostatic Potentials

Empedocles, sometime between 500BC and 400BC imagined the four classical elements (fire, earth, air and water), and suggested they interact with one another through forces of attraction and repulsion he named "love" and "strife", and that these relationships explain the nature of the universe in which we live. Around the same time, Leucippus and his student Democritus proposed that all matter is made of discrete units called "atoms" from the Greek "atomos", meaning "uncuttable" or "indivisible", which remained an accurate descriptor until 1917, more than 2400 years later, the year Rutherford produced the world's first artificially induced nuclear reaction in Manchester, UK. More than 2.5 millennia since its inception, the model has been refined but the ideas remain the same. We continue to consider matter as being made up of atoms, and describe interactive forces as being "attractive" or "repulsive".

Modern concepts surrounding attractive and repulsive forces between atoms and molecules at large-to-intermediate separation primarily concern the electrostatic interactions between charge distributions, which is generally the dominant term. Elaborate schemes exist for the partitioning of molecular charge distributions into atomic contributions, and to thence approximate the potential arising through point-charge models and multipole expansions. The purpose of this chapter is to provide a review of such methods for the approximation of electrostatic potentials, and to set the stage for new research introduced in chapter 5.

4.1 Intermolecular Forces

The energy of the interaction between two molecules, is a function of the distance R between them. The shape of the function depends on both the form of the molcules themselves and their relative orientation. Van der Waals was the first to describe these ideas with any success when he considered gases beyond ideality, and as non-infinitesimal volumes and thus proposed that attractive forces between gaseous molecules in a sealed container reduced the pressure inside. That is, he modified the gas law to

$$\left(p + \frac{a}{V_m^2}\right)(V_m - b) = RT, \tag{4.1}$$

from $pV = nRT$, where b provides some information on the radius of the molecules (assumed to be balls in the van der Waals equation). Parameters a and b provide the correction from the ideal gas law arising from intermolecular forces. The name "van der Waals forces" is used to this day as a general name for intermolecular forces, but lends itself to nothing specific.

Intermolecular forces arise from a number of phenomena, and can be broken into two groups: long and short range interactions. The largest long range effects are electrostatics, induction and dispersion. Electrostatic effects arise from the interaction of two static charge distributions, and may take either a positive or negative sign. Induction effects are a response to the electric field imparted by other molecules to lower the energy and thus always takes a negative sign. Dispersion effects are those which arise as the motions of the electrons in two separate systems correlate and lower the total energy, and by the same logic as the induction effects, are always attractive. In special cases one also has to consider resonance effects, which arise when at least one molecule in an assembly is in a degenerate state. Finally, of no consequence to the work in this thesis are magnetic effects which are very small in magnitude and occur when there are multiple unpaired spins present between nuclei or electrons. The energy of these so-called long range interactions behaves asymptotically as R^{-n}, where n is dependent on the type of interaction and presence of low-rank multipole moments. [26]

Short range interactions arise once molecules are placed sufficiently close to-

gether that their wavefunctions begin to overlap to an extent one cannot neglect. They include exchange-repulsion, charge transfer, penetration and damping. Exchange-repulsion has a net repulsive effect, and is a balancing act between the decrease in the kinetic energy as electrons move in larger distances and the increase in energy arising from Pauli-principle enforced adaptation of the wavefunction. Charge transfer is rather self explanatory - it is a donor-acceptor interaction and only happens when it is energetically favourable and is thus always attractive. The penetration energy is the energy missed by an approximation resting upon Laplace's equation, once in a position where Laplace's equation no longer holds as we shall discuss in more detail later. Finally, damping is a modification to the induction and dispersion effects once electron correlation across the overlapping densities is taken into account, and is repulsive. The energy of the short range interactions behaves as $e^{-\alpha R}$. [26]

4.2 The Multipole Approximation

The work presented in this chapter is primarily concerned with the approximation of electrostatic potentials. As such, this section begins with the electrostatic potential and introduces the multipole moments as they fall out of the equations naturally. The highest working order throughout will be octopole. Cartesian co-ordinates are used where they can add to the discussion, and spherical co-ordinates used otherwise, for compactness.

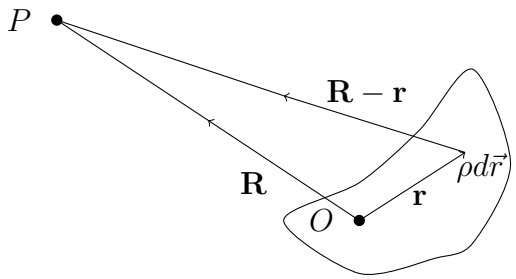

Figure 4.1: Example co-ordinates and notation for a finite and continuous charge distribution.

Consider a finite, origin-containing charge distribution in a vacuum. The charge inside any infinitesimal volume at any position $\mathbf{r}$ is given by $\rho(\mathbf{r})d\vec{r}$, where ρ is any charge density. The electrostatic potential arising from this charge distribution at some point, P located at R is given by the integral

$$V(\mathbf{R}) = \frac{1}{4\pi\epsilon_0}\int_\tau \frac{\rho(\mathbf{r})}{|\mathbf{R}-\mathbf{r}|}d\vec{r}, \tag{4.2}$$

over the volume, τ, occupied by the charge density. A graphical representation of this scenario is shown in figure 4.1. One can perform a Taylor expansion of the denominator in equation 4.2 and obtain

$$|\mathbf{R}-\mathbf{r}|^{-1} = (R^2 - 2\mathbf{R}\cdot\mathbf{r} + r^2)^{-\frac{1}{2}} \tag{4.3}$$

$$= \frac{1}{R}\left(1 + \frac{1}{R^2}\left[r^2 - 2\mathbf{R}\cdot r\right]\right)^{-\frac{1}{2}} \tag{4.4}$$

$$= \frac{1}{R} + \frac{\mathbf{R}\cdot\mathbf{r}}{R^3} + \frac{3(\mathbf{R}\cdot\mathbf{r})^2 - R^2r^2}{2R^5} + \frac{(5\mathbf{R}\cdot\mathbf{r})^3 - 3R^2(\mathbf{R}\cdot\mathbf{r})r^2}{2R^7} + \cdots, \tag{4.5}$$

where terms have been grouped in powers of $\mathbf{r}$. [26–28] Substituting this expansion

into equation 4.2 one obtains the multipole expansion for the electrostatic potential,

$$V(\mathbf{R}) = \frac{1}{4\pi\epsilon_0}\left[\frac{q}{R} + \frac{R_\alpha}{R^3}M_\alpha + \frac{3R_\alpha R_\beta - R^2\delta_{\alpha\beta}}{2R^5}M_{\alpha\beta} + \frac{5R_\alpha R_\beta R_\gamma - R^2(R_\alpha\delta_{\beta\gamma} + R_\beta\delta_{\alpha\gamma} + R_\gamma\delta_{\alpha\beta})}{2R^7}M_{\alpha\beta\gamma} + \cdots\right] \quad (4.6)$$

where

$$q = \int_\tau \rho(\mathbf{r})d\nu, \quad (4.7)$$

$$M_\alpha = \int_\tau r_\alpha\rho(\mathbf{r})d\nu, \quad (4.8)$$

$$M_{\alpha\beta} = \int_\tau r_\alpha r_\beta\rho(\mathbf{r})d\nu, \quad (4.9)$$

$$M_{\alpha\beta\gamma} = \int_\tau r_\alpha r_\beta r_\gamma\rho(\mathbf{r})d\nu, \quad (4.10)$$

are the zeroth through 3rd electric moments, and are referred to hereafter as the primitive moments. The Greek letter subscripts range over x, y and z. It is the usual approach to write these expansions in terms of traceless multipole moments, of which there are fewer independent components at all ranks greater than dipole, as opposed to the primitive moments, and there are several definitions of these available. For consistency with Stone's text (ref. [26]) on intermolecular forces, the definitions contained within are used in this section and for the first three traceless moments read as follows,

$$\mu_\alpha^O = \sum_a e_a r_\alpha, \quad (4.11)$$

$$\Theta_{\alpha\beta}^O = \sum_a e_a\left(\frac{3}{2}r_\alpha r_\beta - \frac{1}{2}r^2\delta_{\alpha\beta}\right), \quad (4.12)$$

$$\Omega_{\alpha\beta\gamma}^O = \sum_a e_a\left[\frac{5}{2}r_\alpha r_\beta r_\gamma - \frac{1}{2}r^2(r_\alpha\delta_{\beta\gamma} + r_\beta\delta_{\alpha\gamma} + r_\gamma\delta_{\alpha\beta})\right], \quad (4.13)$$

where the superscript O indicates that the multipole moments are calculated at the origin. The above are sensitive to the choice of origin for a system if, and only if, all multipoles of lower rank are not zero. Pertinent to the work in this thesis, and as an illustration of the origin independence of the first non-zero terms in the expansion, one can translate multipole moments calculated at the origin to some

other position. [26] For example, the quadrupole moment Θ^O_{zz} at the origin can be translated to some point C and written as

$$\Theta^C_{zz} = \sum_a e_a \left[\frac{3}{2}(r_z - c_z)^2 - \frac{1}{2}\left\{(r_x - c_x)^2 + (r_y - c_y)^2 + (r_z - c_z)^2\right\}\right], \tag{4.14}$$

$$= \sum_a e_a \left[\frac{3}{2}\left(r_z^2 - 2r_z c_z + c_z^2\right) - \frac{1}{2}\left\{a^2 - 2\sum_\alpha c_\alpha r_\alpha - \sum_\alpha c_\alpha^2 q\right\}\right], \tag{4.15}$$

$$= \Theta^O_{zz} - 3\mu^O_z c_z + \frac{3}{2}c_z^2 q + \sum_\alpha \mu^O_\alpha c_\alpha - \frac{1}{2}\sum_\alpha c_\alpha^2 q. \tag{4.16}$$

That is, as a linear combination of the same component of the same rank and multipole moments of lower rank at the original origin. By setting the lower rank multipoles to zero one clearly observes the origin independence of the quadrupole moment if it is the leading term in the expansion. This result holds for all multipole moments at all ranks. As these relationships are simple but time consuming to deduce and there is no easily accessible resource in which to find them online, those up to octopole are provided in appendix A for reference.

Replacing the terms in equation 4.6 with the traceless multipole moments, and taking into account factors in the definitions of each moment, one arrives at [26]

$$V(\mathbf{R}) = Tq - T_\alpha \mu_\alpha + \frac{1}{3}T_{\alpha\beta}\Theta_{\alpha\beta} - \frac{1}{15}T_{\alpha\beta\gamma}\Omega_{\alpha\beta\gamma} + \cdots \tag{4.17}$$

where

$$T = \frac{1}{4\pi\epsilon_0 R}, \tag{4.18}$$

$$T_\alpha = \nabla_\alpha \frac{1}{R} = -\frac{R_\alpha}{4\pi\epsilon_0 R^3}, \tag{4.19}$$

$$T_{\alpha\beta} = \nabla_\alpha \nabla_\beta \frac{1}{R} = -\frac{3R_\alpha R_\beta - R^2\delta_{\alpha\beta}}{4\pi\epsilon_0 R^5}, \tag{4.20}$$

$$T_{\alpha\beta\gamma} = \nabla_\alpha \nabla_\beta \nabla_\gamma \frac{1}{R} = -\frac{15R_\alpha R_\beta R_\gamma - 3R^2(R_\alpha\delta_{\beta\gamma} + R_\beta\delta_{\alpha\gamma} + R_\gamma\delta_{\alpha\beta})}{4\pi\epsilon_0 R^7}, \tag{4.21}$$

$$T_{\alpha\beta\gamma\ldots\delta} = \frac{1}{4\pi\epsilon_0}\nabla_\alpha \nabla_\beta \nabla_\gamma \ldots \nabla_\delta \frac{1}{R}. \tag{4.22}$$

Let us now briefly compare equations 4.2 and 4.17, and explore the benefits of performing a multipole expansion. The presence of $\mathbf{R}$ in equation 4.2 is the source of computational expense in calculating the electrostatic potential; if we wish to

evaluate a molecular potential several thousands of times, we have to evaluate the complicated 3D integral several thousands of times, once for each point, **R**. In contrast, by using equation 4.17, one needs only compute the integrals for the multipole moments once, as **R** is only present in this expression in the prefactors of the expansion, not the operators themselves. Now, although the series of multipole operators runs, in principle, to infinity we know that we usually need only consider the first few terms. This cheapens the computational cost of those thousands of evaluations of the electrostatic potential enormously, as one must only re-evaluate the fraction $(1/R)^n$ where it is needed in the expansion. Performing an expansion also reduces the pressure on numerical accuracy by simplifying the expression of the potential. For example, take the scenario of two separated and opposite charges q and -q, placed at $\pm s = 1$ mm on the z-axis, respectively. Evaluating the potential at +1000 m on the z-axis using equation 4.2,

$$V = \frac{q}{(1000+s)\mathrm{m}} - \frac{q}{(1000-s)\mathrm{m}}, \tag{4.23}$$

$$= \frac{q}{\mathrm{m}}(0.000999999\ldots - 0.001000001\ldots) \approx 2\times 10^{-9}\frac{q}{\mathrm{m}}, \tag{4.24}$$

where the numerical accuracy has been tuned up to 9 decimal places, which is trivial for this very simple example, but for large molecules this integral would be significantly more complex. The dipole for this system is $2\mathrm{mm}\times q$, and calculating the potential arising from the dipole we get

$$V = 0.002\ \mathrm{m}\times q\times\frac{1}{1000^2\ \mathrm{m}^2} = 2\times 10^{-9}\frac{q}{\mathrm{m}}. \tag{4.25}$$

Thus in this simple case we obtain the same potential with one significant figure using the dipole field as we get with numerical integrals tuned to 9 decimal places. That is, the use of the multipole expansion replaces the evaluation of an expensive integral with the evaluation of a simple numerical ratio, and represents an excellent approximation to the exact potential far from the charge distribution, meanwhile removing concerns about numerical errors in the integrals.

Multipole expansions are not limited to pragmatic benefits, but extend to providing some conceptual clarity. Each term in a multipole expansion is a shape descriptor of the density, and the expansion separates the scales beautifully by

having increasing powers of $\frac{1}{R}$. We can see exactly at what distance the test point begins to "see" something other than a ball of charge on the horizon, and at what point the finer details of the charge distribution become relevant. Moreover, one can gather some chemical insights from lower order multipole moments of bonding orbitals, for instance, when there is a polarised bond, one might expect nucleophilic attack at the "positive end". In such a case, the bonding orbital has a large dipole. This insight is simply not possible if the potential is evaluated exactly.

One could feasibly stop here, and use the expansion in equation 4.17 in order to calculate a molecular electrostatic potential, and this would yield good results where P is very far from the electron density. However, given the additivity of the electrostatic potential and the nature of the multipole expansion, there are certain advantages to dividing up the density according to some scheme, and using exactly this formula several times over to calculate the potential arising from each bit of the density, as will be discussed in more detail in section 4.3.

4.2.1 Approximate Electric Fields

The electric field F_α is related to the electrostatic potential by,

$$F_\alpha(\mathbf{R}) = -\frac{\partial V(\mathbf{R})}{\partial R}. \tag{4.26}$$

So, having written down the potential in equation 4.17, and the coefficients in the expansion as $T_{\alpha\beta\ldots\gamma}$ it is, formally at least, very simple to write down the electric field as a multipole expansion. We write the same expansion as previously, take care with dummy variables and add a subscript to each T in the expansion then multiply by -1. [26] That is,

$$F_\alpha(\mathbf{R}) = -T_\alpha q + T_{\alpha\beta}\mu_\beta - \frac{1}{3}T_{\alpha\beta\gamma}\Theta_{\beta\gamma} + \frac{1}{15}T_{\alpha\beta\gamma\delta}\Omega_{\beta\gamma\delta} - \ldots \tag{4.27}$$

where to go up to the quadrupole term, $T_{\alpha\beta\gamma\delta}$ is needed and is given by,

$$\begin{aligned} T_{\alpha\beta\gamma\delta} = \frac{1}{4\pi\epsilon_0 R^9}\big(&105R_\alpha R_\beta R_\gamma R_\delta - 15R^2(R_\alpha R_\beta\delta_{\gamma\delta} + R_\alpha R_\gamma\delta_{\beta\delta} + R_\alpha R_\delta\delta_{\beta\gamma} \\ &+ R_\beta R_\gamma\delta_{\alpha\delta} + R_\beta R_\delta\delta_{\alpha\gamma} + R_\gamma R_\delta\delta_{\alpha\beta}) + 3R^4(\delta_{\alpha\beta}\delta_{\gamma\delta} + \delta_{\alpha\gamma}\delta_{\beta\delta} + \delta_{\alpha\delta}\delta_{\beta\gamma})\big). \end{aligned} \tag{4.28}$$

Identical logic applies to the electric field gradient and higher order derivatives. The termwise differentiation or integration of a power series within its radius of convergence is identical to the power series expansion of the derivative or integral. This is a powerful result and is general to all power series, of which the Taylor series used in this chapter is an example.

4.2.2 Electrostatic Interactions Between Molecules

If one has a potential, $V(\mathbf{r})$, which can be written as the Taylor expansion,

$$V(\mathbf{r}) = V(0) + r_\alpha V_\alpha(0) + \frac{1}{2} r_\alpha r_\beta V_{\alpha\beta}(0) + \frac{1}{3!} r_\alpha r_\beta r_\gamma V_{\alpha\beta\gamma}(0) + \cdots , \tag{4.29}$$

then the operator describing the energy of interaction with a molecule in that potential is given by [26]

$$\hat{\mathcal{H}}' = \sum_a e_a \hat{V}(\mathbf{r}_a), \tag{4.30}$$

$$= V(0) \sum_a e_a + V_\alpha(0) \sum_a e_a a_\alpha + \frac{1}{2} V_{\alpha\beta}(0) \sum_a e_a a_\alpha a_\beta + \cdots , \tag{4.31}$$

$$= qV + \hat{\mu}_a \alpha V_\alpha + \frac{1}{3} \Theta_{\alpha\beta} V_{\alpha\beta} + \cdots , \tag{4.32}$$

where $\mathbf{r}_a$ is the position vector of each particle, a, in the system of charge e_a, and in the last line the primitive moments have been replaced by the traceless multipole moments as before. Suppose now that the potential is one arising from the presence of a molecule located at $\mathbf{A}$, and is denoted V^A and the molecule placed in the electrostatic potential sits at $\mathbf{B}$. We are able to insert into equation 4.32 the expression for V^A from equation 4.17 and obtain the operator describing the electrostatic interaction of molecules A and B, [26]

$$\hat{\mathcal{H}} = q^B V^A + \hat{\mu}^B_\alpha V^A_\alpha + \frac{1}{3} \hat{\Theta}^B_{\alpha\beta} V^A_{\alpha\beta} + \cdots , \tag{4.33}$$

$$\begin{aligned} = q^B & \left[T q^A - T_\alpha \hat{\mu}^A_\alpha + \frac{1}{3} T_{\alpha\beta} \hat{\Theta}^A_{\alpha\beta} + \cdots \right] \\ & + \hat{\mu}^B_\alpha \left[T_\alpha q^A - T_{\alpha\beta} \hat{\mu}^A_\beta + \frac{1}{3} T_{\alpha\beta\gamma} \hat{\Theta}^A_{\beta\gamma} - \cdots \right] \\ & + \hat{\Theta}^B_{\alpha\beta} \left[T_{\alpha\beta} q^A - T_{\alpha\beta\gamma} \hat{\mu}^A_\gamma + \frac{1}{3} T_{\alpha\beta\gamma\delta} \hat{\Theta}^A_{\gamma\delta} - \cdots \right] + \cdots , \end{aligned} \tag{4.34}$$

from which one can calculate the electrostatic interaction by simply inserting the expectation values of the operators. [26] That is, by taking the expectation value of the ground state across the operator $\hat{\mathcal{H}}$. One can further obtain expressions for the polarizabilities of the molecule(s) in terms of multipole moments by performing Rayleigh-Schrödinger perturbation theory to second order, and hyperpolarizabilities by going to fourth order. [26]

While we have placed much emphasis on the work of Stone, we also acknowledge expressions derived by other authors, such as Buckingham, Hirshfelder, Jansen and Leavitt, which are similar to the ones presented in this chapter. [27, 29–31]

4.2.3 A Remark on Co-ordinates

While the cartesian definitions used thus far provide equations which are somewhat intuitively appealing, at high rank these definitions lose their intuitive appeal and become unwieldy. One can combat this by working with spherical co-ordinates, which allow succinct and open-ended definitions of the multipole moments up to arbitrary rank, admittedly with far less conceptual transparency at low rank. The multipole operators associated with an origin, $\vec{A}$, in the spherical tensor formalism are defined by [26, 32]

$$\hat{Q}^A_{lm} = \sum_a e_a \, R_{lm}(\mathbf{r}_a - \mathbf{A}), \tag{4.35}$$

$$R_{lm}(\mathbf{r}) = \sqrt{\frac{4\pi}{2l+1}} \, r^l \, Y_{lm}(\theta, \phi), \tag{4.36}$$

$$I_{lm}(\mathbf{r}) = \sqrt{\frac{4\pi}{2l+1}} \, r^{-l-1} \, Y_{lm}(\theta, \phi), \tag{4.37}$$

where r_a is the position of particle a, e_a is the charge of particle a, $R_{lm}(\vec{r})$ and $I_{lm}(\vec{r})$ are the regular and irregular solid harmonics, and Y_{lm} are the spherical harmonics. [26,32] The expressions for the regular and irregular solid harmonics are obtained by solving the Laplace equation in spherical polar co-ordinates (r, θ, ϕ).

The spherical harmonics are the eigenfunctions of the angular momentum operator, and generate a representation of the rotation group. They are defined on the surface of a sphere of radius $\mathbf{r}$, and provide a basis for the expansion of a potential which naturally behaves according to the appropriate symmetry at each rank, l.

The spherical tensor definitions of the multipole moments have the added benefit of not containing any rotationally invariant terms, as is the case in the cartesian tensor formulation (those along the trace in the primitive moments which are removed in the traceless multipole moments) and thus the spherical tensor formulation is a more natural way to write expansions in terms of multipole moments.

As an example, the expansion of the electrostatic potential given in equation 4.17 can be written more compactly in terms of spherical tensors as, [26]

$$V(\mathbf{r}) = \sum_{lm} (-1)^m Q_{lm} I_{l,-m}(\mathbf{r}), \tag{4.38}$$

and as in the cartesian case can be substituted into the equation for the operator describing the electrostatic interaction of molecules A and B, centered at $\mathbf{A}$ and $\mathbf{B}$, [26]

$$\hat{\mathcal{H}} = \sum_{lm} (-1)^m \hat{Q}^B_{l,-m} V^A_{lm}, \tag{4.39}$$

where

$$V^A_{lm} = \left[(2l-1)!!\right]^{-1} R_{lm}(\nabla) V^A. \tag{4.40}$$

The value returned from the regular solid harmonic of the gradient vector ($R_{lm}(\nabla)$) is a differential operator of an order dependent on l, [26] and thus returns the same expansion as in the cartesian case but is much more compact for large l.

4.3 Distributed Multipole Analysis

Distributed multipole analysis (DMA) was developed to provide improved performance of the multipole expansion close to a molecular charge distribution, compared with the then-common expansion of the entire electron density around a single point. [33] The structure and motivation of the method has remained unchanged since its inception. The structure is

1. Divide an electron density into atomic contributions by some scheme,
2. Calculate the multipole moments arising from the atomic contributions to the electron density,
3. Take a single atomic density and perform the expansion in equation 4.17, and sum over all atoms.

More formally, calculate the potential at $\mathbf{R}$ according to

$$V(\mathbf{R})^{\mathrm{DMA},L} = \sum_{A} \sum_{lm}^{L} (-1)^m Q_{lm}^{A} I_{l,-m}(\mathbf{R} - \mathbf{A}), \tag{4.41}$$

where L is the maximum angular momentum included in the expansion, and is included for reference later and $\mathbf{A}$ is the origin chosen for the expansion, usually the nucleus of the atomic basin from which this term in the potential is calculated.

The motivation arises from the knowledge that the multipole expansion only converges (formally) outside any sphere which contains all of the electron density. But the electron density decays exponentially out to infinity in all directions, so any containing sphere must therefore be infinitely large and the approach infinitely ineffective! In reality, so long as the sphere contains an overwhelming majority of the electron density, the expansion converges. As a consequence, as molecular symmetry reduces, and as larger systems are studied, the expansion of the coulomb integral around a single point becomes less and less reliable; the radius of convergence grows, and the points for which the series will converge are found at increasing distance. The distributed multipole approximation, therefore, by dividing the molecular electron density into atomic contributions reduces one large sphere to a number of smaller spheres and as a result reduces the error associated

with the multipole expansion by exploiting additivity. Moreover, where the one sphere encloses a test point, the other sphere is still far away and thus only the parts of the electrostatic potential arising from density within the sphere enclosing the test point will be erroneous. A schematic showing an example situation where DMA is superior is shown in figure 4.2. Of course, very far from the density, both the multipole expansion of the molecular density and DMA perform equally well.

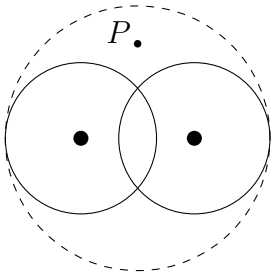

Figure 4.2: A schematic showing a point within the sphere containing most of the molecular electron density (dashed line), but outside both spheres for the atomic densities (solid lines).

The evolution of DMA has been entirely within the scheme used to partition the electron density into atomic contributions. [26, 33–37] The first iteration of the method from Stone, described as an extension to Mulliken population analysis included partitioning the electron density into atomic and bond contributions. Around the same time as Stone published his DMA, Bentley suggested an "atomic multipole analysis", in which bond contributions are not considered, and involved a fitting to experimental multipole data, [38] and thus was less desirable than Stone's formulation. [34] For some time after the first publication, Stone continues to partition the density in different ways, often taking DMA sites between nuclei, i.e an expansion anywhere there is significant overlap between basis functions combined with sites at the nuclei. The issue with this approach was in the sensitivity of the multipole moments at the sites with changing basis sets. [33] Although this of course did not manifest itself in sensitivity in the calculated electrostatic potential. This instability in the multipole moments arises as a consequence of the partitioning taking place in basis function space, and thus in 2005 a revised version of DMA was presented which used real-space partitioning for diffuse functions and the original partitioning schemes for compact functions. [35] This approach yielded extremely stable multipole moments up to hexadecapole. At this time,

the DMA sites were almost always chosen to be the nuclei and the densities to be near-spherical atomic contributions, with the DMA sites along the bonds not receiving a mention. [35]

In its most recent formulation, DMA relies upon a modified form of the iterated stockholder algorithm (ISA) for decomposing a molecular electron density into atomic contributions. [36] The original (real-space) form of the ISA algorithm iterates over two equations,

$$\rho^a(\mathbf{r}) = \rho(\mathbf{r}) \times \frac{w_a(\mathbf{r})}{\sum_b w^b(\mathbf{r})} \tag{4.42}$$

$$w^a(\mathbf{r}) = \langle \rho^a(\mathbf{r}) \rangle_{\text{sph.}} \tag{4.43}$$

for all atoms a in a molecule. [39,40] $w^a(\mathbf{r})$ are functions describing the spherically averaged density of atom a. Convergence is measured by the consistency of the functions $w^a(\mathbf{r})$ iteration to iteration. This was found to converge slowly, and instead a basis-space version of ISA (BS-ISA) was developed by Misquitta *et al.*. [36,41] In this modified scheme the density is expanded in an auxiliary basis through a density-fitting technique. The atomic densities are then expanded in terms of Gaussian type s-orbitals, and a functional such as

$$F_{\text{BS-ISA}} = \sum_a \left|\left| \left(\rho^a - \rho \frac{w^a}{\sum_b w^b} \right)^2 \right|\right| \tag{4.44}$$

is minimised, and the shape functions w^a have been redefined as the expansions in terms of Gaussian s-orbitals,

$$w^a = \sum_p c_p^a \xi_{p,s}^a(\mathbf{r}) \tag{4.45}$$

A full exposition of the BS-ISA method is available in ref. [36], wherein there are a number of more involved steps for dealing with the tails of the shape functions, and an analysis of the performance of DMA with BS-ISA defined sites which is found to out-perform the previous versions of the DMA algorithm, especially at low rank. The details included here are simply to show that DMA in its current form still rests upon an artificial partitioning of the molecular electron density into spherical atomic components. The sites for DMA are then chosen as the nuclei, and

the multipole moments included in the expansion are those of the near spherical densities corresponding to each "atom".

A non-heuristic partitioning of the electron density was suggested by Pullman *et al.* in which the molecular electron density is partitioned into localised orbital contributions, and a multipole expansion performed about each orbital centroid in turn (let us also acknowledge Gordon *et al.* independently arriving at the same scheme; see ref. [42]). [43, 44] This approach is conceptually related to the new work presented in the next chapter, and so we compare its efficacy with that of DMA. We shall refer to Pullman's scheme as the "Orbital Multipole Approxiation" (OMA). The logic of the approach is founded in the use of localised orbitals, which by definition reduce the radius of convergence discussed previously in comparison with canonical orbitals. While this approach removes the need for the assumption that the density can be represented by a sum of near spherical atomic densities, it does introduce a dependence on the chosen localisation algorithm; orbitals localised in different ways will carry different multipole moments. The orbital centroid is the point at which the dipole moment is zero. The dipole moment is calculated as

$$\vec{r_i} = \int d\vec{r} |\psi_i(\vec{r})|^2 \vec{r}, \tag{4.46}$$

and the multipole moments arising at the centroids as

$$Q^i_{lm} = -\int d\vec{r} R_{lm}(\vec{r} - \vec{r_i}) |\psi_i|^2, \tag{4.47}$$

or by calculating them at the global origin and translating the orbital multipole moments to the centroids using the equations provided in appendix A. Two values of Q^i_{lm} are given by construction: the $l, m = 0$ term is -1, and the $l = 1$ term is zero by definition. Further simplifications in the implementation occur in closed shell systems. One can then calculate an approximate potential arising from the multipole expansion of each orbital at its centroid, sum over the orbital index and arrive at the total molecular electrostatic potential at some point, $\mathbf{R}$, by simply providing the L at which to terminate OMA electrostatic potential,

$$V^{\mathrm{OMA},L}(\vec{r}) = \sum_A \frac{Z_A}{|\mathbf{r} - \mathbf{A}|} + \sum_i \sum_{lm}^{L} (-1)^m Q^i_{lm} I_{lm}(\vec{r} - \vec{r_i}). \tag{4.48}$$

This model, of course, suffers the same deficiencies as DMA. Penetration effects will ruin the model potential at short range, and the same arguments about regions of convergence will apply. However, the lack of any nonphysical assumptions that the density is a sum of near-spherical atomic densities is appealing, and arguably the most expensive step of the DMA algorithm (the partitioning of the density) is no longer any concern.

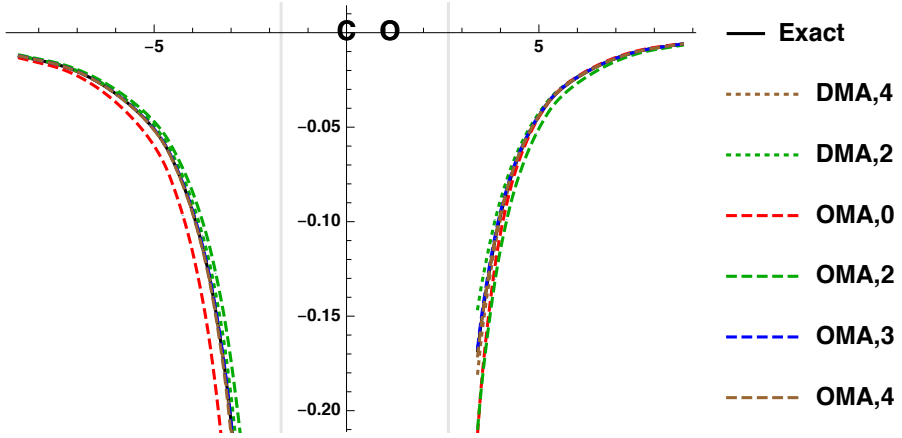

Figure 4.3: DMA,L and OMA,L electrostatic potentials / volt along the molecular axis of CO arising from a B3LYP calculation with the aug-cc-pVQZ basis set. C is at the origin, O is at $(0, 0, r_e = 1.1282$ Å). Distances of one van der Waals radii are shown in grey.

Figure 4.3 shows the exact potential along with $V^{\mathrm{DMA},L}$ and $V^{\mathrm{OMA},L}$ for several L along the molecular axis of carbon monoxide. The data shows that both DMA and OMA yield good approximations to the potential further than 1.5 van der Waals radii away. Significant errors occur where the DMA and OMA expansions are truncated at $L = 2$, more visibly in the OMA,2 case. The difference between the exact potential and the DMA and OMA potentials is shown in figure 4.4. It is clear to see that OMA,0 performs poorly in this example, as expected given that there is no characteristic shape descriptor included in the expansion, and we are at short range. OMA,2 and DMA,2 also perform poorly. OMA,3 and OMA,4 perform best at the oxygen end of the molecule, diverging signficantly closer to the atom than DMA,4. At the other end of the molecule, close to the carbon DMA,4, OMA,3 and OMA,4 all perform roughly as well as each other.

In general there are more OMA sites in a molecule than there are DMA sites - there are usually more orbitals than nuclei in any molecule, given the presence of non-bonding core orbitals. That said, the number of OMA sites can likely be

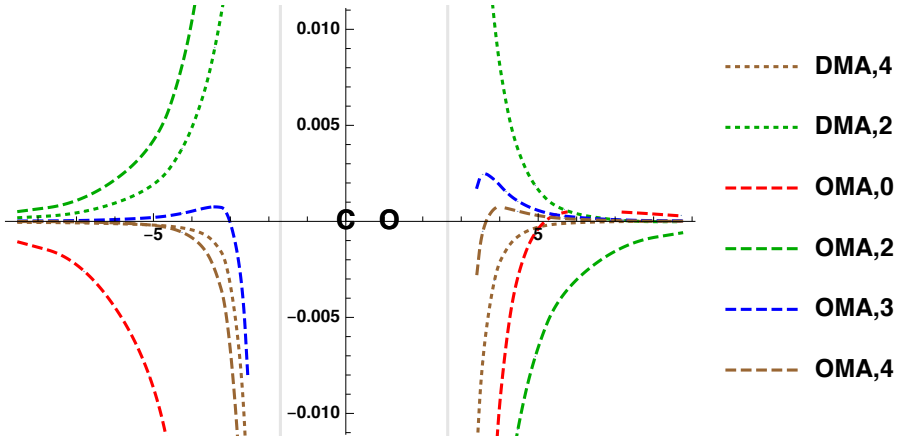

Figure 4.4: Error in OMA,L electrostatic potentials / Volt at points along the molecular axis of CO arising from a B3LYP calculation with the aug-cc-pVQZ basis. C is at the co-ordinate origin, and O at $(0, 0, r_e = 1.1282$ Å). Distances of one van der Waals radii of the atoms ($r_C = 1.70$ Å and $r_{\mathrm{O}} = 1.52$ Å) are indicated in grey. [45]

reduced by representing the core orbitals as monopoles at the nuclei. OMA is, therefore, a viable alternative to DMA and offers a comparable level of accuracy when compared to the exact electrostatic potential.

A more qualitative picture of the accuracy of the OMA can be obtained by investigating a more chemically interesting system. Take, for example, the simplest of the amino acids, glycine. One has within glycine several different functional groups, most of which are polar and produce a more characterful density than the ellipsoidal CO density. Within the restricted formalism of electronic structure, there are 20 molecular orbitals in glycine; 5 core 1s orbitals from each carbon, oxygen and nitrogen atom present, 9 σ bonding molecular orbitals, 1 π bonding orbital and the rest are made up of lobes on each of the carbon, oxygen and nitrogen atoms. The core 1s orbitals are rather uninteresting - they are spherical with stable multipole moments up to high order. They look like small concentrated balls of charge even at short-range, because that is what they are! The lobes, $\sigma-$ and $\pi-$bonds however, are of rather complicated shapes and while at long range they of course look like small balls of charge, at close range the details of their shapes become more important.

Figure 4.5 shows contour maps of the electrostatic potential arising due to the presence of a molecule of glycine. Given the form of equation 4.48, it is not a surprise to see OMA,0 performing poorly at distances close to the molecule - in

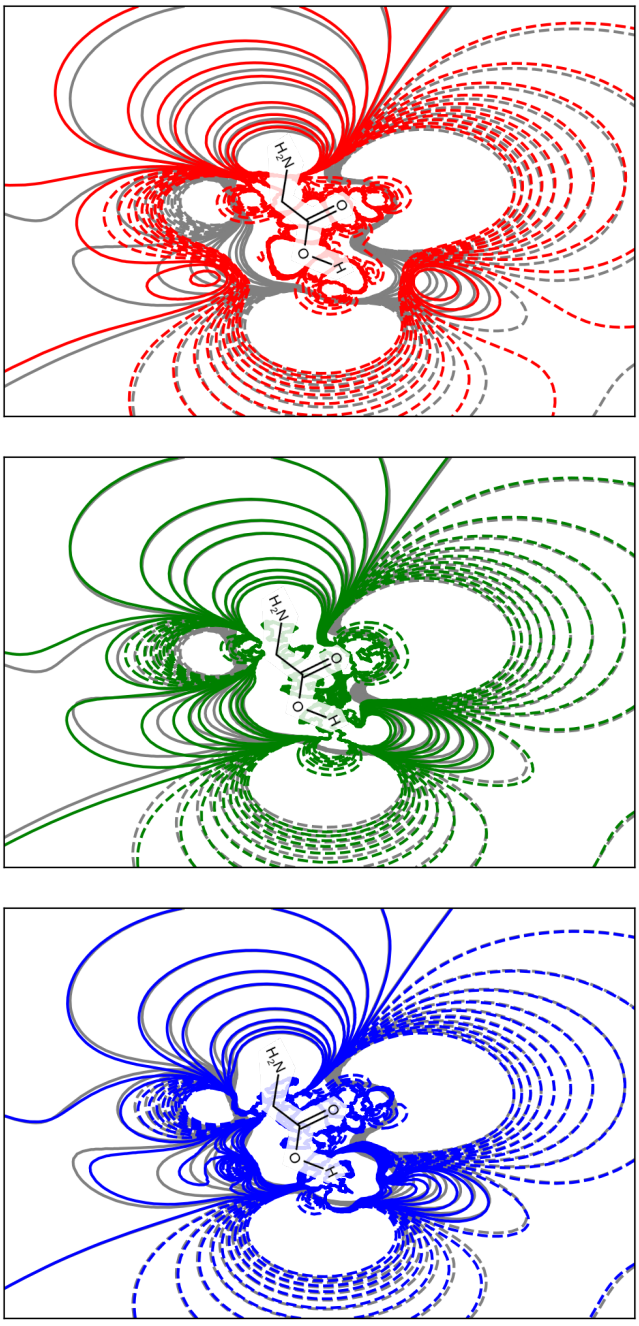

Figure 4.5: Contour maps of the molecular electrostatic potential arising from glycine, calculated using the OMA,0 (top), OMA,2 (middle) and OMA,3 (bottom). Solid and dashed lines indicate positive and negative electrostatic potentials, respectively. The electrostatic potential calculated from the optimised cc-pVTZ B3LYP density (grey) is included for reference in each subfigure. The orbitals used for OMA were localised using the Pipek-Mezey procedure. [46]

OMA,0 there are only point charges (in this case $q = -2$) at the orbital centroids, and the nuclear term. There is no descriptor of the shape of the electron density, and thus once the molecular charge distribution ceases to look like balls of charge very far away, OMA,0 diverges. Once we reach OMA,2 the potential begins to perform much better at close range - the quadrupole term is the first characteristic shape descriptor of the density in the OMA expansion. OMA,3 almost perfectly reproduces the potential far from the molecule. The model naturally still suffers the same problems as DMA once well within the molcular electron density where penetration effects play an enormous role, and no choice of multipole sites could be clever enough to correct for this issue.

4.4 Methods Accounting for Penetration Effects

While the DMA and OMA approximations laid out in the previous section yield good approximations to the electrostatic potential at long range, even at low rank, upon approaching the molecular electron density, the approximation diverges, and any potential within the radius of divergence does not behave as the exact potential behaves. The error in the multipole-expanded interaction energy between two subsystems relative to the non-expanded coulomb interaction is known as the penetration correction. [26, 47, 48] The penetration error becomes significant over distances where charge densities on two subsystems overlap, and the permanent multipole moments of the sub-systems no longer reflect the shape of the density. [49] Traditionally, damping functions have been used to yield better-behaved electrostatic, dispersion and induction energies upon penetration of the electron density. [26, 49–52] Several modern schemes exist which aim to account for the penetration correction by employing a model density, thereby removing the need for parameterised damping functions, and are related to the new research presented in the next chapter. [53–58]

4.4.1 Minimal Basis Iterative Stockholder

In the Minimal Basis Iterative Stockholder (MBIS) algorithm, an approximate atomic density is constructed in terms of Slater-type functions. [56] The centres

for the Slater functions are chosen to be the nuclei, and a procedure similar to the BS-ISA approach is performed, and a so-called "pro-density" is optimised by minimising the information loss. The electrostatic potential arising from this model density can then be calculated at a fraction of the cost of the full electrostatic potential, and given the presence of a suitably optimised model density in the evaluation of the potential, some portion of the penetration correction is recovered. [56] The approach is reasonably new, and systematic improvements to the potential through inclusion of higher order multipole moments forms part of the "future work" section of the initial publication. [56] Partial charges and the potential arising from the pro-density obtained through this scheme have, however, been applied to some systems of chemical interest. [59–61] Assigning partial charges is not of any concern in this thesis, however, methods akin to the MBIS approach which may or may not be used to form approximate electrostatic potentials are benchmarked and discussed in some detail in a recent review article. [62]

4.4.2 Gaussian Electrostatic Model

The Gaussian Electrostatic Model (GEM), similar to the MBIS approach, involves expanding the electron density in terms of an auxiliary basis set. This basis set comprises Hermite-Gaussians which, in the form first introduced, are centred wherever appropriate in order to well-reproduce the molecular electron density. [58, 63] The auxiliary density is generated by performing a density fitting technique. That is, by minimising the self-energy of the error in the density,

$$E_{\text{self}} = \langle \rho - \tilde{\rho} | \frac{1}{r_{12}} | \rho - \tilde{\rho} \rangle \,, \tag{4.49}$$

where the chosen measure in the case of the GEM model is the coulomb operator (but need not be, if one is interested in reducing the cost of evaluating other properties). [58] It is then possible to perform a distributed multipole expansion at each site where the density has been approximately expanded in Hermite-Gaussians, or to evaluate the potential arising from the new density. This approach has been extensively benchmarked, and attempts have been made to incorporate it into popular MM and QM/MM forcefields. [64–66]

4.4.3 Gaussian Multipole Model

If one makes a departure from the use of point-multipoles, which are those presented in the discussion of DMA and OMA, and instead uses *Gaussian multipoles*, which arise as from derivatives of spherical Gaussians and take the form, [67]

$$G^{\xi}_{abc}(\mathbf{r}-\mathbf{r}') = \left(\frac{\xi}{\pi}\right)^{\frac{3}{2}} \frac{(-1)^{a+b+c}}{(a+b+c)!} \frac{\partial^a}{\partial x_a} \frac{\partial^b}{\partial y_b} \frac{\partial^c}{\partial x_c} \exp\left[-\xi(\mathbf{r}-\mathbf{r}')^2\right], \tag{4.50}$$

one arrives at a description of the potential and electrostatic interactions which includes penetration terms for finite ξ. For infinite ξ, the above yields an expression which behaves as a point-multipole expansion. In the Gaussian Multipole Model (GMM), the density arising from the Gaussian multipoles is determined by fitting to accurate values of the electrostatic potential at chosen sites around the molecule. [57]

4.5 Summary

This chapter has covered, in some detail, how one can approximate the electrostatic potential by expanding the coulomb expression in multipole moments. We have also discussed the divergence of the multipole expansion which occurs close to the charge density, and the unphysical singularities in the potential which arise at the multipole sites. These deficiencies are remedied to an extent by reducing the radius of divergence through the use of a distributed multipole approximation, in which several regions of the charge density are represented by several separate multipole expansions. This raises questions of how many multipole sites in a given charge density one should choose, and how they should be chosen. However, no choice of multipole expansion sites is capable of incorporating penetration effects, and the eventual singularities arising still represent a significant flaw in approaches such as DMA and OMA.

Approaches to modelling electrostatic potentials which employ an approximate charge density, such as MBIS, GEM and GMM have the appealing characteristic that they naturally include exponential terms in the electrostatic potential which cancel the multipole terms at points close to, or within the charge density. Methods

based upon building a model density which can be evaluated cheaply represent a promising alternative to established distributed multipole approaches, however, in general they lack the cheap systematic improvement of the approximate potential by the inclusion of higher order multipole terms in an expansion. That is, any improvement of a potential calculated from a model density comes as a result reducing the simplicity of the model density in order to better capture the shape of the density one is attempting to approximate. This controlled approach to the exact potential is appealing in a sense, but taking advantage of it could be seen as counter productive.

In the coming chapter we introduce a new method which aims to include the appealing features of both multipole expansions and model densities for approximating the electrostatic potential. This is achieved by first constructing a set of approximate molecular orbitals, which are in turn used to calculate a model density. The approximate molecular orbitals are obtained by a procedure which matches their charge centroids to a set of accurate molecular orbitals, thus allowing the controlled approach to the exact potential by increasing the basis in which the approximate MOs are expressed. A corrected multipole expansion is then developed at their centroids, allowing the systematic improvement of the potential in terms of multipole moments as in DMA or OMA.

Chapter 5

The Reduced Orbital Potential Approximation

Having provided some survey of the scientific and historic landscape surrounding the issue of approximate molecular potentials, the purpose of this chapter is to introduce a new, computationally efficient method for approximating electrostatic potentials and forcefields arising from molecular electron densities. We first introduce the Reduced Orbital Potential Approximation (ROPA), which aims to incorporate the systematic improvements of a multipole expansion while naturally maintaining some control over penetration effects through the inclusion of a model density expressed in a "reduced basis". Then, we differentiate the expressions obtained as a means to gather approximate expressions for the field, the Orbital Field Approximation (OFA) based on the OMA of the previous chapter, and the Reduced Orbital Field Approximation (ROFA) based on the ROPA expression deduced in this chapter.

We also later consider the impact of orbital localisation on the symmetries of the associated approximate potentials in a case study on the OMA and ROPA electrostatic potentials arising from benzene, and see that ROPA shows surprisingly robust performance when applied with either canonical or localised orbitals of broken symmetry.

5.1 The Reduced Orbital Potential Approximation

By expanding the electrostatic potential around some point in terms of multipole moments, one introduces unphysical singularities into the potential arising from the electrons. This is readily observed from the form of the cartesian definitions of the multipole moments. If R is the distance from the origin chosen for the expansion, then as $R \to 0$, the expansion of the potential quickly approaches infinity. This is true for any choice of multipole site. Thus, while multipole expansions such as those in DMA and OMA provide good approximations to the potential at long range, more care is needed over shorter distances. In the exact calculation of electrostatic potentials, the terms arising from the multipole moments are controlled over small R by exponential terms in the exact potential. [26] The only necessarily surviving singular terms are those arising from point-nuclei. For some time, damping functions have been used as prefactors for the terms in the multipole expansion for returning satisfactory behaviour of the dispersion and induction energies. [26, 50–52, 68, 69] Damping functions constitute some system-specific, parameterised function of intermolecular separation, R, which behaves as R^n over short range when the term being damped behaves as R^{-n}, and tends to unity as $R \to \infty$, and to zero as $R \to 0$. This behaviour thus mutes multipole terms over distances they yield unphysical quantities, and yields a potential equivalent to the un-damped multipole expansion at large R. [26] More recently, schemes have been developed for incorporating damping functions in multipole-expanded expressions of the electrostatic potential. [26, 48] Some of these schemes require fitting to exact values of the molecular potential at various points. [70–73] The deficiency in capturing penetration effects is unique to point-charge and point-multipole approaches, and thus any method which treats all charge-charge interactions according to the non-expanded forms of the operators will yield finite quantities for intermolecular interactions of various types. Thus approaches such as Symmetry Adapted Perturbation Theory (SAPT) do not have associated with them the same issues. [26, 74]

In this section we introduce a new method for approximating molecular electrostatic potentials which, as far as possible, naturally incorporates the charge

penetration correction, without the need for damping functions, by combining the potential arising from a model density with the appealing systematic improvements of a multipole expansion through a point-correction term. The form of the model density is kept as simple as possible in order to increase only minimally the computational expense of a multipole expansion.

Let us first define an auxiliary, "reduced" basis set $\{\bar{\chi}_\mu\}$, which according to the criteria laid out above need only be smaller than the primary basis set (the basis being used for the energy optimisation), but will in general be minimal, as the intention is that the electrostatic potential can be calculated from the density expressed in this basis at little computational expense. An example basis set which is used extensively throughout this thesis is the MINAO basis set in MOLPRO which comprises the valence atomic orbital subset of cc-pVTZ, and will be referred to hereafter without qualification as MINAO. [75] One could of course see more rapid evaluation of the potential under the scheme we present here by replacing MINAO with, say, the STO-3G basis set. A set of molecular orbitals in the reduced basis,

$$|\bar{\psi}_i\rangle = \sum_\mu \bar{C}_{\mu i} \, |\bar{\chi}_\mu\rangle \, , \tag{5.1}$$

can then be generated by projection of the reference molecular orbitals,

$$|\psi_i\rangle = \sum_\alpha C_{\alpha i} \, |\chi_\alpha\rangle \, , \tag{5.2}$$

onto the minimal basis, as is done in some orbital localisation schemes. [76] That is,

$$|\bar{\psi}_i\rangle = |\bar{\chi}_\mu\rangle \, (\bar{\mathbf{S}}^{-1})_{\mu\nu} \, \langle\bar{\chi}_\nu|\chi_\alpha\rangle \, C_{\alpha i} \tag{5.3}$$

$$= |\bar{\chi}_\mu\rangle \, \bar{C}'_{\mu i} \tag{5.4}$$

where

$$\bar{\mathbf{C}}' = \bar{\mathbf{S}}^{-1} \boldsymbol{\Delta} \mathbf{C} \tag{5.5}$$

$$\Delta_{\mu\alpha} = \langle\bar{\chi}_\mu|\chi_\alpha\rangle \, . \tag{5.6}$$

Then finding the MO coefficients in the minimal basis which form the closest orthonormal set in the usual way,

$$\bar{\mathbf{C}} = \bar{\mathbf{C}}'(\bar{\mathbf{C}}'^{\dagger}\bar{\mathbf{S}}\bar{\mathbf{C}}')^{-\frac{1}{2}}. \tag{5.7}$$

One can then minimise the following functional with respect to the coefficients of the reduced orbitals, $\bar{\mathbf{C}}$,

$$F = \sum_i \left|\langle\bar{\psi}_i|\vec{r} - \vec{r}_i|\bar{\psi}_i\rangle\right|^2, \tag{5.8}$$

where

$$\vec{r}_i = \langle\psi_i|\vec{r}|\psi_i\rangle. \tag{5.9}$$

subject to the constraint that the reduced orbitals remain orthonormal. At the minimum of this functional, the dipoles, and by definition the centroids of the reduced orbitals, $\{\bar{\psi}_i\}$, are matched to those of the reference orbitals. It is expected that at least one $F = 0$ can be found, as the dipole in any system can be modified by modifying the ratio of any two coefficients of basis function centred on any two different atoms. By minimising F, one arrives at a reduced density which gives rise to an optimum asymptotic electrostatic potential. This can be done quite simply by making stationary the Lagrangian,

$$L = F - \frac{1}{2}\sum_{ij}\sum_{\mu\nu}\epsilon_{ij}\left\langle\bar{\psi}_i|\bar{\psi}_j\right\rangle. \tag{5.10}$$

However, in the case that the dimension of the minimal basis is greater than the number of electrons (half the number if considering the spin-restricted orbital formalism), as will usually be the case, this is an underdetermined problem; there might exist a number of solutions, which all give the same orbital dipoles and $F = 0$ but different higher-order orbital multipole moments. For instance, for H_2 with a minimal reduced basis the solution to the minimisation is governed by the symmetry of the molecule, and the problem is not underdetermined. For HHe^+, there are two atomic orbitals whose coefficients can be varied to minimise the functional, but only one occupied orbital and thus only one constraint - normalisation. Consequently, changing one coefficient forces change in the other and thus only

one can freely change and exactly one choice of this parameter will give the desired orbital centroid and minimise F. Now, for HLi there are 6 parameters arising from two spatial orbitals and three basis functions; three of these are needed for the orthonormality constraint - for example one orbital varying to remain orthonormal to the other as it is optimised freely, and two are needed for the on-axis co-ordinate of the two orbital centroids. We have thus minimised L but have a parameter left over. This gives rise to an entire family of solutions with identical orbital dipoles and $F = 0$. By its nature, this deficiency will only grow worse as the number of parameters increases. To combat this, we introduce two penalty functions G and H, which are defined below. Both account for the right number of variables, and act as tie-breakers between similar minimisers of F.

$$G = -\sum_i \langle \psi_i | \bar{\psi}_i \rangle, \tag{5.11}$$

$$H = \sum_i \sum_{i \neq j} \left| \langle \psi_j | \bar{\psi}_i \rangle \right|^2. \tag{5.12}$$

The first penalty function, G, provides a means by which one imposes a bias towards minima of F for which the reduced orbitals take a shape as similar as possible to the reference orbitals, thus reducing the magnitude of corrections of higher l in the multipole expansion of the orbitals. The second penalty function, H, places no such bias on the optimisation and allows the orbitals to take whatever shape necessary to minimise F so long as the reduced orbital has nonzero overlap only with the orbital whose centroid is matched by the functional F. This allows greater flexibility in the reduced orbitals, and leads to shapes of the reduced orbitals which are naturally similar to those of the reference orbitals.

We thus arrive at the reduced orbital functional,

$$W = \sum_i \left| \langle \bar{\psi}_i | \vec{r} - \vec{r}_i | \bar{\psi}_i \rangle \right|^2 - w_G \sum_i \langle \psi_i | \bar{\psi}_i \rangle + w_H \sum_i \sum_{i \neq j} \left| \langle \psi_j | \bar{\psi}_i \rangle \right|^2, \tag{5.13}$$

$$= F + w_G G + w_H H, \tag{5.14}$$

where w_G and w_H are the weights of the penalty functions which are chosen to be small enough such that G or H act only as tie-breakers and do not result in the optimisation determining orbitals where the effect of the penalty functions is to

render F significantly different from zero.

The ROPA functional is in itself an interesting optimisation problem, and one for which the Lagrangian approach to the constrained optimisation of equation 5.13 becomes rather tricky when followed through and the form of the multipliers is much less clear than in the optimisation of F alone.[1] Let us first write the derivatives,

$$\frac{\partial F}{\partial \bar{C}_{\mu i}} = 4\left(\vec{\bar{r}}_i - \vec{r}_i\right) \cdot \left(\vec{\bar{r}}_{\mu\nu} - \vec{r}_i\, \bar{S}_{\mu\nu}\right) \bar{C}_{\nu i}, \tag{5.15}$$

$$\frac{\partial G}{\partial \bar{C}_{\mu i}} = -\Delta_{\mu\alpha} C_{\alpha i}, \tag{5.16}$$

$$\frac{\partial H}{\partial \bar{C}_{\mu i}} = 2\sum_{j\neq i} \langle \psi_j | \bar{\psi}_i \rangle \Delta_{\mu\alpha} C_{\alpha j}, \tag{5.17}$$

$$T_{\mu i} = \frac{\partial W}{\partial C_{\mu i}} = \frac{\partial F}{\partial \bar{C}_{\mu i}} + w_G \frac{\partial G}{\partial \bar{C}_{\mu i}} + w_H \frac{\partial H}{\partial \bar{C}_{\mu i}}, \tag{5.18}$$

where the short hand $\vec{\bar{r}}_{\mu\nu}$ is introduced and represents dipole integrals evaluated between basis functions μ and ν,

$$\vec{\bar{r}}_{\mu\nu} = \langle \bar{\chi}_\mu |\, \hat{r}\, | \bar{\chi}_\nu \rangle\,. \tag{5.19}$$

The usual convention applies (greek subscripts correspond to atomic orbital quantities and latin subscripts to molecular orbital quantities, and an overbar denotes the reduced basis). Lagrange's method of undetermined multipliers has been dropped here in favour of an unconstrained optimisation of the elements of an antisymmetric matrix, $\mathbf{X}$, where the reduced orbitals are rewritten as

$$\bar{C}_{\mu i} = \bar{C}_{\mu p}(\exp(\mathbf{X}))_{pi} \approx \bar{C}^0_{\mu i} + \bar{C}^0_{\mu p} X_{pi} + \frac{1}{2}\bar{C}^0_{\mu q} X_{qp} X_{pi} + \mathcal{O}(\mathbf{X}^2). \tag{5.20}$$

where in the last step the update to $\bar{C}_{\mu i}$ is approximated as an expansion, which then allows us to introduce the explicitly skew-symmetric,

$$X^-_{pq} = \frac{1}{2}(X_{pq} - X_{qp}) \qquad \frac{\partial}{\partial X^-_{pq}} = \frac{1}{2}\left(\frac{\partial}{\partial X_{pq}} - \frac{\partial}{\partial X_{qp}}\right) \tag{5.21}$$

[1] The method of undetermined Lagrange multipliers was the the first approach used to attempt to solve the problem of how one can find the optimum reduced orbitals, but keeping track of dummy variables became too difficult as the partial derivatives of different terms in the expressions were found.

which protects against the unwanted introduction of symmetric changes to $\mathbf{X}$ by updating $\bar{C}_{\mu i}$ as

$$\bar{C}_{\mu i} = \bar{C}^0_{\mu i} + \bar{C}^0_{\mu p} X^-_{pi} + \frac{1}{2}\bar{C}^0_{\mu q} X^-_{qp} X^-_{pi} + \mathcal{O}(\mathbf{X}^2), \tag{5.22}$$

thereby ensuring $\mathbf{X}$ remains antisymmetric. This is so that the matrix $\exp(\mathbf{X})$ remains orthogonal, and the rotations it affects in the orbitals do not break their orthonormality. The derivative of $\bar{C}_{\mu k}$ with respect to the elements of $\mathbf{X}^-$ is

$$\frac{\partial \bar{C}_{\mu k}}{\partial X^-_{pq}} = \frac{1}{2}(1 - \hat{\tau}_{pq})(\delta_{qk}\bar{C}^0_{\mu p} + \frac{1}{2}\bar{C}^0_{\mu r} X_{rp}\delta_{kq} + \frac{1}{2}\bar{C}^0_{\mu p} X_{qk}) \tag{5.23}$$

where δ is the Kronecker delta, and τ_{sj} replaces s by j and j by s in the indices of any quantity it acts upon. Equation 5.23 gives the change in the reduced orbital coefficients with respect to only the antisymmetric part of $\mathbf{X}$, which is precisely what is needed. Now write an expression for $\bar{C}^0_{\mu p} T_{\mu k}$ and collect terms, [2]

$$\begin{aligned}\bar{C}^0_{\mu p} T_{\mu k} = C^0_{\mu p} T^0_{\mu k} + 4(\vec{\bar{r}}_k - \vec{r}_k)\cdot(\vec{\bar{r}}_{pr} - \vec{r}_k\delta_{rp})X_{rk} + 8(\vec{\bar{r}}_{rk} - \vec{r}_k\delta_{rk})\cdot(\vec{\bar{r}}_{pk} - \vec{r}_k\delta_{pk})X_{rk} \\ + 2w_H \sum_{j\neq k}\langle\psi_j|\bar{\psi}_r\rangle\langle\psi_j|\psi_p\rangle X_{rk}.\end{aligned} \tag{5.24}$$

It is now possible to find a general expression for the Jacobian by evaluating

$$J_{pq} = \frac{\partial W}{\partial \bar{C}_{\mu k}} \cdot \frac{\partial \bar{C}_{\mu k}}{\partial X^-_{pq}}. \tag{5.25}$$

That is,

$$\begin{aligned}J_{pq} = (1 - \hat{\tau}_{pq})\Bigg(\delta_{qk}\Big(\bar{C}^0_{\mu p} T^0_{\mu k} + 4(\vec{\bar{r}}_k - \vec{r}_k)\cdot(\vec{\bar{r}}_{rp} - \vec{r}_k\delta_{rp})X_{rk} \\ + 8(\vec{\bar{r}}_{rk} - \vec{r}_k\delta_{rk})\cdot(\vec{\bar{r}}_{pk} - \vec{r}_k\delta_{pk})X_{rk} + 2w_H\sum_{j\neq k}\langle\psi_j|\bar{\psi}_r\rangle\langle\psi_j|\bar{\psi}_p\rangle X_{rk}\Big) \\ + \frac{1}{2}\bar{C}^0_{\mu r} T^0_{\mu k} X_{rp}\delta_{qk} + \frac{1}{2}\bar{C}^0_{\mu p} T^0_{\mu k} X_{qk}\Bigg),\end{aligned} \tag{5.26}$$

for which one can write simplified expressions for the occupied and occupied-virtual blocks. The virtual-virtual block is completely unimportant in this, as we only cre-

[2] One should note that the w_G dependence in 5.24 is contained within the term $T^0_{\mu k}$, since the function G is linear in $\bar{C}_{\mu k}$.

ate occupied reduced orbitals in order to reproduce the occupied reference orbitals from which the density is calculated. The occupied block is given by,

$$J_{ji} = (1-\hat{\tau}_{ji})\Big(\bar{C}^0_{\mu j}T^0_{\mu i} + 4(\vec{\bar{r}}_i - \vec{r}_i)\cdot(\vec{\bar{r}}_{rj} - \vec{r}_i\delta_{rj})X_{ri} + 8(\vec{\bar{r}}_{ri} - \vec{r}_i\delta_{ri})\cdot(\vec{\bar{r}}_{ji} - \vec{r}_i\delta_{ji})X_{ri} + 2w_H\sum_{l\neq i}\langle\psi_l|\bar{\psi}_r\rangle\langle\psi_l|\bar{\psi}_j\rangle X_{ri} + \frac{1}{2}\bar{C}^0_{\mu r}T^0_{\mu i}X_{rj} + \frac{1}{2}\bar{C}^0_{\mu j}T^0_{\mu k}X_{ik}\Big) \quad (5.27)$$

where Kronecker deltas have been evaluated wherever possible, likewise for the occupied-virtual block.

$$J_{ai} = \bar{C}^0_{\mu a}T^0_{\mu i} + 4(\vec{\bar{r}}_i - \vec{r}_i)\cdot(\vec{\bar{r}}_{ra} - \vec{r}_i\delta_{ra})X_{ri} + 8(\vec{\bar{r}}_{ri} - \vec{r}_i\delta_{ri})\cdot\vec{\bar{r}}_{ai}X_{ri} + 2w_H\sum_{j\neq i}\langle\psi_j|\bar{\psi}_r\rangle\langle\psi_j|\bar{\psi}_a\rangle X_{ri} + \frac{1}{2}\bar{C}^0_{\mu r}T^0_{\mu k}X_{ra}\delta_{ik} + \frac{1}{2}\bar{C}^0_{\mu a}T^0_{\mu k}X_{ik} - \frac{1}{2}\bar{C}^0_{\mu i}T^0_{\mu k}X_{ak}. \quad (5.28)$$

Having found expressions for the gradient, one might then ask the question of how these equations could be written into a piece of code. The problem is broken down into intermediate quantities,

$$\vec{D}_{pq} = (\vec{\bar{r}}_{pq} - \vec{r}_p\delta_{pq}) \qquad \vec{D}_p = \vec{D}_{pp} \text{ not summed}, \quad (5.29)$$

$$A_{pi} = \bar{C}^0_{\mu p}T^0_{\mu i}, \quad (5.30)$$

$$E_{pi} = \langle\bar{\psi}_p|\psi_i\rangle, \quad (5.31)$$

which gives us

$$J_{ji} = (1-\hat{\tau}_{ji})\Big(A_{ji} + 4\vec{D}_i\cdot(\vec{D}_{jr} + \vec{r}_j\delta_{jr} - \vec{r}_i\delta_{jr})X_{ri} + 8\vec{D}_{ir}\cdot\vec{D}_{ij}X_{ri} + 2w_H\sum_{l\neq i}E_{l\bar{r}}E_{l\bar{j}}X_{ri} + \frac{1}{2}A_{ri}X_{rj} + \frac{1}{2}A_{jk}X_{ik}\Big), \quad (5.32)$$

and

$$J_{ai} = A_{ai} + 4\vec{D}_i \cdot (\vec{D}_{ar} + \vec{r}_a\delta_{ar} - \vec{r}_i\delta_{ra})X_{ri} + 8\vec{D}_{ir} \cdot \vec{D}_{ia}X_{ri} + 2w_H \sum_{j\neq i} E_{j\bar{r}}E_{j\bar{a}}X_{ri} + \frac{1}{2}A_{ri}X_{ra} + \frac{1}{2}A_{ak}X_{ik} - \frac{1}{2}A_{ik}X_{ak}, \quad (5.33)$$

for the occupied and occupied-virtual blocks, respectively. Now define a new matrix, $\mathbf{Q}$ which is just the quantity in brackets in equation 5.32,

$$Q_{pi} = A_{pi} + 4\vec{D}_i \cdot (\vec{D}_{pr} + \vec{r}_p\delta_{pr} - \vec{r}_i\delta_{pr})X_{ri} + 8\vec{D}_{ir} \cdot \vec{D}_{ip}X_{ri} + 2w_H \sum_{l\neq j} E_{l\bar{r}}E_{l\bar{j}} + \frac{1}{2}A_{ri}X_{rp} + \frac{1}{2}A_{pk}X_{ik}, \quad (5.34)$$

which becomes

$$Q_{pi} = A_{pi} + 4\left(\vec{D}_i \cdot \vec{D}_{pr}X_{ri} + \vec{D}_i \cdot \vec{r}_pX_{pi} - \vec{D}_i \cdot \vec{r}_iX_{pi}\right) + 8\vec{D}_{ir} \cdot \vec{D}_{ip}X_{ri} + 2w_H \sum_{l\neq j} E_{l\bar{r}}E_{l\bar{j}} + \frac{1}{2}A_{ri}X_{rp} + \frac{1}{2}A_{pk}X_{ik}. \quad (5.35)$$

One thus arrives at simple formulae for the blocks of the Jacobian, which are

$$J_{ji} = Q_{ji} - Q_{ij}, \quad (5.36)$$

$$J_{ai} = Q_{ai} - \frac{1}{2}A_{ik}X_{ak}. \quad (5.37)$$

Now, let us assume we start very close to the solution, which given the projection we used is not unreasonable, and perturb by some small amount δ,

$$F = \sum_i |\langle\bar{\psi}_i + \delta|\vec{\vec{r}} - \vec{r}_i|\bar{\psi}_i + \delta\rangle|^2 \quad (5.38)$$

$$= \sum_i |\langle\bar{\psi}_i|\vec{r} - \vec{r}_i|\bar{\psi}_i\rangle + 2\langle\delta|\vec{\vec{r}} - \vec{r}_i|\bar{\psi}_i\rangle + \langle\delta|\vec{r} - \vec{r}_i|\delta\rangle|^2 \quad (5.39)$$

The first term inside the modulus goes zero, because F goes to zero. The second term is linear in $\bar{C}_{\mu i}$ and the third term is just some small constant. Thus the square of the linear term gives rise to a quadratic term as the highest power in F. F thus behaves as a quadratic in a sufficiently small neighbourhood of the

minimiser. This makes the BFGS algorithm outlined in section 3 an excellent choice for the minimisation problem.

Having generated the reduced orbitals, we have matched the orbital dipoles and thus expect the electrostatics of any molecule whose potential is dominated by the dipole term would be well represented by the reduced orbitals alone. Hydrogen cyanide is linear, with a dominating dipole term in the expansion of the density and thus is a good test for this hypothesis. If one performs a Kohn-Sham B3LYP calculation on HCN in the MINAO basis, one obtains a density which gives rise to the electrostatic potential mapped out in figure 5.1 (top, orange line). The grey line in the same map is the electrostatic potential arising from the density found performing the same calculation in the aug-cc-pVTZ basis. One can immediately see that the MINAO density fails to reproduce the electrostatics faithfully at all distances in every direction. In contrast, using the MINAO basis as the reduced basis, minimising the ROPA functional ($w_G = 0, w_H = 10^{-9}$) where the reference orbitals are localised Pipek-Mezey[3] (PM) orbitals in the aug-cc-pVTZ basis, one arrives at the red line in figure 5.1 (bottom), which is also shown alongside the aug-cc-pVTZ potential (grey). The potential arising from the reduced orbitals is seen to be remarkably faithful to the "exact" potential, and reproduces the electrostatics almost exactly, especially when one considers the aug-cc-pVTZ basis for this calculation has a dimension of 115, and the MINAO basis has a dimension of 11.

Once the reduced orbitals have been found, and the centroids match those of the reference orbitals, it is possible to define the Reduced Orbital Potential Approximation as,

$$V^{\mathrm{ROPA},L}(\vec{r}) = \sum_A Z_A|\vec{r}-\vec{A}|^{-1} + \sum_i J\left[-\left|\bar{\psi}_i\right|^2\right](\vec{r}) + \sum_i \sum_{lm}^{L} (-1)^m \left(Q_{lm}^i - \bar{Q}_{lm}^i\right) I_{lm}(\vec{r}-\vec{r}_i) \quad (5.40)$$

where the first term is the potential arising from the nuclei, the second is the potential arising from the reduced density, and the last term is a point correction to the

[3]The Pipek-Mezey localisation scheme is discussed in more detail in section 6.3.1.

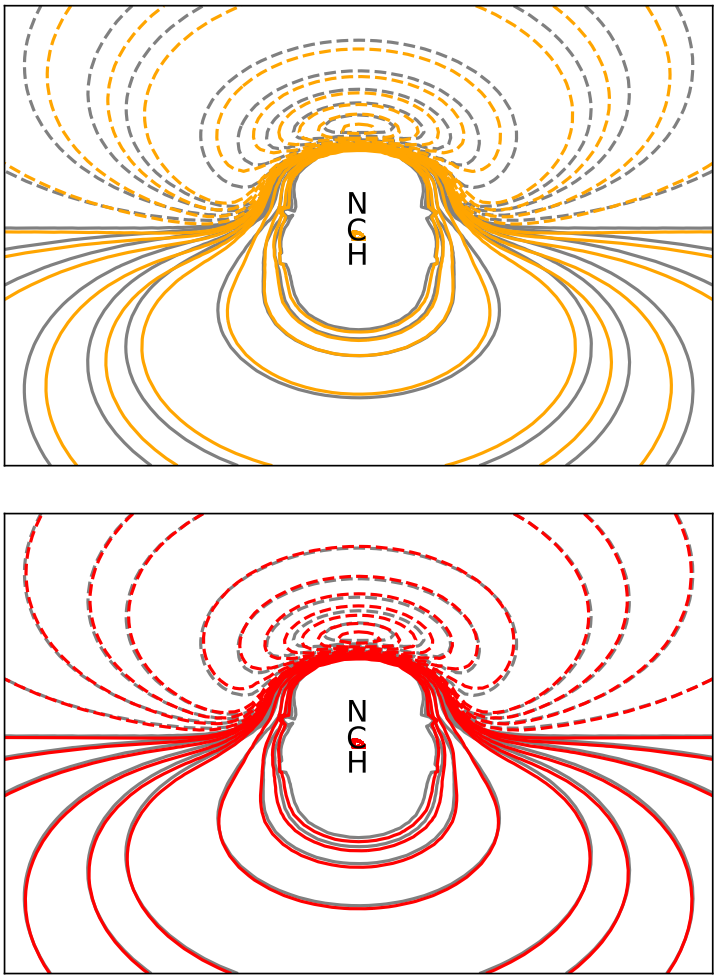

Figure 5.1: Contour plots of the electrostatic potential of HCN arising from the aug-cc-pVTZ Kohn-Sham density (grey line, both), the MINAO Kohn-Sham density (top, orange line), and the ROPA,0 potential with reduced orbitals in the MINAO basis (bottom, red line). Dashed and solid lines correspond to negative and positive values of the potential, respectively. The contour lines are chosen to be logarithmic for image clarity.

reduced orbital multipole moments using the multipole moments of the reference orbitals, i.e, the multipole moments used in OMA. There are several benefits to using this form for the potential as opposed to DMA or OMA. The screening effect upon penetration of the electron density is at least partially accounted for by the second term, and the use of an actual charge density means that at intermediate distances extra definition is added to the shape seen by the test point, without the inclusion of higher order moments. The final term is, however, where the power lies in the ROPA method; a model density is constructed from the reduced orbitals, and then corrections to its shape are made from the perspective of the test points

by using the difference between the multipole moments of the reduced orbitals and those of the reference orbitals. As a consequence, ROPA is expected to perform as well as, or better than OMA. Given that OMA performs approximately as well as DMA, ROPA represents an exciting alternative to both.

Figure 5.2 shows the difference between the exact potential and DMA, OMA and ROPA at a number of points along the molecular axis of carbon monoxide. The electrostatic potential of CO is dominated by the quadrupole moment, and as a consequence ROPA,0 performs poorly. Significant progress is made by the inclusion of the quadrupole moment correction (ROPA,2), but this correction goes too far at the oxygen end of the molecule. By the time one reaches the octopole moment, the potential has begun to converge nicely, and looks more stable. With the inclusion of the hexadecapole moment (DMA,4, OMA,4 and ROPA,4) we see that ROPA outperforms, in general, every other approach.

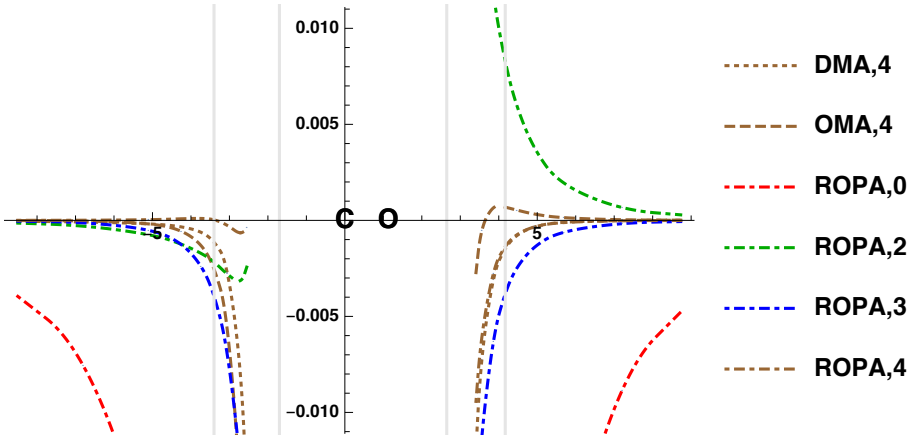

Figure 5.2: Error in ROPA electrostatic potentials / volt at points along the molecular axis of CO arising from a B3LYP calculation with the aug-cc-pVQZ basis. C is at the co-ordinate origin, and O at $(0, 0, r_e = 1.1282\text{Å})$. Distances of one and two van der Waals radii of the atoms ($r_C = 1.70\,\text{Å}$ and $r_\text{O} = 1.52\,\text{Å}$) are indicated in grey. [45]

It is beneficial to consider some more elaborate examples given the additional layer of complexity involved in constructing a ROPA potential. Glycine is again chosen as the test molecule to provide a basis for comparison to the OMA method outlined in the previous chapter, and the first step is to compare the B3LYP MINAO potential and the "exact" potential (in this case, the cc-pVTZ potential). Figure 5.3 shows two maps: the exact molecular electrostatic potential (grey) and the MINAO B3LYP potential (orange) superimposed for comparison. The dotted

lines in this figure represent negative potentials and the solid lines represent positive potentials. One can see immediately, that not only is the shape of the electrostatic potential (ESP) incorrect, there are enormous regions which are attractive when they ought to be repulsive. The electrostatic potential (ESP) to the left side of the glycine molecule is very poorly replicated by the MINAO B3LYP density, and even quite far from the molecule in the lower right corner, the potential is incorrect.

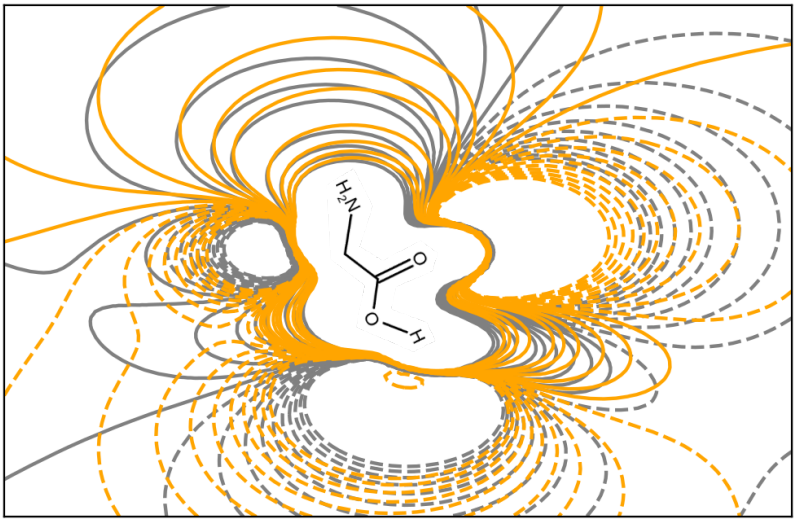

Figure 5.3: Contour maps of the molecular electrostatic potential arising from glycine, calculated with the B3LYP density using cc-pVTZ (grey line) and MINAO (orange line) basis sets. A dashed line indicates contours at negative values, and a solid line indicates contours at positive values.

Figure 5.4 shows the ROPA,0-3 potential maps for glycine. The reference orbitals were optimised in the cc-pVTZ basis, and the reduced basis is MINAO. ROPA,0 clearly outperforms the B3LYP MINAO density when compared to the cc-pVTZ potential (grey line). Regions which are repulsive and attractive are well reproduced. The change in electrostatic potential is not perfect, but the same features are there, and as a model density goes it performs quite well. ROPA,2 is a significant improvement over ROPA,0 and ROPA,3 almost perfectly reproduces the exact potential. Simply including the quadrupole correction term in the expansion largely remedies the errors in the potential at all distances where contours are shown (the pentration effects which only become visible after the inclusion of the quadrupole are clear to see, but less striking than in the OMA case, as should be expected). ROPA,3 continues the trend of convergence and represents an extremely accurate potential. By sampling points close to the van der Waals radius of the

molecule, one obtains an idea of the convergence behaviours and accuracies of both the OMA and ROPA approximations. The OMA,0, OMA,2 and OMA,3 approximations have, in this case, a root mean square error value of 0.2439, 0.1301 and 0.06737 respectively, showing a good increase in accuracy as higher rank multipoles are included in the OMA expansion. However, OMA is significantly outperformed by ROPA in this measure as the ROPA,0, ROPA,2 and ROPA,3 approximations have root mean square error values of 0.0395, 0.02805 and 0.0278, respectively, indicating that to achieve a ROPA,0 level of performance with OMA close to the density one must include terms beyond $L = 3$ in the expansion.

One criticism of the early DMA methods was that the multipoles associated with different atomic DMA sites were unstable under the change of basis set, as discussed in section 4.3, until a new method was suggested by Stone which showed an improvement in the stability of the multipole moments as basis set size was increased. [35] Here the stability of the multipole moments of the reduced and reference orbitals are discussed, with the example being those used to calculate the electrostatic potential for CO in this section. Figure 5.5 shows the absolute multipole moments for the reduced and reference molecular orbitals (top in each subfigure) and the difference between the appropriate aug-cc-pVQZ basis and each data point, to show any convergence behaviour.

Examination of figure 5.5 (a) and (b), noting the scale, one notices that the orbital multipoles for the s-orbitals hardly change with basis set - as one should expect. They begin almost exactly spherical, and remain that way with only some small contamination in high rank multipole moments. They are unimportant, and in future iterations of ROPA will likely be replaced by point charges at the centroid (i.e, on the nucleus). However, strong convergent behaviour is seen for all multipole moments up to octopole, with the hexadecapole moment being slightly erratic in the reduced orbitals. The multipole moments of the lobes on the carbon and oxygen (figures 5.5 (c) and (d)) reveal that for more difficult shapes, the orbital multipoles for both reference and reduced orbitals converge with basis set. In particular this can be seen if the series of augmented and regular basis sets are considered independently, i.e, trace the line between avdz, avtz and avqz and the convergence is clear. One can also see that the reduced orbital multipole moments

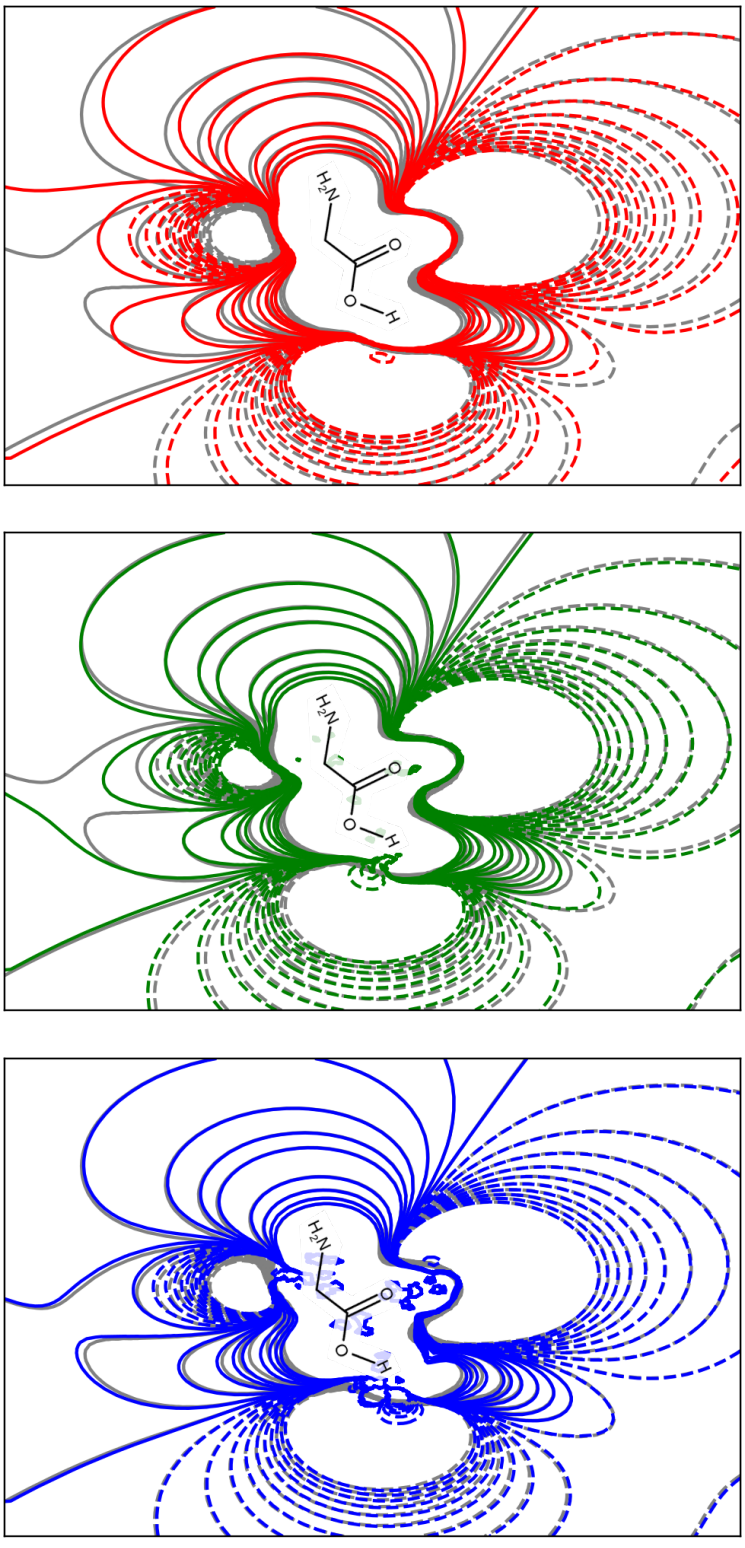

Figure 5.4: Contour maps of the molecular electrostatic potential arising from glycine in the glycine-water dimer, calculated using the ROPA,0, ROPA,2 (middle) and ROPA,3 (bottom). Solid and dashed lines indicate positive and negative electrostatic potentials, respectively. The electrostatic potential calculated from the optimised cc-pVTZ density (grey) is included for reference in each subfigure.

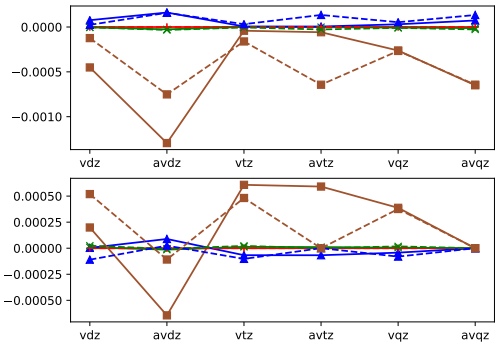

(a) oxygen 1s

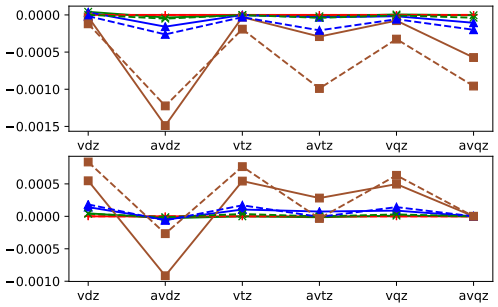

(b) carbon 1s

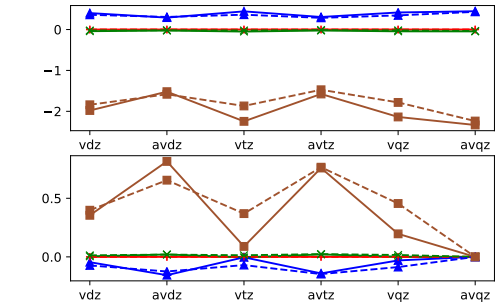

(c) oxygen lobe

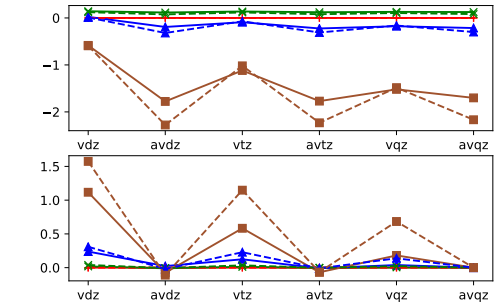

(d) carbon lobe

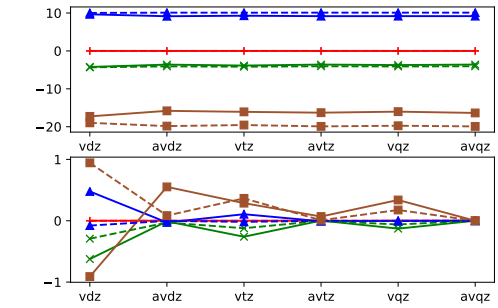

(e) π-bond

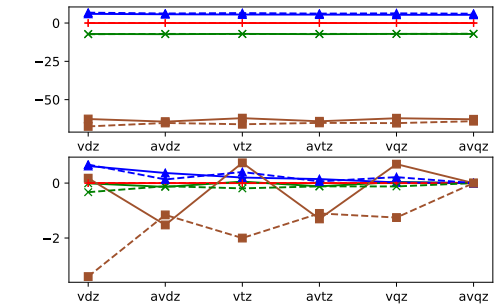

(f) σ-bond

Figure 5.5: Absolute multipole moments (top) for each orbital (solid line) and each reduced orbital (dashed line) for the CO molecule, and the difference compared with the largest basis (bottom) in atomic units. The red lines (+ data markers) correspond to dipoles, green (×) to quadrupoles, blue (▲) to octopoles and brown (■) to hexadecapoles. To avoid duplicate data, only one π-bonding orbital shown.

in general show improved stability over the reference orbitals; this likely arises due to the decrease in variational flexibility when one goes from a large basis set to a minimal one. The most interesting are likely the bonding orbital multipole moments, which show fantastic convergence in the reduced basis, and are very stable up to octopole. The π-bonding orbital shows good stability of all moments. These results can easily be compared to those of Stone. [35] Comparison yields the conclusion that both approaches are similar in terms of stability of the multipoles for the most part, with the stability of Stone's multipole moments for the C and O DMA sites being slightly better. This is not a surprise, given the characterful shapes of the bonding orbitals and lobes in comparison to the almost spherical atomic contributions to the density in that version of DMA. In fact, one might be surprised at the stability of the orbital multipoles.

5.2 The Orbital Field Approximation

In section 4.2.1, the brief discussion of the relationship between the electrostatic potential and the electric field is enough to define an *Orbital Field Approximation* (OFA) to the electric field,

$$F_\alpha^{\mathrm{OFA}}(\vec{r}) = -\sum_A T_\alpha^A Z_A + \sum_i \left[-T_\alpha^i q^i + T_{\alpha\beta}^i \mu_\beta^i - \frac{1}{3} T_{\alpha\beta\gamma}^i \Theta_{\beta\gamma}^i + \frac{1}{15} T_{\alpha\beta\gamma\delta}^i \Omega_{\beta\gamma\delta}^i - \ldots \right] \tag{5.41}$$

which is exactly the derivative of the OMA potential in equation 4.48 with respect to whichever direction happens to be the index α multiplied by minus one, and one specifies the highest order multipole in the same way and truncates the term in the square bracket. For example OMA,2 goes up to quadrupole in the expansion, and OFA,2 truncates after the third term in the square brackets - the quadrupole term. Cartesian co-ordinates are chosen for their simplicity in the differentiation and functional form at low L. Figure 5.6 shows the difference between the "exact" total electric field values along the molecular axis of CO and the OFA total electric field.

One is immediately struck by the accuracy (see the y-axis scale in figure 5.6) of the OFA,3 electric field, which performs better, and diverges closer to the molecule

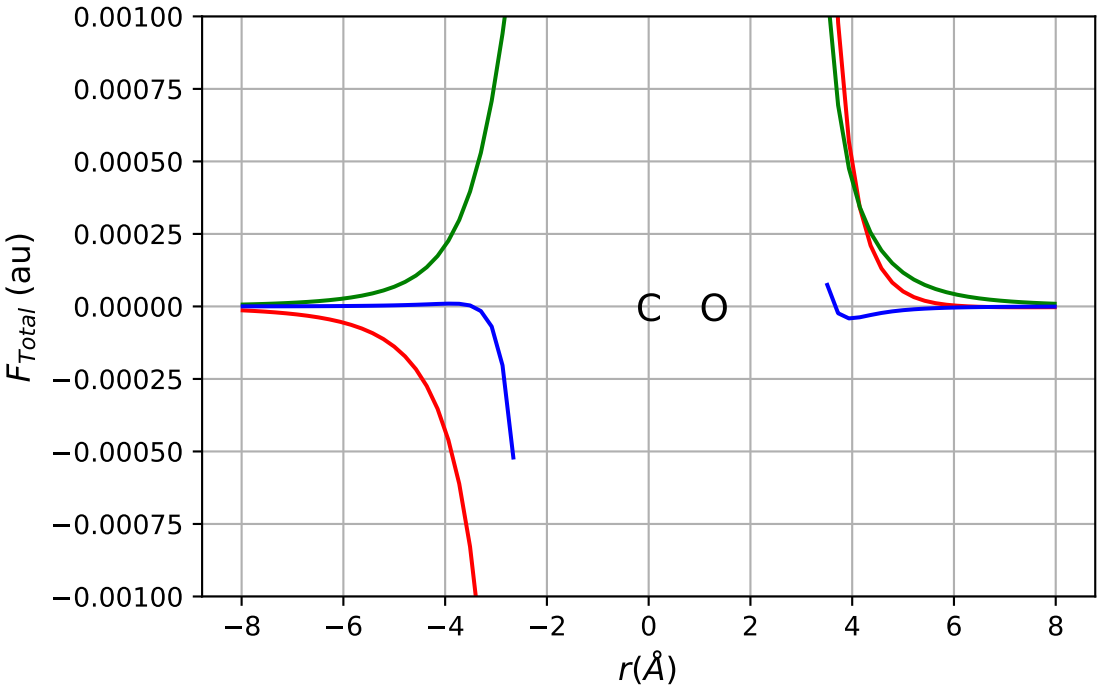

Figure 5.6: Error in OFA total electric field at points along the molecular axis of CO arising from a B3LYP calculation with the aug-cc-pVQZ basis. C is at the coordinate origin, and O at $(0, 0, r_e = 1.1282\text{Å})$. The red line corresponds to OFA,0, green line to OFA,2 and blue line to OFA,3.

than all approximations to the electric field we'll see in this thesis, with OFA,0 performing poorly at both ends of the molecule, and OFA,2 likewise, although an improvement over OFA,0. This is somewhat surprising, and is potentially a fortuitous anomaly. Figure 5.7 shows contour maps of the electric field arising from glycine, i.e, analogous to the plots for the potential in figure 4.5. One sees in this series of plots that OFA,3 outperforms OFA,0 and OFA,2 almost everywhere, but suffers some instability close to the molecule. The accuracy of OFA,0 is perhaps better than one might have expected, and the inclusion of higher order moments has a smaller impact on the shape of the field in comparison to the impact the inclusion of higher order moments in the expansion of the potential has on the shape of the molecular electrostatic potential (MEP). As a result, the rate of convergence to a strong representation of the electric field is less striking, but of course, still present. OFA,2 yields an excellent representation of the field, with some small regions in error (for instance, the lower left corner of the middle image in figure 5.7). OFA,3 yields the best representation, almost exactly reproducing the field in most areas. However, there is some inaccuracy close to the hydroxy oxygen at all ranks.

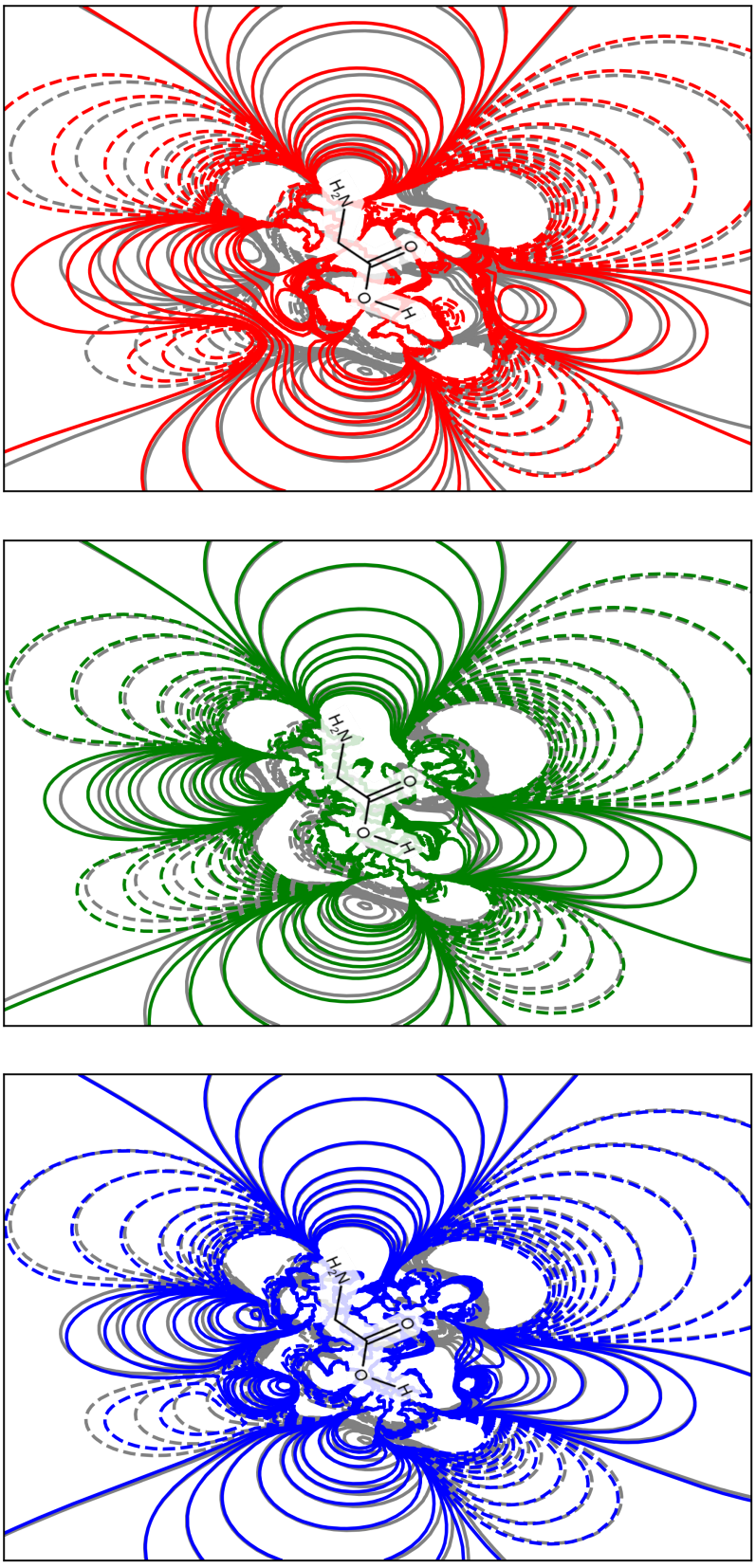

Figure 5.7: The OFA,0 (top, red), OFA,2 (middle, green) and OFA,3 (bottom, blue) approximations to the total electric field of glycine.

In much the same way as the OFA expression was derived, one can write down an expression for G^{OFGA}, the *orbital field gradient approximation* (OFGA),

$$G^{\mathrm{OFGA}}_{\alpha\beta}(\vec{r}) = -\sum_A T^A_{\alpha\beta} Z_A + \sum_i \left[-T^i_{\alpha\beta} q^i + T^i_{\alpha\beta\gamma}\mu^i_\gamma - \frac{1}{3} T^i_{\alpha\beta\gamma\delta}\Theta^i_{\gamma\delta} + \frac{1}{15} T^i_{\alpha\beta\gamma\delta\epsilon}\Omega^i_{\gamma\delta\epsilon} - \ldots \right]. \tag{5.42}$$

5.3 The Reduced Orbital Field Approximation

Differentiating equation 5.40 and multiplying by minus one, one arrives naturally at an expression for the *Reduced Orbital Field Approximation* (ROFA),

$$\begin{aligned} F_\alpha^{\mathrm{ROFA}}(\vec{r}) = &-\sum_A T_\alpha^A Z_A + \sum_i F_\alpha[|\bar{\psi}_i|^2](\vec{r}) \\ &+ \sum_i \left[-T_\alpha^i q^i + T_{\alpha\beta}^i \mu_\beta^i - \frac{1}{3} T_{\alpha\beta\gamma}^i \Theta_{\beta\gamma}^i + \frac{1}{15} T_{\alpha\beta\gamma\delta}^i \Omega_{\beta\gamma\delta}^i - \dots \right] \\ &- \sum_i \left[-\bar{T}_\alpha^i \bar{q}^i + \bar{T}_{\alpha\beta}^i \bar{\mu}_\beta^i - \frac{1}{3} \bar{T}_{\alpha\beta\gamma}^i \bar{\Theta}_{\beta\gamma}^i + \frac{1}{15} \bar{T}_{\alpha\beta\gamma\delta}^i \bar{\Omega}_{\beta\gamma\delta}^i - \dots \right] \end{aligned} \tag{5.43}$$

where in this context $F_\alpha[|\bar{\psi}_i|^2](\vec{r})$ is the electric field arising at a point $\vec{r}$ due to the presence of the reduced density. Figure 5.8 shows the difference between the "exact" total electric field values along the molecular axis of CO and the ROFA total electric field.

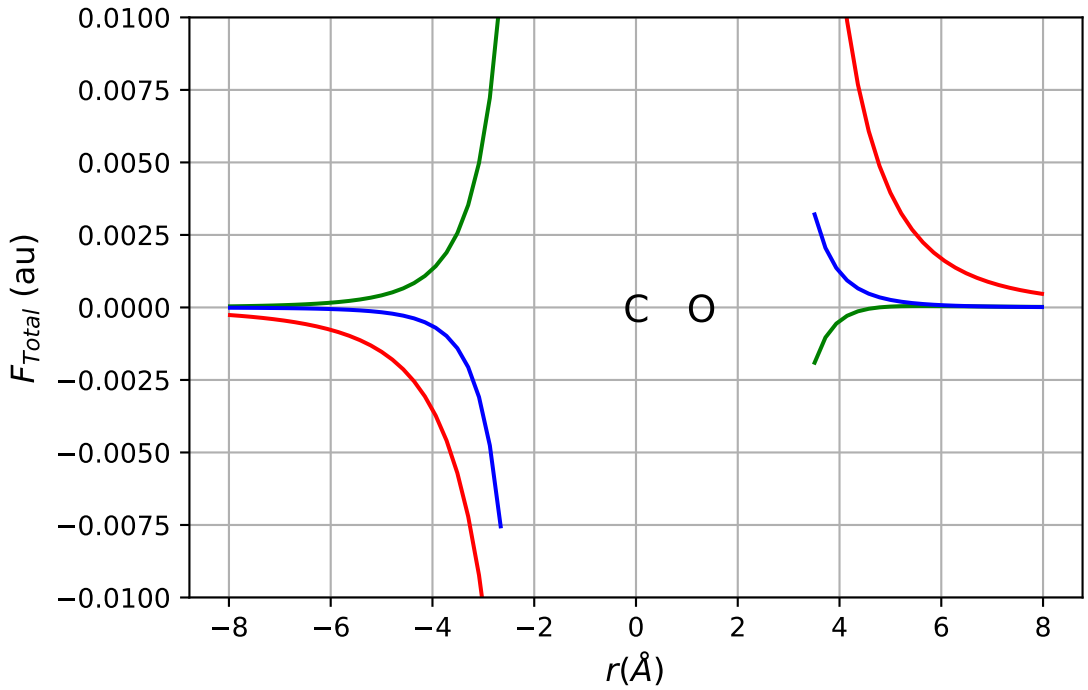

Figure 5.8: Error in ROFA,0 (red), ROFA,2 (green) and ROFA,3 (blue) total electric field at points along the molecular axis of CO arising from a B3LYP calculation with the aug-cc-pVQZ basis. C is at the co-ordinate origin, and O at $(0, 0, r_e = 1.1282\text{Å})$.

The fields calculated using ROFA,0-3 are surprisingly poor in comparison to those calculated using OFA,0-3, though they are still more stable than the ROPA

potentials and are only underwhelming for the CO case as a result of the outstanding results OFA produces. A more fruitful discussion can be had by comparing the data represented in figures 5.9 and 5.7. While both OFA and ROFA produce outstanding approximations to the electric field for glycine, ROFA is the only one of the two closely reproduce the electric field close to the hydroxy oxygen. The presence of an erroneously positive electric field in this region in the OFA,0 and OFA,2 cases is remedied in the ROFA case as a result of the model density.

If one is interested in an approximate field gradient, differentiating the expression for G^{ROFA} provides an expression for the *reduced orbital field gradient approximation* (ROFGA),

$$\begin{aligned} G^{\mathrm{ROFGA}}_{\alpha\beta}(\vec{r}) = &-\sum_A T^A_{\alpha\beta} Z_A + \sum_i G_{\alpha\beta}[|\bar{\psi}_i|^2](\vec{r}) \\ &+ \sum_i \left[-T^i_{\alpha\beta} q^i + T^i_{\alpha\beta\gamma}\mu^i_\gamma - \frac{1}{3} T^i_{\alpha\beta\gamma\delta}\Theta^i_{\gamma\delta} + \frac{1}{15} T^i_{\alpha\beta\gamma\delta\epsilon}\Omega^i_{\gamma\delta\epsilon} - \ldots \right] \\ &- \sum_i \left[-\bar{T}^i_{\alpha\beta} \bar{q}^i + \bar{T}^i_{\alpha\beta\gamma}\bar{\mu}^i_\gamma - \frac{1}{3} \bar{T}^i_{\alpha\beta\gamma\delta}\bar{\Theta}^i_{\gamma\delta} + \frac{1}{15} \bar{T}^i_{\alpha\beta\gamma\delta\epsilon}\bar{\Omega}^i_{\gamma\delta\epsilon} - \ldots \right]. \end{aligned} \tag{5.44}$$

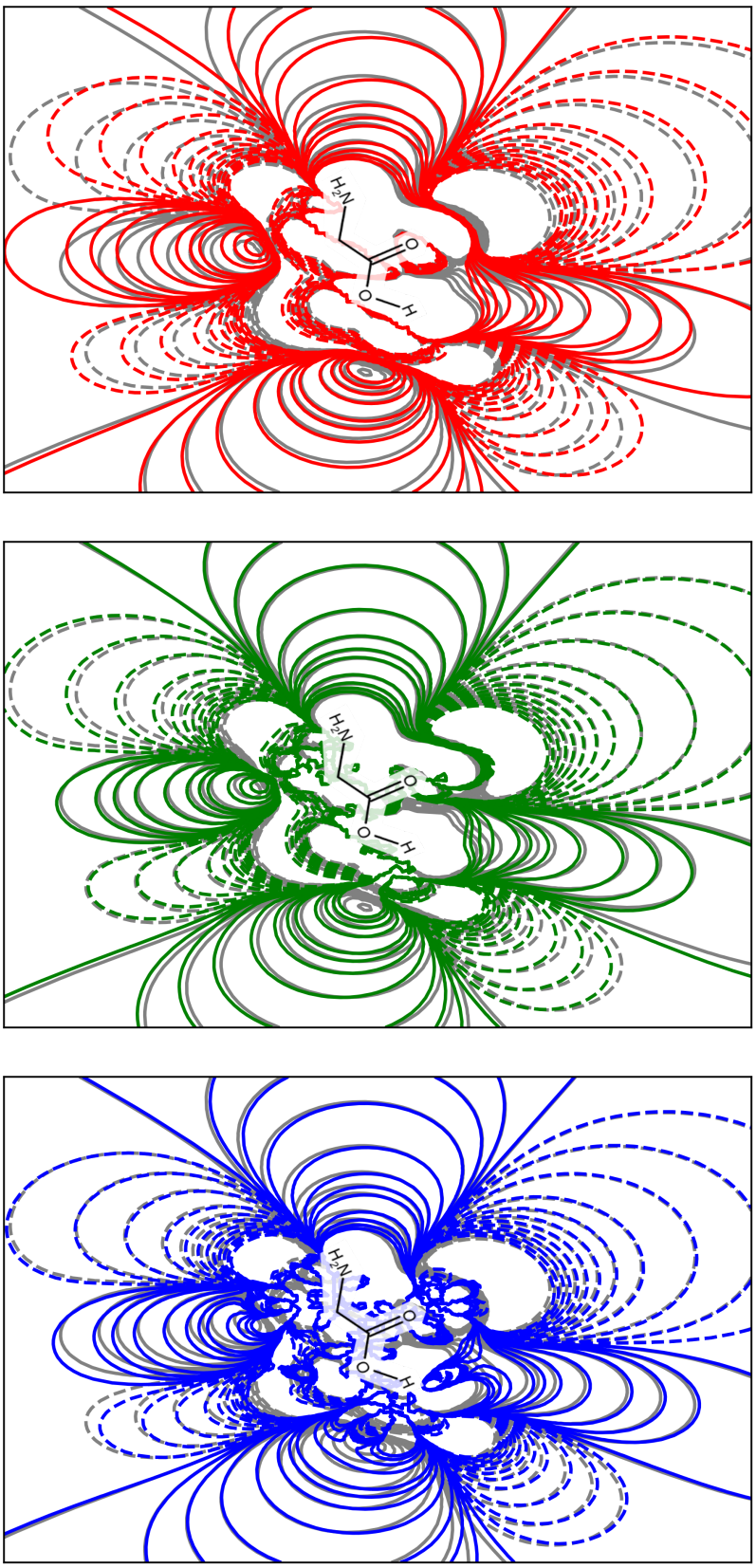

Figure 5.9: The ROFA,0 (top, red), ROFA,2 (middle, green) and ROFA,3 (bottom, blue) approximations to the total electric field of glycine.

5.4 Symmetry: LMOs vs Canonical MOs

Orbital localisation routines often break the D_{6h} symmetry of the benzene canonical orbitals and produce orbitals of D_{3h} symmetry, which closely resemble the orbitals one might expect from a single Kekulé resonance structure. Given that the expansion is performed on each orbital in turn, this could present an issue for the electrostatic potentials calculated using OMA or ROPA. In this section we explore how severe this impact is for both OMA and ROPA when applied to benzene Intrinsic Bond Orbitals (IBOs)[4], and weigh the pros and cons of using canonical orbitals in their stead for cases of high symmetry. [76] Figure 5.10 shows both one canonical and one IBO orbital describing the $\pi-$ system in benzene.

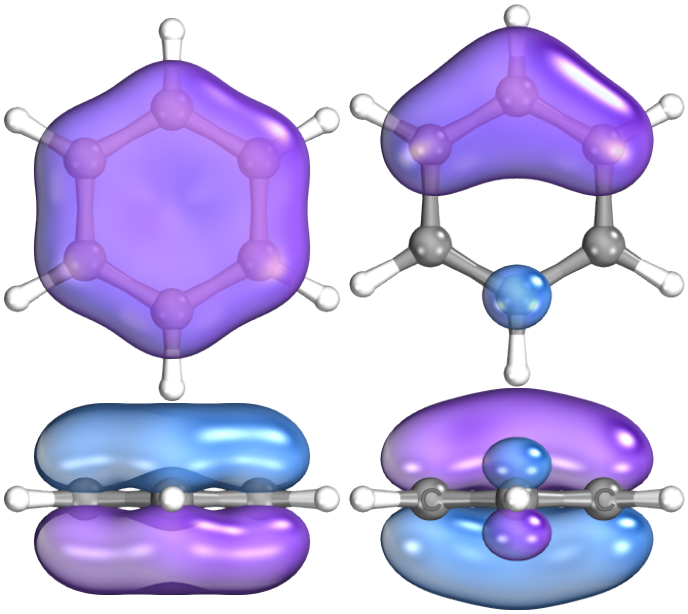

Figure 5.10: Canonical orbital π-system benzene (left column) and one intrinsic bond orbital belonging to the π-system (right column). Both sets of orbitals were generated with the cc-pVTZ basis and the B3LYP density functional.

To assess the impact of breaking the symmetry of the orbitals through localisation, let us perform a short case study on benzene. This case study will involve two identical treatments of two sets of orbitals: a set of IBOs for benzene, the potential arising from which we shall expand according to both the OMA and ROPA recipes, and likewise for a set of canonical orbitals. For consistency the entire study is carried out using the B3LYP density functional and the cc-pVTZ basis set. First, we take an optimised benzene geometry, move the centre of the ring to the origin,

[4]The IBO routine is discussed in more detail in section 6.3.1.

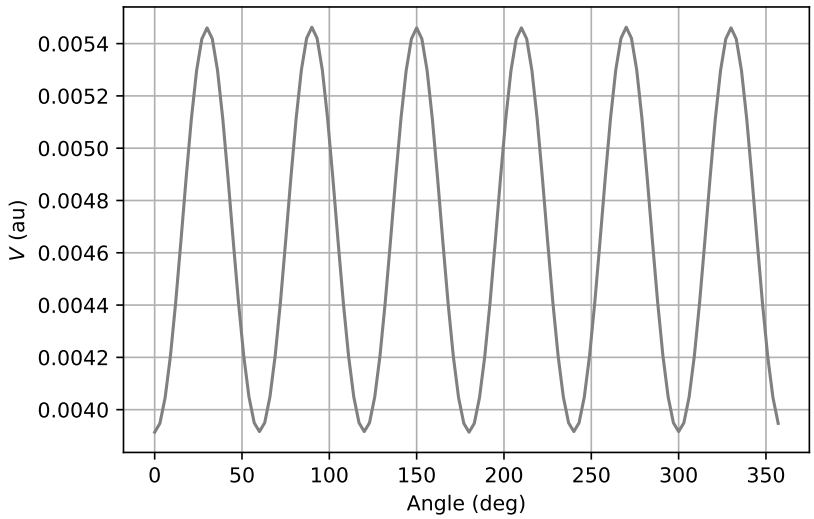

Figure 5.11: The potential arising on the circle around benzene, in the molecular plane, defined by radius $r = ||\vec{r}_{\mathrm{H}}|| + 2\mathrm{H}_{\mathrm{vdW}} = 9.22376$ Bohr, equidistant from all hydrogen atoms. The potential is calculated using the molecular density and not a multipole expansion.

rotate the geometry into the xy-plane, and define a circle in the molecular plane also centred at the origin with radius $r = ||\vec{r}_{\mathrm{H}}|| + 2\mathrm{H}_{\mathrm{vdW}} = 9.22376$ bohr radii (here $\mathrm{H}_{\mathrm{vdW}}$ is the van der Waals radius of hydrogen and $\vec{r}_{\mathrm{H}}$ is the position vector of any H atom in the system). [77] Any point, (x, y), on the circle is thus defined by the angle θ according to $(\cos(\theta), \sin(\theta))$. In this study we take 120 evenly spaced points around the ring. Figure 5.11 shows the potential on the circle as a function of θ calculated using the molecular density and for the purposes of this section shall be referred to as the "exact" potential. As one should expect, there are 6 equivalent minima evenly spaced around the circle, one at each point closest to a H atom and 6 equivalent maxima opposite the centres of each carbon-carbon bond. The exact potential is of $\mathrm{D}_{6\mathrm{h}}$ symmetry.

Figure 5.12 shows the potentials calculated using the OMA and ROPA recipes, where the orbitals used in the large basis are IBOs. Both sets of potentials clearly break the $\mathrm{D}_{6\mathrm{h}}$ symmetry and are of the same symmetry as the IBOs, as one may have expected. ROPA performs better than all OMA expansions even at rank zero; the symmetry breaking and absolute errors are both smaller. The errors reduce upon inclusion of higher order multipole moments for both OMA and ROPA. The $\pi-$bonding IBOs are each centred on every other carbon atom, one centroid every 120°. Thus the potential is expected to have 6 equivalent minima which are slightly

displaced from 60° intervals, and 2 sets of 3 equivalent maxima which alternate around the ring. This is exactly what is seen in figure 5.12 for all expansions but OMA,2, where the nuclear potential overcomes the weak maxima in the expansion of the electronic potential and the symmetry is broken further.

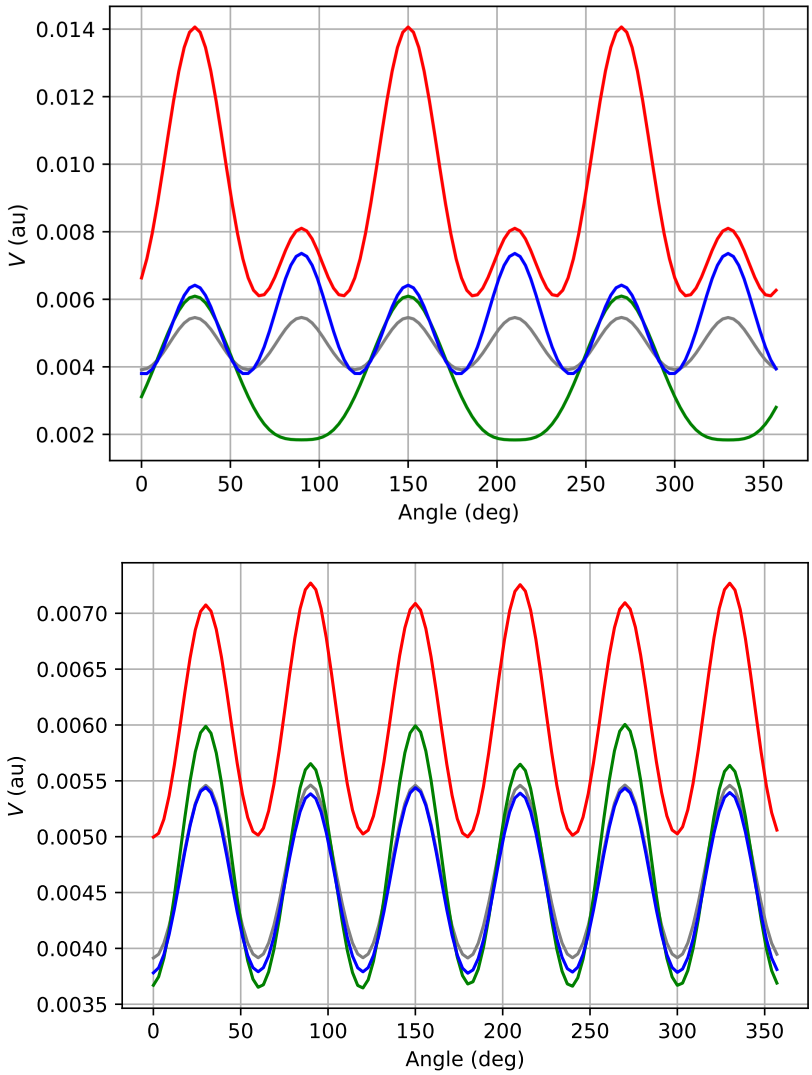

Figure 5.12: The exact (grey), OMA,0 (top, red), OMA,2 (top, green), OMA,3(top, blue), ROPA,0 (bottom, red), ROPA,2 (bottom, green), ROPA,3 (bottom, blue) potentials on a ring around benzene with radius 9.224 au around the centre of mass. The reference orbitals are the B3LYP, cc-pVTZ IBOs.

Table 5.1 contains numerical measures of the symmetry breaking of the OMA and ROPA potentials calculated using both sets of orbitals. The ROPA potentials calculated with localised orbitals clearly approach the correct symmetry, and are extremely close after the inclusion of the octopole moments in the expansion. OMA performed using localised orbitals also approaches the correct symmetry, but much

more slowly than ROPA. In the canonical case ROPA is seen to be far less sensitive to the use of canonical orbitals than one may have expected, and the potentials are extremely close to the exact potential, especially once a quadrupole correction has been included. This is likely due to an absence of localisation tails, and the high symmetry yielding a good approximation to the density through the projection to the MINAO basis alone. The canonical OMA potentials are by far the least accurate, but yield the correct symmetry.

Method	$V_{\max}$	$V_{\min}$	$V(30°) - V(90°)$	$\theta_{\min} - 60°$
Exact	0.00546	0.00391	0.00000	-0.01
Localised orbitals:				
OMA,0	0.01405	0.00610	0.00596	6.95
OMA,2	0.00609	0.00184	0.00425	30.0
OMA,3	0.00735	0.00378	-0.00094	-1.54
ROPA,0	0.00727	0.00501	-0.00020	-0.46
ROPA,2	0.00598	0.00364	0.00033	0.78
ROPA,3	0.00544	0.00379	0.00001	0.00
Canonical orbitals:				
OMA,0	0.13888	0.12556	0	0
OMA,2	0.02144	0.00812	0	0
ROPA,0	0.00595	0.00413	0	0
ROPA,2	0.00571	0.00389	0	0

Table 5.1: Symmetry breaking in the maximum and minimum electrostatic potentials for benzene. Potentials are given in au, angles in degrees. $V_{\max}$, $V_{\min}$ are the maximum and minimum values of the potential, wherever they occur. $V(30°) - V(90°)$ is the difference between the maxima at 30 and 90 degrees which are equivalent maxima if the potential is of the correct (D_{6h}) symmetry, and $\theta_{\min} - 60°$ is the difference in angle of the potential minima from those angles expected by molecular symmetry.

Figure 5.13 shows the potentials calculated using the canonical orbitals for the OMA expansion, and as reference for the ROPA expansion. The centroids are all at the centre of the molecule, and since the octopole operator carries only ungerade representations of D_{6h} the octopole moments are zero by symmetry. OMA,2 is thus the same as OMA,3 and ROPA,2 the same as ROPA,3. The small errors seen in figure 5.13 are perhaps surprising, and show that the canonical orbitals are a reasonable alternative reference set of orbitals for the generation of the reduced orbitals where symmetry makes localisation an unappealing option.

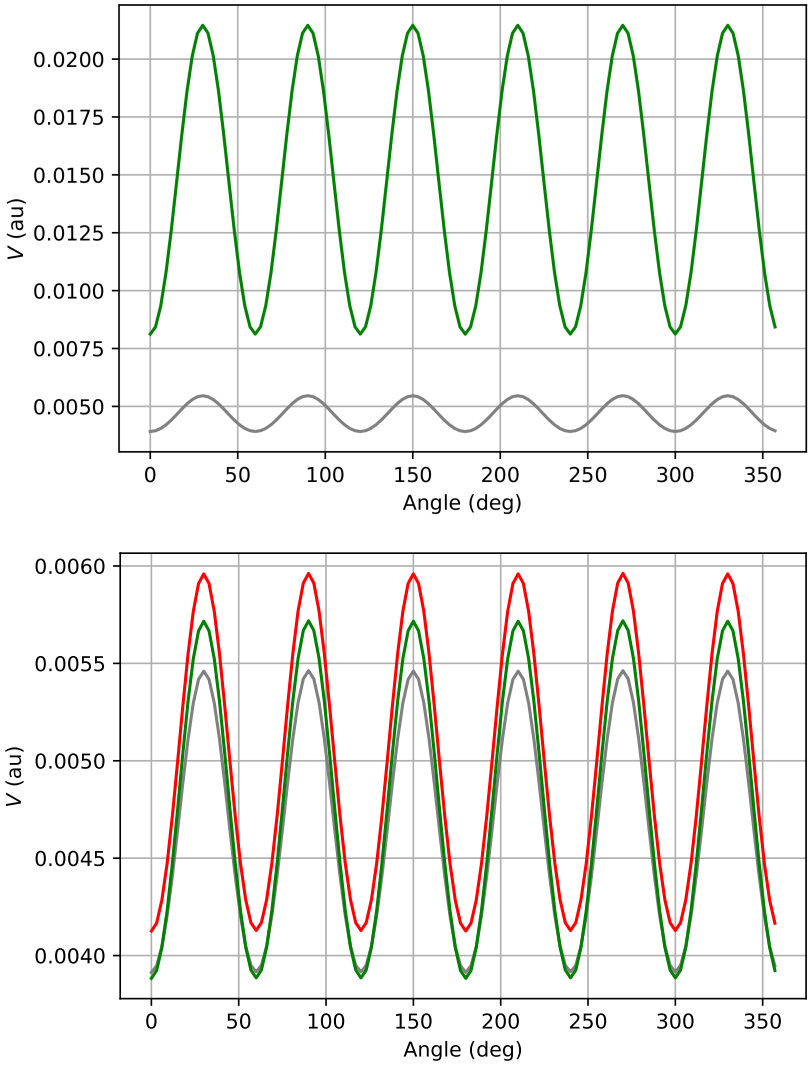

Figure 5.13: The exact (grey), OMA,2 (top, green), ROPA,0 (bottom, red), and ROPA,2 (bottom, green) potentials on a ring around benzene with radius 9.224 au around the centre of mass. The reference orbitals are the canonical orbitals arising from a Kohn-Sham B3LYP calculation in the cc-pVTZ basis.

5.5 Conclusions

On the basis of the data presented in this chapter, and the previous one, it is clear that, in cases where symmetry does not prevent the determination of well-localised orbitals, OMA provides a reasonably good approximation to the molecular electrostatic potential, but must be used with caution in cases of high symmetry and is at all ranks sensitive to the symmetry of the orbitals, rather than the nuclear positions. On the basis of the data shown in this chapter, and the previous one, the only argument for using OMA over ROPA is one of computational expense, and clearly ROPA will always be more expensive than OMA, but the dimension of the reduced basis will always be small and one must ask questions about the balance of accuracy and computational cost on a case by case basis. In systems of high symmetry, it has also been shown that high rank ROPA potentials are very close to the correct symmetry, even if the reference orbitals are not. Of course, one can always fall back on canonical orbitals in cases of doubt and rest assured that the potentials provided by both ROPA and OMA will carry the correct symmetry. The OMA potentials have been shown in this chapter to be inaccurate by comparison to ROPA potentials for benzene. No comment is made concerning the computational expense of DMA, as it entirely depends on the chosen method for partitioning the electron density into atomic regions. Some of these methods are extremely computationally expensive, and some are not, for instance Stone recommends Bader's method of atoms in molecules (AIM), which requires a notoriously expensive, real-space topological analysis of the molecular electron density. [26, 35, 78]

OFA, OFGA are first and second derivatives of the OMA expression (multiplied by minus one), respectively, and will thus carry any of the benefits and defects in OMA, and so they require little further discussion. The same goes for the relationship between ROFA, ROFGA and ROPA. That is, the symmetry of the fields and field gradients obtained from these methods follow the same rules as the potentials provided by OMA and ROPA.

It is anticipated that ROPA may be of interest to those studying large molecules, wishing to extract a model potential without the enormous cost of calculating it exactly. A unique selling point of ROPA,0 is that a good model density can be obtained with knowledge of the orbital centroids alone, and thus one can imagine a

scenario where centroids associated with functional groups are part of a database, and reduced orbitals and their associated potentials can be determined on the fly. Potentials of large molecules are beyond the scope of this thesis but present an interesting challenge which might be partly solved by the use of a simple model density calculated from a set of reduced orbitals. Moreover, the use of localised orbitals allows for predictable locations of orbital centroids for functional groups, and clearly strengthens the case for the development of a "ROPA for large molecules" which would in the same breath provide field and field gradient information by simple differentiation and change of sign.

It is common in molecular mechanics calculations to reduce the multipole expansion to its leading term, and to parameterise forcefields through a fitting procedure which optimises atomic point charges to reproduce the exact electrostatic potential as closely as possible and to then describe other non-bonding effects using a Lennard-Jones potential. In fact, in most commercial molecular mechanics packages and forcefields, there is no inclusion of even dipole moments in the formulae used for electrostatic interactions. [26, 55, 79] As a result, anisotropic features of the electrostatic potential are not well reproduced, and whether or not one obtains "correct" results rests upon ones ability to choose the appropriate forcefield for the simulation. This is a choice which is not always clear as quantitative justification can be difficult to come by. [26] This omission of higher order moments appears to arise through a reluctance to increase computational expense by performing transformations of multipole moments between local and global co-ordinate systems. [8] If, for some reason, this changes and higher order multipoles are included it is beyond any doubt that the chosen method will be the DMA or some other atom-based scheme, as the atomistic description used in molecular mechanics is unlikely to undergo significant change. As a consequence, it is unlikely that the ROPA method will provide a suitable component for molecular mechanics force fields.

Chapter 6

Ab Initio Chemical Bonding Insights

The purpose of this chapter is to provide a review of the current understanding of chemical bonding. As this topic is so large and encompasses most of chemistry, emphasis is placed upon those aspects most relevant to the new work presented in the next chapter.

The first section of this chapter comprises a comparison between the basics of MO theory and valence bond theory, and a justification of why the remainder of the chapter resides within the MO theory framework. The second section is a review of the two prevailing schools of thought on the precise physical description of covalent bonding. The third section briefly covers common practices for gaining insight into chemical bonding in different systems, and there is a strong emphasis placed on those methods which provide energetic insight.

6.1 MO and Valence Bond Methods

In general, when chemists discuss different molecules, they speak of functional groups, atoms and bonds. The MO approach to solving the Schrödinger equation is built upon no such preconception, and as a result when one looks at a computer rendered image of, for instance, a Hartree-Fock canonical orbital it rarely resembles the organic chemist's bonding, anti-bonding or more generally frontier orbital one may have expected to see. Molecular orbitals are just that - *molecular* - with the

exception of the uninteresting core orbitals, they are spread across the molecule and almost never resemble an atomic fragment. This perhaps frustrating property is the price to be paid for a set of orthogonal orbitals which have a host of other desirable properties, such as the invariance of the total wavefunction under rotation of the orbitals, the simple applicability of the coupled cluster operator, and the reduced complexity in variationally optimising the molecular wavefunction.

However, there exists an equally valid approach to solving the Schrödinger equation which may sit more pleasantly among chemists, known as *Valence Bond* (VB) *Theory*. The aim of this section is to briefly compare and contrast the MO and VB approaches, and thus justify the choice of framework for the remainder of the chapter.

In MO theory, one has for minimal basis, single determinant H_2,

$$\Psi_0 = (\chi_A\chi_A + \chi_B\chi_B + \chi_A\chi_B + \chi_B\chi_A)\,[\alpha\beta - \beta\alpha]\,, \tag{6.1}$$

which, as outlined in section 2.5, is a 50:50 mixture of ionic and covalent terms, and is incorrect at the dissociation limit and does not have the requisite flexibility to fix this without including the excited configuration,

$$\Psi_1 = (\chi_A\chi_A + \chi_B\chi_B - \chi_A\chi_B - \chi_B\chi_A)\,[\alpha\beta - \beta\alpha], \tag{6.2}$$

in an expansion of the CI wavefunction,

$$\Psi_{\mathrm{CI}} = c_0\Psi_0 + c_1\Psi_1, \tag{6.3}$$

$$= [(c_0 - c_1)(\chi_A\chi_B + \chi_B\chi_A) + (c_0 + c_1)(\chi_A\chi_A + \chi_B\chi_B)]\,[\alpha\beta - \beta\alpha] \tag{6.4}$$

Now, in valence bond theory one builds a wavefunction by placing s-functions on the H atoms, allowing them to overlap to form a singlet configuration, and antisymmetrizing afterwards, thus arriving at the Heitler-London (HL) function,

$$\Psi_{\mathrm{HL}}^{\mathrm{cov}} = (\chi_A\chi_B + \chi_B\chi_A)[\alpha\beta - \beta\alpha], \tag{6.5}$$

which must then be improved with a second function consisting of the ionic terms,

$$\Psi_{\mathrm{HL}}^{\mathrm{ion}} = (\chi_A\chi_A + \chi_B\chi_B)[\alpha\beta - \beta\alpha], \tag{6.6}$$

to give

$$\Psi_{\mathrm{HL}} = c_0\Psi_{\mathrm{HL}}^{\mathrm{cov}} + c_1\Psi_{\mathrm{HL}}^{\mathrm{ion}}. \tag{6.7}$$

The coefficients c are determined variationally. The CI wavefunction in 6.4 is identical to the above. The HL function is improved upon by the *Fischer-Coulson* function, which allows the AOs to distort in the presence of the other atoms. This distortion is the foundation which most modern VB methods are based upon, and comes at the price of nonorthogonality of the orbitals. For H_2 this is

$$\Psi_{\mathrm{CF}} = (\psi_A\psi_B + \psi_B\psi_A)[\alpha\beta - \beta\alpha], \tag{6.8}$$

$$\psi_A = \chi_A + c\chi_B, \quad \psi_B = \chi_B + c\chi_A. \tag{6.9}$$

The overlap of the VB orbitals ψ_A and ψ_B is

$$\langle\psi_A|\psi_B\rangle = 2c(\langle\chi_A|\chi_A\rangle + \langle\chi_B|\chi_B\rangle) + (1+c^2)\langle\chi_A|\chi_B\rangle, \tag{6.10}$$

$$= 4c + (1+c^2)S_{\mathrm{AB}}. \tag{6.11}$$

Clearly, the Coulson-Fischer function describes appropriately the dissociation of the bond without including further terms in the expansion; as the bond lengths increase, c goes to zero and there are two single atoms with no overlap.

The generalized form of the Coulson-Fischer function one can use for any molecule is known as *Spin Coupled Generalized Valence Bond* (SCGVB) Theory. [80,81] This approach involves coupling unpaired atomic orbitals to produce a singlet spin state and thus a bond. For instance, in a hydrocarbon one would couple unpaired H s-orbitals with the unpaired p-orbitals on the carbons (in different ratios depending on the hybridisation of the carbon centre) to produce C-H bonds, and coupling pairs of p-orbitals to produce the C-C bonds. The spin-coupling coefficients together with the VB orbital coefficients are then optimised variationally to produce an optimal VB wavefunction for which the different combinations of unpaired electrons should all be considered and combined linearly. In simple cases

the combination one would expect from organic chemistry textbooks dominates, and the rest are neglected. For more complicated cases, such as benzene multiple spin couplings must be considered, namely the Kekulé resonance structures and the three states where each carbon has electrons coupled with the carbon opposite and the carbons adjacent. The improvement of a VB wavefunction, much like the improvement of the MO wavefunction, essentially involves adding excited (ionic) states to the ground state VB wavefunction. SCGVB plus the appropriate ionic configurations and CASSCF produce much the same energetic results and thus capture roughly the same amount of electron correlation. The SCGVB wavefunction is more compact, and perhaps more conceptually appealing, whereas the CASSCF wavefunction requires large numbers of Slater determinants to be stored and evaluated.

Why then, is the MO approach dominant in the field of electronic structure and the VB approach relegated to the research interests of small parts of the academic community? The answer to this question is beyond the scope of this thesis, but it is undoubtedly in no small part down to the flexibility of the MO orbitals compared with the SCGVB orbitals. Orthogonal MOs can be freely rotated together without consequence to the total wavefunction, and thus can be manipulated to show us things a chemist might be interested in at no detriment to the total energy (but usually at the cost of the applicability of Koopmans' theorem). Whereas once the SCGVB orbitals have been variationally determined, any modification will destroy their variational character and most likely be of little use. It should be noted however, that the SCGVB orbitals are by their construction rather localised and arguably the most common reason for rotating orthogonal MOs is to localise them! However, the work done in the previous chapter simply could not be done with a valence bond wavefunction. This invariance of the total MO wavefunction under unitary transformation of the MOs is central to this chapter, and the previous one. As such the VB method is parked here, and not picked up again.

6.2 The Nature of the Covalent Bond

In 1916 Lewis' theory that a single chemical bond arises from two atoms sharing a pair of electrons was published. [82] Since then, it has been taught to secondary school students across the globe, and is universally accepted and understood to be true by the scientific community. This model has been applied to virtually every type of compound in "dot structures", and has been adapted to include bonds containing one shared electron since groundbreaking quantum chemical calculations on H_2^+ were performed by the likes of Heitler, London and Barrau. [83, 84] More than 100 years after Lewis' original publication, the precise mechanism of chemical bonding is still a subject of debate between two prevalent schools of thought: one insisting it is an electrostatic phenomenon and the other that covalent bonding is driven by a kinetic energy lowering which accompanies the expansion of electron wavefunction.

The electrostatic argument for covalent bond formation arises quite naturally from things we know from quantum mechanics; bonds are created through the constructive interference of two atomic orbitals on two separate nuclei, and this yields an increase in the electron density in the so-called "binding region" and that at the equilibrium geometry the molecular potential energy is always lower than the sum of the potential energies of the constituent free atoms, whereas the case is reversed for the kinetic energy. One could therefore be forgiven for presuming that the virial theorem,

$$\frac{V}{T} = -2, \tag{6.12}$$

where V and T are the atomic or molecular potential and kinetic energies, respectively, provides rigorous grounding for an appealingly simple electrostatic picture of the chemical bond. Indeed, this was (and arguably still is) the most widely accepted description of covalent bonding, and was strongly supported by incredibly talented scientists such as Slater, Feynman and Coulson. [85–87] More recently, Bader has lent his support to the electrostatic model, with motivation drawn from topological features of the electron density, along with the virial theorem. [88]

At odds with the classical description offered by those in support of the electrostatic description of chemical bonding, Hellmann suggested chemical bonding be

treated as a quantum mechanical effect, and that the lowering of the kinetic energy upon the expansion of the electron waves as delocalisation occurs is responsible for chemical binding. [89] Hellmann's apparent difficulty in aligning his interpretation with the virial theorem was, at least in part, to have his arguments dismissed by the wider scientific community. [90,91] It was not until almost 30 years later that Klaus Ruedenberg provided an in-depth analysis of all of the effects leading to chemical binding in H_2^+, and found himself to be in general agreement with Hellmann; chemical bonding occurs upon the "depression" of the kinetic energy as orbitals overlap and the electrons are free to explore a larger region of space without tunnelling. [92] Since then, Ruedenberg and co-workers have explored molecules ranging from H_2^+ to larger homonuclear diatomics. [92–100] The salient point, however, remains the same; the covalent bond formation is driven by the depression of the kinetic energy. In this respect, then, there is nothing remarkable nor unremarkable about bonds containing one electron.

Several high-profile scientists, such as Nobel Prize winners Mulliken and Fukui, have since aired their agreement with Ruedenberg's description of the chemical bond, among many other prominent researchers in theoretical chemistry. [101–116] However, it would be remiss not to mention that a number of undergraduate textbooks still used today mislead readers by describing covalent bonding as Slater did, more than 80 years ago. It is both surprising and disappointing to see such a fundamental idea, perhaps *the* fundamental idea, in chemistry be given such little regard by the authors that more than 50 years of research and growing scientific consensus on its description should be ignored. This deficiency in common textbooks has been noticed, and several authors have published pedagogical descriptions in educational journals in an attempt to make Ruedenberg's ideas, which do require some knowledge of quantum chemistry in order to grasp, more accessible to the wider chemical community. [106, 110, 117]

6.2.1 Atomic Hydrogen: A Cheat Sheet for Variational Reasoning

The exact solutions to the Schrödinger equation for the hydrogen atom are known. This places it uniquely in a position to provide us with a conceptual understanding,

from a rigorous footing, of precisely what the physical effects are which lead us to a stationary electronic state in the field of point charge "nuclei". The variation principle tells us that the electronic wavefunction assumes whatever shape is necessary in order to minimise the expectation value of the electronic Hamiltonian. The ground state wavefunction is

$$\psi = \left(\frac{\xi^3}{\pi}\right)^{\frac{1}{2}} e^{-\xi r}, \tag{6.13}$$

where the shape is determined by the exponent, ξ, and the requirement that the solution be normalisable. The kinetic energy operator is the radial Laplacian,

$$\hat{T} = -\frac{1}{2r^2}\frac{\partial}{\partial r}\left(r^2\frac{\partial}{\partial r}\right), \tag{6.14}$$

Or, equivalently

$$\hat{T} = \nabla^2 = \left[\left(\frac{\partial}{\partial x}\right)^2 + \left(\frac{\partial}{\partial y}\right)^2 + \left(\frac{\partial}{\partial z}\right)^2\right]. \tag{6.15}$$

The form of the above tells us rather a lot about the behaviour of the kinetic energy of electron waves. If one increases the localisation, the requirement that ψ remains normalised demands the maximum of the orbital be higher. If a maximum in the orbital increases, and the orbital remains normalised, then necessarily the gradient increases. If the gradient increases, then by simple inspection of the above it is clear to see that the kinetic energy must also increase. The pertinent point here is that the *increased localisation of the electron wavefunction must increase the kinetic energy.* [118]

The potential energy operator for a hydrogen-like system is

$$\hat{V} = -\frac{Z}{r}, \tag{6.16}$$

where Z is the nuclear charge. The system contains only one electron and one nucleus, so of course the terms for electron-electron and internuclear repulsion are missing and the potential energy is clearly always negative. All of these are classical electrostatic interactions, of which the attractive term dominates. As a

consequence, even in systems of many electrons and nuclei the potential energy is negative.

The kinetic and potential energy integrals of ψ are

$$\langle \hat{T} \rangle = \frac{\xi^2}{2m}, \tag{6.17}$$

$$\langle \hat{V} \rangle = -\xi Z, \tag{6.18}$$

where m is the mass of the electron. This tells us that the potential energy reaches a minimum as $\xi \to \infty$, whereas the kinetic energy reaches a minimum as $\xi \to 0$. The total energy is given by

$$E = \frac{\xi^2}{2m} - \xi Z. \tag{6.19}$$

The optimum choice for the exponent is found by simply setting the derivative of the energy with respect to the exponent to zero, and solving for ξ. For the H atom that, in atomic units, is

$$\frac{dE}{d\xi} = \xi - 1 = 0, \tag{6.20}$$

$$\xi = 1. \tag{6.21}$$

It is clear, then, that the potential and kinetic energies oppose one-another. The kinetic energy drives the electrons towards complete delocalisation, and the potential energy drives the electrons towards collapse onto the nuclei and complete localisation to a point. The interaction between the kinetic and potential energies can be thus described as the potential driving contraction against the resistance of the kinetic energy driving expansion, or vice versa; the kinetic energy drives expansion against the pull of the attractive force between the electrons and the nuclei. [91, 95, 118]

Figure 6.1 shows the dependence of the kinetic, potential and total energies of atomic hydrogen upon changing the orbital exponent according to the above. Also shown is one side of the virial equation $(-V/2)$, which intersects the kinetic energy, i.e shows the virial theorem is satisfied only with an orbital exponent of 1. The kinetic energy, which is always positive, and has a minimum at an orbital exponent of zero, thus drives orbital delocalisation, or synonymously, orbital ex-

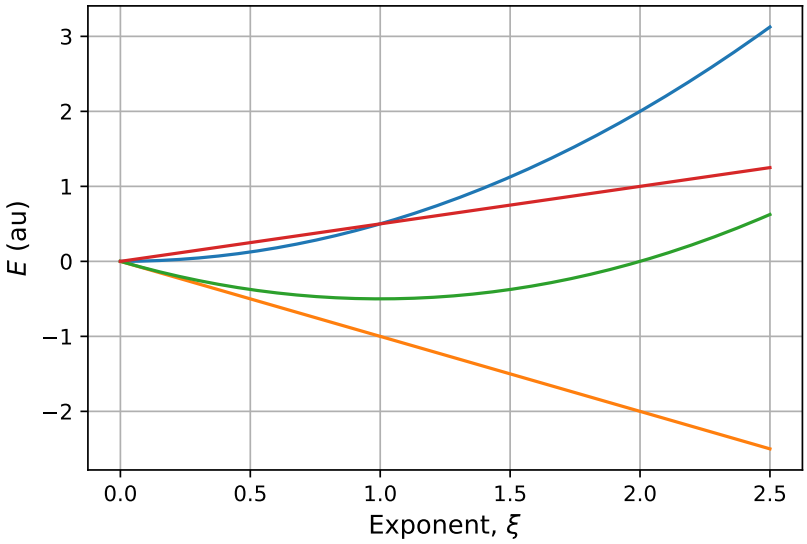

Figure 6.1: The kinetic (blue), potential (orange) and total (green) energies of the H atom as a function of orbital exponent. The red line is $-V/2$ where V is the potential energy.

pansion. The potential energy drives orbital contraction. The total energy is of course a balance of the two. One can thus draw the conclusion that wherever the kinetic energy decreases and the potential energy becomes less negative, the orbitals are expanding, and contracting where the case is reversed. Now considering the fabricated case, where the nuclear mass remains the same, but the charge of the nucleus is doubled, i.e $Z = 2$. The kinetic energy remains the same, whereas the electron feels double the attraction to the nucleus, and as a consequence the energy minimum is at $\xi = 2$, as shown in figure 6.2. [118]

One could likewise reduce the kinetic energy pressure, as Ruedenberg calls it in his original publication, by increasing m in equation 6.17. [92] The kinetic energy pressure can be increased absolutely by decreasing m, or relatively by decreasing Z and thereby reducing the pull the electrons feel towards the nuclei. [118]

6.2.2 The Chemical bond in H_2^+

With the results of the previous subsection in mind, let us now examine how the kinetic, potential and total energies change as the bond in H_2^+ is shortened, from the dissociation limit to slightly shorter than the equilibrium bond distance of 2 Bohr radii, as seen in figure 6.3. When the proton and the hydrogen atom are

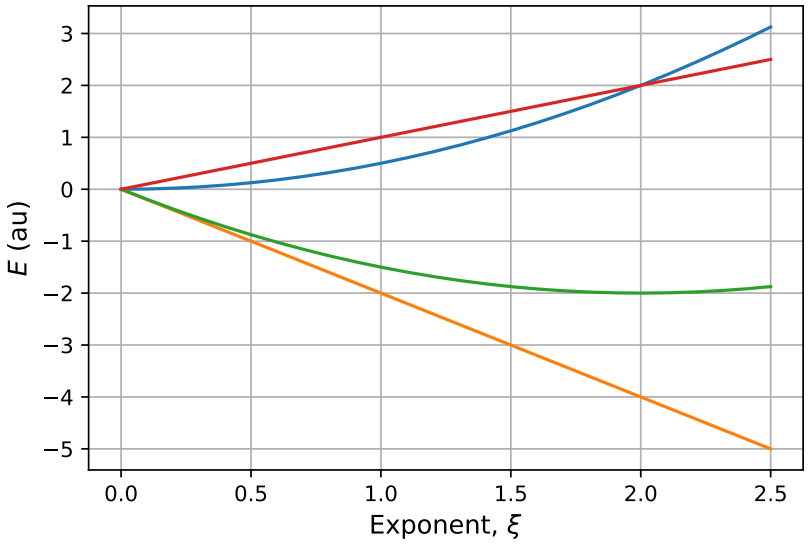

Figure 6.2: The kinetic (blue), potential (orange) and total (green) energies of one electron in the field of a point charge of +2 as a function of orbital exponent. The red line is $-V/2$ where V is the potential energy.

brought together from far apart attraction initially arises as the s-orbitals overlap, leading to a lowering of the kinetic energy as the molecular orbital expands between the nuclei and occupies a larger region of space. In terms of the results of the preceding section: the orbital exponents decrease, thereby decreasing the kinetic energy against the resistance of the potential energy. The adaptation of the orbital exponent to the bonding situation can be mimicked closely by using a sufficiently large basis set, wherein as long the coefficients in the linear combinations of atomic orbitals are able to provide adequate flexibility in the variational optimisation of the wavefunction, one sees the same behaviour for the kinetic, potential and total energies as if one optimised the exponents, as in VB theory.

As the proton and hydrogen atom come close together the physical effects become somewhat more complicated. There is a contraction of the orbitals perpendicular to the bond direction, which drives further delocalisation along the bond and thus lowers the kinetic energy overall, but increases the kinetic energy in the "intra-atomic" region. Bacskay *et al.* examined the individual components of the kinetic energy operator and found that the bond-perpendicular component shows an increase, whereas the bond-parallel component shows a substantial decrease as the bond is shortened. [114] The intra-atomic contractions naturally cause a de-

crease in the intra-atomic potential energy, and oppose the inter-atomic kinetic and potential energy changes which are driving bond formation; the intra-atomic orbital contraction drives delocalization along the bond, thus increasing the inter-atomic potential energy and decreasing the inter-atomic kinetic energy. The total intra-atomic energy increases as a result of the contractions; the intra-atomic kinetic energy increase is slightly larger than the magnitude of the intra-atomic potential energy decrease. As the nuclear separation approaches equilibrium bond length, the intra-atomic effects become so large that they become larger than the inter-atomic effects. Thus the total kinetic energy increases, and becomes greater than that of the electron in atomic hydrogen, whereas the total potential energy decreases, and becomes less than that in atomic hydrogen. However, on balance, the total energy goes down, as the absolute value of the sum of the inter- and intra-atomic potential energies at equilibrium is greater than the sum of the inter- and intra-atomic kinetic energies, as demanded by the virial theorem. [91] The orbitals contract wherever possible against the resistance of the kinetic energy, which is lessened by the increase in delocalisation along the bond. The role of orbital contraction in covalent bond formation, might thus be attributed to the restoration of the virial ratio at equilibrium bond length. Head-Gordon and co-workers recently suggested that in some larger molecules the role of orbital contraction is taken over by polarization. [119]

The difference between the bond in H_2^+ and the bonds between other elements, or in molecules that most chemists might have an interest in, is likely to arise primarily from the presence of other occupied orbitals which could interfere with the electron-nuclear term through electron-electron coulomb and exchange integrals. Ruedenberg *et al* provided some insight into this case while investigating a range of homonuclear diatomics. [97,99,100,118] In each case the energy curves are similar to those in H_2^+ and the variational reasoning remains the same. The same group more recently showed that orbital contraction is responsible for the restoration of the virial coefficient by calculating the increase in intra-atomic electron-electron repulsions, and increase in nuclear-electronic attraction in a range of homonuclear diatomics compared with the constituent free atoms. [91]

Let us now consider covalent bonding in a basis set without the necessary flex-

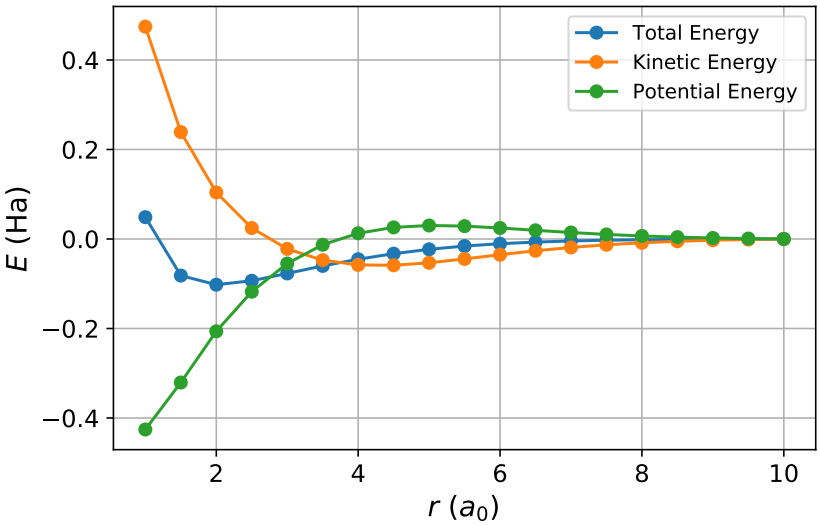

Figure 6.3: The total (blue line), kinetic (orange line) and potential (green line) energy against nuclear separation for H_2^+. The energies are calculated using the cc-pVQZ basis set, and have been shifted by their respective asymptotic values.

ibility to contract the atomic regions but expand along the bond direction, nor distort strongly from the free atom shapes. That is, let us perform the same calculation on H_2^+, but using a minimal basis set with fixed atomic orbital exponents. Figure 6.4 shows the energy components over the same internuclear distances as in figure 6.3. One should immediately notice the violation of the virial theorem at the equilibrium bond length. The kinetic energy is lower in the molecule than in the separate atoms, whereas the potential energy is larger in the molecule than in the consitituent free atoms! The delocalisation of the electron over both nuclei as the atomic orbitals overlap causes the decrease in the kinetic energy against the resistance of the potential energy pulling the electrons towards the nuclei. However, the wavefunction lacks the flexibility to contract in the atomic regions and thus lower the total potential energy and increase the total kinetic energy - there are no p-functions to allow bond-perpendicular contraction, only s-functions whose contraction would decrease delocalisation in the bond-parallel direction, and increase the kinetic energy. The variational balance over the nuclear separations is to never have the potential energy decrease. Thus the potential energy contribution to the covalent binding, i.e the orbital contraction, is completely missing, and the minimum in the total energy arises only due to the kinetic energy.

The salient points, in order of occurrence in the chemical bond formation in

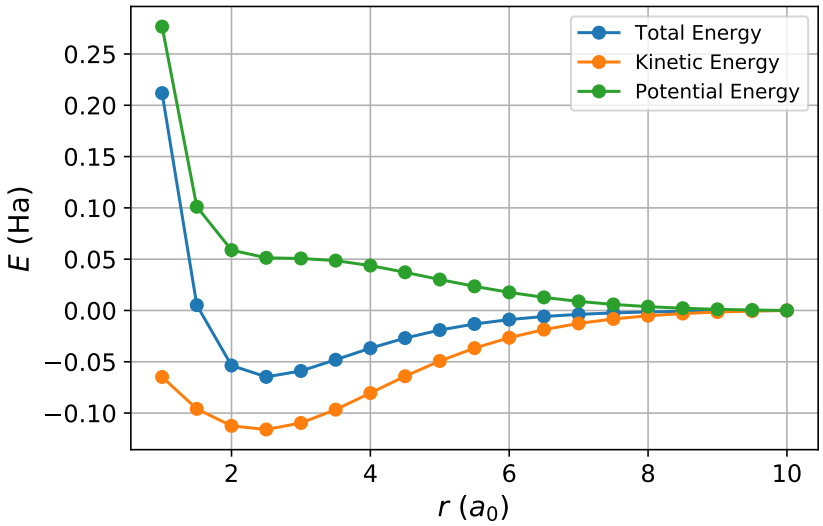

Figure 6.4: The total (blue line), kinetic (orange line) and potential (green line) energy against nuclear separation for H_2^+. The energies are calculated using the MINAO minimal basis set, and have been shifted by their respective asymptotic values.

H_2^+, as the nuclear separation is decreased, are: [118]

1. The overlapping s-functions and consequential delocalisation of the electron over both protons is the only covalent interaction at large nuclear separation. There is no orbital contraction perpendicular to the bond. The kinetic energy decreases against the resistance of the potential energy increase which accompanies the accumulation of charge between the nuclei.

2. The kinetic energy decreases further, and the electron wavefunction becomes more and more delocalised. The inter-atomic potential energy remains an antibonding effect over all internuclear distances.

3. As the nuclear separation becomes smaller, there is an intra-atomic contraction and consequential lowering of the intra-atomic potential energy. This contraction facilitates further shifting of charge into the bonding region, thus lowering the kinetic energy further.

4. At roughly two times the equilibrium bond distance, the total molecular kinetic energy begins to increase as the intra-atomic contractions increase the intra-atomic kinetic energy. The total potential energy begins to decrease at

the same point because the orbital contraction places the electron closer to the nuclei.

5. Once equilibrium bond length has been reached, the intra-atomic kinetic energy has increased to such a degree, due to the intra-atomic orbital contraction, that it overwhelms the inter-atomic kinetic energy and thus yields a larger total kinetic energy than the constituent free atoms. The potential energy in the intra-atomic region lowers and likewise overwhelms the inter-atomic potential energy through the intra-atomic contraction of the orbitals, leaving us with a negative total potential energy relative to the consituent free atoms. The virial ratio is thereby restored.

Where there are additional shells of electrons, or where bonds are delocalised over 3 or more nuclear centres, the interpenetration of the electron wavefunctions will clearly increase the coulombic repulsion, which is missing entirely from the H_2^+ example. This increase is counteracted by dynamic electron correlation to a certain degree. The overall effect of occupied inner shells of electrons is one which aids in the restoration of the virial ratio, through a delicate balance of correlation, coulomb and one-electron effects. [91]

6.3 Wavefunctions and Chemical Bonding

Many different approaches exist for extracting bonding information from molecular wavefunctions. Many groups exist which focus primarily upon using quantities which can be calculated using the appropriate operators and indirectly yield information on the types and strengths of chemical bonds. Such approaches include NICS, ring-current methods, magnetic methods, and many more. There is no discussion of methods such as these in this chapter as, despite their value, they are not related to the original work presented in later sections. Instead, we focus on methods which provide direct qualitative and quantitative information on bonding through the shapes of orbitals, energetic quantities or both.

6.3.1 Orbital Localisation

Localised Molecular Orbitals LMOs) are, as the name suggests, canonical orbitals which have been transformed in order to reduce their spatial volume. The most attractive features of LMOs are that they are usually consistent across molecules containing the same functional groups; they usually reflect the chemist's picture of bonding and they facilitate the development of electronic structure methods where only local correlations are included in an expansion or perturbation. It is common to generate LMOs at several points over a reaction co-ordinate; doing so can be qualitatively rather illuminating, and certainly provides conceptual insight into how a reaction proceeds. However, this kind of analysis is not necessarily based on any physical quantities and yields no quantitative energetic information which might *really* be used to help an experimentalist design experiments. Over the years, there have been many localisation methods developed. In this subsection we briefly discuss a selection of methods, and their benefits and drawbacks in what is far from a complete discussion.

Pipek-Mezey Localised Orbitals

Pipek-Mezey (PM) LMOs, (as used frequently throughout chapters 4 and 5) are those orbitals which maximise the sum of (originally Mulliken) atomic charges. [46]

The orbital coefficients are those which minimise the functional,

$$F_{\mathrm{PM}} = -\sum_{A}^{N_{\mathrm{atom}}} (Q_A)^2, \tag{6.22}$$

where Q_A is the charge allocated to atom A. Although it is common to use Mulliken atomic charges, any method for allocating atomic charge which depends on the orbital coefficients can be used whenever the basis set employed is a large one and the Mulliken atomic charges become erratic. PM LMOs are used widely, and usually reflect orbitals one might draw through intuition. Pipek-Mezey orbitals are popular as they, in general, separate σ- and π-orbitals. The application of PM localization can come at a cost in highly symmetrical systems. The go-to example is benzene, whose canonical orbitals are of D_{6h} symmetry but under PM transformation has orbitals of D_{3h} symmetry, as was discussed in chapter 4.

Boys' Localised Orbitals

The *Foster-Boys* (FB) localisation method perhaps more intuitively decreases the spatial extent of the canonical orbitals by explicitly referencing the square of the distance between two electrons in a minimisation of the functional, [120, 121]

$$F_{\mathrm{FB}} = \sum_{i}^{N_{\mathrm{orb}}} \langle \psi_i \psi_i | (\mathbf{r}_1 - \mathbf{r}_2)^2 | \psi_i \psi_i \rangle \tag{6.23}$$

with respect to the orbital coefficients. FB localization yields orbitals which are perhaps less intuitive as far as $\pi-$bonding is concerned, as the σ/π separation is rarely preserved and one ends up with "banana bonds", but essentially serve the same purpose as PM orbitals.

Intrinsic Bond Orbitals

Knizia's Intrinsic Bond Orbitals (IBOs) are related to PM orbitals, with a different choice of exponent in the objective function, and the atomic charges used are those arising from the intrinsic atomic orbitals of the same paper, wherein he proposes a new method for calculating atomic charges which are convergent with increasing size of the basis set by projection onto a minimal basis and back. The orbitals

are then reconstructed in the large basis by a further projection, and the atomic charges obtained by performing a Mulliken atomic population analysis. [76] The choice of exponent 4 is inspired by work which has shown it to be effective in suppressing unwanted orthogonalisation tails. [76, 122, 123]

Natural Orbitals

Natural orbitals are the eigenfunctions of the one-electron density matrix, the associated eigenvalues are the orbital occupation numbers. Natural orbitals also have the attractive feature of providing the fastest possible convergence to the full CI energy when the occupation numbers are used to guide the choice of excited determinants when one includes the largest occupations in excited determinants first. [8] Natural orbitals often resemble localised orbitals, and are one of the most widely used approaches in computational chemistry for gaining insight into how atomic orbitals interact in a given system to give rise to bonding. The procedures involved are the *natural atomic orbital* (NAO) and *natural bond orbital* (NBO) analyses of Weinhold *et al.* [124] The natural atomic orbitals are those which diagonalise blocks of the density matrix arising from basis functions on each atom; the natural atomic orbitals on atom A are the eigenfunctions of the sub matrix of the density arising only from atomic orbitals centred on A. The diagonalisation is then performed for each block in the density matrix associated with each atom. The resulting natural atomic orbitals are not mutually orthogonal, and must thus be orthogonalised using an appropriate algorithm. The natural orbitals in general resemble the pure atomic orbitals, and the orthogonalisation ensures a sum over the diagonal elements of the new density matrix formed from the NAOs is equal to the number of electrons, and the trace of each block yields the atomic charge arising from the electrons in the setting of the molecule. However, this approach to calculating partial charges is hostage to the same effects as Mulliken populations; whenever a basis set containing diffuse functions is chosen, electronic charge far from the basis function centre will be attributed to the atom erroneously.

Following the definition of the NAOs, bonds between atoms are formed by simple inspection of the off diagonal blocks of the NAO basis density matrix. Orbitals with occupations very close to 2 have their contributions to the density matrix

removed and are thereafter considered core orbitals, a lower threshhold is set for so-called "lone-pair" orbitals, whose contributions to the density matrix are treated similarly. Removing the contributions of these orbitals to the density matrix leaves us with off diagonal blocks between atomic centres. These blocks are diagonalised, and the eigenfunctions filtered by their corresponding eigenvalues (occupation numbers) until the correct number of bonding orbitals have been found; these are the natural bond orbitals, and can be written in terms of the NAOs, thus providing insight into which atomic orbitals contribute to the bonds, and the occupation number giving at least something close to quantitative insight into relative bond strengths.

6.3.2 Energy Decomposition Analyses

Several schemes have been published which go a step further than the orbital localisation pictures and aim to give numerical quantities which can be associated with bond strength, or in some cases, numerical quantities for each physical effect associated with bond formation (i.e distortion from the atomic state, orbital contraction, spin-coupling effects, and so on). There have been a large number of methods developed for the energy decomposition of non-covalent interactions, with some proving to be very successful. [119,125–137] The general validty of EDAs and their inevitable shortcomings and benefits was the topic of a recent review article. [138] As we shall see later, we are concerned in this chapter only with covalent bonding, and so we limit ourselves to associated energy decomposition schemes. Even so, a large number of EDAs exist for covalent bond energy decomposition, and so this subsection outlines several popular methods, but could not possibly cover all available approaches.

Quasi-atomic Orbitals and Chemical Bonding

Ruedenberg and co-workers have, with success, developed a black-box algorithm for drawing bonding information from *ab initio* wavefunctions for electronic states through a sequence of orbital localisations. [125] The aim of the approach is to separate the one electron potential from the electron correlation potential. This is achieved by dividing the full orbital space into three components: the inner-shell

core space, the valence-internal space and valence-external space.

The core orbital space is always a subset of the occupied orbitals, they are always closed and orthogonal to the valence and external spaces. In order to determine the quasi-atomic core orbitals, the HF core orbitals are projected onto a set of minimal basis atomic orbitals and a singular value matrix decomposition (SVD) is performed. The non-zero values then correspond to the core orbitals. These core HF orbitals are then symmetrically orthogonalised, and the resulting orbitals are the quasi-atomic core orbitals.

The valence-internal orbital basis is generated similarly. The HF virtual orbitals are projected onto the full space of minimal basis orbitals, the SVD is performed and the HF orbitals corresponding to the minimal basis virtual orbitals are those with the maximal singular values. They are then cast into a basis which diagonalises the Fock operator, and the resulting orbitals are named the *canonical valence-virtual orbitals*. Together with the occupied HF canonical orbitals, they make up the canonical valence-internal space. The valence-external space are simply those HF virtual orbitals whose singular values did not qualify them as part of the canonical valence-virtual space.

Now that we have the three well-defined canonical orbital subspaces, what remains is to find a quasi-atomic representation of the canonical orbitals. The SVD of the overlap matrix between the full canonical orbital space and the minimal atomic orbital basis is then performed. The number of non-zero singular values is exactly equal to the number of minimal basis orbitals, and since each minimal basis orbital is associated with an atom, the associated singular vector in canonical valence-internal space is taken to be the local contributions of each atomic orbital to that internal space. By performing this for all orbitals and for each atom, a set of localised basis orbitals is generated. The orbitals must then be orthogonalised, as they are in general non-orthogonal between atomic centres. Ruedenberg and co-workers dubbed these orbitals *canonical quasi-atomic valence orbitals*.

All that is left is to now orient these canonical quasi-atomic valence orbitals, by maximising the sum of the off-diagonal inter-atomic one-particle density matrix elements to the fourth power, and thus yielding those orbitals which interact with as few other orbitals as possible. These are the *oriented quasi-atomic orbitals*. In

the first publication about such orbitals, an illustrative example of quinone showed that the bond orders they yield are rather insightful, even revealing information as to the aromaticity of the system through the $\sigma - \pi$ bond orders. [125]

Further modifications were made to this approach in a series of papers. [126–128] The modification in the first instance was the generalisation to wavefunctions beyond HF wavefunctions, which is beyond the scope of this thesis, as we shall concern ourselves in this section only with closed shell single configurational systems. However, the introduction of a "kinetic binding energy" in the second publication as a measure of bond strength is of particular interest. [126] The difficulty in controlling the phases of the quasi-atomic orbitals in large systems, and negative bond-orders sometimes being associated with bonding interactions led the authors to multiply the bond-orders by a kinetic energy interference term. This term is taken to be the kinetic energy integrals between different quasi-atomic centres. They further assert that "since the kinetic energy is responsible for covalent bonding, it is likely that the [inter-quasi-atomic kinetic energy integrals] reflect bond strengths and can serve a similar purpose as 'resonance energies' ", and that adjusting the kinetic bond orders empirically (multiplying by 0.1) provides a numerical measure of the bonding indicated by the one-particle density matrix. [126–128] The last two publications were applications to specific molecules, with the last being a unimolecular diradical dissociation reaction. [127, 128]

A full energy decomposition scheme has since been developed by the same group, and is based upon these quasi-atomic orbitals. [139] The total energy is written in terms of five different quantities,

$$E = E_1 + E_{2C} + E_{2I} + E_{3I} + E_{4I}, \tag{6.24}$$

where E_1 is the intra-atomic energy, E_{2C} is the energy arising from two-centre coulomb interactions and E_{XI} are the interference interactions across X centres. In order to associate terms in the above equation with physical quantities, the wavefunction is first partitioned into two parts: one part which is an assembly of unbound quasi-atoms and one part which is responsible for bonding. A determinant which describes the wavefunction of atom A is taken as being the antisymmetrised product of all quasi-atomic orbitals centred on A, and the total molecular wavefunc-

tion is the further antisymmetrised product of all wavefunctions for all atoms. The atomic wavefunctions which consist of a number of quasi atomic orbitals which is equal to the nuclear charge are combined linearly to give a wavefunction describing a set of non-bonded quasi-atoms,

$$\Psi^0 = \sum_i c_i^0 D_i^0, \tag{6.25}$$

where D_i^0 are the antisymmetrised atomic determinants. A whole host of properties of Ψ^0 which indicate it is indeed a wavefunction of unbound atoms are calculable and discussed in some detail in ref [139], but most notable is the absence of any inter-atomic density matrix elements. A second wavefunction is generated similarly from the wavefunctions of atoms whose number of constituent quasi-atomic orbitals is *not* equal to the atomic charge,

$$\Psi' = \sum_j c_j' D_j'. \tag{6.26}$$

The energy of these wavefunctions then correspond to parts of the energy associated with notional zero charge migration, E^{nm}, and the part associated with charge migration and thus bonding, E^{m}. That is,

$$E = \langle \Psi | \hat{\mathrm{H}} | \Psi \rangle + E_{\mathrm{nuc}}, \tag{6.27}$$

$$E^{\mathrm{nm}} = \langle \Psi^0 | \hat{\mathrm{H}} | \Psi^0 \rangle + E_{\mathrm{nuc}} \tag{6.28}$$

$$E^{\mathrm{m}} = E - E^{\mathrm{nm}} = 2c^0 c' \langle \Psi^0 | \hat{\mathrm{H}} | \Psi' \rangle + (c')^2 \left[\langle \Psi' | \hat{\mathrm{H}} | \Psi' \rangle - \langle \Psi^0 | \hat{\mathrm{H}} | \Psi^0 \rangle \right], \tag{6.29}$$

where E^{nm} is the energy associated with the wavefunction describing unbound quasi-atoms and E is the energy arising from the total wavefunction, which can be written as

$$\Psi = c^0 \Psi^0 + c' \Psi', \tag{6.30}$$

subject to the constraint that $(c^0)^2 + (c')^2 = 1$). It is found that the energy lowering associated with chemical bonding arises through the kinetic energy integrals, particularly those in the cross term, $\langle \Psi^0 | \hat{\mathrm{T}} | \Psi' \rangle$, where $\hat{\mathrm{T}}$ is the kinetic energy operator of the one electron Hamiltonian. [139]

The energy terms in equation 6.24 for E^{nm} correspond to the energies of the quasi-atoms (E_1), the quasi-classical energy (E_{2C}) and the energy of antisymmtrisation (E_{2I}). The terms in the equation for E^{m} correspond to the sharing-intra-atomic energy (E_1), the sharing-coulombic energy (E_{2C}), sharing-interference energy over X centres (E_{XC}). The goal of the EDA is to write an explicit form for the bonding energy,

$$E(\text{bonding}) = E(\text{quasi-atom formation}) + E(\text{quasi-classical}) + E(\text{electron sharing}) + E(\text{charge-transfer}). \quad (6.31)$$

The quasi-classical term naturally falls out of the expression for E^{nm} as the two centre coulomb interaction between any two quasi-atoms. The quasi-atom formation energy requires a second calculation on the free-atom ground states, and is the difference between the energies of those free atoms and the corresponding quasi-atoms. The electron sharing and charge transfer terms are together encompassed by the sum of the sharing-intra-atomic and sharing-coulombic terms which both arise through E^{m}. An illustrative example investigating the bonding in C_2 was included in the original publication, which shows what one may expect; the atoms are not bound without the interference terms. [139]

In subsequent publications concerning the quasi-atomic orbital approach to extracting bonding information from molecular wavefunctions, Ruedenberg *et al* have not performed analyses similar to the one they performed for C_2, and instead focus on elucidating information through those quantities defined earlier in this section: the kinetic bond orders and bond orders arising from the one particle density matrix. [140–142]

Absolutely Localised Molecular Orbital Energy Decomposition

A novel approach to the problem of isolating bonding energies and their various contributing quantities has been suggested by Head-Gordon *et al.*, wherein a series of constraints are placed on a wavefunction in a gradual relaxation to the ground state. [119, 130–132, 135, 143] Under the absolutely localised molecular orbital (ALMO) EDA scheme, the energy of interaction of two molecular fragments

is written as [119]

$$\Delta E_{\mathrm{INT}} = \Delta E_{\mathrm{GEOM}} + \Delta E_{\mathrm{FRZ}} + \Delta E_{\mathrm{SC}} + \Delta E_{\mathrm{POL}} + \Delta E_{\mathrm{CT}}. \tag{6.32}$$

The procedure begins with calculations on isolated fragments A and B of molecule AB in their ground states, and then in their respective geometries in AB but with no interaction with the molecular environment, in order to obtain the term ΔE_{GEOM}, which is the energy change associated with the geometric distortion of each fragment. The orbitals then remain unmodified, but are allowed to experience the presence of those on the other fragment. The associated energy change is ΔE_{FRZ} and consists of Pauli-repulsion, classical electrostatic interactions and dispersion. The MO matrix is block-diagonal and if bonding occurs in the nonorthogonal meeting of the fragments, the system is placed in a high-spin electronic state. A flip of the spin of one of the electrons is thus performed, and a lower spin configuration formed. The energy change associated with the spin flipping of electrons in the frozen orbitals is thus the spin coupling energy change, ΔE_{SC}. To define ΔE_{POL}, an optimisation of the orbitals local to each fragment is carried out through the mixing of same-fragment occupied and virtual orbitals capable of describing wavefunction polarization, and the difference is taken relative to the previous state. The final term, ΔE_{CT}, which is associated with charge transfer is then defined as the change in the energy upon the removal of all constraints, and the optimal mixing of the orbitals across the fragments. By definition, then, the quantites which are overall repulsive are ΔE_{FRZ} and ΔE_{GEOM}. All other quantities are manifestly attractive. [132]

Partitioning the energy of interaction according to the ALMO-EDA scheme has led Head-Gordon and co-workers to suggest that orbital contraction be replaced by orbital polarization in the discussion of bonding for elements heavier than hydrogen. [119] The partitioning is modified in the extension of the ALMO-EDA for MP2 calculations by the inclusion of an additional dispersion term. This inclusion is an attractive prospect: the dispersion is in general only a small contribution to the energy, but plays the dominant role in the formation of the bond in the helium dimer. [133–135]

In some publications the ALMO-EDA has been applied to systems at several

points along a reaction co-ordinate. [131, 133–135] The method is shown to yield an energetic "fingerprint" for different types of bond. At the time of writing, however, no studies of covalent bonds of greater order than 1 have been published. The high resolution of this EDA can come at considerable computational expense, depending on the nature of its use; if one is interested in the nature of the changes in, say, 5 bonds in a molecule along a reaction co-ordinate then one must perform calculations on 10 isolated fragments (both in their equilibrium geometry and in the geometry they take in the molecular setting) in turn, and perform the entire series of optimisations for each bond at each geometry along the reaction co-ordinate. It could well be that the information it provides is worth the cost for systems of specific interest, but it is unlikely to be the case for exploratory calculations.

Seminal Energy Decomposition Analyses

Early EDAs similar in concept to the ALMO-EDA include the Extended Transition State EDA (ETS-EDA) and the Kitaura-Morokuma EDA (KM-EDA). [136, 137] Although the early energy decomposition schemes were aimed at understanding noncovalent interactions, they have been modified and redeployed as a means to gain insight into bonding interactions. [129] The ETS-EDA decomposes the energy as

$$\Delta E = \Delta E_{\mathrm{GEOM}} + \Delta E_{\mathrm{EL}} + \Delta E_{\mathrm{PAULI}} + \Delta E_{\mathrm{ORB}}, \tag{6.33}$$

where ΔE_{GEOM} is the energy change associated with the reorganisation of the nuclei from the ground state to the arrangement in the molecular environment; that is, precisely the same as the corresponding term in the ALMO-EDA. ΔE_{EL} is the coulombic repulsion between two fragments of a molecule. $\Delta E_{\mathrm{PAULI}}$ is the repulsive interaction arising from the antisymmtrization of the wavefunction, and ΔE_{ORB} is the stabilising energy associated with the mixing of the orbitals from different fragments; this form of energy partitioning wherein all bonding interactions are grouped into a single orbital interaction term is common. The ALMO-EDA is the exception in providing further clarity.

6.4 Summary

We have introduced in this chapter some popular orbital localisation schemes which aim to provide qualitative insight into chemical bonding and reactions. We have also introduced a number of EDA methods, the first of which is the one of Ruedenberg *et al.* [125–128], in which the orbital space is divided into a number of subspaces and a series of orbital optimisations are performed and an empirical measure of covalency is obtained by scaling a set of "inter-quasi-atomic" kinetic energy integrals. An energy of bonding is also calculated through some combination of interference terms. The number of quantities defined in this EDA is large, and in order to obtain a bonding energy requires multiple calculations on the system of interest.

The ALMO EDA was also covered in significant detail, and represents a large number of other EDAs which are built upon a similar partitioning of the energy, such as the KM-EDA and ETS-EDA. In the ALMO EDA, a series of constraints placed upon a wavefunction are relaxed, and the energy differences attributed to different quantitative effects, such as polarization, and charge transfer. This EDA has received a lot of praise in the literature, and seems to provide the best results in this particular class of EDAs. However, no single quantity points at how covalent a bond might be, and the approach requires several calculations to be carried out in order to obtain certain terms, such as the energy of the geometry adjusting to nearby molecular fragments, as well as a series of relaxing constraints and is thus quite computationally taxing.

A review of the work which isolated, for the first time, the physical effects which give rise to chemical bonding has formed a large part of this chapter. We have emphasised the differences in the roles of the kinetic and potential energies in the formation of a chemical bonds in large and minimal basis sets, as these differences form the central motivation of the new method introduced in the coming chapter, which aims not to compete with the other EDAs presented in this thesis, but to provide quantitative justification for curly arrow mechanisms in chemistry at little computational expense. The new method aims to sacrifice the resolution of the rigorous EDAs, and equip the computational chemist with a new tool to help form conceptual pictures of chemical change over the course of a reaction.

Chapter 7

Reaction Orbitals

Curly arrow mechanisms are ubiquitous in chemistry. One need only open any modern organic text book and be presented with a myriad of different reactions with different names, all with their own unique curly arrow reaction mechanism to be convinced of this. [144] The original example and use is usually attributed to Robinson in his study on resonance in a conjugated system. [145] Since their inception, curly arrows have proven to be remarkably powerful and reliable tools for predicting the outcome of chemical reactions, and are a cornerstone of every chemistry student's education. In general, they are used to describe the motions of pairs of electrons over the course of a reaction; half-arrows are used, where necessary, to describe the motions of single electrons. The tail of the arrow is where they begin, and the head is where they end in that particular "step" of the reaction. Their place centre-stage in organic chemistry has led to them becoming a preoccupation of some theoretical chemists whose aim has been to place them on a more formal footing. [146–155]

Vidossich and co-workers suggest the concentration of orbitals to their charge centroids, and that the motions of the centroids be tracked and used to gather curly-arrow information. [146] Knizia and Klein apply their IBO routine and use measures of orbital change to inform them of those orbitals involved in the reaction and thus connect curly arrows to the IBO representation of the wavefunction. [147, 154] Weinhold and Glendening lean upon a modification to their NBO methods. [153] Liu and co-workers discard the MO model and interpret the wavefunction in tiles and draw conclusions from electron motion among and across those tiles. [151]

Other existing methods rest upon topological features of the electron density. [148–150]

In what ensues, we present a new method for drawing chemical bonding information across a reaction co-ordinate, with the ultimate aim of providing quantitative justification for the use of curly arrow mechanisms by connecting the ideas discussed in the previous section on energy partitioning and orbital localisation.

7.1 Reaction Orbitals: A Framework

The use of curly arrows in chemistry, usually comes with little-to-no quantitative justification. This is hardly a surprise. Their unrelenting success in describing chemical transformation can understandably lead to some complacency and readiness in their application. The reasoning associated with curly arrow mechanisms is often classical in nature. One could therefore suggest that the current nature of their application is one at odds with quantum mechanics, and inconsistent with what we have known of the nature of covalent bonds since the work of Ruedenberg in 1962. [92] If one were to write down some approximations and assumptions in a bid to justify the use of curly arrows, they might be

1. Electron correlation effects are negligible; molecular orbital theory can be applied.

2. Orthogonal, localised molecular orbitals can be found which correspond to the familiar chemical picture of bonds and lone pairs.

3. The total energy can be written as a sum of orbital energies.

4. Most of the molecular orbitals do not need to be considered as their energy contribution does not change over the reaction co-ordinate.

The neglect of correlation effects is common in large systems, and MO wavefunctions are the most widely used approximation to exact wavefunctions in quantum chemistry. The second item is almost always true, and one has at one's disposal a whole arsenal of orbital localization methods to choose from which are designed to produce orbitals resembling bonds and lone pairs. The third item is formally true

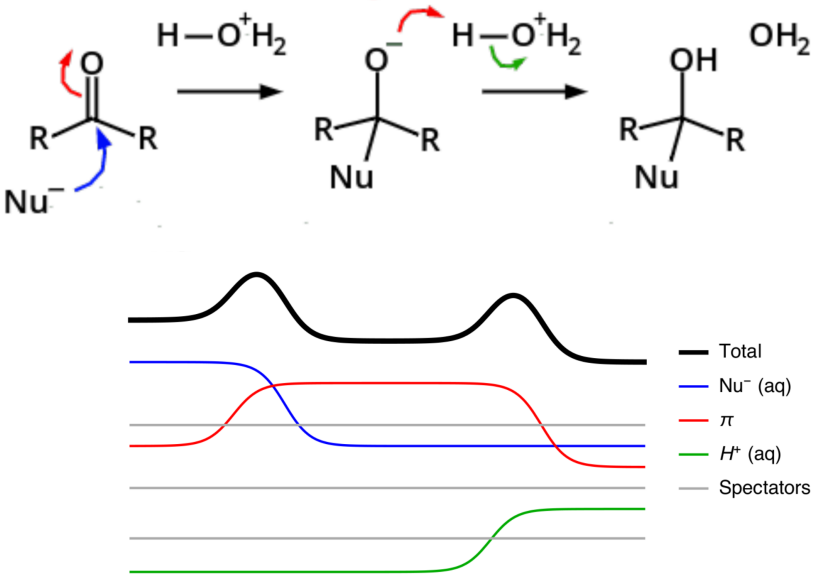

Figure 7.1: An example reaction mechanism (H_3O^+ is abbreviated to H^+) and orbital energies one may expect to see if the list of assumptions are all assumed valid.

in the case of the HF approximation. If the fourth item were also true, one would arrive at the familiar Walsh diagram picture of the reaction, and be able to plot the orbital energies along a reaction co-ordinate and obtain something similar to that shown in figure 7.1. That is, orbitals we shall refer to hereafter as "spectator" orbitals do not change in energy at all, and those involved in the making and breaking of bonds are responsible for the entirety of the energy changes over the reaction co-ordinate. In this make-believe scenario, the connection of curly arrows to the wavefunction is clear; as the orbitals spread themselves over more centres, and the atomic orbitals overlap, they decrease in energy, and as orbitals reduce the number of nuclei they're spread over, they increase in energy (see the blue and red lines in figure 7.1, respectively). The curly arrows are thus drawn in coincidence with those experiencing the energy changes (those whose shape and/or location changes significantly over the reaction).

In reality, it is easy to show item 4 is *not* true. The spectator orbitals experience strong energy changes through changing coulomb interactions with the electrons in all of the other orbitals, and with the nuclei. It transpires that these spectator orbital changes are very significant, as illustrated by the orbital energy changes shown in figure 7.2 for a simple reaction between a fluoride ion and hydrogen

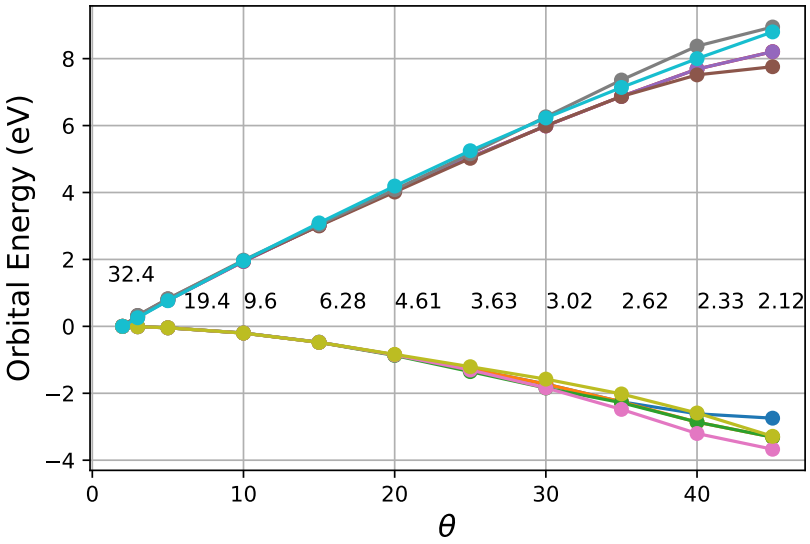

Figure 7.2: HF canonical orbital energy changes for the reaction F^- + HF in the aug-cc-pVQZ basis. The abscissa is the angle θ (degrees) and the H-F distances are $R_1 = R\cos(\theta)$ and $R_2 = R\sin(\theta)$. A selection of bond lengths (in atomic units) are indicated at points along the reaction co-ordinate.

fluoride. It is clear that drawing any conclusions about which orbital is which, and which ones are involved in the bond forming and bond breaking processes from the numbers alone is not straightforward. The reaction orbitals problem can thus be summarized as follows: to define a physically meaningful quantity associated with chemical bonding which, in contrast to the orbital eigenvalues, makes reasonable item 4 in the list of assumptions and approximations.

As a solution to the reaction orbitals problem we propose that we first partition the orbital energies into one-part classical and non-bonding effects, and one-part interactions leading to covalent bonding. The magnitude of the latter interactions will be refered to hereafter as 'covalency'. Upon the extraction of covalency from each orbital, we then propose uniquely optimised reaction orbitals be determined through the minimisation of an appropriate functional, referencing the newly-defined orbital covalency energies. This minimisation should be designed to concentrate the changes in orbital covalency into as few orbitals as yields physically reasonable results.

7.2 A Minimal Basis Energy Decomposition Scheme

We wish to define tensorially a quantity, V_{global}, which contains for any given restricted, closed-shell wavefunction all classical, electrostatic interactions and any quantity not culpable for the formation of covalent bonds. That is, we wish to acquire the ability to write the total energy for a system as,

$$\mathrm{E} = V_{\text{global}} + \sum_i H_{ii}, \tag{7.1}$$

where **H** is the "covalency matrix". The effects described by the elements of **H** depend upon the nature of the chosen basis set. In a minimal basis, orbital relaxation effects which drive bond formation are absent; there are too few Gaussians to provide the requisite flexibility. As a consequence, the variational balance is simply to have the kinetic energy decrease upon basis function overlap. This is seen clearly in fig 6.4. Thus the quantities responsible for covalent bonding along the reaction co-ordinate, given a set of optimum molecular orbitals are the kinetic energy integrals in the AO basis[1] in off-diagonal, inter-atomic elements.

An expression for the off-diagonal kinetic energy AO basis integrals in terms of those not arising through the overlap of basis functions can be found by constructing a matrix, $\mathbf{t}'$ in a basis whose member functions, and their second derivatives, are orthogonal. For a minimal basis containing two orbitals this is,

$$\mathbf{t}' = \begin{bmatrix} t'_{11} & 0 \\ 0 & t'_{22} \end{bmatrix}. \tag{7.2}$$

The diagonal elements of this AO basis kinetic energy matrix remain constant regardless of separation of two molecules or atoms, and the depression of the kinetic energy seen in figure 6.4 is absent. Transforming $\mathbf{t}'$ into a non-orthogonal basis capable of accounting for covalency with the overlap matrix,

$$\mathbf{S} = \begin{bmatrix} 1 & s \\ s & 1 \end{bmatrix} \tag{7.3}$$

[1]The term "in the AO basis" shall be used frequently throughout this chapter to describe integrals between basis functions.

raised to the power of a half yields a new kinetic energy matrix whose diagonal elements take a value dependent on the overlap of basis functions. This new matrix is

$$\mathbf{t}'' = \mathbf{S}^{\frac{1}{2}}\mathbf{t}'\mathbf{S}^{\frac{1}{2}} \tag{7.4}$$

$$= \begin{bmatrix} \frac{1}{2}(t'_{11} + (f(s))(t'_{11} - t'_{22}) + t'_{22}) & \frac{1}{2}(t'_{11} + t'_{22})s \\ \frac{1}{2}(t'_{11} + t'_{22})s & \frac{1}{2}(t'_{22} + (f(s))(t'_{22} - t'_{11}) + t'_{11}) \end{bmatrix}, \tag{7.5}$$

$$\text{where } f(s) = (1 - s^2)^{\frac{1}{2}}. \tag{7.6}$$

The corrections in the diagonal terms arising through overlap of different functions come only from the inter-atomic coupling terms, and are dependent on $f(s)$. Assuming basis function 1 and 2 are centred on the same atom, the corrections disappear as functions in minimal basis sets centred on the same atom are orthogonal by symmetry. In the case that orbitals 1 and 2 are centred on different atoms, the corrections do *not* disappear, and we must consider their influence. They contribute only what $f(s)$ allows, and as bonding in the minimal basis is present only through inter-atomic coupling across the kinetic energy operator, the energy changes associated with bond formation, which come from the diagonal elements, are characterized by the derivative of $f(s)$,

$$\frac{\mathrm{d}f(s)}{\mathrm{d}s} = -\frac{s}{(1 - s^2)^{\frac{1}{2}}}. \tag{7.7}$$

Figure 7.3 shows how the term governing the changes in the diagonal elements in equation 7.5 ($f(s)$) behaves, and its derivative with respect to overlap (equation 7.7). The results are those one should expect. For positive s, the gradient is negative, indicative of covalent bonding, and in the negative direction the gradient is positive (anti-bonding interactions between the basis functions, where the destructive interference results in the electrons being more confined, and thus the kinetic energy increasing). If we wish for the diagonal elements of $\mathbf{t}'$ to contain no covalent bonding effects, we must remove all terms dependent on s. Performing a Taylor expansion on equation 7.6 provides some clarity as to how this should be done.

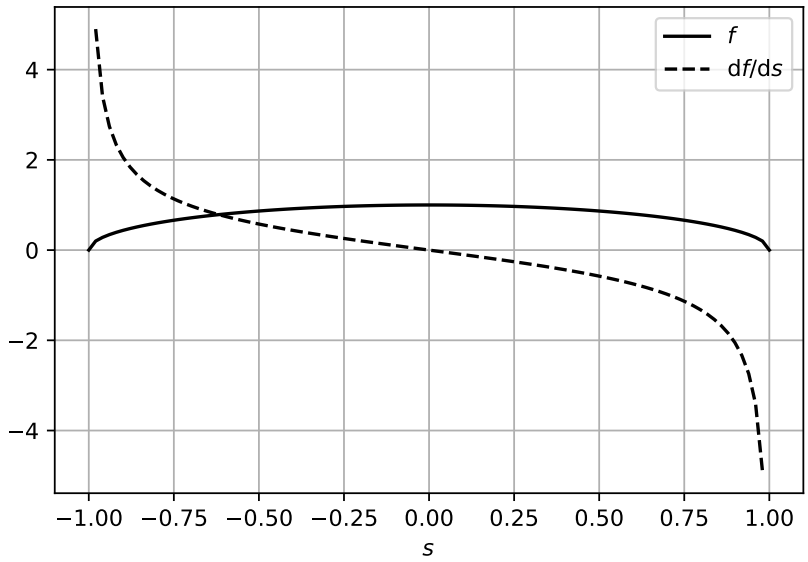

Figure 7.3: $f(s)$ (equation 7.6) and $\frac{\mathrm{d}f(s)}{\mathrm{d}s}$ (equation 7.7) over the interval $[-1, 1]$.

Assuming that s is small, and performing an expansion about zero one obtains

$$f(s) = 1 - \frac{s^2}{2} - \frac{s^4}{8} - \frac{s^6}{16} + \mathcal{O}(s^8). \tag{7.8}$$

Thus by simply setting $f(s) = 1$, we arrive at an expression for the kinetic energy integrals in a non-orthogonal AO basis set, the elements of which contain no covalent terms and are given by

$$\bar{T}_{\mu\nu} = \frac{1}{2}(T_{\mu\mu} + T_{\nu\nu})S_{\mu\nu}, \tag{7.9}$$

where $T_{\mu\mu}$ are the regular kinetic energy integrals between basis functions in a non-orthogonal basis set, or some other approximation to the diagonal elements expected as part of equation 7.2.

In reality, when one symmetrically orthogonalises the AO basis, the kinetic energy matrix is not diagonal, as in the model case shown in equation 7.2. The accuracy of this approach is reliant on a good choice of the elements $t'_{\mu\mu}$. Finding an appropriate equation for calculating the values of the diagonals is not straightforward. One option is to simply use the diagonals of the kinetic energy matrix in the non-orthogonal AO basis, and another is to set the inter-atomic elements of the non-orthogonal AO basis overlap and kinetic energy matrix elements to zero to form matrices $\mathfrak{S}$ and $\mathfrak{T}$, respectively, then symmetrically orthogonalise $\mathfrak{T}$ with

$\mathfrak{S}^{\frac{1}{2}}$, and transform back to the non-orthogonal basis by substituting $\mathfrak{T}_{\epsilon\epsilon}$ for $T_{\epsilon\epsilon}$ in equation 7.9. One further option is to use the eigenvalues of $\mathfrak{T}$ as the elements $T_{\epsilon\epsilon}$ in equation 7.9. At the time of writing, the solution to this problem remains to be found, and is still under investigation. We shall proceed under the assumption that the non-orthogonal AO basis diagonal elements of the kinetic energy matrix are reasonable approximations to t' in equation 7.9.

The nuclear part of the long range interaction energy between two molecules is controlled by the one electron potential. This is manifest in the form of the one electron potential energy operator, but let us briefly show this using an illustrative model. Say we have a pair of AOs, ϕ_1 and ϕ_2 are centred on two positive charges at positions $-r$ and 0, respectively, which are in the field of a negative point charge at R, such that $R \gg r$ in a linear system. A graphical representation of the system is shown below.

$$\overset{+1}{\underset{-r}{\bullet}} - \overset{+1}{\underset{0}{\bullet}} \cdots\cdots\cdots\cdots\cdots \overset{-1}{\underset{R}{\bullet}} \tag{7.10}$$

The total wavefunction in this model is normalised, plays host to two electrons and is written as a linear combination of the undefined atom-centred AOs,

$$\Psi = c_1\phi_1 + c_2\phi_2. \tag{7.11}$$

Given the presence of only two atomic orbitals one can write the coefficients in the expansion above as,

$$c_1 = \sin(\theta), \tag{7.12}$$

$$c_2 = \cos(\theta), \tag{7.13}$$

and naturally obtain $c_1^2 + c_2^2 = 1$. The interactions of the point charges (let us say the positive point charges on the left are two hydrogen nuclei, and the negative charge is a negative ion far away, and can be treated as a negative point) gives rise to the nuclear energy, and the energy of the nuclei interacting with the distant

point charge,

$$V_{\text{nuc}} = -R^{-1} - (r+R)^{-1} + r^{-1}, \tag{7.14}$$

$$\approx r^{-1} - (2R^{-1} + rR^{-2} + \mathcal{O}(R^{-3})), \tag{7.15}$$

which are grouped into one term for brevity. The nuclear energy thus changes approximately according to R^{-1} and must be appropriately controlled by a term in the electronic potential energy to recover the R^{-2} expected from a pure charge-dipole interaction. The one-electron potential energy integrals in the AO basis arising through interaction with the distant point charge are,

$$V_e = \int dr_e \quad \phi^* |R + r_e|^{-1} \phi, \tag{7.16}$$

$$= \int dr_e \quad \phi^* \left| R^{-1} \left(1 - \frac{r_e}{R}\right) \right|^{-1} \phi, \tag{7.17}$$

$$\approx \int dr_e \quad \phi^* \left(R^{-1} + R^{-2} r_e + \mathcal{O}(R^{-3})\right) \phi, \tag{7.18}$$

which in matrix form evaluate to

$$\mathbf{V}_e^{AO} = R^{-1}\mathbf{S} + R^{-2} \begin{bmatrix} 0 & -\frac{1}{2}sr \\ -\frac{1}{2}sr & -r \end{bmatrix}. \tag{7.19}$$

The sum of the one-electron potential and nuclear asymptotic energies in the molecular orbital basis is given by,

$$2V_e^{MO} + V_{\text{nuc}} = \left(\frac{rR^{-2}}{2(1-s^2)^{\frac{1}{2}}} \right) \cos(2\theta) + r^{-1}. \tag{7.20}$$

Thus the nuclear term is controlled by the one-electron potential alone, and the correct R^{-2} dependence is recovered. The charge-dipole interaction is given by μR^{-2}. The dipole for this system is $\mu = r\cos(2\theta)$. The pure charge-dipole term can clearly be seen in equation 7.20. The r^{-1} term naturally arises as part of the energy, is constant, and unimportant in our current discussion of long-range interactions and can thus be ignored.

In a minimal basis, then, where the kinetic energy is the driver of covalent bond formation, we now have an expression for V_{global} which contains no covalent effects

arising from the kinetic energy integrals,

$$V_{\text{global}} = \sum_i (\mathbf{C}^\dagger(\bar{\mathbf{T}} + \mathbf{V} + g[\mathbf{D}])\mathbf{C})_{ii}, \tag{7.21}$$

where $g[\mathbf{D}]$ is the two electron part of the HF energy calculated from the density $\mathbf{D}$ arising from the outer products of the optimum orbitals $\mathbf{C}$. Given the design of V_{global}, and the quantities we wish for it to contain, we may reasonably place the demand upon it that it have the same dependence upon intermolecular separation as the total energy at long range. The modification of the kinetic energy integrals also has the potential to influence this dependence through the induction energy. The kinetic energy truncation shown in equation 7.9 is deduced from a simple model with only one MO expressed as a sum of two atomic orbitals. Thus there are no intra-atomic kinetic energy integrals present. This raises the question of whether the AO integrals between atomic centres ought to be truncated, and those AO integrals which are intra-atomic be left untouched, or whether all AO basis kinetic energy integrals need to be treated in the same way if we are to ensure the induction energy remain a part of V_{global}, and does not pollute our covalency matrix. Allowing this pollution of the covalency energy would yield a V_{global} which does not behave appropriately at large inter-molecular separation. An answer can be found by investigating how the AO basis integrals influence the total kinetic energy in the molecular orbital basis. In order to do this, let us define a decomposition of the AO basis kinetic energy integrals into diagonal, inter- and intra-atomic components,

$$T_{\mu\nu}^{\text{inter}} = \begin{cases} T_{\mu\nu}, & \text{if } \nu \notin A \\ 0, & \text{otherwise,} \end{cases} \tag{7.22}$$

$$T_{\mu\nu}^{\text{diag}} = \begin{cases} T_{\mu\nu}, & \text{if } \mu = \nu \\ 0, & \text{otherwise,} \end{cases} \tag{7.23}$$

$$T_{\mu\nu}^{\text{intra}} = T_{\mu\nu} - T_{\mu\nu}^{\text{inter}} - T_{\mu\nu}^{\text{diag}}, \tag{7.24}$$

where $T_{\mu\nu}$ is the kinetic energy integral between basis functions μ and ν and A is the set of basis functions centred at the same position as μ. The full kinetic energy

matrix in the AO basis can thus be reconstructed as a sum of the above,

$$\mathbf{T} = \mathbf{T}^{\text{diag}} + \mathbf{T}^{\text{inter}} + \mathbf{T}^{\text{intra}}. \tag{7.25}$$

The quantities in equation 7.25 will be referred to as the *exact* diagonal, inter- and intra-atomic kinetic energy integrals in the AO basis. The matrix defined by equation 7.9 can be decomposed similarly, into

$$\bar{T}^{\text{inter}}_{\mu\nu} = \begin{cases} \bar{T}_{\mu\nu}, & \text{if } \nu \in A, \\ 0, & \text{otherwise,} \end{cases} \tag{7.26}$$

$$\bar{T}^{\text{diag}}_{\mu\nu} = \begin{cases} \bar{T}_{\mu\nu}, & \text{if } \mu = \nu, \\ 0, & \text{otherwise,} \end{cases} \tag{7.27}$$

$$\bar{T}^{\text{intra}}_{\mu\nu} = \bar{T}_{\mu\nu} - \bar{T}^{\text{inter}}_{\mu\nu} - \bar{T}^{\text{diag}}_{\mu\nu}. \tag{7.28}$$

These components can then be summed together to give the "scheme 1" kinetic energy in the AO basis. It is constructed of a full set of truncated AO basis integrals, with only the diagonal elements remaining unchanged. A final kinetic energy matrix,

$$T'_{\mu\nu} = \bar{T}^{\text{inter}}_{\mu\nu} + T^{\text{diag}}_{\mu\nu} + T^{\text{intra}}_{\mu\nu}, \tag{7.29}$$

is defined and referred to as the kinetic energy in the AO basis under "scheme 2". This is the kinetic energy matrix one obtains by truncating the AO basis integrals according to 7.9 only if basis functions with index μ and ν are centred on different atoms. The energy (or property) associated with the AO basis integrals in the MO basis can be calculated by substituting the appropriate matrix in place of $\mathbf{X}$ in

$$E_X = \sum_i (\mathbf{C}^\dagger \mathbf{X} \mathbf{C})_{ii}, \tag{7.30}$$

where the matrix $\mathbf{X}$ is any matrix of AO basis integrals.

Figure 7.4 shows the energy associated with the intra-atomic, diagonal, inter-atomic, and full kinetic energy integrals, in their exact form and under schemes 1 and 2, as a function of R over the interval [30, 40] Bohr radii, where R is the

distance between the H in HF and an F^- ion in the constrained linear system,

$$F^- \cdots\cdots\overset{R}{\cdots\cdots} H - F. \tag{7.31}$$

The change in the exact, inter-atomic kinetic energy integrals (solid blue line) is small, given the nuclear separations but still noticeable. It is also the only contribution to the total kinetic energy which decreases as R decreases. The exact intra-atomic contributions to the total kinetic energy increase sharply as R decreases. The contributions dependent on the diagonal integrals increase most steeply of all, but take values which are consistent across all schemes. The solid grey line is the total kinetic energy in the MO basis, and is the sum of the solid coloured lines. The increase in the kinetic energy at these large distances is due to the kinetic contribution to the induction energy, where the overlap between the basis functions on the ion and those in the molecule is basically zero, but the electrostatically induced dipole in the molecular orbitals on the molecule yields an overall increase in the kinetic energy of the system. The desired outcome of the truncation scheme is thus that the total truncated kinetic energy will change at the same rate as the exact MO basis total kinetic energy, but without any covalent interactions included, thereby incorporating the induction energy into V_{global}. The dashed lines are those obtained under scheme 1; all kinetic energy integrals are treated the same way, and truncated according to equation 7.9. The scheme 1 intra-atomic contributions once transformed into the MO basis do not change with the nuclear separation; they're dependent on the overlap of orthogonal functions and manifestly zero. Rather, the change is forced in its entirety into the inter-atomic contributions which increase as R decreases. The sums of the coloured dashed lines, and the green solid line is the total kinetic energy under scheme 1 (black dashed line), and agrees with the change in the exact MO basis total kinetic energy almost perfectly. Under scheme 1, then, the $R-$dependence must be retained. Under scheme 2, the total, truncated kinetic energy in the MO basis is shown by the dotted black line, which shows a significant deviation from the exact total kinetic energy in the MO basis. The $R-$dependence is thus destroyed if this scheme is used; the total kinetic energy under scheme 2 (black dotted line) is given by the sum of the solid green, dotted blue and solid red lines. In summary, truncating *all* kinetic energy integrals yields a kinetic energy

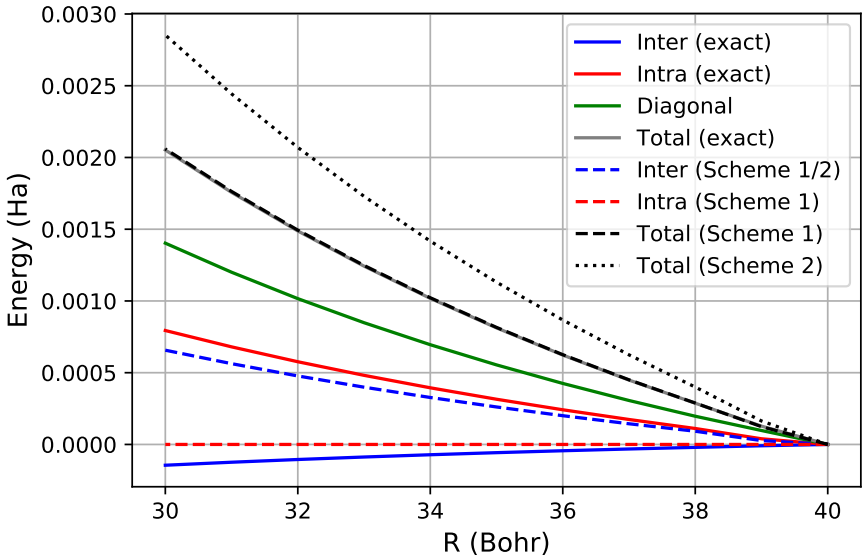

Figure 7.4: The contributions of various kinetic energy matrices to the MO basis kinetic energy. Solid lines are various contributions to the atomic orbital basis kinetic energy integrals transformed into the MO basis. The dashed lines correspond to those contributions defined in equations 7.26, 7.28 and 7.9 in order of appearance in the legend. The dotted line corresponds to the equation 7.29. The scheme(s) each quantity is part of is indicated in brackets in the legend.

matrix whose intra- and inter-atomic terms cancel appropriately, and intra-atomic kinetic energy contributions to the MO basis kinetic energy do not change along the reaction co-ordinate. Truncating the inter-atomic kinetic energy integrals alone leads to a kinetic energy matrix whose inter- and intra-atomic contributions to the total MO basis kinetic energy do *not* cancel sufficiently and the $R-$dependence is ruined.

Figure 7.5 shows the total HF energy in the MINAO basis, along with V_{global} and the pure dipole-charge interaction μR^{-2} for the same example. V_{global} is calculated according to equation 7.21, and the kinetic energy integrals are truncated under scheme 1. It is clear to see that the R-dependence is retained, and the change in V_{global} with reaction co-ordinate agrees well with the change in the total energy. Both V_{global} and the RHF energy agree nicely with the pure dipole-charge interaction, which is a reasonable approximation for the energy change of this system at such large ion-molecule separation. It is assumed hereafter that any reference to the truncation of the kinetic energy integrals concerns scheme 1. The difference between V_{global} and the RHF energy at each point in figure 7.5 is, according to equation 7.1, the change in the covalency energy of the system.

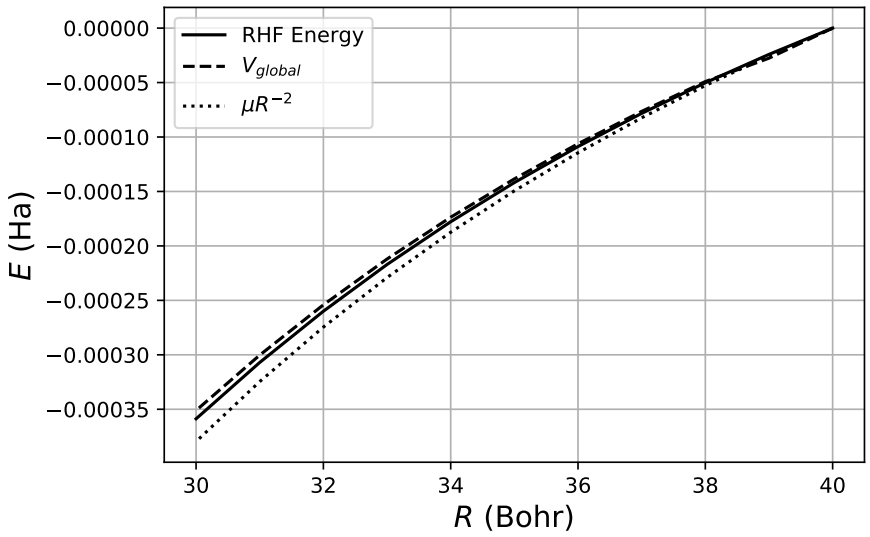

Figure 7.5: The RHF energy, V_{global} (computed using scheme 1 kinetic energy matrix) and dipole-charge interaction for the constrained linear F^- ion interacting with a hydrogen fluoride molecule as a function of the F^--H distance, R.

We have now derived an energy decomposition scheme for minimal basis wavefunctions, which in principle should provide us with an energy associated with each orbital which is constant for the "spectator" orbitals as discussed in section 7.1, and changes strongly only for those involved in bond breaking or bond forming processes. Thus we have made reasonable the list of necessary assumptions presented in section 7.1 for the use of curly arrows and frontier orbitals. We shall persist with the same example as shown in equation 7.31, and first inspect the behaviour of V_{global} and the covalency energy as the trace of their respective matrices, and then on an orbital-by-orbital basis. The charge-dipole interaction between the distant F^- ion and the dipolar HF molecule is attractive, and thus when decreasing R one approaches a minimum in the energy at the point where $R = r$, and by symmetry any further decrease in R leads to an $r > R$ and produces a mirror image of the energy surface already explored. Figure 7.6 shows how the overlap integral between the atomic basis hydrogen 1s and both atomic basis $2p_z$ orbitals changes as R is decreased, and indicates that any change in the covalency energy of orbitals describing bonding between the H and F^- where $R > 9$ must be erroneous. One should expect, then, that V_{global} keep the same R-dependence as the total energy until R is somewhere in the region of 8 to 4 Bohr radii before deviating, and the covalency should remain approximately constant until the same R by construction.

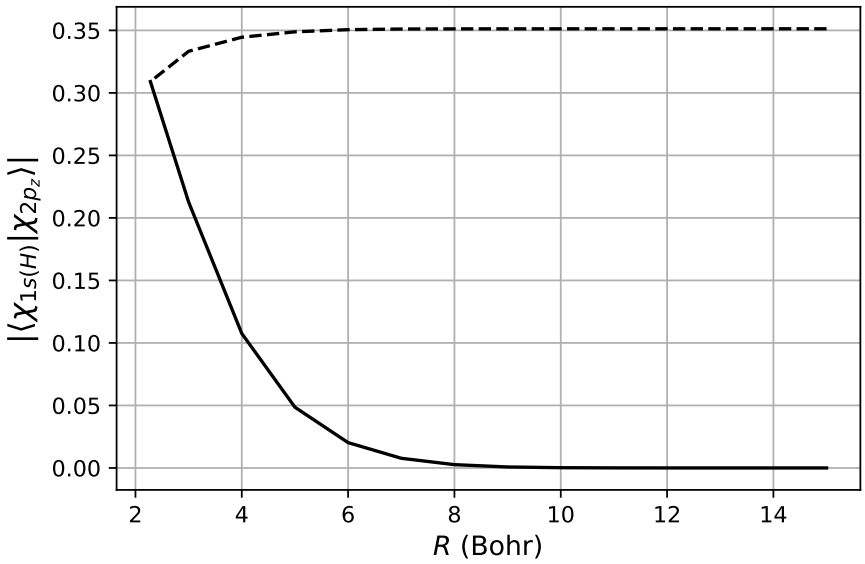

Figure 7.6: The modulus of the overlap integral between the atomic basis 1s function centred on the hydrogen in HF and the atomic basis $2p_z$ function centred on the incoming fluoride ion at distance R (solid line), and the same basis function centred on the F atom in the HF molecule (dashed line) and as a function of ion-molecule separation.

Figure 7.7 shows V_{global} and the total RHF and covalency energies of the system over the reaction co-ordinate. It is immediately clear that V_{global} shows the same R-dependence at long range as the total energy, and that the total covalency energy of the system remains constant until approximately 3.5Å separation. This is in line with what one should expect given the overlaps shown in figure 7.6.

While one would normally use localised orbitals for drawing conclusions about chemical change along a reaction co-ordinate in order to minimise the number of molecular orbitals changing strongly in shape, canonical orbitals provide a deep link with molecular orbital diagrams used in organic and inorganic chemistry. This link is especially strong when MOs are expressed in a minimal basis where the experimental chemists "symmetry adapted linear combinations" (SALCs) of atomic orbitals really are the molecular orbitals yielded by the RHF procedure, and not complicated combinations of large numbers of valence orbitals. We first perform the energy decomposition using canonical orbitals and later consider the use of localised orbitals. The linear combinations of atomic orbitals one expects from classical MO theory are those shown in figure 7.8. That is, that covalent bonding arises through σ bonding interactions between 1s functions on each fluorine atom,

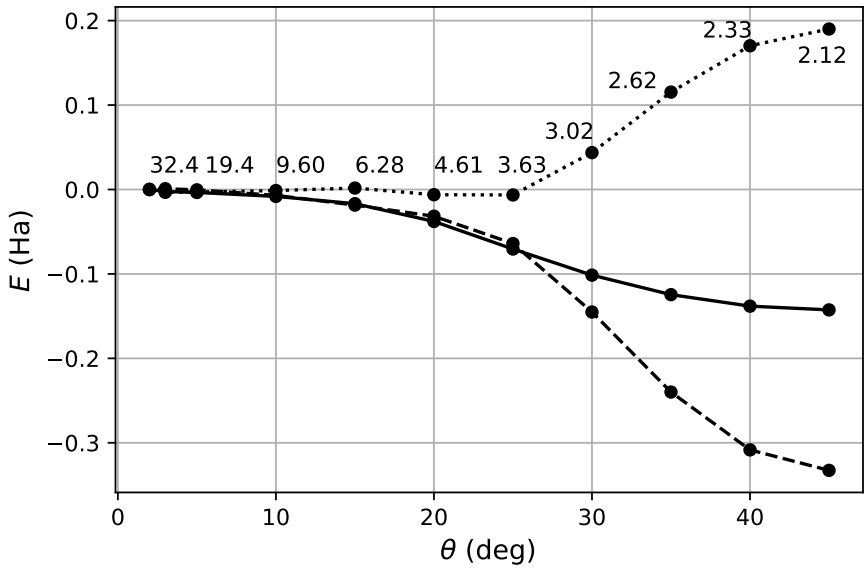

Figure 7.7: V_{global} (dashed line), total RHF (solid line) and covalency energy (dotted line) along the reaction co-ordinate for F^-+HF defined by the angle θ where the HF bond distances are $R = \lambda\cos(\theta)$ $r = \lambda\sin(\theta)$, where λ is optimised at each θ. R (Å) is shown at all points along the line for the covalency energy except the asymptotic point at $R = 48.3$ Å$(\theta = 2°)$.

2s functions on each fluorine atom, and the combination of the 1s on the hydrogen and the two p_z orbitals on the fluorine atoms. There is further splitting through π interactions between the p_x and p_y functions on each fluorine. The energy levels are then filled appropriately with 20 electrons to account for the charge on the molecule. The unoccupied orbital σ_3^* is the combination of the phase-flipped 1s on the hydrogen with the A_g orbital. Of course, in the mission to deduce curly arrow mechanisms, this is not ideal. It is more desirable to have covalency energy changes in a smaller number of orbitals. It is, however, beneficial to consider first an example for which we have an expected outcome and can therefore gauge the success of the energy partitioning without the question of how using localised orbitals will impact the picture by reducing the number of orbitals changing in energy. The use of canonical orbitals avoids the difficult problem of assessing whether any spurious results arise through a deficiency in the energy partitioning or as artefacts of the chosen localisation procedure.

Here it is worth stressing the physical interpretation of equation 7.1. That is, positive changes in the covalency energy are manifestly anti-bonding quantities, whereas decreases in the orbital covalency energy are bonding quantities; positive

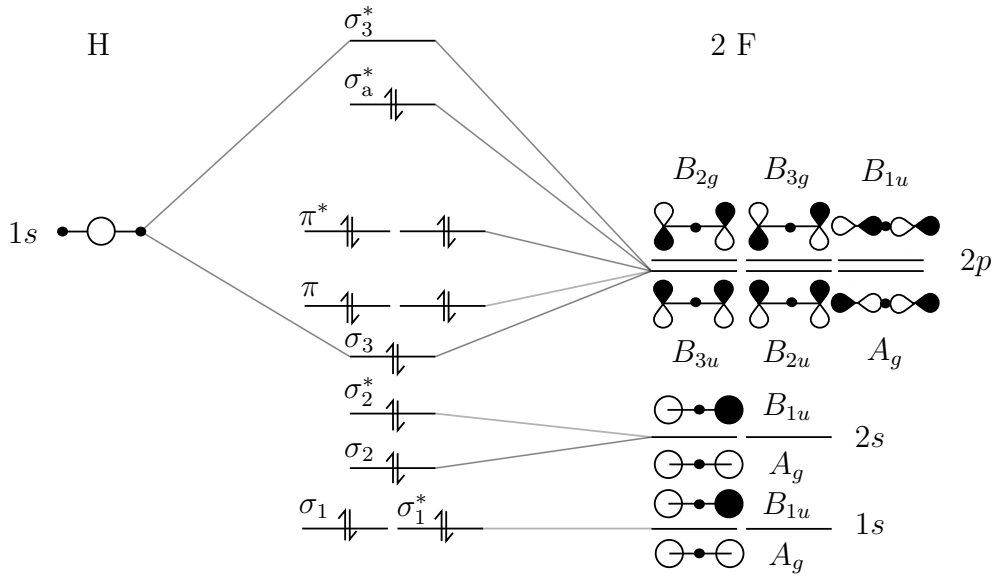

Figure 7.8: Molecular orbital diagram for $[FHF]^-$. The symmetry labels are dropped in the molecular orbitals for better agreement with the scan of the reaction co-ordinate, in which the symmetry changes.

changes increase the energy of the system and negative changes decrease the energy of the system, with the difference being made up by V_{global}. Figure 7.9 shows the changes in orbital covalency for the RHF canonical orbitals in the MINAO basis. The changes in covalency are consistent with what is expected from the MO diagram; the σ_1 and σ_1^* orbitals experience hardly any change in covalency over the reaction co-ordinate, with the out-of-phase combination showing a very small increase in the covalency energy and the in-phase combination showing a small decrease, these changes cancel in the trace. The σ_2 orbital shows a decrease in covalency energy and is thus bonding as expected. The σ_2^* contribution requires additional explanation, and will be discussed shortly. The MO arising from the in-phase combination of the two $2p_z$ orbitals shows a negative change in covalency energy. The anti-bonding complement σ_3^* is a virtual orbital and thus not shown. The π orbital contributions cancel appropriately, and the respective bonding and anti-bonding properties are recovered; in-phase combination shows a decrease in the covalency energy whereas the out-of-phase, anti-bonding combination of the AOs shows an increase. The orbitals obtained from a calculation at the ground state geometry ($\theta = 45°$ in figures 7.7 and 7.9), except the σ_1 and σ_1^* orbitals, can be seen in figure 7.10.

The σ_2^* orbital, while anti-bonding at the ground state of the system, is seem-

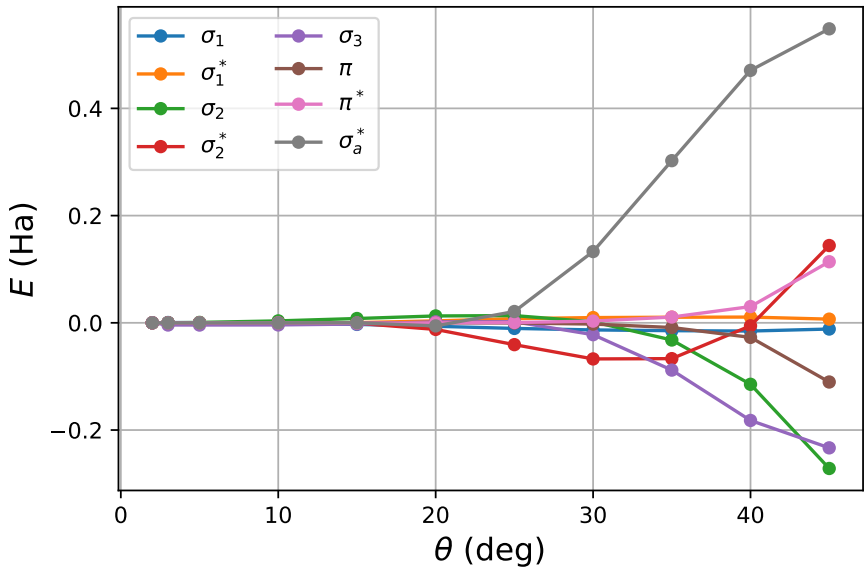

Figure 7.9: Orbital covalencies of the canonical RHF orbitals in the MINAO. The labels correspond to those orbitals shown in figure 7.8.

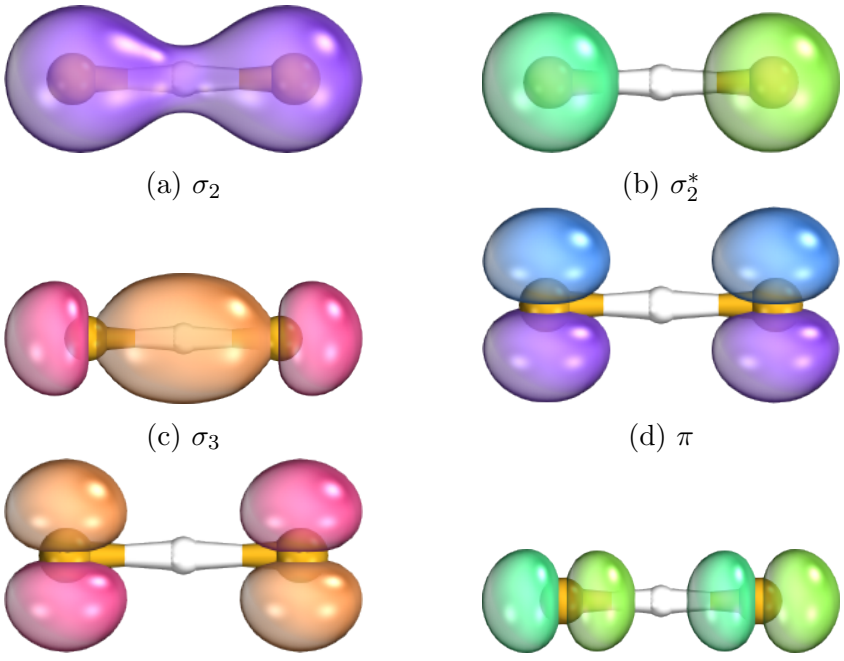

(a) σ_2 (b) σ_2^*

(c) σ_3 (d) π

(e) π^* (f) σ_a

Figure 7.10: The canonical orbitals arising from a HF calculation on $[FHF]^-$ at the ground state. The labels coincide with those shown in the MO diagram in figure 7.8.

ingly a bonding orbital at increased ion-molecule separation (in truth, it is not an antibonding orbital at smaller θ, it is an MO which very closely resembles the atomic $2s$ function). An explanation for this is found by inspecting figure 7.11, which shows the form of the so-called σ_2^* orbital at $\theta = 40°$ in figure 7.9, that is, at

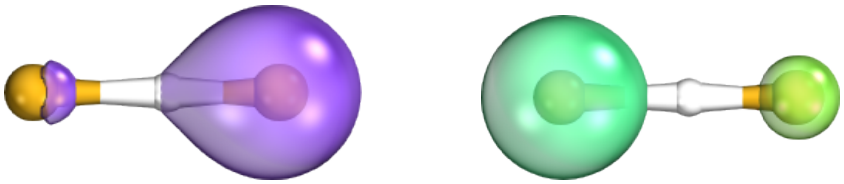

(a) $\sigma_2,\ \theta = 40°$ (b) $\sigma_2^*,\ \theta = 40°$

Figure 7.11: The σ_2 and σ_2^* canonical orbitals arising from a HF calculation on $[FHF]^-$ at the ground state at $\theta = 40°$ on the reaction co-ordinate in figure 7.7. The labels coincide with those shown in the MO diagram in figure 7.8.

the value of θ that the covalency energy associated with the "σ_2^*" approaches the point at which it becomes anti-bonding. The σ_2 orbital is also shown, and provides clarity to the fact that the σ_2^* orbital becomes anti-bonding as a consequence of the orthonormality constraint; also visible is the distortion of the $2s$ function on the approaching fluoride ion in the σ_2^* as the s function on the hydrogen has become available, and the out-of-phase contribution from the other $2s$ orbital maintaining the orthogonality of the σ_2^* MO with the σ_2 MO. Thus, the bonding behaviour shown in the covalency energy arising from the "σ_2^*" orbital is due to the distortion of the $2s$ upon the approach of the ion over distances where the orthogonality constraint does not require large contributions from the other $2s$ orbital.

The results suggest, then, that the minimum in this complex is found through predominantly electrostatic and classical effects, and in fact, the covalent interaction is *destabilising* once all orbital covalencies are taken into account.

At the beginning of this chapter, we set out with the intention of connecting curly arrows and frontier orbitals to *ab initio* wavefunctions. While we have managed to extract parts of the Fock eigenvalues associated with covalent bonding, the picture is more complex than one which might allow us to draw the two curly arrows an organic chemist might anticipate from this reaction co-ordinate. Usually, the computational chemist turns to localised orbitals in order to minimise the change in the shapes of those orbitals not involved in a chemical transformation and to generate orbitals which resemble frontier orbitals, and are more conceptually appealing. An attractive feature of the tensorial definition of V_{global} is that the transformation of the molecular orbitals on which it depends is usually performed by orbital rotations after a variational calculation. These rotations leave the trace of any symmetric matrix unchanged, and thus the total V_{global}, and total

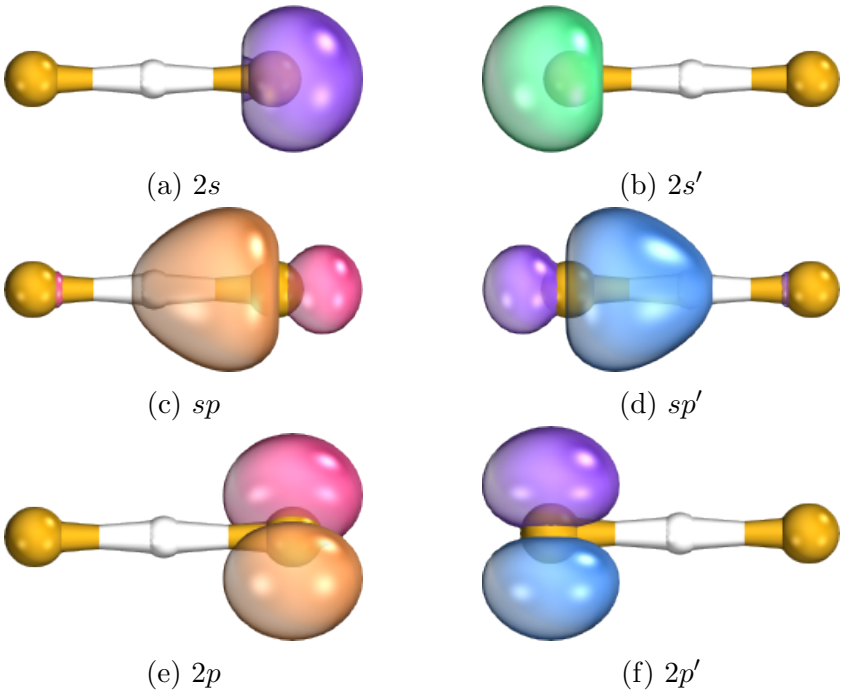

(a) $2s$ (b) $2s'$

(c) sp (d) sp'

(e) $2p$ (f) $2p'$

Figure 7.12: The Pipek-Mezey orbitals arising from a HF calculation on $[FHF]^-$ in its ground state geometry. The labels are chosen according to their appearance and evident hybridisation. A prime denotes orbitals centred on the approaching fluoride ion in a scan of the reaction co-ordinate.

covalency is invariant to localisation, as long as it is performed by applying unitary transformations to the orbital coefficient matrix. The orbital contributions to the total covalency and total V_{global} will of course change upon mixing through rotation. Localising our set of molecular orbitals, then, one should expect to see a dampening of the orbital covalency energy changes in the spectator orbitals, as their shape changes are less significant over the course of the reaction. Figure 7.12 shows a selection of the Pipek-Mezey orbitals generated from a HF calculation at the equilibrium geometry. They clearly coincide well with the orbitals one expects to see from frontier orbital theory.

The covalency energies associated with the PM orbitals are shown in figure 7.13. The orbital covalencies of the spectator orbitals are almost constant over the whole reaction co-ordinate, with the exception of $2s'$ which requires further discussion. The orbitals which change in covalency energy strongly are those one might expect. The sp and sp' orbitals change most strongly, and are those involved in the bond making and bond breaking. The decrease in the orbital covalency of the sp' orbital comes through the expansion over the H atom as R is decreased. The increase

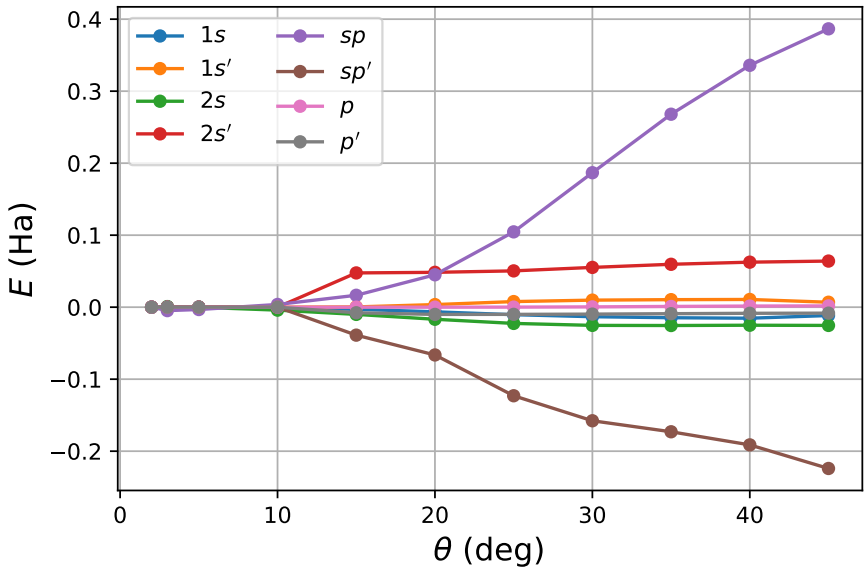

Figure 7.13: Orbital covalencies of the PM orbitals generated from a RHF wavefunction in the MINAO basis. The labels correspond to those orbitals shown in figure 7.8.

in orbital covalency seen in the sp orbital is an antibonding effect which arises as the orbital is forced to contract upon the approach of the sp' orbital. The core $1s$ orbitals are *not* localised and correspond to the σ_1 and σ_1^* orbitals of the canonical investigation. This is because enforcing the localisation of the full occupied orbital space leads to large and unphysical changes in the covalency energies of the core orbitals. The reason for this in a minimal basis is unclear, and the topic of further investigation, a likely cause is the small expansions and contractions of the core orbitals which do not cancel as they do in the canonical case, where there are contributions from two $1s$ orbitals with opposing behaviour; where one contracts the other necessarily expands.

The kink in the orbital covalency for the $2s'$ orbital in figure 7.13 is an artefact of the localisation procedure. The sp-hybridisation changes from being weakly sp^3 to the expected $2s$ orbital and thus there is a rapid change in shape, which is shown in the covalency energy. This is demonstrated in figure 7.14. Promisingly, for all $\theta > 15°$, and all $\theta < 10°$ the covalency remains constant. In a later section we shall explore an extension to this analysis which ensures this does not happen, regardless of the localisation procedure.

(a) $2s'$, $\theta = 10°$ (b) $2s'$, $\theta = 15°$

Figure 7.14: The $2s'$ Pipek-Mezey orbital arising from a HF calculation on $[FHF]^-$ on the reaction co-ordinate in figure 7.7.

7.3 Generalisation to Large Basis Sets

The properties of the minimal basis wavefunction which make the analysis in the previous section possible are not present in large basis sets containing polarisation functions. The processes which lead to covalent bond formation are more delicately balanced, as discussed earlier in this chapter, and demonstrated in figure 6.3. That is, as orbitals overlap and bonds are formed, the kinetic energy decreases initially as the electrons delocalise in the bonding direction. A critial point is reached in the interaction where the potential energy, which was increasing, begins to decrease as the kinetic energy pressure decreases; once the electrons are delocalised and the kinetic energy decreases, the potential energy begins to decrease against the reduced resistance of the kinetic energy. This decrease drives orbital contraction, or orbital polarisation, which is not present in a minimal basis description as it lacks the appropriate functions. The kinetic energy then begins to increase, hostage to the virial theorem.

Thus, the generalisation of the procedure outlined in section 7.2 to large basis sets cannot be a direct translation; the variational flexibility of a larger basis wavefunction ensures we cannot simply apply the same recipes and expect to remove the covalency while calculating V_{global}. At least, not without also trying to derive equations for the truncation of the one- and two-electron potentials, and the former is left in its exact form in the previous section to control the nuclear repulsion. Thus, any truncation of off-diagonal elements runs the risk of breaking the long range R-dependence of V_{global}. Although the difference in the effects driving bonding between minimal and large bases complicates the picture somewhat, it also provides us with the means to generalise the results of the previous section in an indirect way. If we are able to remove covalent effects in a minimal basis, and if that basis contains too few functions to describe the orbital relaxation responsible

for the potential energy lowering seen in large basis wavefunctions, any minimal basis representation of a large basis wavefunction which accurately describes the long range electrostatic and non-covalent interactions can simply have its associated V_{global} matrix projected into the large basis and subtracted from the large basis Fock matrix to yield a covalency matrix for a more accurate wavefunction. The diagonals of this covalency matrix will thus contain the covalent effects of the large basis associated with kinetic energy depression, *and* orbital relaxation.

In the following we make use of two basis sets; a large, primary basis set, B_1, and a minimal basis set, B_2, such that $B_2 \subset B_1$. We shall be deducing formulae for moving between bases, and while there will always be information lost in the transformation from the primary to the minimal basis set, we are able to eliminate all of the error associated with the transformation from the minimal to primary basis set by imposing the requirement that B_2 be a subset of B_1. This requirement is not essential to the method, but is the only sensible way here to choose a minimal basis. The data lost in the transformation to the minimal basis are the finer details of large basis orbitals arising primarily through relaxation. Also not reproducible in a minimal basis are the kinetic energy integrals between functions which are not orthogonal over larger ranges than they might be in a minimal basis, as a result of the inclusion of diffuse functions in the large basis set. Again, these are not bonding effects we wish to be able to reproduce and thus pose no concern. An unavoidable issue in this approach is that the minimal basis representation of the wavefunction will never be able to capture *all* of the electrostatic, non-bonding effects present in the large basis. This will lead to some contamination of the orbital covalency energies with quantities we would rather have placed in V_{global}. However, it is hoped that the contamination over long range will be close to zero, and over short range only make up a small percentage of the orbital covalency energies.

Many of the equations used in chapter 4, inspired by those in Knizia's IBO procedure will be repeatedly used again here. [76] For clarity of communication these equations will be presented again here, as if for the first time. Let us define

two projection operators,

$$\mathbb{P} = |\chi_\alpha\rangle \left(\mathbf{S}^{-1}\right)_{\alpha\beta} \langle\chi_\beta| \,, \tag{7.32}$$

$$\bar{\mathbb{P}} = |\bar{\chi}_\mu\rangle \left(\bar{\mathbf{S}}^{-1}\right)_{\mu\nu} \langle\bar{\chi}_\nu| \,, \tag{7.33}$$

where we have introduced a notation we shall lean upon heavily for the remainder of this section; an overbar denotes a quantity defined in, or member function of the minimal basis, B_2. The symbol χ is used for atomic basis functions. Any quantity or basis function presented which does not have an overbar is defined in B_1. We shall also refer to functions in B_2 with indices μ, ν and ϵ and ξ, and functions in B_1 with indices α, β, γ and δ. A set of molecular orbitals $\{\psi_i\}$ defined in B_1 by a linear combination,

$$|\psi_i\rangle = \sum_\alpha \chi_\alpha C_{\alpha i}, \tag{7.34}$$

can be projected onto the minimal basis by applying the projection operator defined in equation 7.33 to yield a new set of molecular orbitals, $\{\bar{\psi}_i'\}$. That is,

$$|\bar{\psi}_i{}'\rangle = \bar{\mathbb{P}} \, |\chi_\alpha\rangle \, C_{\alpha i} \tag{7.35}$$

$$= |\bar{\chi}_\mu\rangle \left(\bar{\mathbf{S}}^{-1}\right)_{\mu\nu} \Delta_{\nu\alpha} C_{\alpha i}, \tag{7.36}$$

$$= |\bar{\chi}_\mu\rangle \, \bar{C}'_{\mu i}, \tag{7.37}$$

where

$$\Delta_{\mu\alpha} = \langle\bar{\chi}_\mu|\chi_\alpha\rangle \,, \tag{7.38}$$

$$\bar{\mathbf{C}}' = \bar{\mathbf{S}}^{-\mathbf{1}} \boldsymbol{\Delta} \mathbf{C}. \tag{7.39}$$

The Einstein summation convention has been used in the above, and will be used throughout this section. The orbitals $\{\bar{\psi}_i'\}$ will not necessarily be mutually orthogonal, but can be symmetrically orthogonalised to form a new set of minimal basis molecular orbitals $\{\bar{\psi}_i\}$ with coefficients,

$$\mathbf{C} = \bar{\mathbf{C}}' \bar{\mathbf{\Lambda}}^{-\frac{1}{2}}, \tag{7.40}$$

where

$$\bar{\Lambda}_{ij} = \langle \bar{\psi}_i | \bar{\psi}_j \rangle \,, \tag{7.41}$$

$$\bar{\mathbf{\Lambda}} = \bar{\mathbf{C}}'^{\dagger} \bar{\mathbf{S}}^{-1} \bar{\mathbf{C}}'. \tag{7.42}$$

These orbitals then represent a starting point which one can perform some unitary transformations according to criteria in order to generate a set of minimal basis orbitals which represent the large basis, long-range electrostatic effects faithfully. As we discussed at length in chapter 4, a variationally optimised minimal basis wavefunction does *not* produce accurate electrostatics and therefore is not an option for generating optimal $\bar{\mathbf{C}}$. Moreover, it is preferable to find orbitals in the minimal basis through some reference to the large basis orbitals, such that V_{global} is sensitive to the choice of the large basis set. A suitable procedure for this was laid out in detail in section 5.1 in determining the reduced orbitals of ROPA.

Having optimised the minimal basis MO coefficients to yield, say, reduced orbitals, one can *exactly* reproduce them in B_1 (if $B_2 \subset B_1$) as the set of molecular orbitals, $\{\phi_i\}$, by projection onto B_1,

$$|\phi_i\rangle = \mathbb{P} \, |\bar{\psi}_i\rangle \,, \tag{7.43}$$

$$= |\chi_\alpha\rangle \left(\mathbf{S}^{-1}\right)_{\alpha\beta} \left(\Delta^{\dagger}\right)_{\beta\mu} \bar{C}_{\mu i}, \tag{7.44}$$

$$= |\psi_\alpha\rangle \, \tilde{C}_{\alpha i}, \tag{7.45}$$

where

$$\tilde{\mathbf{C}} = \mathbf{S}^{-1} \mathbf{\Delta}^{\dagger} \bar{\mathbf{C}} \tag{7.46}$$

and $\tilde{\mathbf{C}}$ is the matrix of optimal minimal basis molecular orbital coefficients expressed in the large basis. The B_1 representation of the orthonormal B_2 molecular orbitals will naturally require no orthogonalisation. The B_2 atomic orbital integrals can similarly be exactly transformed into B_1 by

$$I^{B_1}_{\alpha\beta} = (\mathbf{\Delta}^{\dagger})_{\alpha\mu} (\bar{\mathbf{S}}^{-1})_{\mu\nu} I^{B_2}_{\nu\epsilon} (\bar{\mathbf{S}}^{-1})_{\epsilon\xi} \Delta_{\xi\beta}. \tag{7.47}$$

The B_1 integrals can similarly be transformed, and reduced, into B_2 by

$$I^{B_2}_{\mu\nu} = \Delta_{\mu\alpha}(\mathbf{S}^{-1})_{\alpha\beta} I^{B_1}_{\beta\gamma} (\bar{\mathbf{S}}^{-1})_{\gamma\delta} (\mathbf{\Delta}^{\dagger})_{\delta\nu}. \tag{7.48}$$

where I is any integral across basis functions in the basis indicated in the superscript, and by the subscript notation outlined previously. The total V_{global} for the system expressed in B_1 is then defined as the trace of the matrix,

$$\mathbf{V}_{\text{global}} = \sum_i \left(\tilde{\mathbf{C}}^{\dagger} \mathbf{\Delta}^{\dagger} \bar{\mathbf{S}}^{-\mathbf{1}} (\bar{\mathbf{T}}^{\text{trunc}} + \bar{\mathbf{V}} + g[\bar{\mathbf{D}}]) \bar{\mathbf{S}}^{-1} \mathbf{\Delta} \tilde{\mathbf{C}} \right)_{ii}, \tag{7.49}$$

where $\mathbf{T}^{\text{trunc}}$ is the kinetic energy matrix in B_2 truncated according to the scheme 1, $\bar{\mathbf{V}}$ is the minimal basis one-electron potential energy matrix, and $g[\bar{\mathbf{D}}]$ is the matrix of two-electron integrals in the minimal basis calculated with the density arising from the optimal $\bar{\mathbf{C}}$, which in this thesis will always be chosen as the set of reduced orbitals given by the procedure in section 5.1. The individual terms in the sum in equation 7.49 are the V_{global} associated with each orbital, i. The total covalency energy is the trace of the covalency matrix, the elements of which are given by,

$$H_{ij} = F_{ij} - V^{\text{global}}_{ij}, \tag{7.50}$$

where $\mathbf{F}$ is the B_1 Fock matrix in the MO basis.

As a basis for comparison, and to gauge the success of the generalised approach, we shall perform the same analysis on the same system as in the previous section, first using canonical orbitals, and then using localised orbitals. It is worth mentioning the scheme presented in this section that if the choice of orbitals changes, the value of V_{global} will also change. For instance, if reduced orbitals are used, they will change depending on whether the reference set of orbitals in the large basis are localised or not, and so will the associated V_{global}. Let us add to the MINAO basis those s- and p-functions not already contained within MINAO but are a part of the cc-pVTZ basis set to the fluorine atoms, and the additional s-functions to the hydrogen. That is, define B_1 as the subset of cc-pVTZ s- and p-functions for atoms which are not hydrogen, and the subset of cc-pVTZ s-functions for hydrogen atoms, roughly tripling the dimension of the basis. This subset of cc-pVTZ will be

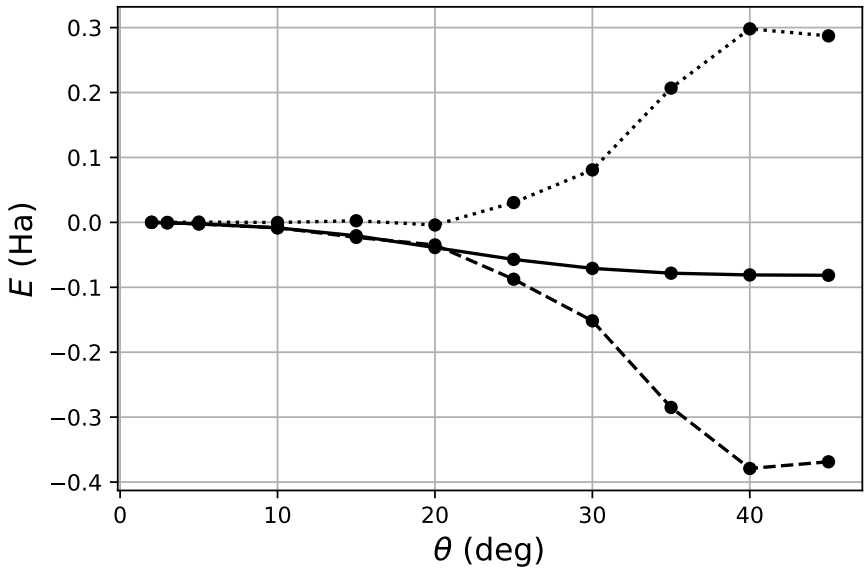

Figure 7.15: Total (solid line), covalency (dotted line) and global potential (dashed line) energies calculated using MINAO reduced orbitals, with canonical reference orbitals in the cc-pVTZ(p/s) basis, over the reaction co-ordinate for $[FHF]^-$ formation as a function of the angle θ. The HF bond distances are $R = \lambda\cos(\theta)$ $r = \lambda\sin(\theta)$, where λ is optimised at each θ.

denoted cc-pVTZ(p/s) hereafter. The associated total V_{global}, energy and covalency energy, calculated with reduced orbitals which are generated by reference to cc-pVTZ(p/s) canonical Fock orbitals, are shown in figure 7.15 which shows that the global potential, when calculated in this way, faithfully reproduces the long-range energy change arising primarily through electrostatic interactions. The changes in total covalency, and total global potential are more severe than seen in the minimal basis example in the previous section. While there is bound to be some pollution of the covalency energy with non-covalent effects, this is not necessarily the source of the increased deviation. Inspection of the energy changes accompanying bond formation in H_2^+ shown in figure 6.3, reveals much stronger changes in the energy constituents than in a minimal basis as the virial ratio is restored. This behaviour is reflected in the global potential and covalency energies. Qualitatively this is perhaps expected; the more diffuse functions overlap to a larger extent, and the orthogonality constraint has more of an impact on the shapes of the orbitals. The attractive interaction described by V_{global} is also of larger magnitude, and again, may be qualitatively anticipated as the inclusion of polarisation functions allow greater flexibility in the description of the multipole moments.

Before partitioning the total covalency energy into orbital contributions, it is beneficial to consider how one expects this picture to differ from the one obtained for a minimal basis wavefunction. We know from the work of Ruedenberg, Bacskay *et al.* that intra-atomic orbital contraction plays a central role in the formation of a chemical bond, in that it restores the virial ratio by driving up the intra-atomic kinetic energy and driving down the intra-atomic potential energy. [91,95,114] More specifically, these authors have shown the contraction occurs perpendicular to the bond direction and in intra-atomic orbitals, with bond parallel components not showing contraction to the same degree. One might therefore expect the covalency energies of the bond-parallel orbitals, σ_2, σ_3 and σ_a^* to have similar behaviour to those in the minimal basis picture as orbital contraction will play only a minor role, and the "intra-atomic" and bond-perpendicular orbitals, σ_1, σ_1^*, σ_2^*, π and π^* to deviate significantly from the minimal basis example as orbital contraction plays a major role in a large basis wavefunction and is absent in a minimal basis wavefunction. One can see in figure 7.16 that this is precisely the case; there is a decrease in the π contributions, both bonding and antibonding likely arising through orbital contraction and thus decreased overlap, and a significant increase in magnitude of the orbital covalency changes in the σ_1 and σ_1^* orbitals through contraction as the overall covalency in the system increases. The bond-parallel components show little difference from those discussed in the minimal basis covalency energies.

Applying this procedure once one has localised the orbitals is not straightforward. The recipe remains the same, but increasing the dimension of the basis set introduces significant risk in the use of PM orbitals for instance, that many artefacts such as the one seen in the minimal basis example in figure 7.12 will arise. The use of Mulliken population analysis further increases the likelihood of spurious localised orbitals. To this end, we use Boys' localisation procedure which makes direct reference to the spatial extent of each orbital. [121] It is important to note that while this adds a layer of robustness to the procedure, it does not guarantee the localised orbitals will change smoothly over the reaction co-ordinate. Figure 7.17 shows the total changes in the total, global potential, and covalency energies in the cc-pVTZ(p/s) basis over the reaction co-ordinate. The long range behaviour is well reproduced under the formulation presented in this section, and the energy

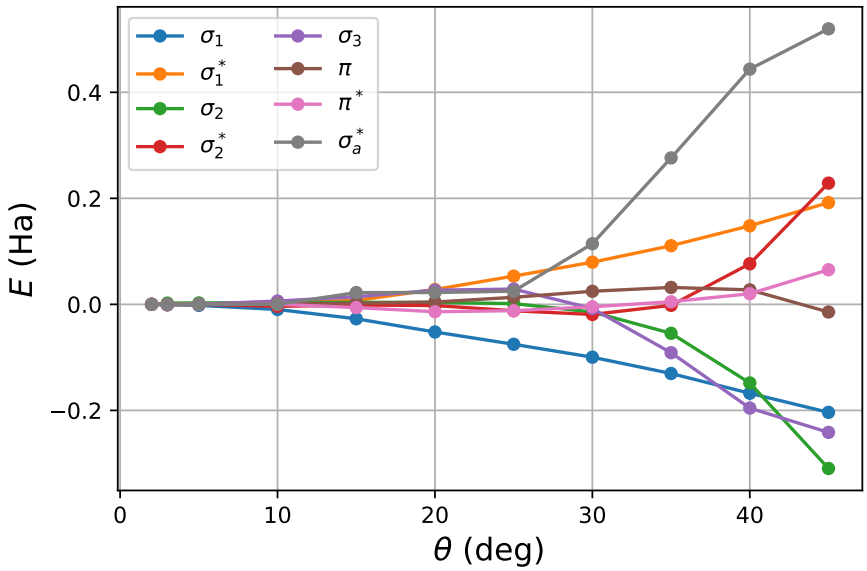

Figure 7.16: Orbital covalencies of the canonical RHF orbitals in the cc-pVTZ(p/s) basis. The labels correspond to those orbitals shown in figure 7.8.

breakdown closely resembles that seen in the minimal basis. The associated orbital covalencies are shown in figure 7.18. The nonbonding sp^3 orbitals show little change in covalency over the reaction co-ordinate, with the majority of the change being seen in the core σ_1 and σ_1^* orbitals and the bonding sp^3 orbitals. It is difficult to assess the extent to which this generalisation to a large basis has been successful. The behaviour of the core orbitals, while not unexpected, perhaps exhibits larger changes than might expect. How this approach can be effectively generalised to large basis sets remains an open question and part of future research plans.

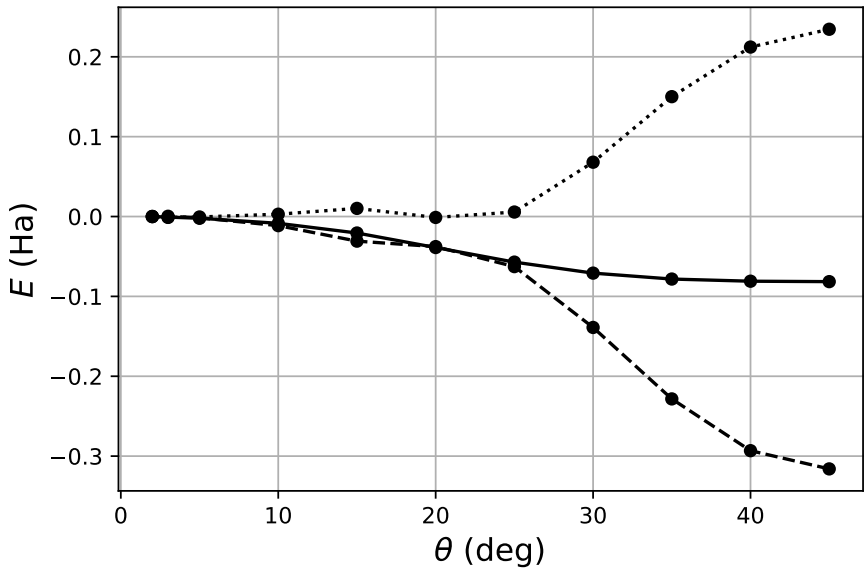

Figure 7.17: Total (solid line), covalency (dotted line) and global potential (dashed line) energies calculated using MINAO reduced orbitals, with Boys localised reference orbitals in the cc-pVTZ(p/s) basis, over the reaction co-ordinate for $[FHF]^-$ formation as a function of the angle θ. The HF bond distances are $R = \lambda\cos(\theta)$ $r = \lambda\sin(\theta)$, where λ is optimised at each θ.

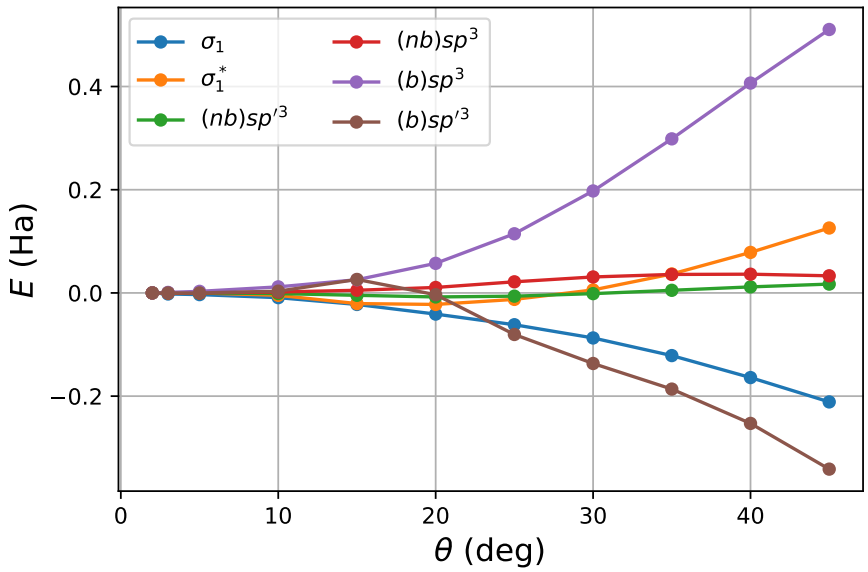

Figure 7.18: Orbital covalencies of the Boys localised RHF orbitals in the cc-pVTZ(p/s) basis. The core orbitals are not localised, and the valence orbitals are sp^3 hybridised as a result of the localisation. A prime indicates an orbital centred on the approaching F^- ion, and (b) and (nb) indicate an sp^3 orbital pointing along, or away from the bond, respectively.

7.4 Reaction Orbitals: Optimisation

In the previous sections in this chapter a new approach for decomposing the energy into covalent parts and a part arising through electrostatic and non-covalent interactions has been presented, and has been performed in some exploratory calculations. It has also been demonstrated that some core localised orbitals such as those obtained through Pipek-Mezey localisation fail to remain consistent enough in shape over the course of a simple reaction to have their covalency energies remain constant. In this section we explore some new approaches to orbital localisation over a reaction co-ordinate, making use of the new measures of covalency. That is not to say that we discard old fashioned, discrete methods of localisation at each point in a reaction; rather, we rely on them but modify the orbitals they generate at each point through reference to orbital covalencies at previous points.

The changes in the Pipek-Mezey orbital covalencies provide quantitative insight into which orbitals are involved in the bond breaking and bond forming process in the reaction between F^- and HF. An unfortunate artefact of the localisation process was seen as a core orbital changed suddenly in energy midway along the reaction co-ordinate. To combat this, one approach is to choose those orbitals one expects to change, and define them as the set of reaction orbitals (ROs), $\{\phi_{\mathrm{RO}}\}$, then to minimise through orbital rotations the sum

$$ {}^1F = \sum_{i \notin \{\phi_{\mathrm{RO}}\}} (H_{ii}^{(0)} - H_{ii}^{(n)})^2, \tag{7.51} $$

where $H_{ii}^{(n)}$ is the covalency energy of the ith orbital at the nth step along the reaction co-ordinate. One could also consider modifying the above functional by weighting each term in the sum with some value which is proportional to the inverse of its importance to the reaction. That is, modifying ${}^1F$ to be,

$$ {}^2F = \sum_i (H_{ii}^{(0)} - H_{ii}^{(n)})^2 w_i, \tag{7.52} $$

where w_i is the weight for orbital i. The weight for the frontier, or "reaction orbitals" should be small (or zero, as in ${}^1F$), so only a very small amount of pressure is placed upon them to remain constant over the reaction, and very large for the

spectator orbitals whose orbital covalency energy we wish to remain constant. Finding suitable quantities for w_i are part of ongoing investigation. In a recent publication, Knizia and Klein use orbital contributions to atomic charges as a measure of orbital change, which they define as

$$f_i = \sqrt{\sum_{A}^{N_{\text{atoms}}} (n_{A,i}(\bar{n}) - n_{A,i}(\bar{n}=0))^2}, \tag{7.53}$$

where $n_{A,i}(n)$ is the contribution of orbital i to the atomic charge n of atom A at the $\bar{n}^{\text{th}}$ point on the reaction co-ordinate, which represents a potential alternative for future investigation. [154]

Here we shall consider only the orbital covalencies, and orbitals, obtained by finding the minimum of the functional defined in equation 7.51, and choose the orbitals we expect to change by inspecting the orbitals by eye. In the future, it is hoped that the detection of the appropriate orbitals can be done automatically, and step-to-step, such that applications to wider problems, such as on-the-fly active space detection are possible. If this cannot be done, an analysis of the covalency after a full reaction co-ordinate scan presents a simpler problem for which one could consider using the inverse of the area between the curve describing each orbital's covalency energy change and the x-axis as the weight, w_i, in equation 7.52.

Let us again consider the same reaction between a fluoride ion and a hydrogen fluoride molecule. With the present goal in mind, which is to reduce the number of orbitals whose covalency energy changes to *two* orbitals, consistent with a frontier orbital and curly arrow picture of the reaction, the Pipek-Mezey orbitals reflect a better starting point. This is simply because the choice of orbitals associated with bond breaking/forming is more clear, and more in line with the pictures chemists generally think of as bonding orbitals than the Fock eigenfunctions. Let us begin by optimising the functional shown in equation 7.51 at each point along the reaction co-ordinate. The chosen basis is MINAO, and the initial orbitals are PM orbitals. The unoptimised orbital energies are shown in figure 7.13, and showed a kink in the $2s'$ orbital energy as the hybridisation changed. Figure 7.19 shows that, as a result of the orbital rotations, this kink is removed and, in fact, when rotated together with the sp' orbital, the change in both of them is delayed until larger θ;

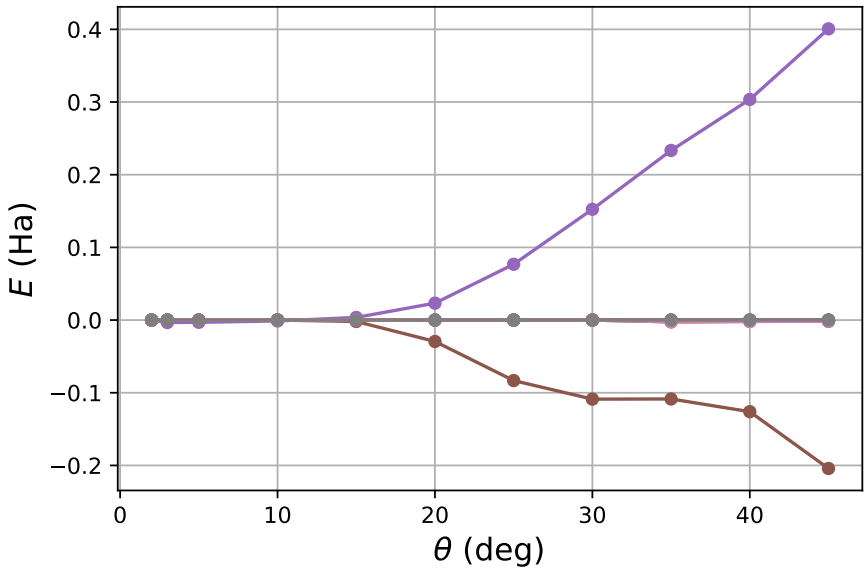

Figure 7.19: Orbital covalencies of the PM orbitals generated from a RHF wavefunction in the MINAO basis, which have then been optimised along the reaction co-ordinate by minimisation of the functional in equation 7.51. The labels correspond to those orbitals shown in figure 7.12, orbitals not in the reaction orbital set are practically super imposed at E=0.

the rotations mix them appropriately until the change is completely cancelled in both. The sp' orbital covalency energy changes less severely over the reaction as a consequence of the change which was erroneously attributed to the $2s'$ orbital in the original PM picture, which has an opposite sign to the original sp' data, and so flattens the curve. Likewise, the change in the sp orbital, once mixed with the other orbitals is delayed. This is all acheived by choosing sp and sp' as being the orbitals making up the reaction orbital set $\{\phi_{\mathrm{RO}}\}$ in equation 7.51. This allows the spectator orbitals to rotate freely together and for any remaining covalency to be localised into the reaction orbitals.

Given the symmetry of the molecule, any effective orbital optimisation should yield covalency energies of the sp and sp' orbitals which cross at the transition state, and, in order to recover the barrier to the bond formation seen in the total covalency energy in figure 7.7, should show an increase in the sp orbital covalency which is larger than the decrease in the sp' orbital. Figure 7.20 shows that this is, in fact, the case. Thus the barrier to bond formation is approximately 0.2 Ha, which is generally consistent with the bond energy one may expect from a single bond. This provides further clarity to the nature of the reaction. There is indeed

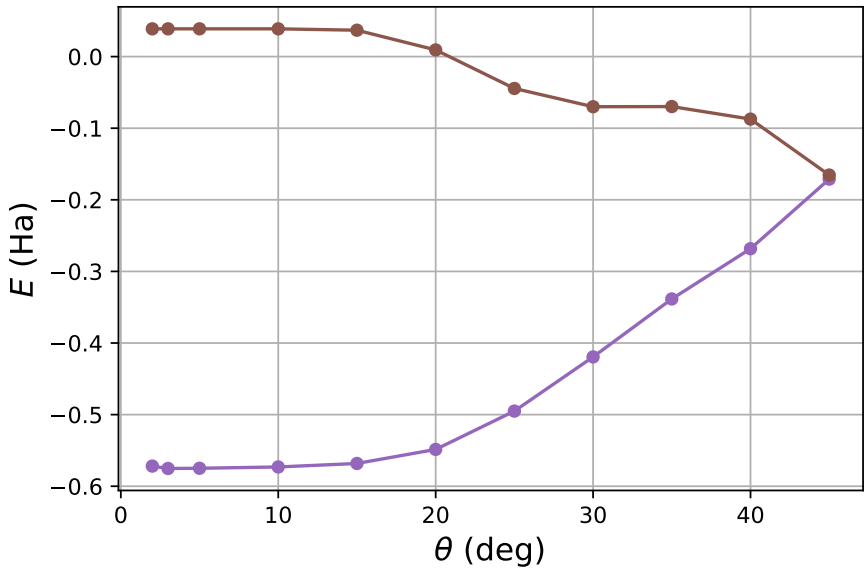

Figure 7.20: Orbital covalencies of the sp (purple) and sp' (brown) orbitals shown in figure 7.12 after optimisation using the functional in equation 7.51.

an energy barrier associated with forming a new covalent bond as the old one is broken, as one should expect. However, the net decrease in the total energy arises in this instance from the electrostatic attraction between the charge and the dipole, and is strong enough to significantly overcome the bond forming/breaking process. It should be noted that we are assuming that the single determinantal description of this reaction is valid, which may not be true, and an extension of this method to multi-determinantal methods forms part of future research plans for this project.

Having built a picture of this reaction in which the changes in covalency really do only occur in two of the ten available orbitals, we have made true the list of assumptions and approximations outlined in section 7.1 and are able to begin thinking about how one might draw curly arrows from first principles for the first time. The decreasing covalency energy of the sp' orbital has a stabilising impact on the total energy, and is thus favourable. The increase in the sp orbital covalency is destabilising and is the source of the energy barrier to covalent bond formation in this system, and were it not for the prevailing electrostatic attraction coupled with the decrease in the covalency energy of the sp' orbital, would prevent this reaction from being barrierless. In the context of "pushing" curly arrows, which are concerned only with the skeletal structure of a molecule, one could only feasibly begin a curly on the incoming sp' and draw it to the H atom, thereby decreasing

its covalency energy and as a consequence increase the covalency energy of the *sp* orbital by drawing a second curly arrow from the H-F bond in the molecule to the F, creating a new fluoride ion.

7.5 Case study: An S_N2 Reaction

A reaction related to the one seen previously, but which provides more of a test of the reaction orbitals approach is the S_N2 reaction between a fluoride ion and methyl fluoride,

$$F^- + CH_3 - F \quad \longrightarrow \quad F - CH_3 + F^-, \tag{7.54}$$

for which we should expect to see changes in the orbital covalencies of the localised orbitals associated with the C-H bonds as well as the C-F bonds, as the C-H bonds change in length and location as we approach the transition state. In the subsequent optimisation of the reaction orbitals, we shall investigate how the chosen $\{\phi_{\mathrm{RO}}\}$ impact the results obtained using the reaction orbitals algorithm, and how reasonable constant orbital covalencies for the C-H bonding orbitals are, and thus whether the textbook mechanism, the one in which only the C-F bonds change, can really be thought of as a reasonable approximation. The Boys localisation procedure is chosen as it yields one bonding orbital per hydrogen attached to the central carbon atom, and one bonding orbital between the carbon atom and each fluorine atom and thus provides us with exactly the picture we wish to examine. The PM orbitals, however, as well as the IBOs yield orbitals delocalised over multiple hydrogen atoms and not consistent with a frontier orbital model for the reaction. Thus, the use of PM or IBO orbitals in this example makes the expected behaviour of the covalency energy unclear. The reaction co-ordinate is optimised in the aug-cc-pVTZ(p/s) basis.

The MINAO Boys localised orbitals at the transition state where both C-F bond lengths are identical are shown in figure 7.21. As the coordination number of the carbon atom approaches 5, one should anticipate positive changes in the σ_{CH} covalencies, a positive change in the σ_{CF} covalency corresponding to bond weakening, and a large, negative change in the $\sigma_{CF'}$ covalency energy, where F′ is the approaching fluorine atom, corresponding to a bond forming interaction as the "negative charge" is stabilised. The associated energies as a function of reaction co-ordinate in both the large (aug-cc-pVTZ(p/s)) and minimal (MINAO) bases are shown in figure 7.22. The barrier height in the minimal basis is seen to be siginificantly smaller than the barrier height in the large basis. One should therefore

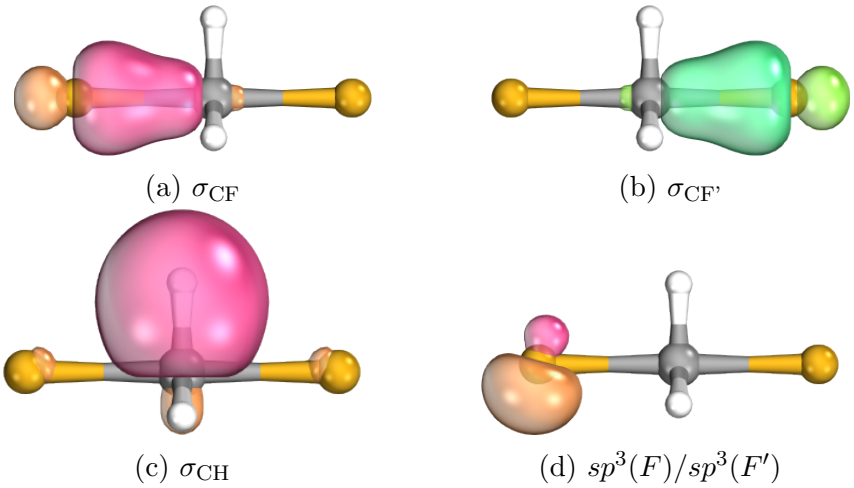

(a) σ_{CF} (b) $\sigma_{\mathrm{CF'}}$

(c) σ_{CH} (d) $sp^3(F)/sp^3(F')$

Figure 7.21: The Boys orbitals arising from a MINAO RHF calculation on $[FCH_3F]^-$ at the transition state. The labels are chosen according to their appearance and evident hybridisation. The sp^3 orbital in (d) is given by reflection through the plane bisecting the three σ_{CH} bonds. A prime denotes orbitals centred on the approaching fluoride ion in a scan of the reaction co-ordinate.

expect that, in the minimal basis, the covalency energy increase associated with the breaking bond in the minimal basis is much smaller than the bond-forming energy decrease. One should also anticipate that in the large basis, the energy increase associated with the breaking bond is in finer balance with the energy decrease in the forming bond. One should also not neglect to consider the impact on the total covalency of the σ_{CH} bonding orbitals, of which there are three and have a covalency energy which, pre-optimisation, *should* change.

The total covalency energy changes in both the large and minimal bases can be seen in figure 7.23. Rather surprisingly, the total covalency is seen to have a stabilising impact on the total energy at the transition state, as the geometry becomes trigonal bipyramidal. In contrast, the total global potential, which by definition looks much like a mirror image of the total covalency energy, has a maximum at the transition state. This may be less surprising, as the coulomb interactions become larger and larger and the dipole in what was the methyl fluoride molecule becomes vanishingly small, consequently destroying the attractive charge-dipole interaction.

The orbital covalency energy changes in the Boys localised orbitals in the MINAO basis are shown in figure 7.24. The core orbitals, as was seen in the illustrative $[FHF]^-$ example remain approximately constant. The anti-bonding increase in the

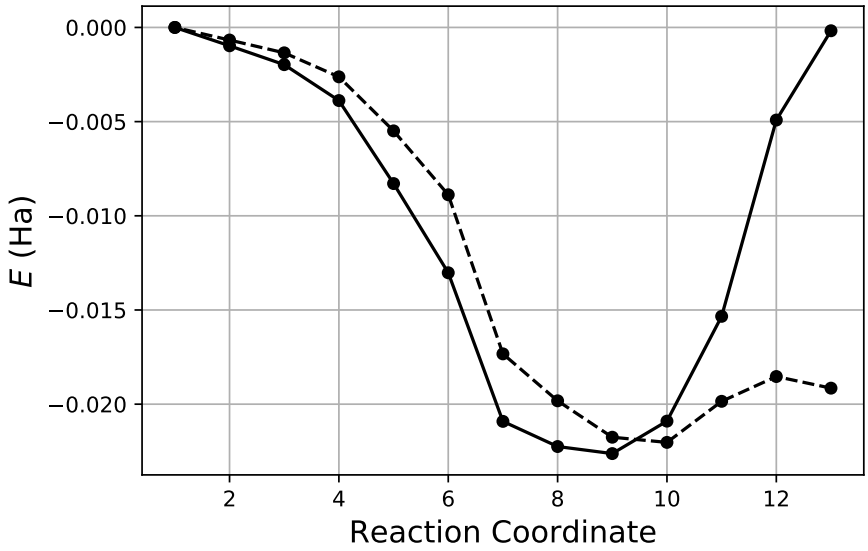

Figure 7.22: Total energy along the reaction co-ordinate defined by aug-cc-pVTZ(p/s) optimised geometry parameters in the MINAO (dashed line) and aug-cc-pVTZ(p/s) (solid line) bases. The transition state is at point 13 along the reaction co-ordinate. C-F′ bond lengths can be seen in figure 7.24.

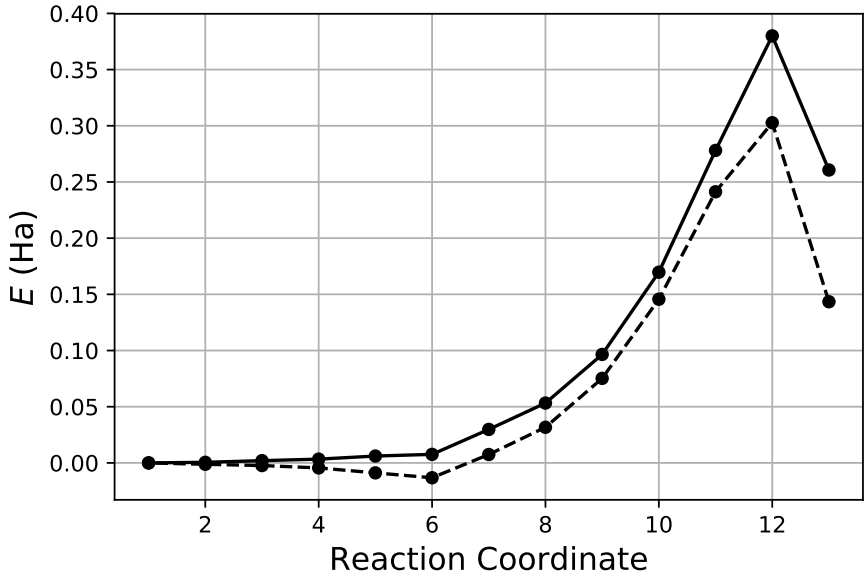

Figure 7.23: Total covalency along the reaction co-ordinate defined by aug-cc-pVTZ(p/s) optimised geometry parameters in the MINAO (dashed line) and aug-cc-pVTZ(p/s) (solid line) bases. Transition state is at point 13 along the reaction co-ordinate. C-F′ bond lengths can be seen in figure 7.24.

covalency energy in the σ_{CF} orbital is strikingly small, and occurs only close to the transition state, with the majority of the increase in the covalency energy accounted for by the three σ_{CH} bonding orbitals. As anticipated, the $\sigma_{CF'}$ orbital has an associated strong covalency energy decrease upon the formation of the new C-F

bond. The strong changes in the σ_{CH} orbital covalency energies raise an interesting question; can one really localise all of the changes in covalency into two orbitals and retain a physically reasonable picture from which one can draw chemical conclusions and, ultimately, curly arrows? If one selects the set of reaction orbitals as $\{\phi_{RO}\} = \{\sigma_{CF}, \sigma_{CF'}\}$, and optimises the functional 7.51, i.e, if one attempts to recover a curly arrow picture, the orbital covalency energies shown in figure 7.25 are obtained.

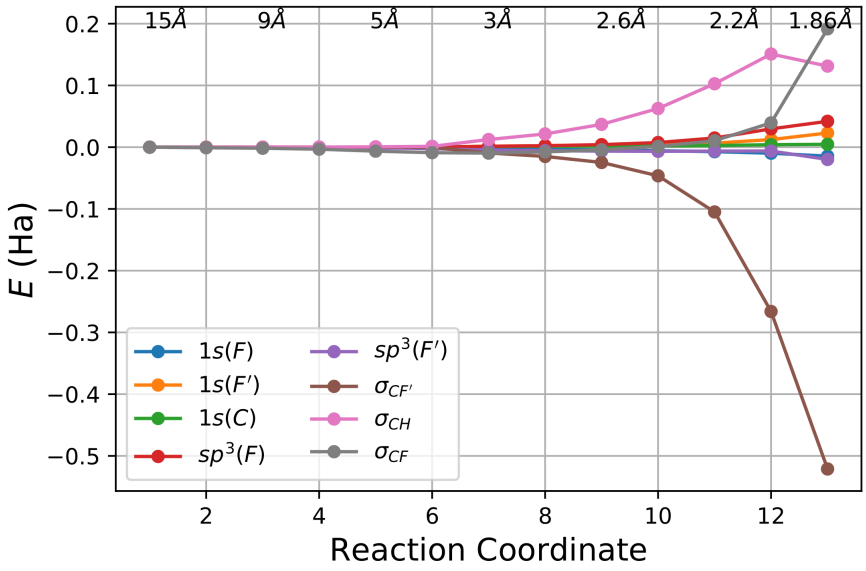

Figure 7.24: Orbital covalencies of the Boys localised orbitals generated from a RHF wavefunction in the MINAO basis. The labels of the valence orbitals correspond to those orbitals shown in figure 7.21. Core orbital labels are self-explanatory. Also shown along the top of the figure are some of the C-F′ bond lengths.

The unfortunate artefact of the optimisation which results in an unphysical increase in the covalency energy of the $\sigma_{CF'}$ orbital highlights the need for a more sophisticated reaction orbital optimisation than the one provided by equation 7.51. Whether the increased sophistication should come through weighting the terms in the functional, as in equation 7.52 or whether the design of a new functional is necessary is unclear. A reduction in the change in the covalencies of the orbitals whose covalency we do not expect to change in the reaction, however, does not provide physically unreasonable results under the current scheme. That is, by updating our chosen set of reaction orbitals as $\{\phi_{RO}\} = \{3\sigma_{CH}, \sigma_{CF}, \sigma_{CF'}\}$ and thence minimising equation 7.51. The resulting orbital covalency energy changes

are shown in figure 7.26. The changes in orbital covalency can be rationalised as follows: The dipole induced in the C-F bond by the approaching F^- yields a response in the molecule which strengthens the C-F bond by the distortion of the geometry and the C-H bonding orbitals, which are in turn weakened, then, upon closer approach the C-F bond elongates until a trigonal bypyramidal geometry is obtained and the dipole in the direction along the F→F vector becomes zero. The distortion of the σ_{CH} bonding orbitals becomes symmetric through the molecular mirror plane, and the vanishing dipole along the F→F results in a stabilisation of the σ_{CH} bonds. The $\sigma_{CF'}$ orbital experiences a strong negative change in the covalency energy as a bond is formed.

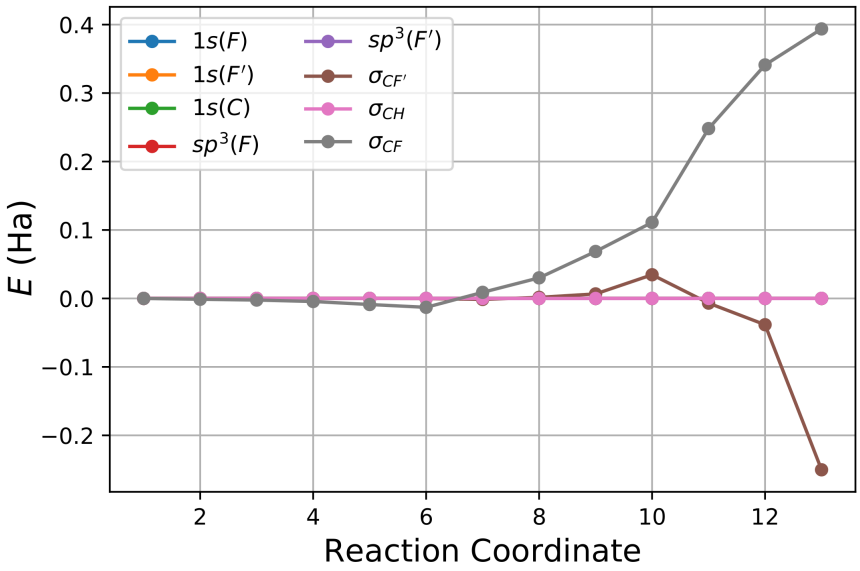

Figure 7.25: Optimised orbital covalencies of the Boys localised orbitals generated from a RHF wavefunction in the MINAO basis. The labels of the valence orbitals correspond to those orbitals shown in figure 7.21. Core orbital labels are self-explanatory. Only $\sigma_{CF'}$ and σ_{CF} change strongly, the other orbitals are practically superimposed at E=0.

Performing the same analysis in aug-cc-pVTZ(p/s) basis, and choosing our minimal basis orbitals to be reduced orbitals, defined by reference to Boys localised orbitals in the large basis, one arrives at the orbital covalency energy changes shown in figure 7.27. Strong changes are observed in the un-optimised core orbitals upon contraction, as discussed previously. These changes mostly cancel and can be removed by optimisation. The large, positive change in the σ_{CF} bonding orbital is more in line with expectation. The $\sigma_{CF'}$ orbital experiences a large decrease

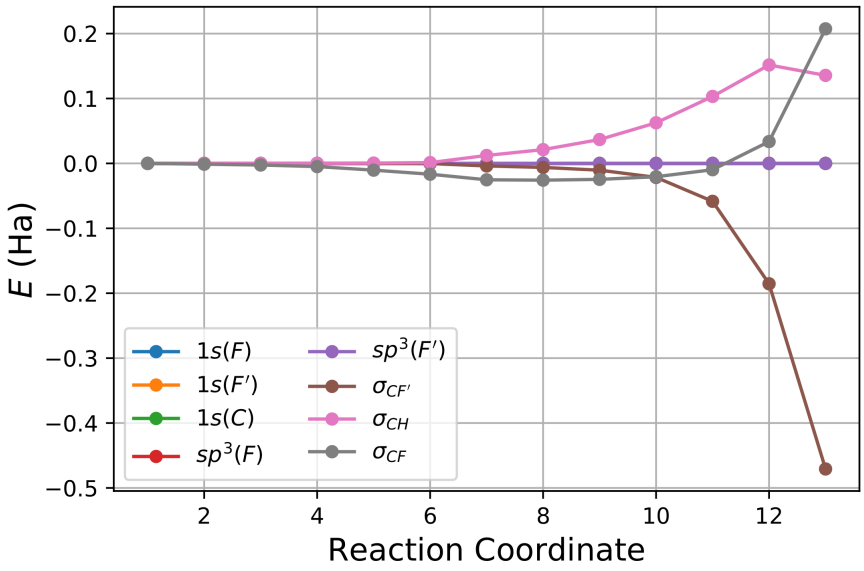

Figure 7.26: Optimised orbital covalencies of the Boys localised orbitals generated from a RHF wavefunction in the MINAO basis. The labels of the valence orbitals correspond to those orbitals shown in figure 7.21. Core orbital labels are self-explanatory. Also shown along the top of the figure are some of the C-F′ bond lengths. The 3 σ_{CH}, σ_{CF}, $\sigma_{\mathrm{CF'}}$, are exempted from optimisation.

in covalency energy, whereas the σ_{CH} orbitals experience less change than they did in the minimal basis. This is likely through the increased flexibility in the wavefunction to describe the distortion of the orbitals in the field of the charge.

Attempting to recover a curly arrow description of the reaction through the optimisation of equation 7.51 with a set of reaction orbitals defined by $\{\phi_{RO}\} = \{\sigma_{CF}, \sigma_{CF'}\}$ represents a difficult challenge. Since the initial results were less erratic in the minimal basis, and the optimisation of the same functional with the same chosen set of reaction orbitals yields unphysical results, it is no surprise that the optimised reaction orbital covalency energies shown in figure 7.28 offer little chemical insight, and further highlight the need for development of the reaction orbital optimisation procedure. Similar to the minimal basis case, one can improve the picture significantly by including in the reaction orbital space the σ_{CH} orbitals. The results obtained by updating the selection of the reaction orbital space are shown in figure 7.29.

It is worth stressing that the inclusion of further orbitals in the reaction orbital space does not ruin the validity of the scheme. In fact, it removes some ambiguity from the model, and ensures that the appropriate crossing of the orbital covalency

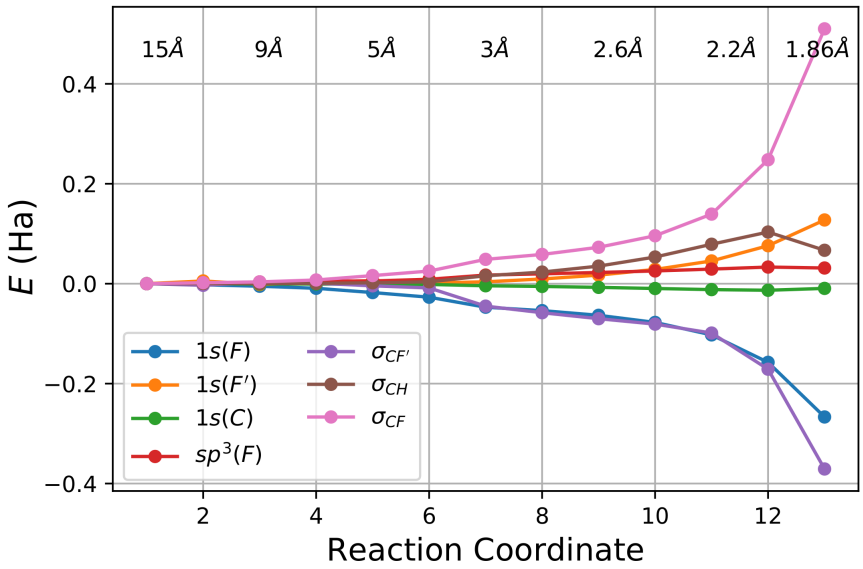

Figure 7.27: Orbital covalencies of the Boys localised orbitals generated from a RHF wavefunction in the aug-cc-pVTZ(p/s) basis. The labels of the valence orbitals correspond to those orbitals shown in figure 7.21. Core orbital labels are self-explanatory. Also shown along the top of the figure are some of the C-F′ bond lengths.

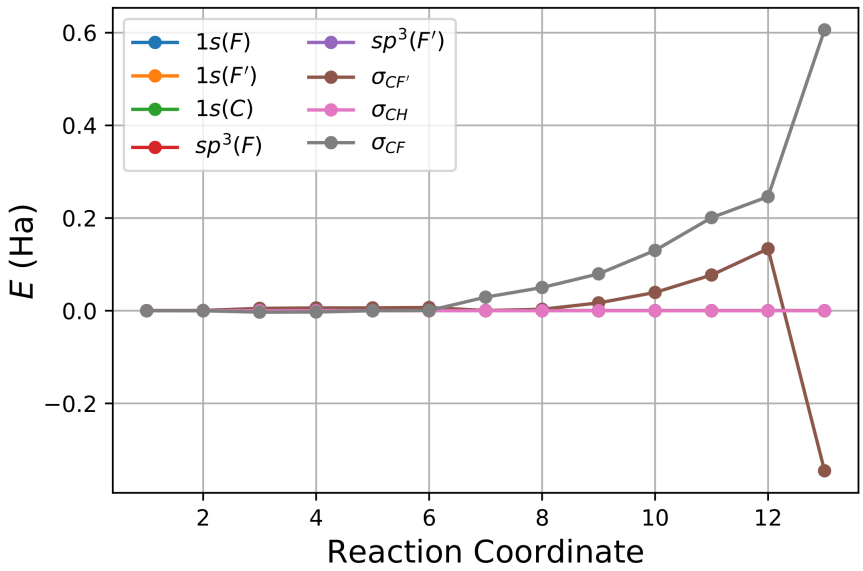

Figure 7.28: Optimised orbital covalencies of the Boys localised orbitals generated from a RHF wavefunction in the aug-cc-pVTZ(p/s) basis. The labels of the valence orbitals correspond to those orbitals shown in figure 7.21. Core orbital labels are self-explanatory. Also shown along the top of the figure are some of the C-F′ bond lengths.

energies at the transition state is preserved, which is not the case when one also spreads the orbital covalencies of the σ_{CH} bonds among the σ_{CF} and $\sigma_{CF'}$ orbitals.

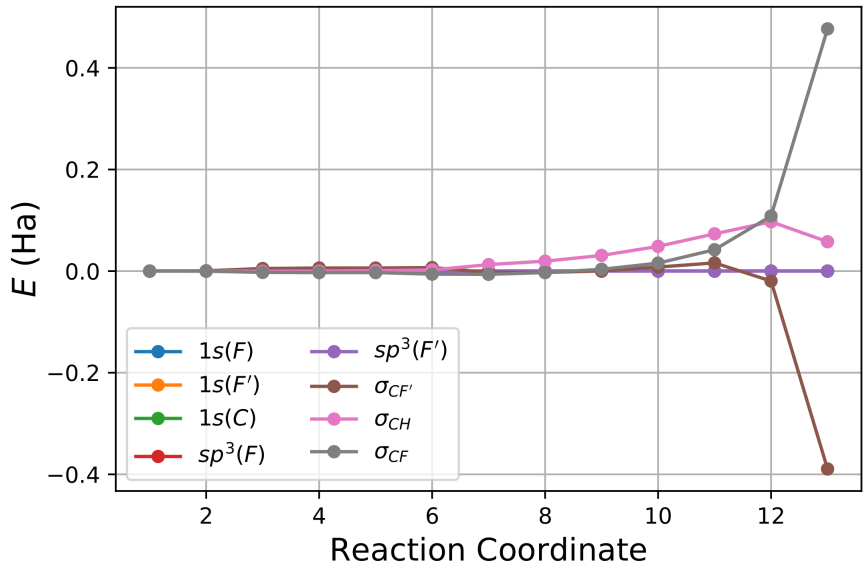

Figure 7.29: Optimised orbital covalencies of the Boys localised orbitals generated from a RHF wavefunction in the aug-cc-pVTZ(s/p) basis. The labels of the valence orbitals correspond to those orbitals shown in figure 7.21. Core orbital labels are self-explanatory. Also shown along the top of the figure are some of the C-F′ bond lengths. The 3 σ_{CH}, σ_{CF}, $\sigma_{\mathrm{CF'}}$, are exempted from optimisation.

This retention in the crossing behaviour is seen clearly in figure 7.30.

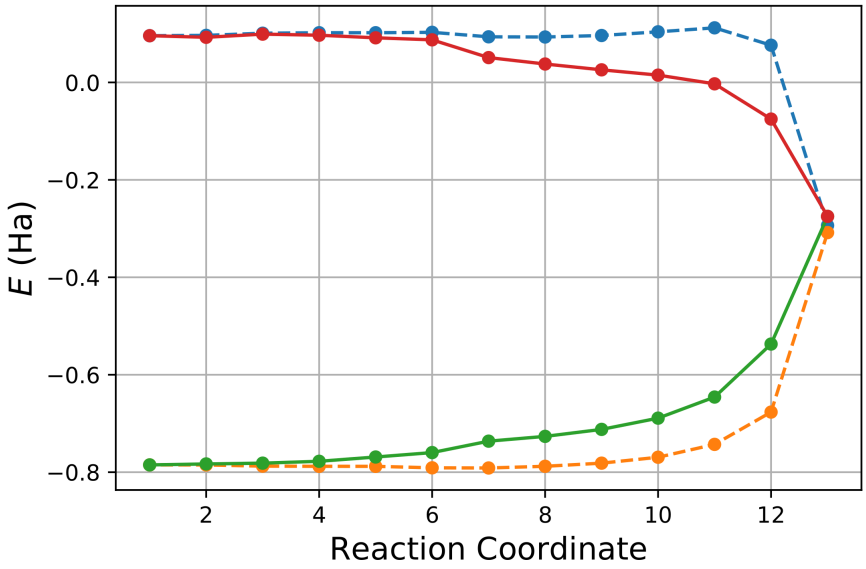

Figure 7.30: Optimised (dashed line) and unoptimised (solid line) covalency energies of the σ_{CF} and $\sigma_{CF'}$ orbitals in the aug-cc-pVTZ(p/s) basis. In both cases the $\sigma_{CF'}$ orbital decreases in covalency energy and the σ_{CF} orbital increases in covalency energy. The reaction orbital set omitted in the optimisation of equation 7.51 was $\{3\sigma_{CH}, \sigma_{CF}, \sigma_{CF'}\}$.

7.6 Conclusions

In this section we have presented a promising new method for, as far as possible, making true the assumptions and approximations one makes in the application of curly arrows and frontier orbitals for restricted Hartree-Fock wavefunctions. While there are several issues requiring further attention, such as a more effective scheme for the attenuation of the kinetic energy integrals and a robust and automatic detection and optimisation of reaction orbitals, the method itself, and the associated framework shows promising signs of one day becoming a black-box procedure for providing curly-arrows and frontier orbitals from first principles, along with a quantitative measure of covalency which can be broken down into orbital contributions. The scheme has been shown to work well for a small test case, and has also shown its limitations in a more complicated reaction with several bonds whose covalency energy must be accounted for.

Several avenues in this project now exist which can be explored and iterative improvements made to the procedure; for instance, one could imagine the definition of a new basis in which the kinetic energy matrix is diagonal and can be related back to a minimal basis of Gaussian functions. Or perhaps a new localisation procedure which accounts for covalency in the system and naturally results in unchanging covalency energies for the core orbitals. Solutions to this problem have implications beyond providing insights into chemical bonding, and have the potential to provide some clarity or automation for the choices of active spaces in CASSCF calculations.

Extension of this analysis to other methods may also be required once the algorithm is taken beyond prototypical stage for restricted HF methods. For instance an immediate extension can be formulated for Kohn-Sham calculations by partitioning the molecular density into orbital squares and performing the same truncation scheme for the kinetic energy integrals, though one must be careful of the kinetic correlation corrections in the exchange functional. For perturbative and coupled cluster methods one must appeal to both one and two-electron density matrices; this represents a greater challenge.

Chapter 8

Closing Remarks

This thesis contains new solutions to two problems; how to mitigate the computational expense associated with electrostatic potential evaluation without sacrificing too much accuracy, and the other is how to quantitatively justify widely used conceptual descriptors of chemical change. The overall success of the new methods is unknown at the time of writing, but both form promising directions for future research.

Both methods are distinct from one another, in accordance with how they have been presented. It is worth keeping in mind, however, that the ROPA method came about as a result of needing a minimal basis wavefunction for the expression of V_{global}, which formed the largest part of this research and is thus designed with the reaction orbital scheme in mind.

The methods as they are presented in the pages of this thesis are the product of an enormous number of unsuccessful attempts at solving various problems, in particular finding a suitable form for the V_{global}. For the reader interested in pursuing the same research direction, some of these failed attempts at forming optimal reduced orbitals are mentioned here in a series of short sections.

Calculating V_{global} Using Population Analysis

In this approach we tried a crude Mulliken population analysis approach to approximating the electrostatics using the resultant charges of atoms in the system of interest. That is, we took the electronic population for each atom, n_A, and summed over the orbital contributions to the atomic populations, subtracted this

electronic charge from the atomic number and used the charge-charge interactions of the atoms as our V_{global} quantity.

Putting aside the issues associated with Mulliken populations when large basis sets are used, the use of a charge-charge model makes for a particularly poor approximation to the MEP. For instance, if we consider the co-linear hydrogen fluoride dimer in which the dipole-dipole interaction is the dominant one electrostatically, a charge-charge model will fail to appropriately describe the long-range behaviour of the global potential: it will result in an R^{-1} asymptotic potential, rather than the correct R^{-3} asymptotic potential. As such this approach was dropped.

Calculating V_{global} Using Projected Orbitals

The final version of V_{global} presented in this thesis is the trace of a modified, minimal basis Fock matrix. This form for the global potential came about rather early on in the project. We made the assumption that the primary basis orbitals, once projected onto the minimal basis, would provide a better approximation to the electrostatic potential than the optimised minimal basis wavefunction. This turned out to be incorrect. Applications to simple monomers, such as hydrogen fluoride showed that the total dipole moment of the RHF minimal basis wavefunction was much closer to the exact dipole moment than the dipole moment of the projected minimal basis wavefunction. This first hint that a projection alone would not be enough to obtain orbitals for which V_{global} behaved appropriately was then borne out in a number of experiments on several small systems. As a result, the approach in the following section was developed.

Using the minimal basis RHF orbitals to calculate V_{global}

The RHF orbitals from a separate calculation on the same system but in the minimal basis were then used as a trial form for V_{global}. However, as was discussed at length in chapter 5.1, the density arising from a minimal basis calculation turns out to be inaccurate, and even sometimes taking the wrong sign when compared to an accurate calculation. Thus, again, the approach was dropped. Moreover, this approach would leave the minimal basis orbitals invariant to the basis the reference orbitals are expressed in, which would be an unappealing feature for the reaction

orbitals method.

Calculating $V_{\mathbf{global}}$ Using Density Fitting

The deficiency of the minimal basis RHF orbitals led to a series of investigations in which different operators were used as a measure of similarity, and the similarity between the minimal basis orbitals and the primary basis orbitals maximised. The first of these approaches was to employ a density fitting approach, in which the following was minimised,

$$F = (\rho - \bar{\rho}|\rho - \bar{\rho}). \tag{8.1}$$

Where $\bar{\rho}$ is density calculated from the minimal basis orbitals and ρ is the density arising from the primary basis orbitals. This approach performed surprisingly poorly. Perhaps in part because the function being minimised is takes the minimal basis density as an argument and not the orbital coefficients. This logic led to the use of a number of operators being used for approaches with the measure of similarity being a number of one electron operators.

Calculating $V_{\mathbf{global}}$ Using One-Electron Operators

In finding the reduced orbitals, which form the basis of V_{global} in all of the examples in this thesis, one minimises the reduced orbital functional. While attempting to deduce the appropriate form for V_{global}, a number of operators were substituted into a similar functional,

$$F = \sum_i \left(\langle \bar{\psi}_i | \hat{O} | \bar{\psi}_i \rangle - \langle \psi_i | \hat{O} | \psi_i \rangle \right)^2, \tag{8.2}$$

where $\hat{O}$ is some one-electron operator. Some attempts which are of note and came before the eventual dipole operator are the $\hat{r}^2$ operator, inspired by Boys localisation and the overlap operator. The dipole operator was the first to give results which could be considered reasonable, and had the added benefit of matching the orbital centroids and thus a possible incorporation of a point corrected multipole expansion of the potential which eventually became the ROPA approximation.

Efforts continued along this line for a short time, in which higher rank multipole moments were included in a linear combination of operators, with the expectation

that this would yield a better potential from the density alone, without the extra point correction. After some investigation it became clear that the improvement was marginal, if it existed at all. Moreover, by including higher rank multipole moments, the centroids no longer necessarily match and the point correction in the ROPA equation is rendered invalid. The decision was then made that the reduced orbitals of the ROPA scheme were sufficient for the reaction orbitals algorithm.

8.1 Future Work

The ROPA method requires heavily benchmarking in order to establish its place in the literature, and to assess whether it outperforms existing methods. This is perhaps the most pressing piece of work which must be done on the molecular potentials research presented in this thesis. A second interesting piece of work which could be carried out on the ROPA method is to see how the errors behave as the basis set is changed. For instance, using STO-1G as the reduced basis would yield a density which is exceptionally cheap to evaluate. Moreover, if it is possible to demonstrate that the errors behave predictably as the dimension of the reduced basis is increased, perhaps a semi-empirical form of the ROPA potential could be devised in which the potentials are improved according to some regression function after employing a very small reduced basis.

The reaction orbitals scheme is not yet in a position that it can be applied reliably on any system. The elements of the truncated kinetic energy matrix, while logically presented in this thesis, may not represent the best choice and further work is needed in this direction. The same can be said of the form of the reaction orbital functional by which the orbital covalencies of the spectator orbitals are made flat over the course of a reaction, which holds a great deal of promise. The application of the reaction orbitals procedure to the detection of active spaces in active space methods is a particularly exciting application of the reaction orbitals method, and represents a potential solution to a long-standing problem. Further work is needed in order to aid in the detection of virtual orbitals of importance. However, the other issues must be solved before this research can be done.

Bibliography

[1] E. Schrödinger, *Collected Papers on Wave Mechanics*, vol. 302. American Mathematical Society, 2003.

[2] R. Shankar, *Principles of Quantum Mechanics*. Springer Science & Business Media, 2012.

[3] A. Szabo and N. S. Ostlund, *Modern Quantum Chemistry: Introduction to Advanced Electronic Structure Theory*. Dover, 1996.

[4] J. C. Slater, "The Theory of Complex Spectra," *Physical Review*, vol. 34, pp. 1293–1322, 1929.

[5] J. C. Slater, "Cohesion in Monovalent Metals," *Physical Review*, vol. 35, pp. 509–529, 1930.

[6] E. U. Condon, "The Theory of Complex Spectra," *Physical Review*, vol. 36, no. 7, p. 1121, 1930.

[7] T. Helgaker, P. Jørgensen, and J. Olsen, *Molecular Electronic-Structure Theory*. John Wiley & Sons, 2014.

[8] F. Jensen, *Introduction to Computational Chemistry*. John Wiley & Sons, 2017.

[9] L. Laaksonen, P. Pyykkö, and D. Sundholm, "Fully Numerical Hartree-Fock Methods for Molecules," *Computer Physics Reports*, vol. 4, pp. 313–344, 1986.

[10] E. A. McCullough, "Numerical Hartree-Fock Methods for Diatomic Molecules: A Partial-Wave Expansion Approach," *Computer Physics Reports*, vol. 4, pp. 265–312, 1986.

[11] C. M. Reeves and R. Fletcher, "Use of Gaussian Functions in the Calculation of Wavefunctions for Small Molecules. III. The Orbital Basis and its Effect on Valence," *Journal of Chemical Physics*, vol. 39, p. 4073, 1963.

[12] C. M. Reeves and M. C. Harrison, "Use of Gaussian Functions in the Calculation of Wavefunctions for Small Molecules. II. The Ammonia Molecule," *Journal of Chemical Physics*, vol. 39, pp. 11–17, 1963.

[13] R. D. Bardo and K. Ruedenberg, "Even-Tempered Atomic Orbitals. VI. Optimal Orbital Exponents and Optimal Contractions of Gaussian Primitives for Hydrogen, Carbon, and Oxygen in Molecules," *Journal of Chemical Physics*, vol. 60, no. 3, pp. 918–931, 1974.

[14] M. W. Schmidt and K. Ruedenberg, "Effective Convergence to Complete Orbital Bases and to the Atomic Hartree–Fock Limit Through Systematic Sequences of Gaussian Primitives," *Journal of Chemical Physics*, vol. 71, no. 10, pp. 3951–3962, 1979.

[15] C. A. Coulson and H. C. Longuet-Higgins, "CVII. Notes on the Validity and Application of the Method of Molecular Orbitals," *The London, Edinburgh, and Dublin Philosophical Magazine and Journal of Science*, vol. 40, no. 310, pp. 1172–1177, 1949.

[16] J. Townsend, J. K. Kirkland, and K. D. Vogiatzis, "Post-Hartree-Fock Methods: Configuration Interaction, Many-Body Perturbation Theory, Coupled-Cluster Theory," in *Mathematical Physics in Theoretical Chemistry*, pp. 63–117, Elsevier, 2019.

[17] B. O. Roos, "A New Method for Large-Scale CI Calculations," *Chemical Physics Letters*, vol. 15, no. 2, pp. 153–159, 1972.

[18] C. Møller and M. S. Plesset, "Note on an Approximation Treatment for Many-Electron Systems," *Physical Review*, vol. 46, no. 7, pp. 618–622, 1934.

[19] D. Cremer, "Møller-Plesset Perturbation Theory: From Small Molecule Methods to Methods for Thousands of Atoms," *Wiley Interdisciplinary Reviews: Computational Molecular Science*, vol. 1, pp. 509–530, 2011.

[20] P. Hohenberg and W. Kohn, "Inhomogeneous Electron Gas," *Physical Review*, vol. 136, p. B864, 1964.

[21] L. J. Bartolotti and K. Flurchick, "An Introduction to Density Functional Theory," *Reviews in Computational Chemistry*, vol. 7, pp. 187–260, 1996.

[22] R. G. Parr and W. Yang, *Density-Functional Theory of Atoms and Molecules*, vol. 3. Springer, Dordrecht, 1980.

[23] T. Ziegler, "Approximate Density Functional Theory as a Practical Tool in Molecular Energetics and Dynamics," *Chemical Reviews*, vol. 91, pp. 651–667, 1991.

[24] W. Kohn and L. J. Sham, "Self-Consistent Equations Including Exchange and Correlation Effects," *Physical Review*, vol. 140, no. 4A, p. A1133, 1965.

[25] R. Fletcher, *Practical Methods of Optimization*. John Wiley & Sons, 2013.

[26] A. J. Stone, *The Theory of Intermolecular Forces*. Oxford University Press, 2013.

[27] A. D. Buckingham, P. W. Fowler, and J. M. Hutson, "Theoretical Studies of van der Waals Molecules and Intermolecular Forces," *Chemical Reviews*, vol. 88, no. 6, pp. 963–988, 1988.

[28] R. E. Raab and O. L. De Lange, *Multipole Theory in Electromagnetism: Classical, Quantum, and Symmetry Aspects, with Applications*, vol. 128. Oxford University Press, 2005.

[29] J. O. Hirschfelder and M. A. Eliason, "Electrostatic Hellmann—Feynman Theorem Applied to the Long-Range Interaction of Two Hydrogen Atoms," *Journal of Chemical Physics*, vol. 47, no. 3, pp. 1164–1169, 1967.

[30] L. Jansen, "Tensor Formalism for Coulomb Interactions and Asymptotic Properties of Multipole Expansions," *Physical Review*, vol. 110, no. 3, p. 661, 1958.

[31] B. L. Cardon, H. Oona, and J. A. Leavitt, "Equilibrium Charge-State Distributions and Multiple-Scattering Angles of 1-and 2-MeV Krypton Ions in Carbon Foils," *Physical Review A*, vol. 21, no. 2, p. 515, 1980.

[32] R. J. A. Tough and A. J. Stone, "Properties of the Regular and Irregular Solid Harmonics," *Journal of Physics A: Mathematical and General*, vol. 10, no. 8, p. 1261, 1977.

[33] A. J. Stone and M. Alderton, "Distributed Multipole Analysis: Methods and Applications," *Molecular Physics*, vol. 56, no. 5, pp. 1047–1064, 1985.

[34] A. J. Stone, "Distributed Multipole Analysis, or how to Describe a Molecular Charge Distribution," *Chemical Physics Letters*, vol. 83, no. 2, pp. 233–239, 1981.

[35] A. J. Stone, "Distributed Multipole Analysis: Stability for Large Basis Sets," *Journal of Chemical Theory and Computation*, vol. 1, pp. 1128–1132, 2005.

[36] A. J. Misquitta, A. J. Stone, and F. Fazeli, "Distributed Multipoles from a Robust Basis-Space Implementation of the Iterated Stockholder Atoms Procedure," *Journal of Chemical Theory and Computation*, vol. 10, no. 12, pp. 5405–5418, 2014.

[37] P. Politzer and D. G. Truhlar, *Chemical Applications of Atomic and Molecular Electrostatic Potentials: Reactivity, Structure, Scattering, and Energetics of Organic, Inorganic, and Biological Systems*. Springer Science & Business Media, 2013.

[38] P. Politzer and D. G. Truhlar, *Chemical Applications of Atomic and Molecular Electrostatic Potentials*. Plenum Press, 1981.

[39] T. C. Lillestolen and R. J. Wheatley, "Redefining the Atom: Atomic Charge Densities Produced by an Iterative Stockholder Approach," *Chemical Communications*, no. 45, pp. 5909–5911, 2008.

[40] T. Verstraelen, P. W. Ayers, V. Van Speybroeck, and M. Waroquier, "The Conformational Sensitivity of Iterative Stockholder Partitioning Schemes," *Chemical Physics Letters*, vol. 545, pp. 138–143, 2012.

[41] A. J. Misquitta and A. J. Stone, "ISA-Pol: Distributed Polarizabilities and Dispersion Models from a Basis-Space Implementation of the Iterated Stockholder Atoms Procedure," *Theoretical Chemistry Accounts*, vol. 137, no. 11, p. 153, 2018.

[42] M. S. Gordon and W. England, "Localized Charge Distributions. III. Transferability and Trends of Carbon-Hydrogen Moments and Energies in Acyclic Hydrocarbons," *Journal of the American Chemical Society*, vol. 94, no. 15, pp. 5168–5178, 1972.

[43] C. Etchebest, R. Lavery, and A. Pullman, "The Calculation of Molecular Electrostatic Potentials from a Multipole Expansion Based on Localized Orbitals and Developed at their Centroids: Accuracy and Applicability for Macromolecular Computations," *Theoretica Chimica Acta*, vol. 62, no. 1, pp. 17–28, 1982.

[44] R. Lavery, C. Etchebest, and A. Pullman, "Calculation of the Molecular Electrostatic Potential from a Multipole Expansion Based on Localized Orbitals," *Chemical Physics Letters*, vol. 85, no. 3, pp. 266–270, 1982.

[45] A. Bondi, "Van der Waals Volumes and Radii," *The Journal of Physical Chemistry*, vol. 68, no. 3, pp. 441–451, 1964.

[46] J. Pipek and P. G. Mezey, "A Fast Intrinsic Localization Procedure Applicable for *ab initio* and Semiempirical Linear Combination of Atomic Orbital Wave Functions," *The Journal of Chemical Physics*, vol. 90, no. 9, pp. 4916–4926, 1989.

[47] H. C. Longuet-Higgins, "The Electronic States of Composite Systems," *Proceedings of the Royal Society of London. Series A. Mathematical and Physical Sciences*, vol. 235, no. 1203, pp. 537–543, 1956.

[48] A. J. Stone, "Electrostatic Functions and the Penetration Energy," *The Journal of Physical Chemistry A*, vol. 115, no. 25, pp. 7017–7027, 2011.

[49] K. Ng, W. J. Meath, and A. Allnatt, "Charge Overlap Effects and the Validity of the Multipole Results for First-Order Molecule-Molecule Intermolecular

Forces Using Pair Interactions Involving the Ground State H_2, N_2, CO_2, HF and LiH Molecules as Models," *Molecular Physics*, vol. 38, no. 2, pp. 449–463, 1979.

[50] P. J. Knowles and W. J. Meath, "Non-Expanded Dispersion Energies and Damping Functions for Ar_2 and Li_2," *Chemical Physics Letters*, vol. 124, no. 2, pp. 164–171, 1986.

[51] P. J. Knowles and W. J. Meath, "Non-expanded dispersion and induction energies, and damping functions, for molecular interactions with application to hf-he," *Molecular Physics*, vol. 59, no. 5, pp. 965–984, 1986.

[52] P. J. Knowles and W. J. Meath, "A Separable Method for the Calculation of Dispersion and Induction Energy Damping Functions With Applications to the Dimers Arising from He, Ne and HF," *Molecular Physics*, vol. 60, no. 5, pp. 1143–1158, 1987.

[53] V. Kairys and J. H. Jensen, "Evaluation of the Charge Penetration Energy Between Non-Orthogonal Molecular Orbitals Using the Spherical Gaussian Overlap Approximation," *Chemical Physics Letters*, vol. 315, no. 1-2, pp. 140–144, 1999.

[54] M. A. Spackman, "The Use of the Promolecular Charge Density to Approximate the Penetration Contribution to Intermolecular Electrostatic Energies," *Chemical Physics Letters*, vol. 418, no. 1-3, pp. 158–162, 2006.

[55] J. Wang, R. M. Wolf, J. W. Caldwell, P. A. Kollman, and D. A. Case, "Development and Testing of a General AMBER Force Field," *Journal of Computational Chemistry*, vol. 25, no. 9, pp. 1157–1174, 2004.

[56] T. Verstraelen, S. Vandenbrande, F. Heidar-Zadeh, L. Vanduyfhuys, V. Van Speybroeck, M. Waroquier, and P. W. Ayers, "Minimal Basis Iterative Stockholder: Atoms in Molecules for Force-Field Development," *Journal of Chemical Theory and Computation*, vol. 12, no. 8, pp. 3894–3912, 2016.

[57] D. M. Elking, G. A. Cisneros, J.-P. Piquemal, T. A. Darden, and L. G. Pedersen, "Gaussian Multipole Model (GMM)," *Journal of Chemical Theory and Computation*, vol. 6, no. 1, pp. 190–202, 2010.

[58] G. A. Cisneros, D. Elking, J.-P. Piquemal, and T. A. Darden, "Numerical Fitting of Molecular Properties to Hermite Gaussians," *The Journal of Physical Chemistry A*, vol. 111, no. 47, pp. 12049–12056, 2007.

[59] A. Maslechko, T. Verstraelen, T. S. van Erp, and E. Riccardi, "Multiscale Partial Charge Estimation on Graphene for Neutral, Doped and Charged Flakes," *Physical Chemistry Chemical Physics*, vol. 20, no. 31, pp. 20678–20687, 2018.

[60] B. Kelly and W. R. Smith, "Alchemical Hydration Free-Energy Calculations Using Molecular Dynamics with Explicit Polarization and Induced Polarity Decoupling: an On-the-Fly Polarization Approach," *Journal of Chemical Theory and Computation*, 2020.

[61] M. Riquelme and E. Vöhringer-Martinez, "SAMPL6 Octanol–Water Partition Coefficients from Alchemical Free Energy Calculations with MBIS Atomic Charges," *Journal of Computer-Aided Molecular Design*, pp. 1–8, 2020.

[62] M. Cho, N. Sylvetsky, S. Eshafi, G. Santra, I. Efremenko, and J. M. Martin, "The Atomic Partial Charges Arboretum: Trying to See the Forest for the Trees," *A European Journal of Chemical Physics and Physical Chemistry*, 2020.

[63] G. A. Cisneros, J.-P. Piquemal, and T. A. Darden, "Generalization of the Gaussian Electrostatic Model: Extension to Arbitrary Angular Momentum, Distributed Multipoles, and Speedup with Reciprocal Space Methods," *The Journal of chemical physics*, vol. 125, no. 18, p. 184101, 2006.

[64] G. A. Cisneros, "Application of Gaussian Electrostatic Model (GEM) Distributed Multipoles in the AMOEBA Force Field," *Journal of Chemical Theory and Computation*, vol. 8, no. 12, pp. 5072–5080, 2012.

[65] H. Torabifard, O. N. Starovoytov, P. Ren, and G. A. Cisneros, "Development of an AMOEBA Water Model using GEM Distributed Multipoles," *Theoretical Chemistry Accounts*, vol. 134, no. 8, p. 101, 2015.

[66] J.-P. Piquemal and G. A. Cisneros, "Status of the Gaussian Electrostatic Model, a Density-Based Polarizable Force Field," 2016.

[67] R. J. Wheatley, "Gaussian Multipole Functions for Describing Molecular Charge Distributions," *Molecular Physics*, vol. 79, no. 3, pp. 597–610, 1993.

[68] K. Tang and J. P. Toennies, "An Improved Simple Model for the van der Waals Potential Based on Universal Damping Functions for the Dispersion Coefficients," *The Journal of chemical physics*, vol. 80, no. 8, pp. 3726–3741, 1984.

[69] S. Grimme, J. Antony, S. Ehrlich, and H. Krieg, "A Consistent and Accurate *Ab Initio* Parametrization of Density Functional Dispersion Correction (DFT-D) for the 94 Elements H-Pu," *Journal of Chemical Physics*, vol. 132, no. 15, p. 154104, 2010.

[70] M. A. Freitag, M. S. Gordon, J. H. Jensen, and W. J. Stevens, "Evaluation of Charge Penetration Between Distributed Multipolar Expansions," *Journal of Chemical Physics*, vol. 112, no. 17, pp. 7300–7306, 2000.

[71] J. Piquemal, N. Gresh, and C. G, "Improved Formulas for the Calculation of the Electrostatic Contribution to the Intermolecular Interaction Energy from Multipolar Expansion of the Electronic Distribution," *The Journal of Physical Chemistry A*, vol. 107, no. 48, pp. 10353–10359, 2003.

[72] G. A. Cisneros, J.-P. Piquemal, and T. A. Darden, "Quantum Mechanics/Molecular Mechanics Electrostatic Embedding with Continuous and Discrete Functions," *The Journal of Physical Chemistry B*, vol. 110, no. 28, pp. 13682–13684, 2006.

[73] L. V. Slipchenko and M. S. Gordon, "Electrostatic Energy in the Effective Fragment Potential Method: Theory and Application to Benzene Dimer," *Journal of Computational Chemistry*, vol. 28, no. 1, pp. 276–291, 2007.

[74] K. Szalewicz, "Symmetry-Adapted Perturbation Theory of Intermolecular Forces," *Wiley Interdisciplinary Reviews: Computational Molecular Science*, vol. 2, no. 2, pp. 254–272, 2012.

[75] T. H. Dunning Jr, "Gaussian Basis Sets for use in Correlated Molecular Calculations. I. The Atoms Boron Through Neon and Hydrogen," *Journal of Chemical Physics*, vol. 90, no. 2, pp. 1007–1023, 1989.

[76] G. Knizia, "Intrinsic Atomic Orbitals: An Unbiased Bridge Between Quantum Theory and Chemical Concepts," *Journal of Chemical Theory and Computation*, vol. 9, no. 11, pp. 4834–4843, 2013.

[77] G. Herzberg, "Molecular Spectra and Molecular Structure. Vol. 3: Electronic Spectra and Electronic Structure of Polyatomic Molecules," *New York: Van Nostrand, Reinhold*, 1966.

[78] R. F. Bader, "Atoms in Molecules," *Accounts of Chemical Research*, vol. 18, no. 1, pp. 9–15, 1985.

[79] B. R. Brooks, R. E. Bruccoleri, B. D. Olafson, D. J. States, S. a. Swaminathan, and M. Karplus, "CHARMM: A Program for Macromolecular Energy, Minimization, and Dynamics Calculations," *Journal of Computational Chemistry*, vol. 4, no. 2, pp. 187–217, 1983.

[80] D. Cooper, *Valence Bond Theory*. Elsevier, 2002.

[81] D. L. Cooper, J. Gerratt, and M. Raimondi, "Applications of Spin-Coupled Valence Bond Theory," *Chemical Reviews*, vol. 91, no. 5, pp. 929–964, 1991.

[82] G. N. Lewis, "The Atom and the Molecule," *Journal of the American Chemical Society*, vol. 38, no. 4, pp. 762–785, 1916.

[83] W. Heitler and F. London, "Wechselwirkung Neutraler Atome und Homöopolare Bindung nach der Quantenmechanik," *Zeitschrift für Physik*, vol. 44, no. 6-7, pp. 455–472, 1927.

[84] Ø. Burrau, "Berechnung des energiewertes des wasserstoffmolekel-ions im normalzustand," *Naturwissenschaften*, vol. 15, no. 1, pp. 16–17, 1927.

[85] J. C. Slater, "The Virial and Molecular Structure," *The Journal of Chemical Physics*, vol. 1, no. 10, pp. 687–691, 1933.

[86] R. P. Feynman, "Forces in Molecules," *Physical Review*, vol. 56, no. 4, p. 340, 1939.

[87] C. Coulson, *Valence*. Oxford University Press, 1961.

[88] R. F. Bader, J. Hernández-Trujillo, and F. Cortés-Guzmán, "Chemical Bonding: From Lewis to Atoms in Molecules," *Journal of computational chemistry*, vol. 28, no. 1, pp. 4–14, 2007.

[89] H. Hellmann, "Zur Rolle der Kinetischen Elektronenenergie für die Zwischenatomaren Kräfte," *Zeitschrift für Physik*, vol. 85, pp. 180–190, 1933.

[90] H. Hellmann, *Einführung in die Quantenchemie: von... Hans Hellmann,...* F. Deuticke, 1937.

[91] G. B. Bacskay, S. Nordholm, and K. Ruedenberg, "The Virial Theorem and Covalent Bonding," *The Journal of Physical Chemistry A*, vol. 122, no. 39, pp. 7880–7893, 2018.

[92] K. Ruedenberg, "The Physical Nature of the Chemical Bond," *Reviews of Modern Physics*, vol. 34, no. 2, pp. 326–376, 1962.

[93] M. Feinberg, K. Ruedenberg, and E. L. Mehler, "The Origin of Binding and Antibinding in the Hydrogen Molecule-lon," in *Advances in quantum chemistry*, vol. 5, pp. 27–98, Elsevier, 1970.

[94] M. Feinberg and K. Ruedenberg, "Heteropolar one-electron bond," *The Journal of Chemical Physics*, vol. 55, no. 12, pp. 5804–5818, 1971.

[95] K. Ruedenberg, "The Nature of the Chemical Bond, an Energetic View," in *Localization and Delocalization in Quantum Chemistry*, pp. 223–245, Springer, 1975.

[96] K. Ruedenberg and M. W. Schmidt, "Why Does Electron Sharing Lead to Covalent Bonding? A Variational Analysis," *Journal of Computational Chemistry*, vol. 28, no. 1, pp. 391–410, 2007.

[97] T. Bitter, K. Ruedenberg, and W. Schwarz, "Toward a Physical Understanding of Electron-Sharing Two-Center Bonds. I. General Aspects," *Journal of Computational Chemistry*, vol. 28, no. 1, pp. 411–422, 2007.

[98] K. Ruedenberg and M. W. Schmidt, "Physical Understanding Through Variational Reasoning: Electron Sharing and Covalent Bonding," *The Journal of Physical Chemistry A*, vol. 113, no. 10, pp. 1954–1968, 2009.

[99] T. Bitter, K. Ruedenberg, and W. Schwarz, "Toward a Physical Understanding of Electron-Sharing Two-Center Bonds. I. General Aspects," *Journal of Computational Chemistry*, vol. 28, no. 1, pp. 411–422, 2007.

[100] M. W. Schmidt, J. Ivanic, and K. Ruedenberg, "Covalent Bonds are Created by the Drive of Electron Waves to Lower their Kinetic Energy Through Expansion," *Journal of Chemical Physics*, vol. 140, no. 20, p. 204104, 2014.

[101] R. Mulliken, *Diatomic Molecules: Results of Ab Initio Calculations*. Elsevier, 1977.

[102] K. Fukui, "Chemical Reactions and Electronic Orbitals," 1976.

[103] C. W. Wilson and W. A. Goddard, "The Role of Kinetic Energy in Chemical Binding," *Theoretica Chimica Acta*, vol. 26, no. 3, pp. 195–210, 1972.

[104] W. Kutzelnigg, "The Physical Mechanism of the Chemical Bond," *Angewandte Chemie*, vol. 12, no. 7, pp. 546–562, 1973.

[105] W. Kutzelnigg and W. Schwarz, "Formation of the Chemical Bond and Orbital Contraction," *Physical Review A*, vol. 26, no. 5, p. 2361, 1982.

[106] N. C. Baird, "The Chemical Bond Revisited," *Journal of Chemical Education*, vol. 63, no. 8, p. 660, 1986.

[107] S. Nordholm, "Delocalization the Key Concept of Covalent Bonding," *Journal of Chemical Education*, vol. 65, no. 7, p. 581, 1988.

[108] S. Shaik, P. Maitre, G. Sini, and P. C. Hiberty, "The charge-shift bonding concept. electron-pair bonds with very large ionic-covalent resonance ener-

gies," *Journal of the American Chemical Society*, vol. 114, no. 20, pp. 7861–7866, 1992.

[109] G. B. Bacskay, J. R. Reimers, and S. Nordholm, "The Mechanism of Covalent Bonding," *Journal of Chemical Education*, vol. 74, no. 12, p. 1494, 1997.

[110] F. Rioux, "The Covalent Bond Examined using the Virial Theorem," *Chem Educator*, vol. 8, pp. 10–12, 2003.

[111] P. C. Hiberty, R. Ramozzi, L. Song, W. Wu, and S. Shaik, "The physical origin of large covalent–ionic resonance energies in some two-electron bonds," *Faraday discussions*, vol. 135, pp. 261–272, 2007.

[112] S. Nordholm and W. Eek, "Ergodicity and rapid electron delocalization–the dynamical mechanism of atomic reactivity and covalent bonding," *International Journal of Quantum Chemistry*, vol. 111, no. 9, pp. 2072–2088, 2011.

[113] S. Nordholm and G. B. Bacskay, "The Role of Quantum Dynamics in Covalent Bonding- A Comparison of Thomas-Fermi and Hückel Models," *Advances in Quantum Theory*, pp. 107–152, 2012.

[114] G. B. Bacskay and S. Nordholm, "Covalent Bonding: The Fundamental Role of the Kinetic Energy," *The Journal of Physical Chemistry A*, vol. 117, no. 33, pp. 7946–7958, 2013.

[115] G. B. Bacskay and S. Nordholm, "Covalent Bonding in the Hydrogen Molecule," *The Journal of Physical Chemistry A*, vol. 121, no. 48, pp. 9330–9345, 2017.

[116] D. W. O. de Sousa and M. A. C. Nascimento, "One-electron bonds are not "half-bonds"," *Physical Chemistry Chemical Physics*, vol. 21, no. 24, pp. 13319–13336, 2019.

[117] G. B. Bacskay, W. Eek, and S. Nordholm, "Is Covalent Bonding a One-Electron Phenomenon? Analysis of a Simple Potential Model of Molecular Structure," *Chemical Educator*, vol. 15, pp. 42–54, 2010.

[118] M. W. Schmidt, J. Ivanic, and K. Ruedenberg, "The Physical Origin of Covalent Bonding," *The Chemical Bond. Fundamental Aspects of Chemical Bonding; Frenking, G., Shaik, S.*, 2014.

[119] D. S. Levine and M. Head-Gordon, "Quantifying the Role of Orbital Contraction in Chemical Bonding," *The Journal of Physical Chemistry Letters*, vol. 8, no. 9, pp. 1967–1972, 2017.

[120] J. M. Foster and S. F. Boys, "Canonical Configurational Interaction Procedure," *Reviews of Modern Physics*, vol. 32, no. 2, p. 300, 1960.

[121] S. F. Boys, "Construction of Some Molecular Orbitals to be Approximately Invariant for Changes from One Molecule to Another," *Reviews of Modern Physics*, vol. 32, no. 2, p. 296, 1960.

[122] B. Jansík, S. Høst, K. Kristensen, and P. Jørgensen, "Local Orbitals by Minimizing Powers of the Orbital Variance," *The Journal of Chemical Physics*, vol. 134, no. 19, p. 194104, 2011.

[123] I. Høyvik, B. Jansik, and P. Jørgensen, "Trust Region Minimization of Orbital Localization Functions," *Journal of chemical theory and computation*, vol. 8, no. 9, pp. 3137–3146, 2012.

[124] A. E. Reed, R. B. Weinstock, and F. Weinhold, "Natural Population Analysis," *Journal of Chemical Physics*, vol. 83, no. 2, pp. 735–746, 1985.

[125] A. C. West, M. W. Schmidt, M. S. Gordon, and K. Ruedenberg, "A Comprehensive Analysis of Molecule-Intrinsic Quasi-Atomic, Bonding, and Correlating Orbitals. I. Hartree-Fock Wave Functions," *The Journal of Chemical Physics*, vol. 139, no. 23, p. 234107, 2013.

[126] A. C. West, M. W. Schmidt, M. S. Gordon, and K. Ruedenberg, "A Comprehensive Analysis in Terms of Molecule-Intrinsic, Quasi-Atomic Orbitals. II. Strongly Correlated MCSCF Wave Functions," *The Journal of Physical Chemistry A*, vol. 119, no. 41, pp. 10360–10367, 2015.

[127] A. C. West, M. W. Schmidt, M. S. Gordon, and K. Ruedenberg, "A Comprehensive Analysis in Terms of Molecule-Intrinsic, Quasi-Atomic Orbitals. III.

The Covalent Bonding Structure of Urea," *The Journal of Physical Chemistry A*, vol. 119, no. 41, pp. 10368–10375, 2015.

[128] A. C. West, M. W. Schmidt, M. S. Gordon, and K. Ruedenberg, "A Comprehensive Analysis in Terms of Molecule-Intrinsic Quasi-Atomic Orbitals. IV. Bond breaking and Bond Forming Along the Dissociative Reaction Path of Dioxetane," *The Journal of Physical Chemistry A*, vol. 119, no. 41, pp. 10376–10389, 2015.

[129] L. Zhao, M. von Hopffgarten, D. M. Andrada, and G. Frenking, "Energy Decomposition Analysis," *Wiley Interdisciplinary Reviews: Computational Molecular Science*, vol. 8, no. 3, p. e1345, 2018.

[130] P. R. Horn, Y. Mao, and M. Head-Gordon, "Probing Non-Covalent Interactions with a Second Generation Energy Decomposition Analysis using Absolutely Localized Molecular Orbitals," *Physical Chemistry Chemical Physics*, vol. 18, no. 33, pp. 23067–23079, 2016.

[131] D. S. Levine, P. R. Horn, Y. Mao, and M. Head-Gordon, "Variational Energy Decomposition Analysis of Chemical Bonding. 1. Spin-Pure Analysis of Single Bonds," *Journal of Chemical Theory and Computation*, vol. 12, pp. 4812–4820, 2016.

[132] D. S. Levine and M. Head-Gordon, "Energy Decomposition Analysis of Single Bonds within Kohn–Sham Density Functional Theory," *Proceedings of the National Academy of Sciences*, vol. 114, pp. 12649–12656, 2017.

[133] J. Thirman and M. Head-Gordon, "An Energy Decomposition Analysis for Second-Order Møller–Plesset Perturbation Theory Based on Absolutely Localized Molecular Orbitals," *The Journal of Chemical Physics*, vol. 143, no. 8, p. 084124, 2015.

[134] J. Thirman and M. Head-Gordon, "Efficient Implementation of Energy Decomposition Analysis for Second-Order Møller–Plesset Perturbation Theory and Application to Anion- π Interactions," *The Journal of Physical Chemistry A*, vol. 121, no. 3, pp. 717–728, 2017.

[135] J. Thirman, E. Engelage, S. M. Huber, and M. Head-Gordon, "Characterizing the Interplay of Pauli Repulsion, Electrostatics, Dispersion and Charge Transfer in Halogen Bonding with Energy Decomposition Analysis," *Physical Chemistry Chemical Physics*, vol. 20, no. 2, pp. 905–915, 2018.

[136] T. Ziegler and A. Rauk, "On the Calculation of Bonding Energies by the Hartree Fock Slater Method," *Theoretica Chimica Acta*, vol. 46, no. 1, pp. 1–10, 1977.

[137] K. Kitaura and K. Morokuma, "A New Energy Decomposition Scheme for Molecular Interactions within the Hartree-Fock Approximation," *International Journal of Quantum Chemistry*, vol. 10, no. 2, pp. 325–340, 1976.

[138] J. Andrés, P. W. Ayers, R. A. Boto, R. Carbó-Dorca, H. Chermette, J. Cioslowski, J. Contreras-García, D. L. Cooper, G. Frenking, C. Gatti, *et al.*, "Nine Questions on Energy Decomposition Analysis," *Journal of Computational Chemistry*, vol. 40, no. 26, pp. 2248–2283, 2019.

[139] A. C. West, M. W. Schmidt, M. S. Gordon, and K. Ruedenberg, "Intrinsic Resolution of Molecular Electronic Wave Functions and Energies in Terms of Quasi-Atoms and their Interactions," *The Journal of Physical Chemistry A*, vol. 121, no. 5, pp. 1086–1105, 2017.

[140] A. C. West, J. J. Duchimaza-Heredia, M. S. Gordon, and K. Ruedenberg, "Identification and Characterization of Molecular Bonding Structures by *Ab Initio* Quasi-Atomic Orbital Analyses," *The Journal of Physical Chemistry A*, vol. 121, no. 46, pp. 8884–8898, 2017.

[141] J. J. Duchimaza Heredia, K. Ruedenberg, and M. S. Gordon, "Quasi-Atomic Bonding Analysis of Xe-Containing Compounds," *The Journal of Physical Chemistry A*, vol. 122, no. 13, pp. 3442–3454, 2018.

[142] G. Schoendorff, M. W. Schmidt, K. Ruedenberg, and M. S. Gordon, "Quasi-Atomic Bond Analyses in the Sixth Period: II. Bond Analyses of Cerium Oxides," *The Journal of Physical Chemistry A*, vol. 123, no. 25, pp. 5249–5256, 2019.

[143] M. Loipersberger, Y. Mao, and M. Head-Gordon, "Variational Forward-Backward Charge Transfer Analysis Based on Absolutely Localized Molecular Orbitals: Energetics and Molecular Properties," *Journal of Chemical Theory and Computation*, 2020.

[144] J. Clayden, N. Greeves, S. Warren, and P. Wothers, *Organic Chemistry*. Oxford University Press, 2001.

[145] W. O. Kermack and R. Robinson, "LI.—An Explanation of the Property of Induced Polarity of Atoms and an Interpretation of the Theory of Partial Valencies on an Electronic Basis," *Journal of the Chemical Society, Transactions*, vol. 121, pp. 427–440, 1922.

[146] P. Vidossich and A. Lledós, "The Use of Localised Orbitals for the bonding and Mechanistic Analysis of Organometallic Compounds," *Dalton Transactions*, vol. 43, no. 29, pp. 11145–11151, 2014.

[147] G. Knizia and J. E. Klein, "Electron Flow in Reaction Mechanisms—Revealed from First Principles," *Angewandte Chemie*, vol. 54, no. 18, pp. 5518–5522, 2015.

[148] A. J. Proud, D. E. Mackenzie, and J. K. Pearson, "Exploring electron pair behaviour in chemical bonds using the extracule density," *Physical Chemistry Chemical Physics*, vol. 17, no. 31, pp. 20194–20204, 2015.

[149] J. Andrés, S. Berski, and B. Silvi, "Curly Arrows Meet Electron Density Transfers in Chemical Reaction Mechanisms: from Electron Localization Function (ELF) Analysis to Valence-Shell Electron-Pair Repulsion (VSEPR) Inspired Interpretation," *Chemical Communications*, vol. 52, no. 53, pp. 8183–8195, 2016.

[150] J. Andrés, P. González-Navarrete, V. S. Safont, and B. Silvi, "Curly Arrows, Electron Flow, and Reaction Mechanisms from the Perspective of the Bonding Evolution Theory," *Physical Chemistry Chemical Physics*, vol. 19, no. 43, pp. 29031–29046, 2017.

[151] Y. Liu, P. Kilby, T. J. Frankcombe, and T. W. Schmidt, "Calculating Curly Arrows from *Ab Initio* Wavefunctions," *Nature Communications*, vol. 9, no. 1, pp. 1–7, 2018.

[152] I. Frank and P. Kraus, "The Tardy Dance of Molecular Orbitals," *International Journal of Quantum Chemistry*, vol. 118, no. 20, p. e25718, 2018.

[153] E. Glendening and F. Weinhold, "Resonance Natural Bond Orbitals: Efficient Semilocalized Orbitals for Computing and Visualizing Reactive Chemical Processes," *Journal of chemical theory and computation*, vol. 15, no. 2, pp. 916–921, 2019.

[154] J. E. Klein, G. Knizia, and H. S. Rzepa, "Epoxidation of Alkenes by Peracids: From Textbook Mechanisms to a Quantum Mechanically Derived Curly-Arrow Depiction," *ChemistryOpen*, vol. 8, no. 10, pp. 1244–1250, 2019.

[155] G. Sciortino, A. Lledós, and P. Vidossich, "Bonding Rearrangements in Organometallic Reactions: From Orbitals to Curly Arrows," *Dalton Transactions*, vol. 48, no. 42, pp. 15740–15752, 2019.

Appendix A

Translation of Multipole Moments

The formulae here are for the translation of cartesian multipole moment components, up to octopole from the origin, $O = (0, 0, 0)$, to a point, $C = (c_x, c_y, c_z)$.

For the dipole moment we have,

$$\mu_x^C = \mu_x^O - qc_x, \tag{A.1}$$

$$\mu_y^C = \mu_y^O - qc_y, \tag{A.2}$$

$$\mu_z^C = \mu_z^O - qc_z. \tag{A.3}$$

For the quadrupole moment,

$$\Theta_{xx}^C = \Theta_{xx}^O - 3\mu_x^O c_x + \frac{3}{2}c_x^2 q + \sum_\alpha \mu_\alpha^O c_\alpha - \frac{1}{2}\sum_\alpha c_\alpha^2 q, \tag{A.4}$$

$$\Theta_{yy}^C = \Theta_{yy}^O - 3\mu_y^O c_y + \frac{3}{2}c_y^2 q + \sum_\alpha \mu_\alpha^O c_\alpha - \frac{1}{2}\sum_\alpha c_\alpha^2 q. \tag{A.5}$$

$$\Theta_{zz}^C = \Theta_{zz}^O - 3\mu_z^O c_z + \frac{3}{2}c_z^2 q + \sum_\alpha \mu_\alpha^O c_\alpha - \frac{1}{2}\sum_\alpha c_\alpha^2 q, \tag{A.6}$$

$$\Theta_{xy}^C = \Theta_{xy}^O - \frac{3}{2}(\mu_x^O c_y + \mu_y^O c_x - c_x c_y q), \tag{A.7}$$

$$\Theta_{xz}^C = \Theta_{xz}^O - \frac{3}{2}(\mu_x^O c_z + \mu_z^O c_x - c_x c_z q), \tag{A.8}$$

$$\Theta_{yz}^C = \Theta_{yz}^O - \frac{3}{2}(\mu_y^O c_z + \mu_z^O c_y - c_y c_z q). \tag{A.9}$$

Finally, for the octopole moment,

$$\Omega^C_{zzz} = \Omega^O_{zzz} - 3\Theta^O_{zz}c_z + 2(\Theta^O_{xz}c_x + \Theta^O_{yz}c_y) + \frac{9}{2}\mu^O_z c_z^2 - \frac{3}{2}||c||(\mu^O_z - c_z q) - 3(\mu^O_x c_x c_z + \mu^O_y c_y c_z) - \frac{5}{2}c_z^3 q, \quad \text{(A.10)}$$

$$\Omega^C_{yyy} = \Omega^O_{yyy} - 3\Theta^O_{yy}c_y + 2(\Theta^O_{xy}c_x + \Theta^O_{yz}c_z) + \frac{9}{2}\mu^O_y c_y^2 - \frac{3}{2}||c||(\mu^O_y - c_y q) - 3(\mu^O_z c_z c_y + \mu^O_x c_x c_y) - \frac{5}{2}c_y^3 q, \quad \text{(A.11)}$$

$$\Omega^C_{xxx} = \Omega^O_{xxx} - 3\Theta^O_{xx}c_x + 2(\Theta^O_{zx}c_z + \Theta^O_{yx}c_y) + \frac{9}{2}\mu^O_x c_x^2 - \frac{3}{2}||c||(\mu^O_x - c_x q) - 3(\mu^O_z c_z c_x + \mu^O_y c_y c_x) - \frac{5}{2}(c_x^3 q), \quad \text{(A.12)}$$

$$\Omega^C_{xyz} = \Omega^O_{xyz} - \frac{5}{3}(\Theta^O_{yz}c_x + \Theta^O_{xz}c_y + \Theta^O_{xy}c_z) + \frac{5}{2}(\mu^O_z c_y c_x + \mu^O_y c_x c_z + \mu^O_x c_y c_z - c_x c_y c_z q), \quad \text{(A.13)}$$

$$\Omega^C_{xzz} = \Omega^O_{xzz} - \frac{8}{3}\Theta^O_{xz}c_z + \frac{2}{3}\Theta^O_{xy}c_y - \Theta^O_{zz}c_x + \frac{2}{3}(\Theta^O_{xx} - \Theta^O_{zz})c_x + 4\mu^O_z c_z c_x - \mu^O_y c_x c_y + \frac{5}{2}\mu^O_x c_z^2 - \mu^O_x c_x^2 - \frac{1}{2}||c||(\mu^O_x - c_x q) - \frac{5}{2}c_z^2 c_x q, \quad \text{(A.14)}$$

$$\Omega^C_{yzz} = \Omega^O_{yzz} - \frac{8}{3}\Theta^O_{yz}c_z + \frac{2}{3}\Theta^O_{xy}c_x - \Theta^O_{zz}c_y + \frac{2}{3}(\Theta^O_{yy} - \Theta^O_{zz})c_y + 4\mu^O_z c_z c_y - \mu^O_x c_x c_y + \frac{5}{2}\mu^O_y c_z^2 - \mu^O_y c_y^2 - \frac{1}{2}||c||(\mu^O_y - c_y q) - \frac{5}{2}c_z^2 c_y q, \quad \text{(A.15)}$$

$$\Omega^C_{xxy} = \Omega^O_{xxy} - \frac{8}{3}\Theta^O_{xy}c_x + \frac{2}{3}\Theta^O_{yz}c_z - \Theta^O_{xx}c_y + \frac{2}{3}(\Theta^O_{yy} - \Theta^O_{xx})c_y + 4\mu^O_x c_x c_y - \mu^O_z c_z c_y + \frac{5}{2}\mu^O_y c_x^2 - \mu^O_y c_y^2 - \frac{1}{2}||c||(\mu^O_y - c_y q) - \frac{5}{2}c_x^2 c_y q, \quad \text{(A.16)}$$

$$\Omega^C_{xxz} = \Omega^O_{xxz} - \frac{8}{3}\Theta^O_{xz}c_x + \frac{2}{3}\Theta^O_{yz}c_y - \Theta^O_{xx}c_z + \frac{2}{3}(\Theta^O_{zz} - \Theta^O_{xx})c_z$$
$$+ 4\mu^O_x c_x c_z - \mu^O_y c_y c_z + \frac{5}{2}\mu^O_z c_x^2 - \mu^O_z c_z^2 - \frac{1}{2}||c||(\mu^O_z - c_z q) - \frac{5}{2}c_x^2 c_z q, \quad \text{(A.17)}$$

$$\Omega^C_{yyz} = \Omega^O_{yyz} - \frac{8}{3}\Theta^O_{yz}c_y + \frac{2}{3}\Theta^O_{xz}c_x - \Theta^O_{yy}c_z + \frac{2}{3}(\Theta^O_{zz} - \Theta^O_{yy})c_z$$
$$+ 4\mu^O_y c_y c_z - \mu^O_x c_x c_z + \frac{5}{2}\mu^O_z c_y^2 - \mu^O_z c_z^2 - \frac{1}{2}||c||(\mu^O_z - c_z q) - \frac{5}{2}c_y^2 c_z q, \quad \text{(A.18)}$$

$$\Omega^C_{xyy} = \Omega^O_{xyy} - \frac{8}{3}\Theta^O_{xy}c_y + \frac{2}{3}\Theta^O_{xz}c_z - \Theta^O_{yy}c_x + \frac{2}{3}(\Theta^O_{xx} - \Theta^O_{yy})c_x$$
$$+ 4\mu^O_y c_y c_x - \mu^O_z c_x c_z + \frac{5}{2}\mu^O_x c_y^2 - \mu^O_x c_x^2 - \frac{1}{2}||c||(\mu^O_x - c_x q) - \frac{5}{2}c_y^2 c_x q. \quad \text{(A.19)}$$